ERDC/CHL TR-12-22

Coastal and Hydraulics Laboratory

US Army Corps
of Engineers®
Engineer Research and
Development Center

Great Lakes Coastal Flood Study, 2012 Federal Inter-Agency Initiative

Cross-Shore Numerical Model CSHORE for Waves, Currents, Sediment Transport and Beach Profile Evolution

Bradley D. Johnson, Nobuhisa Kobayashi,
and Mark B. Gravens

September 2012

Approved for public release; distribution is unlimited.

Great Lakes Coastal Flood Study, 2012
Federal Inter-Agency Initiative

ERDC/CHL TR-12-22
September 2012

Cross-Shore Numerical Model CSHORE for Waves, Currents, Sediment Transport and Beach Profile Evolution

Bradley D. Johnson and Mark B. Gravens

Coastal and Hydraulics Laboratory
U.S. Army Engineer Research and Development Center
3909 Halls Ferry Road
Vicksburg, MS 39180

Nobuhisa Kobayashi

Center for Applied Coastal Research
Ocean Engineering Laboratory
University of Delaware
Newark, Delaware 19716

Final report

Prepared for U.S. Army Corps of Engineers
441 G Street NW
Washington, DC 20314-1000

Abstract

The majority of the world shoreline is experiencing some form of erosion, which will become more serious if the mean sea level rise accelerates because of the greenhouse effect. The recent increase of coastal storm damage necessitates the development of numerical models for predicting the damage progression and breaching of beaches, coastal stone structures and earthen levees during extreme storms. This report summarizes the continuing effort to improve our quantitative understanding of beach morphology and structural damage progression with the goal to develop simple and robust models that are suited for engineering applications. Our effort for the last 10 years has produced the cross-shore numerical model CSHORE, which is presently limited to the case of alongshore uniformity. CSHORE consists of the following components: a combined wave and current model based on time-averaged continuity, cross-shore and longshore momentum, wave action, and roller energy equations; a sediment transport model for suspended sand and bedload; a permeable layer model to account for porous flow and energy dissipation; empirical formulas for irregular wave runup, overtopping and seepage; and a probabilistic model for an intermittently wet and dry zone for the purpose of predicting wave overwash and structural damage progression. The wet and dry model, which is the latest addition to CSHORE, is calibrated and verified using our 107 small-scale tests for irregular wave overtopping and overflow on a levee as well as 118 Dutch tests for low-exceedance wave overtopping, in which velocities and water depths were measured on the crest and landward (inner) slope of dikes. Finally, the computer program CSHORE is explained to facilitate use and modifications, if necessary. In the near future, CSHORE will be compared with wave overwash experiments and structural damage progression experiments.

Contents

Figures

Figures

Preface

This study has been supported by the Flood and Coastal Systems Research and Development Program The work performed at CHL was under the general supervision of Dr. Ty V. Wamsley, Chief, Coastal Processes Branch; Bruce A. Ebersole, Chief, Coastal Flood and Storm Protection Division; William R. Curtis, Technical Director for Flood and Storm Damage Reduction. The Director of the Coastal and Hydraulics Laboratory was Dr. William D. Martin.

COL Kevin J. Wilson was Commander and Executive Director of ERDC. Dr. Jeffery P. Holland was Director.

1 Introduction

A sand beach with a wide berm and a high dune provides storm protection and damage reduction, recreational and economical benefits, and biological habitats for plants and animals. Most sandy beaches are eroding partly due to sea level rise. Beach nourishment is widely adopted to maintain a wide beach for a developed coastal community if a suitable beachfill is available in the vicinity of an eroding beach. Empirical methods based on field data have been developed for the design of beach fills (Headquarters, U.S. Army Corps of Engineers (HQUSACE) 2002). The design of the cross-shore beachfill profile is normally based on the concept of an equilibrium beach profile. The alongshore spreading of the beachfill is generally predicted using a one-line model coupled with the Coastal Engineering Research Center (CERC) formula or the formula by Kamphuis (1991) for the longshore sediment transport rate. These simple beachfill design methods have been criticized and a number of more process-based models have been proposed. However, the process-based models may not necessarily be more accurate at present.

Sediment transport is caused by the combined action of waves and currents. Our capabilities of predicting wave and current fields have improved steadily over the last 30 years. However, the predictive capability of sediment transport on beaches has not improved to the same degree. The major reason for this discrepancy is that no dynamic equation is available to describe the motion of a large number of sediment particles. Consequently, sediment transport models are essentially empirical and dependent on reliable sediment transport data. Unfortunately, sediment dynamics on beaches are highly complex and involve wide ranges of morphological scales in time and space. Correspondingly, available sediment transport models have become more complex and less transparent. We have tried to synthesize available data and formulas to develop simple and transparent formulas for the cross-shore and longshore transport rates of suspended sand and bedload on beaches. The simple formulas need to include basic sediment dynamics sufficiently so that the formulas will be applicable to small-scale and large-scale laboratory beaches and eventually prototype beaches. Furthermore, the morphological model should be computationally efficient to allow calibration and verification using extensive data sets. The hydrodynamic input required for the morphological model should be limited to quantities that can be predicted routinely and reliably. These considerations have guided our development of the cross-shore numerical model CSHORE presented in this report.

Coastal storm damage has been increasing mostly due to the recent growth of coastal population and assets and possibly due to the intensification of hurricanes caused by global warming. Coastal structures including earthen levees (dikes) have been designed conventionally for no storm surge overflow and minor wave overtopping during a design storm. Empirical formulas for wave overtopping rates are used for a preliminary design where EurOtop Manual (2007) recommends the latest formulas. Physical model testing is normally conducted in a wave flume or basin for a detailed design. Various numerical models have also been developed to predict detailed hydrodynamics that are difficult to measure even in a laboratory (Kobayashi and Otta 1987; Kobayashi 1999; van Gent 2001). The latest numerical models for hydrodynamics are reviewed by Losada et al. (2008) and Neves et al. (2008). However, our improved predictive capabilities for the hydrodynamics have not really improved our predictive capability for damage progression partly because damage to a coastal structure is cumulative (Melby and Kobayashi 1998). As a result, a performance or risk-based design of a coastal structure relies on empirical formulas for damage (e.g., Kobayashi et al. 2003). This practical difficulty is similar to that for sediment transport on beaches. Alternatively, the computationally-efficient CSHORE calibrated with extensive data sets has been developed for the design of inclined structures with relatively small wave reflection where damage progression models for stone structures and earthen levees will be developed by modifying the sediment transport model in this report. The eventual goal is to predict the performance of an inclined structure located on a movable bottom.

2 History of CSHORE Development

The history of the cross-shore model CSHORE is summarized to provide an overview of CSHORE and acknowledge a number of graduate students and visiting scientists who contributed to the development of CSHORE. The present version of CSHORE includes the various capabilities added to the initial model developed in 1998. The different stages of development are summarized in the following where the detail of each stage can be found in the listed publications.

The cross-shore model CSHORE was developed initially to predict the cross-shore transformation of irregular nonlinear waves using the time-averaged continuity, momentum, and wave energy equations together with a non-Gaussian probability distribution of the free surface elevation. However, empirical formulas of limited generality were required to parameterize the wave nonlinearity. The present version of CSHORE is based on linear wave theory and the Gaussian probability distribution to reduce the degree of empiricism (Kobayashi et al. 1998; Kobayashi and Johnson 1998; Johnson and Kobayashi 1998; Kearney and Kobayashi 2000; Johnson and Kobayashi 2000).

The next stage of the CSHORE development was motivated by the need of a computationally-efficient time-averaged model that can be used for the design of porous coastal structures. The linear-wave version of the initial CSHORE was modified to account for the effects of a permeable layer for the case of normally incident waves. The permeable version of CSHORE was called CSHOREP. The permeability effects are extended to obliquely incident waves in the present CSHORE (Meigs and Kobayashi 2004; Meigs et al. 2004; de los Santos and Kobayashi 2005; Ota et al. 2006; de los Santos et al. 2006; de los Santos and Kobayashi 2006; Kobayashi et al. 2007b; Kobayashi and de los Santos 2007; Ota et al. 2007; Kobayashi et al. 2008b).

Concurrently, the impermeable version of CSHORE is being extended to predict the cross-shore and longshore transport rates of suspended sand and bedload on beaches. A series of extensions were made in the following publications to make the model both versatile and better verified (Zhao and Kobayashi 2005; Kobayashi et al. 2005; Agarwal and Kobayashi 2005;

Schmied et al. 2006a and b; Agarwal et al. 2006; Payo et al. 2006; Kobayashi et al. 2007a; Buck et al. 2007; Gencarelli et al. 2007; Kobayashi et al. 2008a and b; Payo et al. 2009 Buck et al. 2008; Gencarelli et al. 2008a and b. The impermeable and permeable versions of CSHORE have been merged in the present CSHORE to expand the range of practical applications.

The following papers summarized the progress of the CSHORE development concisely up to 2008(Kobayashi 2006; Kobayashi 2008; Kobayashi et al. 2008e). These publications were based on the earlier version of CSHORE limited to the wet zone below the mean water level. To extend CSHORE to the zone which is intermittently wet and dry, laboratory experiments were conducted for wave overtopping and overflow on fixed levees. The laboratory data were used for the development of a probabilistic model for the wet and dry zone on an impermeable bottom. This hydrodynamic model coupled with the sediment transport model in CSHORE has been used to predict wave overwash of dunes. The hydrodynamic model has also been extended to the wet and dry zone on a permeable bottom for the prediction of wave overtopping of rubble mound structures. This model coupled with the CSHORE bedload formula modified for stone has been shown to be capable of predicting the evolution of damaged stone armor layers (Farhadzadeh et al. 2007; Kobayashi et al. 2007c; Farhadzadeh et al. 2008; Kobayashi and Farhadzadeh 2009; Johnson et al. 2009; Figlus et al. 2009; Figlus et al. 2010; Farhadzadeh et al. 2009; Farhadzadeh et al. 2010; Kobayashi et al. 2010a; Kobayashi et al. 2010b).

3 Wave and Current Models

Cross-shore sediment transport on beaches has been investigated extensively (e.g., Kriebel and Dean 1985; van Rijn et al. 2003) but we still cannot predict beach profile evolution accurately. To improve our predictive capabilities, sediment transport models have become more sophisticated but less transparent. For example, Thornton et al. (1996) and Gallagher et al. (1998) used the energetics-based total load model of Bailard (1981) to explain the offshore movement of a bar at Duck, NC, during storms. The onshore bar migration on the same beach was predicted by both Hoefel and Elgar (2003), using the skewed acceleration effect on bedload, and Henderson et al. (2004), using a suspended sediment model. The contribution of bedload and suspended load are not clear at present. Kobayashi et al. (2008a) made an attempt to synthesize and simplify existing cross-shore sediment transport models with the aim of developing a simple and robust model that is suited for engineering applications including the berm and dune erosion. This model has been extended to predict the cross-shore and longshore transport rates of bedload and suspended load under the combined wave and current action predicted by the time-averaged, probabilistic model by Kobayashi et al. (2007a).

Sediment transport on beaches is caused by the combined action of waves and currents. The hydrodynamic input required for a sediment transport model depends on whether the sediment transport model is time-dependent (phase-resolving) or time-averaged over a number of waves. A time-dependent sediment transport model such as that by Kobayashi and Johnson (2001) is physically appealing because it predicts intense but intermittent sand suspension under irregular breaking waves (Kobayashi and Tega 2002). However, the time-dependent model requires considerable computation time and is not necessarily more accurate in predicting slow morphological changes than the corresponding time-averaged model presented in the following. Horizontally two-dimensional (2-D) wave and current models are presented first before the cross-shore model CSHORE, which is based on the assumption of alongshore uniformity.

Figure 1 shows obliquely incident irregular waves on an essentially straight shoreline where the cross-shore coordinate x is positive onshore and the longshore coordinate y is positive in the downwave direction. The beach is

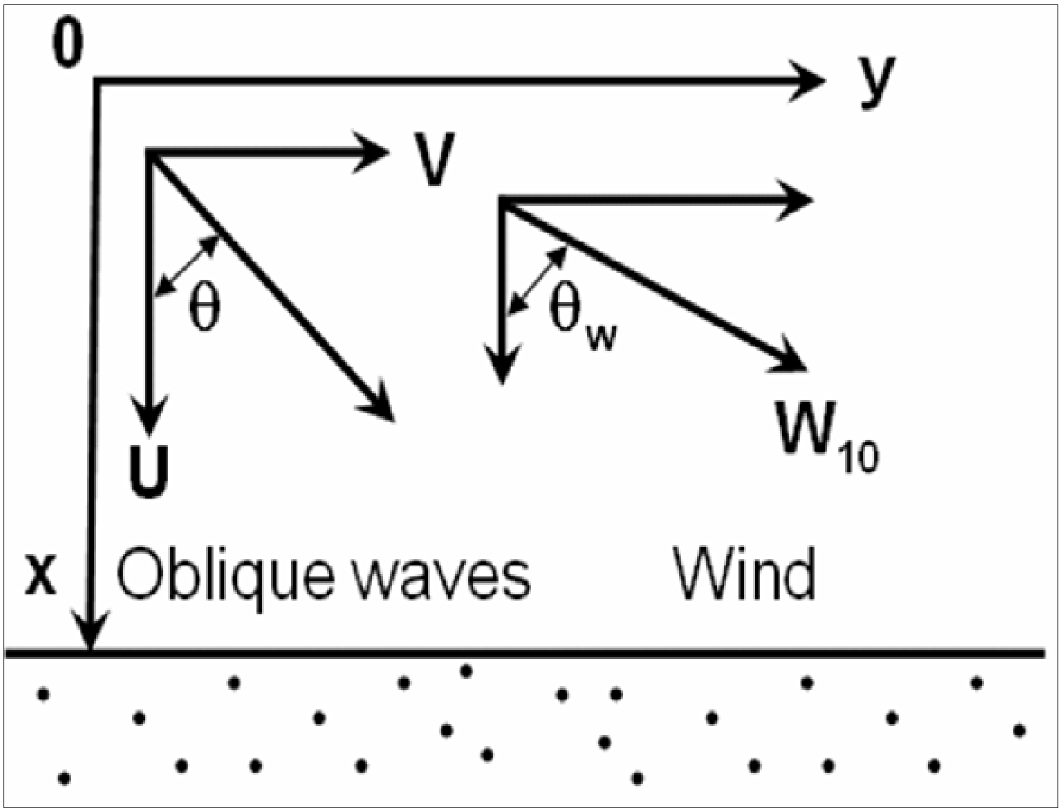

Figure 1. Definition sketch for incident irregular waves and wind on beach.

assumed to be impermeable. The depth-averaged cross-shore and longshore velocities are denoted by U and V, respectively. Incident waves are assumed to be unidirectional with θ equal to the incident angle relative to the shore normal. The height and period of the irregular waves are represented by the root-mean-square (*rms*) wave height H_{rms} and the spectral peak period T_p specified at the seaward boundary located at $x = 0$. The wave angle θ is assumed to be in the range of $|\theta| < 90$ degrees to ensure that the incident waves propagate landward. The wind speed and direction at the elevation of 10 m above the sea surface are denoted by W_{10} and θ_w, respectively.

The mean water depth $\bar{h}$, with the over bar indicating time-averaging ,is given by:

$$\bar{h} = \left(\bar{\eta} + S - z_b\right) \tag{1}$$

where $\bar{\eta}$ = wave setup above the still water level (SWL) ; and S = storm tide above the datum $z_b = 0$ which is assumed to be uniform in the computation domain, where z_b = bottom elevation relative to the datum $z = 0$ with z = vertical coordinate taken to be positive upward. Linear wave and current theory for wave refraction (e.g., Phillips 1977; Mei 1989; Dalrymple 1988) is used to predict the spatial variations of H_{rms} and θ. The dispersion relation for linear waves is expressed as:

$$\omega^2 = kg\tanh\left(k\bar{h}\right);\omega_p = \omega + k\left(Q_x\cos\theta + Q_y\sin\theta\right)/\bar{h} \tag{2}$$

where ω = intrinsic angular frequency; k = wave number; g = gravitational acceleration; ω_p = absolute angular frequency given by $\omega_p = 2\pi / T_p$; Q_x and Q_y = time-averaged volume flux per unit width in the x and y directions, respectively, and θ = incident wave angle. Equation 2 can be solved iteratively to obtain k *and* ω for known $\omega_p, \bar{h}, \theta, Q_x$ and Q_y. The phase velocity C and the group velocity C_g are given by:

$$C = \omega / k;C_g = nC;n = \frac{1}{2}\left[1 + \frac{2k\bar{h}}{\sinh\left(2k\bar{h}\right)}\right] \tag{3}$$

The wave angle θ is computed using the irrotationality of the wave number:

$$\frac{\partial}{\partial x}\left(k\sin\theta\right) - \frac{\partial}{\partial y}\left(k\sin\theta\right) = 0 \tag{4}$$

The *rms* wave height H_{rms} defined as $H_{rms} = \sqrt{8}\,\sigma_\eta$ with σ_η = standard deviation of the free surface elevation (η) is computed using the wave action equation:

$$\frac{\partial}{\partial x}\left[\frac{E}{\omega}\left(C_g\cos\theta + \frac{Q_z}{h}\right)\right] + \frac{\partial}{\partial y}\left[\frac{E}{\omega}\left(C_g\sin\theta + \frac{Q_y}{h}\right)\right] = \frac{D_B + D_f}{\omega} \tag{5}$$

with

$$E = \rho G\sigma_\eta^2 = \frac{1}{8}\rho g H_{rms}^2 \tag{6}$$

where E = specific wave energy; ρ = fluid density; and D_B and D_f = wave energy dissipation rate per unit horizontal area due to wave breaking and bottom friction, respectively. The formulas for D_B and D_f are presented later in relation to the cross-shore model CSHORE.

The time-averaged volume fluxes Q_x and Q_y in Equation 2 are expressed as:

$$Q_x = \bar{h}\bar{U} + Q_{wx} \; ; Q_y = \bar{h}\bar{V} + Q_{wy} \tag{7}$$

with

$$Q_{wx} = \frac{g\sigma_\eta^2 \cos\theta}{C} + q_r \cos\theta \; ; Q_{wy} = \frac{g\sigma_\eta^2 \sin\theta}{C} + q_r \sin\theta \tag{8}$$

where $\bar{U}$ and $\bar{V}$ = time-averaged, depth-averaged velocities in the x and y directions; Q_{wx} and Q_{wy} = wave-induced volume fluxes in the x and y directions; $\left(g\sigma_\eta^2/C\right)$ = volume flux due to linear waves propagating in the direction of θ; and q_r = volume flux of a roller on the front of a breaking wave. The roller volume flux q_r is estimated using the roller energy equation, as explained by Kobayashi et al. (2005, 2007a):

$$\frac{\partial}{\partial x}\left(\rho C^2 q_r \cos\theta\right) + \frac{\partial}{\partial y}\left(\rho C^2 q_r \sin\theta\right) = D_B - D_r \tag{9}$$

with

$$D_r = \rho g \beta_r q_r \; ; \beta_r = \left(0.1 + S_b\right) \geq 0.1 \tag{10}$$

$$S_b = \frac{\partial z_b}{\partial x}\cos\theta + \frac{\partial z_b}{\partial y}\sin\theta \tag{11}$$

where D_r = roller dissipation rate; β_r = wave-front slope; S_b = bottom slope in the direction of wave propagation. The wave front slope β_r is assumed to be 0.1 unless it is increased by the positive bottom slope S_b.

The mean water depth $\bar{h}$ and the current velocities $\bar{U}$ and $\bar{V}$ are computed using the time-averaged continuity and momentum equations (Phillips 1977; Svendsen et al. 2002):

$$\frac{\partial}{\partial x}\left(Q_x\right) + \frac{\partial}{\partial y}\left(Q_y\right) = 0; \tag{12}$$

$$\frac{\partial}{\partial x}\left(\frac{Q_x^2}{\bar{h}}\right)+\frac{\partial}{\partial y}\left(\frac{Q_x Q_y}{\bar{h}}\right)+g\bar{h}\frac{\partial\bar{\eta}}{\partial x}+\frac{\tau_{bx}}{\rho}=\tau_{wx}+\frac{\tau_{sx}}{\rho}; \tag{13}$$

$$\frac{\partial}{\partial x}\left(\frac{Q_x Q_y}{\bar{h}}\right)+\frac{\partial}{\partial y}\left(\frac{Q_y^2}{\bar{h}}\right)+g\bar{h}\frac{\partial\bar{\eta}}{\partial x}+\frac{\tau_{by}}{\rho}=\tau_{wy}+\frac{\tau_{sy}}{\rho}; \tag{14}$$

with

$$\tau_{wx}=-\frac{\partial}{\partial x}\left(\frac{S_{xx}}{\rho}-\frac{Q_{wx}^2}{\bar{h}}\right)-\frac{\partial}{\partial y}\left(\frac{S_{xy}}{\rho}-\frac{Q_{wx}Q_{wy}}{\bar{h}}\right); \tag{15}$$

$$\tau_{wy}=-\frac{\partial}{\partial x}\left(\frac{S_{xy}}{\rho}-\frac{Q_{wx}Q_{wy}}{\bar{h}}\right)-\frac{\partial}{\partial y}\left(\frac{S_{yy}}{\rho}-\frac{Q_{wy}^2}{\bar{h}}\right); \tag{16}$$

$$S_{xx}=\left(nE+M_r\right)\cos^2\theta+E\left(n-\frac{1}{2}\right);\ M_r=\rho C q_r; \tag{17}$$

$$S_{xy}=\left(nE+M_r\right)\cos\theta\sin\theta\,;\ S_{yy}=\left(nE+M_r\right)\sin^2\theta+E\left(n-\frac{1}{2}\right) \tag{18}$$

where τ_{bx} and τ_{by} = bottom shear stresses in the x and y directions; τ_{sx} and τ_{sy} = wind stresses on the sea surface in the x and y directions; and S_{xx}, S_{xy} and S_{yy} = radiation stresses including the momentum flux M_r of a roller propagating with the phase speed C. It is noted that the terms $Q_{wx}^2, Q_{wx}Q_{wy}$ and Q_{wy}^2 in Equations 15 and 16 included by Phillips (1977) are of 4-th order in terms of the wave height and are normally neglected. The present circulation model based on Equations 12-18 is a simplified version of SHORECIRC (Svendsen et al. 2002) for irregular waves where SHORECIRC assumes monochromatic waves. The formulas for τ_{bx}, τ_{by}, τ_{sx} and τ_{sy} are presented later in relation to the cross-shore model CSHORE.

A horizontally 2-D model C2SHORE is also being developed (Johnson and Grzegorzewski, 2011). The directional spectral wave model STWAVE (Smith et al. 2001) is used to predict the wave transformation. The wave-induced fluxes Q_{wx} and Q_{wy} and the radiation stresses S_{xx}, S_{xy} and S_{yy} are computed from the predicted directional wave spectra. The roller effects included in Equations 8, 17, and 18 are neglected. The circulation model is based on

Equations 12-16 with the formulas for τ_{bx}, τ_{by}, τ_{sx} and τ_{sy} used in CSHORE. The wave and circulation models are coupled. The wave field is computed to estimate τ_{wx} and τ_{wy} given by Equations 15 and 16 for the circulation model which computes the wave setup and wave-induced currents. An efficient finite difference method is used to solve Equations 12-14 as described in Shi et al. 2007. Johnson and Grzegorzewski (2011) compared C2SHORE results with morphologic change data for Ship Island in Mississippi Sound, with good results.

4 Combined Wave and Current Model in Wet Zone

The cross-shore model CSHORE assumes alongshore uniformity but computes the wave and current fields simultaneously. The depth-integrated continuity equation of water given by Equation 12 requires that the cross-shore volume flux Q_x is constant and equal to the wave overtopping rate q_o at the landward end of the computation domain. Equations 7 and 8 yield:

$$Q_x = \overline{h}\overline{U} + \frac{g\sigma_\eta^2}{C}\cos\theta + q_r\cos\theta = q_o \tag{19}$$

$$Q_y = \overline{h}\overline{V} + \frac{g\sigma_\eta^2}{C}\sin\theta + q_r\sin\theta \tag{20}$$

where $\overline{h}$ = mean water depth; $\overline{U}$ = mean cross-shore velocity; which is negative and offshore because cos θ > 0 if $q_o = 0$ (no wave overtopping); g = gravitational acceleration; σ_η = standard deviation of the free surface elevation η; C = linear wave phase velocity in the mean water depth $\overline{h}$ corresponding to the spectral peak period T_p; and q_r = volume flux of a roller on the front of a breaking wave. If the incident wave angle θ is small, Equation 20 can be approximated by $Q_y \simeq \overline{h}\overline{V}$ for most applications.

For the case of alongshore uniformity, Equation 4 reduces to Snell's law:

$$k\sin\theta = \text{constant} \tag{21}$$

which is used to obtain the wave direction θ.

The constant value is obtained from the values of θ, $\overline{h}$, and T_p specified at the seaward boundary $x = 0$ located outside the surf zone where ω can be approximated by ω_p in Equation 2. Reflected waves are neglected in this model.

The cross-shore and longshore momentum Equations 13 and 14 are simplified as:

$$\frac{d}{dx}\left(S_{xx}+\rho\frac{Q_x^2}{\bar{h}}\right)=-\rho g\bar{h}\frac{d\bar{\eta}}{dx}-\tau_{bx}+\tau_{sx} \tag{22}$$

$$\frac{d}{dx}\left(S_{xy}+\rho\frac{Q_xQ_y}{\bar{h}}\right)=-\tau_{by}+\tau_{sy} \tag{23}$$

where S_{xx} = cross-shore radiation stress; ρ = water density; τ_{bx} = cross-shore bottom stress; τ_{sx} = cross-shore wind stress on the sea surface; S_{xy} = shear component of the radiation stress; τ_{by} = longshore bottom stress; and τ_{sy} = longshore wind stress on the sea surface. The wind shear stresses may not be negligible especially outside surf zones on natural beaches (Lentz et al. 1999). Linear wave theory for progressive waves is used to estimate S_{xx} and S_{xy} as in Equations 17 and 18. For the sake of clarity, the equations are again given as:

$$S_{xx}=\left(nE+M_r\right)\cos^2\theta+E\left(n-\frac{1}{2}\right);S_{xy}=\left(nE+M_r\right)\cos\theta\sin\theta \tag{24}$$

with

$$n=C_g/C\,;E=\rho g\sigma_\eta^2\,;M_r=\rho Cq_r \tag{25}$$

where C_g = linear wave group velocity; E = specific wave energy with the rms wave height defined as H_{rms} = $\sqrt{8}\,\sigma_\eta$; and M_r = momentum flux of a roller propagating with the phase velocity C.

The time-averaged bottom shear stresses in Equations 22 and 23 are written as:

$$\tau_{bx}=\frac{1}{2}\rho f_b\overline{UU_a}\,;\tau_{by}=\frac{1}{2}\rho f_b\overline{VU_a}\,;U_a=\left(U^2+V^2\right)^{0.5} \tag{26}$$

where U = depth-averaged cross-shore velocity; V = depth-averaged longshore velocity; f_b = bottom friction factor; and the overbar indicates time averaging. The bottom friction factor f_b is of the order of 0.015 but should be calibrated using longshore current data because of the sensitivity of longshore currents to f_b. The equivalency of the time and probabilistic averaging is assumed to express τ_{bx} and τ_{by} in terms of the mean and standard deviation of the depth-averaged velocities U and V expressed as:

$$U = \sigma_T F_U \; ; V = \sigma_T F_V \; ; U_a = \sigma_T F_a \; ; F_a = \left(F_U^2 + F_V^2\right)^{0.5} ; \tag{27}$$

with

$$F_U = U_* + r\cos\theta \, ; F_V = V_* + r\sin\theta \, ; U_* = \frac{\overline{U}}{\sigma_T} \, ; V_* = \frac{\overline{V}}{\sigma_T} ; \tag{28}$$

where $\overline{U}$ and $\overline{V}$ = depth-averaged cross-shore and longshore currents; σ_T = standard deviation of the oscillatory (assumed Gaussian) depth-averaged velocity U_T with zero mean; and r = Gaussian variable defined as $r = U_T/\sigma_T$ whose probability density function is given by:

$$f(r) = \frac{1}{\sqrt{2\pi}} \exp\left(-\frac{r^2}{2}\right) \tag{29}$$

Linear progressive wave theory is used locally to express U_T in terms of the oscillatory free surface elevation $\left(\eta - \overline{\eta}\right)$:

$$U_T = \frac{C}{\overline{h}} (\eta - \overline{\eta}) \tag{30}$$

which yields the standard deviation σ_T of the oscillatory velocity U_T:

$$\sigma_T = C\sigma_* \; ; \sigma_* = \sigma_\eta / \overline{h} \tag{31}$$

It is noted that that $U_* = \overline{U} / \sigma_T$ and $V_* = \overline{V} / \sigma_T$ are of the order of unity or less. The standard deviations of U and V are given by:

$$\sigma_U = \sigma_T \cos\theta \, ; \sigma_V = \sigma_T \left|\sin\theta\right| \tag{32}$$

where cos θ > 0 but sin θ can be negative. Substitution of Equation 27 into Equation 26 yields:

$$\tau_{bx} = \frac{1}{2} \rho f_b \sigma_T^2 G_{bx} \; ; \tau_{by} = \frac{1}{2} \rho f_b \sigma_T^2 G_{by} \tag{33}$$

with

$$G_{bx} = \int_{-\infty}^{\infty} F_U F_a f(r)\, dr\,;\, G_{by} = \int_{-\infty}^{\infty} F_V F_a f(r)\, dr \tag{34}$$

which must be integrated numerically.

The wind shear stress in Equations 22 and 23 are expressed as:

$$\tau_{sx} = \rho_a C_D W_{10}^2 \cos\theta_w\,;\, \tau_{sy} = \rho_a C_D W_{10}^2 \sin\theta_w \tag{35}$$

where ρ_a = air density ($\rho_a \simeq 1.225$ kg/m3); C_D = drag coefficient, W_{10} = 10-m wind speed; and θ_w = wind direction defined in Figure 1. The formula by Large and Pond (1981) is used to estimate C_D where C_D = 0.0012 for W_{10} < 11 m/s and C_D = (0.00049 + 0.000065 W_{10}) for $W_{10} \geq$ 11 m/sec. It is noted that the measured values of C_D during tropical cyclones by Powell et al. (2003) indicated no increase of C_D with the increase of W_{10} much above 25 m/sec. In short, available data are insufficient to estimate C_D for extreme wind conditions.

The wave action Equation 5 for the case of alongshore uniformity becomes:

$$\frac{d}{dx}\left[\frac{E}{\omega}\left(C_g \cos\theta + \frac{Q_x}{\bar{h}}\right)\right] = -\frac{D_B + D_f}{\omega} \tag{36}$$

which reduces to the wave energy equation if ω is constant and $Q_x = 0$. In this case, the wave energy equation is given by:

$$\frac{dF_x}{dx} = -D_B - D_f\,;\, F_x = EC_g \cos\theta \tag{37}$$

where F_x = cross-shore energy flux based on linear progressive wave theory; and D_B and D_f = energy dissipation rates due to wave breaking and bottom friction, respectively. The energy dissipation rate D_B, due to wave breaking, in Equation 36 is estimated using the formula by Battjes and Stive (1985), which was modified by Kobayashi et al. (2005) to account for the local bottom slope and to extend the computation to the lower swash zone. The modified formula is expressed as:

$$\begin{gathered} D_B = \frac{\rho g a Q H_B^2}{4T}\,;\, \frac{Q-1}{\ln(Q)} = \left(\frac{H_{rms}}{H_m}\right)^2; \\ H_m = \frac{0.88}{k}\tanh\left(\frac{\gamma k\bar{h}}{0.88}\right);\, a = \frac{2\pi S_b}{3k\bar{h}} \geq 1 \end{gathered} \tag{38}$$

where a = slope effect parameter; Q = fraction of breaking waves; H_B = breaker height used to estimate D_B; T = intrinsic wave period given by $T = 2\pi/\omega$ with ω obtained using Equation 2; $H_{rms} = \sqrt{8}\sigma_\eta$ = local *rms* wave height; H_m = local depth-limited wave height; k = wave number; $\overline{h}$ = mean water depth including wave setup; γ = empirical breaker ratio parameter; and S_b = local bottom slope given by Equation 11. The parameter a is the ratio between the wave length ($2\pi/k$) and the horizontal length ($3\,\overline{h}/S_b$) imposed by the small depth and relatively steep slope where the lower limit of a = 1 corresponds to the formula by Battjes and Stive (1985), who also assumed $H_B = H_m$. The fraction Q is zero for no wave breaking and unity when all waves break. The requirement of $0 \le Q \le 1$ implies $H_{rms} \le H_m$ but H_{rms} can become larger than H_m in very shallow water. When $H_{rms} > H_m$, Q is set to one and H_B equal to H_{rms}. In addition, the upper limit of $\sigma_* = \sigma_\eta/\overline{h}$ from Equation 31 is imposed as $\sigma_* \le 1$ in very shallow water (Kobayashi et al. 1998). The breaker ratio parameter γ in Equation 38 is typically in the range of $\gamma = 0.5 - 1.0$ (Kobayashi et al. 2007a) but should be calibrated to obtain a good agreement with the measured cross-shore variation of σ_η if such data are available. The default value for field applications is $\gamma = 0.5$. An option is provided in CSHORE to estimate γ with the empirical formula developed by Apotsos et al. (2008) using field data.

On the other hand, the energy dissipation rate D_f due to bottom friction in Equation 36 is expressed as:

$$D_f = \frac{1}{2}\rho f_b \overline{U_a^3} \tag{39}$$

Substitution of U_a given in Equation 27 into Equation 39 yields:

$$D_f = \frac{1}{2}\rho f_b \sigma_T^3 G_f \; ; G_f = \int_{-\infty}^{\infty} F_a^3 f(r)\,dr \tag{40}$$

where $f(r)$ is given by Equation 29.

The energy equation for the roller given by Equation 9 reduces to that used by Ruessink et al. (2001) for the case of alongshore uniformity:

$$\frac{d}{dx}\left(\rho C^2 q_r \cos\theta\right) = D_B - D_r \; ; D_r = \rho g \beta_r q_r \tag{41}$$

where the roller dissipation rate D_r is assumed to equal the rate of work to maintain the roller on the wave-front slope β_r which is of the order of 0.1. Use is made of the empirical formula given by Equation 10 proposed by Kobayashi et al. (2005) who included the local bottom slope effect. If the roller is neglected, $q_r = 0$ and Equation 41 yields $D_r = D_B$. The roller effect improves the agreement between computed and observed for the longshore current (Kobayashi et al. 2007a).

Equations 19-41 are the same as those used by Kobayashi et al. (2007a) who assumed $Q_x = q_o = 0$ in Equation 19 and neglected the wind shear stresses in Equations 22 and 23, and used linear shallow-water wave theory with $C = (g\,\bar{h})^{0.5}$ in Equation 30. Substitution of Equation 31 and 32 into Equation 19 yields:

$$\bar{U} = -\frac{g\bar{h}}{C^2}\sigma_U \sigma_* \left(1 + \frac{Cq_r}{g\sigma_\eta^2}\right) + \frac{Q_x}{\bar{h}} \tag{42}$$

The landward-marching computation starting from $x = 0$ outside the surf zone is the same as that of Kobayashi et al. (2007a).

Approximate analytical equations of G_{bx}, G_{by} and G_f given by Equations 34 and 40 are obtained by Kobayashi (2009a) to reduce the computation time and improve the numerical stability. The function F_a given in Equation 27 with Equation 28 is rewritten as:

$$F_a = \left[(r - r_m)^2 + F_m^2\right]^{0.5} \tag{43}$$

with

$$r_m = -(U_* \cos\theta + V_* \sin\theta)\,;\, F_m = V_* \cos\theta - U_* \sin\theta \tag{44}$$

Equation 43 is approximated as:

$$\begin{aligned} F_a &= (r - r_m) + |F_m| \,\text{for}\, r \geq 0; \\ F_a &= -(r - r_m) + |F_m| \,\text{for}\, r < 0 \end{aligned} \tag{45}$$

Substituting Equation 45 into Equations 34 and 40 and integrating the resulting equations analytically, we obtain approximate expressions for G_{bx}, G_{by} and G_f:

$$G_{bx} = \sqrt{\frac{2}{\pi}}\left(U_* - r_m \cos\theta\right) + U_* \left|F_m\right|; \tag{46}$$

$$G_{by} = \sqrt{\frac{2}{\pi}}\left(V_* - r_m \sin\theta\right) + V_* \left|F_m\right|; \tag{47}$$

$$G_f = 2\sqrt{\frac{2}{\pi}} + \left(1 + U_*^2 + V_*^2\right)\left|F_m\right| + \sqrt{\frac{2}{\pi}}\left(U_*^2 + V_*^2 + 2r_m^2\right) \tag{48}$$

which depends on sinθ (cos θ > 0 assumed), r_m and F_m where Equation 44 yields $U_* = -(r_m \cos\theta + F_m \sin\theta)$ and $V_* = (F_m \cos\theta - r_m \sin\theta)$.

For the case of normally incident waves with no wind, sin θ = 0 and $V_* = 0$. Equations 46-48 yield $G_{bx} = 1.6\ U_*$, $G_{by} = 0$, and $G_f = (1.6 + 2.4\ U_*^2)$. Equation 23 requires $\tau_{by} = 0$ for $Q_x = 0$ (no wave overtopping) and Equation 33 yields $G_{by} = 0$. As a result, Equation 47 is exact. For sin θ = 0 and $V_* = 0$, G_{bx} and G_f, given by Equations 34 and 40, can be integrated analytically as presented by Kobayashi et al. (2007b) who approximated the analytical expressions of G_{bx} and G_f as $G_{bx} = 1.64\ U_*$ and $G_f = (1.6 + 2.6\ U_*^2)$. These approximate equations are very similar to the above equations obtained from Equations 46 and 48. For the case of $|\sin\theta| \ll 1$ and $|U_*| \ll |V_*|$, Equation 47 can be approximated as $G_{by} = V_*(0.8 + |V_*|)$. Using field data and probabilistic analyses, Feddersen et al. (2000) obtained $G_{by} = V_*(1.16^2 + V_*^2)^{0.5}$. The difference between these two approximate equations for G_{by} is less than 20 percent for $|V_*| < 1.4$, which is typically satisfied.

Kobayashi et al. (2009a) compared the approximate values of G_{bx}, G_{by} and G_f given by Equations 46-48 with the exact values of G_{bx}, G_{by} and G_f obtained by the numerical integration of Equations 34 and 40. The percentage error was typically about 10 percent and always less than 35 percent for the ranges of $|\sin\theta| < 1$, $|r_m| < 1$ and $|F_m| < 1$. This error is probably less than the uncertainty of the bottom friction factor f_b.

5 Sediment Transport Model in Wet Zone

The combined wave and current model CSHORE predicts the spatial variations of the hydrodynamic variables used in the following sediment transport model for given beach profile, water level and seaward wave conditions at $x = 0$. The bottom sediment is assumed to be uniform and characterized by d_{50} = median diameter; w_f = sediment fall velocity; and s = sediment specific gravity. The sediment transport model developed for CSHORE is modified slightly for the horizontally 2-D model C2SHORE.

The spatial variation of the degree of sediment movement is estimated using the critical Shields parameter ψ_c (Madsen and Grant 1976) which is taken as $\psi_c = 0.05$. The instantaneous bottom shear stress τ'_b is assumed to be given by $\tau'_b = 0.5\,\rho f_b U^2_a$ with U_a given in Equation 26. The sediment movement is assumed to occur when τ'_b exceeds the critical shear stress, $\rho g(s-1)d_{50}\,\psi_c$. The probability P_b of sediment movement can be shown to be the same as the probability of $(r-r_m)^2 > F_b^2 = (R_b^2 - F_m^2)$ where $R_b = [2\,g\,(s-1)\,d_{50}\,\psi_c f_b^{-1}]^{0.5}/\sigma_T$ and r_m and F_m are defined in Equation 44. For the Gaussian variable r given by Equation 29, P_b is given by:

$$P_b = \frac{1}{2} erfc\left(\frac{F_b - r_m}{\sqrt{2}}\right) + \frac{1}{2} erfc\left(\frac{F_b + r_m}{\sqrt{2}}\right) \text{for } F_b^2 > 0 \qquad (49)$$

and $P_b = 1$ for $F_b^2 \le 0$ where *erfc* is the complementary error function. The value of P_b computed from $x = 0$ located outside the surf zone increases landward and fluctuates in the surf and swash zones, depending on the presence of a bar or a terrace that increases the local fluid velocity.

The spatial variation of the degree of sediment suspension is estimated using the experimental finding of Kobayashi et al. (2005) who showed that the turbulent velocities measured in the vicinity of the bottom were related to the energy dissipation rate due to bottom friction. Representing the magnitude of the instantaneous turbulent velocity by $(D'_f/\rho)^{1/3}$ with $D'_f = 0.5\,\rho f_b\,U_a^3$ in light of Equation 39, the probability P_s of sediment suspension is assumed to be the same as the probability of $(D'_f/\rho)^{1/3}$ exceeding the sediment fall velocity w_f. The probability P_s is then equal to the probability of $F_S^2 = (R_S^2 - F_m^2)$ with $R_s = [(2/f_b)^{1/3}\,w_f/\sigma_T]$ and is given by:

$$P_s = \frac{1}{2} erfc\left(\frac{F_s - r_m}{\sqrt{2}}\right) + \frac{1}{2} erfc\left(\frac{F_s + r_m}{\sqrt{2}}\right) for\ F_s^2 > 0 \qquad (50)$$

and $P_s = 1$ for $F_s^2 \leq 0$. If $P_s > P_b$, use is made of $P_s = P_b$ assuming that sediment suspension occurs only when sediment movement occurs. Fine sands on beaches tend to be suspended once their movement is initiated.

The suspended sediment volume V_s per unit horizontal bottom area is estimated by modifying the sediment suspension model by Kobayashi and Johnson (2001):

$$V_s = P_s \frac{e_B D_r + e_f D_f}{\rho g(s-1) w_f}\left(1+S_{bx}^2\right)^{0.5}\left(1+S_{by}^2\right)^{0.5} ; S_{bx} = \frac{\partial z_b}{\partial x} ; S_{by} = \frac{\partial z_b}{\partial y} \qquad (51)$$

where S_{bx} = cross-shore bottom slope; S_{by} = longshore bottom slope; and e_B and e_f = suspension efficiencies for the energy dissipation rates D_r and D_f due to wave breaking and bottom friction, respectively. Use is made of $e_B = 0.005$ and $e_f = 0.01$ as typical values in the computation of berm and dune erosion but the value of e_B is uncertain and should be calibrated if V_s is measured (Kobayashi et al. 2007a). The sediment suspension probability P_s is added to Equation 51 to ensure $V_s = 0$ if $P_s = 0$. The term involving S_{bx} and S_{by} is the actual bottom area per unit horizontal bottom area and essentially unity except for very steep slopes. For the case of alongshore uniformity, $S_{by} = 0$. The cross-shore and longshore suspended sediment transport rates q_{sx} and q_{sy} are expressed as:

$$q_{sx} = a_x \bar{U} V_s ; q_{sy} = \bar{V} V_s ; a_x = \left[a + \left(S_{bx} / \tan\varphi\right)^{0.5}\right] \geq a \qquad (52)$$

where a = empirical suspended load parameter and ϕ = angle of internal friction of the sediment with $\tan\phi = 0.63$ for sand (Bailard 1981). The parameter a accounts for the onshore suspended sediment transport due to the positive correlation between the time-varying cross-shore velocity and suspended sediment concentration. The value of a increases to unity as the positive correlation decreases to zero. For the three small-scale equilibrium profile tests conducted by Kobayashi et al. (2005), a was of the order of 0.2. The effect of the cross-shore bottom slope on a_x was included by Kobayashi et al. (2009b) to increase berm and dune erosion. For $S_{bx} \leq 0$, a_x = a. The cross-shore suspended sediment transport rate q_{sx} is negative (offshore) because the return (undertow) current $\bar{U}$ is negative (offshore). On the other hand, the longshore suspended sediment transport rate q_{sy} in Equation 52 neglects the correlation between the time-varying longshore velocity and suspended sediment concentration, which appears to be very small if the longshore current $\overline{V}$ is sufficiently large. Payo et al. (2009) verified Equation 52 using velocities and sand concentrations measured along 20 transects at the Field Research Facility (FRF) at Duck, North Carolina during a storm in 1997.

The formulas for the cross-shore and longshore bedload transport rates q_{bx} and q_{by} are devised somewhat intuitively because bedload in the surf zone has never been measured. The time-averaged rates q_{bx} and q_{by} are tentatively expressed as:

$$q_{bx} = B\overline{\left(U^2+V^2\right)U}\ ; q_{by} = B\overline{\left(U^2+V^2\right)V} \tag{53}$$

where B = empirical parameter. Equation 53 may be regarded as a quasi-steady application of the formula of Meyer-Peter and Mueller (e.g., Ribberink 1998). Substitution of U and V given in Equation 27 with Equations 28 and 29 into Equation 53 yields:

$$q_{bx} = B\sigma_T^3\left(b_* + U_*V_*^2 + 2F_m\sin\theta\right) \tag{54}$$

$$q_{by} = B\sigma_T^3\left[V_*\left(1+U_*^2+V_*^2\right) - 2r_m\sin\theta\right] \tag{55}$$

where $b_* = \left(3U_* + U_*^3\right)$ and F_m and r_m are defined in Equation 44.

Equation 54 and 55 yield $q_{bx} = b_*B\sigma_T^3$ and q_{by} = 0 for normally incident waves with $\sin\theta = 0$ and $V_* = 0$. The expressions of B and b_* are obtained by requiring that $q_{bx} = b_*B\sigma_T^3$ reduces to the onshore bedload formula proposed by Kobayashi et al. (2008a) for normally incident waves, which synthesized existing data. The proposed formulas are written as:

$$q_{bx} = \frac{bP_b}{g(s-1)}\sigma_T^3\left(1+U_*V_*^2+2F_m\sin\theta\right)G_s\left(S_{bx}\right) \tag{56}$$

$$q_{by} = \frac{bP_b}{g(s-1)}\sigma_T^3\left[V_*\left(1+U_*^2+V_*^2\right)-2r_m\sin\theta\right]G_s\left(S_{by}\right) \tag{57}$$

where b = empirical bedload parameter; and G_s = bottom slope function. The sediment movement probability P_b given in Equation 49 accounts for the initiation of sediment movement. It is noted that b_* = 1 in Equation 56 to compensate for the limitations of Equation 53 and the Gaussian distribution of the horizontal velocity used in Equations 28 and 29, as discussed by Kobayashi et al. (2008a). They calibrated b = 0.002 using the 20 water tunnel tests of Ribberink and Al-Salem (1994), the four large-scale wave flume tests of Dohmen-Janssen and Hanes (2002), and the 24 sheet flow tests by Dohmen-Janssen et al. (2002). Furthermore, this simple bedload formula is consistent with the sheet flow model for onshore bar migration by Trowbridge and Young (1989) and the energetics-based bedload formula for steady flow by Bagnold (1966) if the steady flow formula is applied in the time-averaged manner. The onshore bedload transport predicted by Equation 56 is consistent with the field observations of onshore ripple migration by Becker et al. (2007) and Masselink et al. (2007). The offshore suspended sediment transport predicted by Equation 52 is consistent with the field measurement during a storm by Madsen et al. (1994). The condition of $\left(q_{bx}+q_{sx}\right)=0$ for an equilibrium profile along with additional assumptions can be shown to yield the equilibrium profile popularized by Dean (1991).

The bottom slope function $G_s(S_{bx})$ was introduced by Kobayashi et al. (2008a) to account for the effect of the steep cross-shore slope S_{bx} on the bedload transport rate and is expressed as:

$$G_s\left(S_{bx}\right)=\tan\varphi/\left(\tan\varphi+S_{bx}\right)\text{for} \quad -\tan\varphi<S_{bx}<0 \tag{58}$$

$$G_s\left(S_{bx}\right)=\left(\tan\varphi-2S_{bx}\right)/\left(\tan\varphi-S_{bx}\right)\text{for} \quad o<S_{bx}<\tan\varphi \tag{59}$$

where G_s = 1 for S_{bx} = 0. Equation 58 corresponds to the functional form of G_s used by Bagnold (1966) for steady stream flow on a downward slope with S_{bx} < 0 where the downward slope increases q_{bx}. Equation 59 ensures that G_s approaches negative infinity as the upward slope S_{bx} approaches tan ϕ. Equations 58 and 59 reduce to $G_s = (1 - S_{bx}/\tan\phi)$ for $|S_{bx}| \ll \tan\phi$. Equation 56 with G_s given by Equations 58 and 59 implies that the bedload transport rate q_{bx} is positive (onshore) for $S_{bx} < (\tan\phi)/2$ and negative (offshore) for $S_{bx} > (\tan\phi)/2$. Use is made of $|G_s| < G_m = 10$ to avoid an infinite value in the computation. The computed profile change is not very sensitive to the assumed value of G_m because the beach profile changes in such a way to reduce a very steep slope except in the region of scarping (e.g., Seymour et al. 2005). The effect of the longshore bottom slope S_{by} is included in Equation 57 using the same bottom slope function $G_s(S_{by})$ but has never been validated for lack of suitable data.

The landward marching computation of the present time-averaged model ends at the cross-shore location $x = x_m$ where the mean water depth $\bar{h}$ is less than 1 cm. No reliable data exists for suspended sand and bedload transport rates in the zone which is wet and dry intermittently. Consequently, the following simple procedure was proposed by Kobayashi et al. (2008a) to deal with the zone with a bottom slope $S_{bx} > \tan \phi$. The cross-shore total sediment transport rate $q_x = (q_{sx} + q_{bx})$ at $x = x_m$ is denoted by q_{xm}. If q_{xm} is negative (offshore), q_x is extrapolated linearly to estimate q_x on the scarped face with $S_{bx} > \tan \phi$ such that:

$$q_x = q_{xm}\left(x_e - x\right) / \left(x_e - x_m\right) \; for \; x_m < x < x_e \tag{60}$$

where x_e = landward limit of the scarping zone with $S_{bx} > \tan \phi$. The extrapolated q_x is in the range of $q_{xm} \leq q_x \leq 0$ and the scarping zone is eroded due to the offshore sediment transport. This simple procedure is effective for a high and wide dune, that is typical in the Netherlands (e.g., van Gent et al. 2006), but does not allow onshore sediment transport due to overwash. As a result, no wave overtopping has been allowed so far and $q_o = 0$ in Equation 19.

The beach profile change is computed using the continuity equation of bottom sediment:

$$\left(1 - n_p\right)\frac{\partial z_b}{\partial t} + \frac{\partial q_x}{\partial x} + \frac{\partial q_y}{\partial y} = 0 \tag{61}$$

where n_p = porosity of the bottom sediment which is normally taken as $n_p = 0.4$; t = slow morphological time for the change of the bottom elevation z_b; and $q_y = (q_{sy} + q_{by})$ = longshore total sediment transport rate. For the case of alongshore uniformity, the third term in Equation 61 is zero. Equation 61 is solved using an explicit Lax-Wendroff numerical scheme (e.g., Nairn and Southgate 1993) to obtain the bottom elevation at the next time level. This computation procedure is repeated starting from the initial bottom profile until the end of a profile evolution test.

6 Permeable Layer Model in Wet Zone

The combined wave and current model CSHORE is extended to allow the presence of a permeable layer in the computation domain. Figure 2 shows an example of irregular wave overtopping of a permeable slope where x = onshore coordinate: z = vertical coordinate, $\overline{\eta}$ = mean free surface elevation above SWL; Mean Water Level (MWL) is the SWL + $\overline{\eta}$; S = storm tide above $z = 0$; z_b = bottom elevation; $\bar{h}$ = mean water depth; U = instantneous depth-averaged cross-shore velocity above the bottom; z_p = elevation of the lower boundary of the permeable layer; $h_p = (z_b - z_p)$ = vertical thickness of the permeable layer; and U_p = instantaneous cross-shore discharge velocity inside the permeable layer. The cross-shore profiles of $z_b(x)$ and $z_p(x)$ are specified as input where $h_p = 0$ in the zone of no permeable layer. The lower boundary located at $z = z_p$ is assumed to be impermeable for simplicity. Kobayashi et al. (2007b) developed a permeable layer model in the wet zone for normally incident waves. This model is extended to obliquely incident waves in the following but the extended model has not yet been verified.

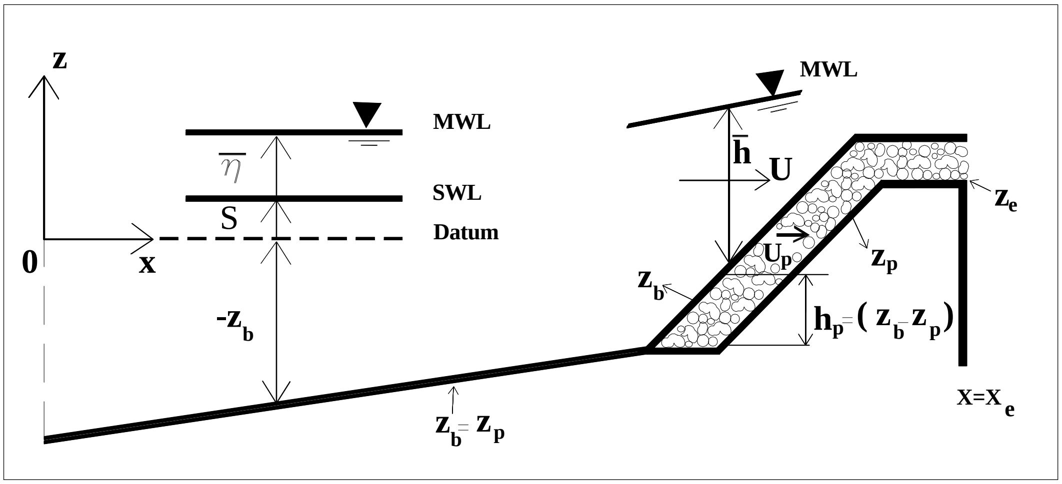

Figure 2. Definition sketch of permeable layer model.

The time-dependent model for the flow over a permeable layer in shallow water developed by Kobayashi and Wurjanto (1990) and Wurjanto and Kobayashi (1993) is time-averaged and simplified to account for the permeable layer in the cross-shore model CSHORE. The vertically-integrated continuity Equation 19 is modified as:

$$Q_x = \bar{h}\bar{U} + \frac{g\sigma_\eta^2}{C}\cos\theta + q_r\cos\theta\,; Q_x + h_p\overline{U_p} = q_o \tag{62}$$

where $\overline{U_p}$ = time-averaged cross-shore discharge velocity; $\left(h_p\overline{U_p}\right)$ = water flux inside the permeable layer with its vertical thickness h_p; and q_o = combined wave overtopping rate above and through the permeable layer. The cross-shore and longshore momentum Equations 22 and 23 are assumed to remain the same, neglecting the momentum fluxes into and out of the permeable layer where the bottom friction factor f_b for τ_{bx} and τ_{by} given by Equation 33 includes the effect of the surface roughness of the permeable layer and was calibrated in the range of f_b = 0.01 – 0.05 (Kobayashi et al. 2007b). For the case of alongshore uniformity and negligible momentum fluxes into and out of the permeable layer, the time-averaged longshore discharge velocity $\overline{V_p}$ is assumed to be zero because of no, or negligible, driving force to cause the longshore discharge inside the permeable layer. It is noted that the assumption of $\overline{V_p} = 0$ cannot be validated at present for lack of suitable data.

On the other hand, the wave action Equation 36 is modified as:

$$\frac{d}{dx}\left[\frac{E}{\omega}\left(C_g\cos\theta + \frac{Q_x}{\bar{h}}\right)\right] = -\frac{D_B + D_f + D_P}{\omega} \tag{63}$$

where D_p = energy dissipation rate due to flow resistance in the permeable layer, assuming that the energy influx into the permeable layer equals the dissipation rate D_p per unit horizontal area. The dissipation rate D_p is expressed as (Wurjanto and Kobayashi 1993):

$$D_p = \rho h_p\left[\alpha_p\left(\overline{U_p^2 + V_p^2}\right) + \beta_p\left(\overline{U_p^2 + V_p^2}\right)^{1.5}\right] \tag{64}$$

where α_p and β_p = laminar and turbulent flow resistance coefficients, respectively, and V_p = instantaneous longshore discharge velocity. Kobayashi et al. (2007b) modified the formulas for α_p and β_p proposed by van Gent (1995) as follows:

$$\alpha_p = \alpha_0 \frac{\left(1-n_p\right)^2}{n_p^2} \frac{\upsilon}{D_{n50}^2}; \beta_p = \beta_1 + \frac{\beta_2}{\sigma_p} \quad (65)$$

with

$$\beta_1 = \frac{\beta_0\left(1-n_p\right)}{n_p^3 D_{n50}}; \beta_2 = \frac{7.5\beta_0\left(1-n_p\right)}{\sqrt{2}n_p^2 T} \quad (66)$$

where α_0 and β_0 = empirical parameters calibrated as α_0 = 1,000 and β_0 = 5; n_p = porosity of the permeable layer consisting of stone; ν = kinematic viscosity of the fluid; D_{n50} = nominal stone diameter defined as $D_{n50} = \left(M_{50}/\rho_s\right)^{1/3}$ with M_{50} = median stone mass and ρ_s = stone density; σ_p = standard deviation of the instantaneous discharge velocity; and T = intrinsic wave period used in Equation 38.

The discharge velocities U_p and V_p in Equation 64 are assumed to be expressed as:

$$U_p = \overline{U_p} + r\sigma_p \cos\theta; V_p = r\sigma_p \sin\theta; \quad (67)$$

where r = Gaussian variable whose probability density function is given by Equation 29; and θ = incident wave angle for the oscillatory velocity direction above and inside the permeable layer. The assumptions of the Gaussian velocity distribution and $\overline{V_p} = 0$ allow one to represent the discharge velocities by the mean cross-shore discharge velocity $\overline{U_p}$ and the standard deviation σ_p. Substitution of Equation 67 into Equation 64 yields:

$$D_p = \rho h_p \left\{\alpha_p\left(\overline{U_p}^2 + \sigma_p^2\right) + \sqrt{\frac{2}{\pi}}\left(\beta_2 + \beta_1\sigma_p\right)\left[2\sigma_p^2 + \overline{U_p}^2\left(1+2\cos^2\theta\right)\right]\right\} \quad (68)$$

where use is made of the approximate expression of G_f given by Equation 48 and the assumption of $\left|\overline{U_p}\sin\theta\right| \ll \sigma_p$ to simplify Equation 68. Approximate equations for $\overline{U_p}$ and σ_p are derived in the following.

Neglecting the inertia terms in the cross-shore momentum equation for the flow inside the permeable layer (Kobayashi and Wurjanto 1990), the local force balance between the cross-shore hydrostatic pressure gradient and flow resistance is assumed to be:

$$g\frac{\partial\eta}{\partial x}+\alpha_p U_p+\beta_p U_p\left(U_p^2+V_p^2\right)^{0.5}=0 \tag{69}$$

Equation 69 is averaged probabilistically using Equation 67. For the case of alongshore uniformity, the averaged force balance equation is expressed as:

$$g\frac{d\overline{\eta}}{dx}+\overline{U_p}\left[\alpha_p+\sqrt{\frac{2}{\pi}}\left(\beta_2+\beta_1\sigma_p\right)\left(1+\cos^2\theta\right)\right]=0 \tag{70}$$

where use is made of the approximate expression of G_{bx} given by Equation 46 and the assumption of $\left|\overline{U_p}\sin\theta\right|\ll\sigma_p$ to simplify Equation 70. It is noted that the local force balance between the longshore hydrostatic pressure gradient and flow resistance yields $\overline{V_p}=0$ for the case of alongshore uniformity where $\overline{\eta}$ is independent of the longshore coordinate y. To derive an equation for σ_p, the approximate analytical method used by Kobayashi et al. (2007b) is adopted. Equation 69 is linearized as:

$$g\frac{\partial\eta}{\partial x}+\left(\alpha_p+1.9\beta_p\sigma_p\right)U_p=0 \tag{71}$$

which is used to obtain:

$$\left[\alpha_p+1.9\left(\beta_2+\beta_1\sigma_p\right)\right]\sigma_p=gk\overline{h}\sigma_*\;;\sigma_*=\sigma_\eta/\overline{h} \tag{72}$$

where the wave number k is computed using Equation 2. Equation 72 can be solved analytically to obtain σ_p for known $k\overline{h}\sigma_*$. After σ_p is obtained, Equation 70 is used to calculate $\overline{U_p}$ for known $d\overline{\eta}/dx$. The energy dissipation rate D_p is computed using Equation 68. Equation 62 for assumed q_o is used to obtain Q_x and $\overline{U}$ where $\overline{U}$ is expressed by Equation 42.

7 Irregular Wave Runup and Overtopping

The time-averaged model CSHORE does not predict the shoreline oscillations on beaches and coastal structures unlike time-dependent models (e.g., Wurjanto and Kobayashi 1993). To compensate for this shortcoming of CSHORE, Kobayashi et al. (2008b) proposed a probabilistic model for irregular wave runup as illustrated in Figure 3. The shoreline oscillation is assumed to be measured by a runup wire (RW in Figure 3) placed parallel to the bottom elevation z_b at a vertical height of δ_r. The runup wire measures the instantaneous elevation η_r above SWL of the intersection between the wire and the free surface elevation. The mean $\overline{\eta}_r$ and standard deviation σ_r of η_r are estimated using the computed cross-shore variations of $\overline{\eta}(x)$ and $\sigma_\eta(x)$ of the free surface elevation η above SWL. The probabilities of η_r exceeding $\left(\overline{\eta}_r+\sigma_r\right)$, $\overline{\eta}_r$, and $\left(\overline{\eta}_r-\sigma_r\right)$ are assumed to be the same as the probabilities of η exceeding $\left(\overline{\eta}+\sigma_\eta\right)$, $\overline{\eta}$, and $\left(\overline{\eta}-\sigma_\eta\right)$, respectively. The elevations of Z_1, Z_2, and Z_3 of the intersections of $\left(\overline{\eta}+\sigma_\eta\right)$, $\overline{\eta}$, and $\left(\overline{\eta}-\sigma_\eta\right)$ with the runup wire are obtained for the given wire elevation (z_b + δ_r). The obtained elevations are assumed to correspond to $Z_1=\left[\overline{\eta}_r+\sigma_r\right]$, $Z_2=\overline{\eta}_r$, and $Z_3=\left(\overline{\eta}_r-\sigma_r\right)$. The mean and standard deviation of η_r are estimated as:

$$\overline{\eta}_r=\left(Z_1+Z_2+Z_3\right)/3\,;\sigma_r=\left(Z_1-Z_3\right)/2 \tag{73}$$

In CSHORE, $\overline{\eta}$ and σ_η are replaced by $\left(P_w\overline{h}+z_b\right)$ and $P_w\sigma_\eta$ for the computation of Z_1, Z_2 and Z_3 to account for the transition from the wet zone (P_w = 1) to the wet and dry zone (P_w < 1) where P_w is the wet probability explained in Chapter 8.

The runup height R is defined as the crest height above SWL of the temporal variation of η_r. The probability distribution of linear wave crests above the mean water level (MWL) is normally given by the Rayleigh distribution. For the case of no wave overtopping, the runup height $\left(R-\overline{\eta}_r\right)$ above the mean elevation $\overline{\eta}_r$ is assumed to be given by the Rayleigh distribution (Kobayashi et al. 2008b). The exceedance probability $P(R)$ of the runup height R above SWL is given as:

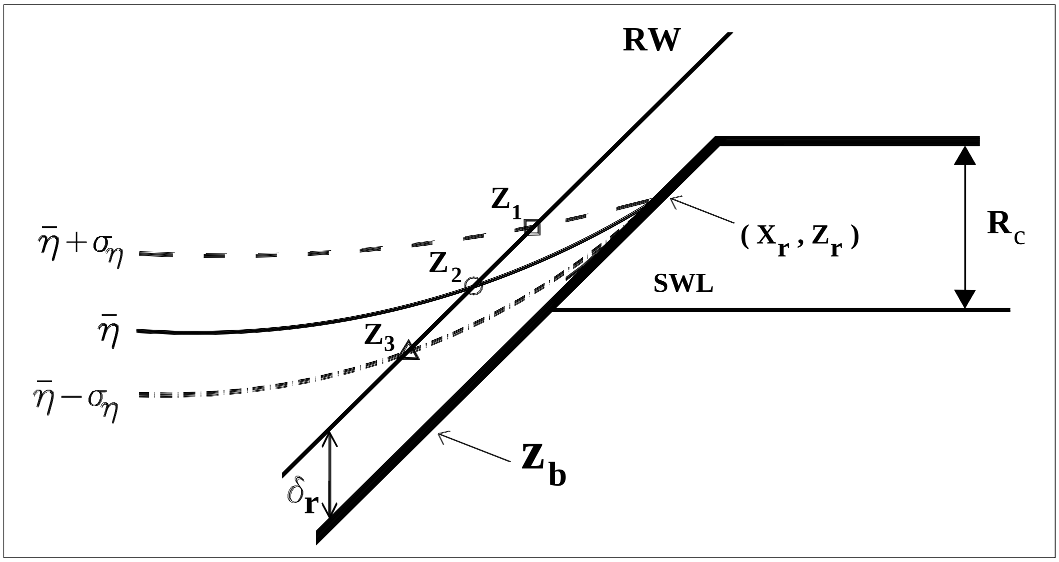

Figure 3. Definition sketch for probabilistic model for irregular wave runup.

$$P(R) = \exp\left[-2\left(\frac{R-\bar{\eta}_r}{R_{1/3}-\eta_r}\right)\right] \qquad (74)$$

where $R_{1/3}$ = significant runup height which is defined as the average of 1/3 highest values of R.

The mean $\bar{\eta}_r$ related to wave setup is normally neglected in Equation 74 for the prediction of irregular wave runup on steep coastal structures. For the 1/5 and 1/2 permeable slope experiments conducted by Kobayashi et al. (2008b), $R_{1/3}$ was estimated as:

$$R_{1/3} = \bar{\eta}_r + (2+\tan\theta)\sigma_r \qquad (75)$$

where θ = seaward slope angle from the horizontal and tan θ = 0.2 and 0.5 in the experiments. It is cautioned that Equations 74 and 75 have been calibrated only for permeable slopes with tan θ = 0.2 - 0.5 in the absence of wave overtopping.

Wave overtopping occurs when the individual runup height R above SWL exceeds the structure crest height R_c above SWL as depicted in Figure 3. Wave overtopping reduces R exceeding R_c because of overtopping flow on the crest. Kobayashi and de los Santos (2007) adopted the following Weibull distribution:

$$P(R) = \exp\left[-2\left(\frac{R-\bar{\eta}_r}{R_{1/3}-\bar{\eta}_r}\right)^{K}\right] \tag{76}$$

with

$$\kappa = 2 + 0.5R_*^{-3}\ ;\ R_* = \left(R_c - \bar{\eta}_r\right)/\left(R_{1/3}-\bar{\eta}_r\right) \tag{77}$$

where κ = shape parameter with κ = 2 for the Rayleigh distribution given by Equation 74; and R_* = normalized crest height related to the wave overtopping probability P_o. The probability P_o of R exceeding R_c in Equation 76 is given by:

$$P_o = \exp\left(-2R_*^{\kappa}\right) \tag{78}$$

It should be noted that the empirical formula for κ given by Equation 77 has been calibrated using only 22 permeable slope tests so far. The formula for $R_{1/3}$ given by Equation 75 has been found to be applicable to these 22 tests. The runup height $R_{2\%}$ for the two percent exceedance probability obtained using Equation 76 is given by

$$R_{2\%} = \bar{\eta}_r + (1.40)^{2/\kappa}\left(R_{1/3}-\bar{\eta}_r\right) \tag{79}$$

where the shape parameter κ given by Equation 77 accounts for the decrease of $R_{2\%}$ due to the decrease of the normalized crest height R_* and the resulting increase of the wave overtopping probability P_o given by Equation 78.

The wave overtopping rate q_o in Equation 19 for an impermeable slope and in Equation 62 for a permeable slope needs to be estimated if wave overtopping occurs at the landward end of the computation domain located at $x = x_e$ in Figure 2. For permeable slopes, Kobayashi and de los Santos (2007) proposed the following empirical formula:

$$q_o = a_*\left(P_o\right)^{b_*} q_{SWL} + q_s \tag{80}$$

with

$$q_{SWL} = \frac{g\sigma_\eta^2}{C}\cos\theta \quad \text{at} \quad x = x_{SWL} \tag{81}$$

where a_* and b_* = empirical parameters; P_o = wave overtopping probability; q_{SWL} = wave-induced onshore flux in Equation 62 evaluated at the still water shoreline located at $x = x_{SWL}$ with $z_b(x_{SWL}) = S$ in Figure 2; and q_s = seepage rate through the permeable layer. It is noted that the roller effect has been neglected for permeable slopes because of its negligible effect and $q_r = 0$ in Equation 62. The empirical parameters a_* and b_* are assumed to depend on the horizontal width L_h of the permeable surface above the upper limit of wave setup located at (x_r, z_r) in Figure 3, where the infiltration of overtopped water is assumed to be vertical due to gravity. The empirical formulas based on 32 tests were expressed as:

$$a_* \exp(-0.1L_*) ; b_* = 1 + 0.1L_* ; L_* = L_h / D_{n50} \qquad (82)$$

where L_* = infiltration width normalized by the nominal stone diameter D_{n50}, crudely representing the horizontal number of stones above the maximum wave setup.

On the other hand, Kobayashi and de los Santos (2007) estimated the seepage rate q_s for normally incident waves as:

$$q_s = 0.2(z_r - z_e)^{1.5} \left[\frac{g}{(x_e - x_r)\beta_1} \right]^{0.5} \quad \text{for} \quad z_r > z_e \qquad (83)$$

where z_e = elevation of the landward end of the impermeable surface z_p as shown in Figure 2; and β_1 = turbulent flow resistance coefficient defined in Equation 66. To derive Equation 83, the seepage flow was assumed to be driven by the horizontal pressure gradient from the point (x_r, z_r) to the point (x_e, z_e). Consequently, $q_s = 0$ if $z_r < z_e$. If $x_r = x_e$, the permeable layer is always wet and $q_s = h_p \overline{U}_P$ at $x = x_e$ where the water flux $h_p \overline{U}_P$ in the permeable layer is included in the continuity equation given in Equation 62.

Kobayashi et al. (2007c) examined the transition from little wave overtopping to excessive wave overtopping and overflow on an impermeable smooth levee with a seaward slope of 1/5 in wave-flume experiments consisting of 107 tests. For the impermeable slope, Equations 75 and 77 used for the permeable slope had to be modified as:

$$R_{1/3} = \overline{\eta}_r + 4\sigma_r \ ; \kappa = 2 \tag{84}$$

The wave overtopping probability P_o is given by Equation 78 with κ = 2 where the normalized crest height R_* above SWL is defined in Equation 77 with $R_{1/3}$ given by Equation 84. It is noted P_o = 1 if $R_* < 0$. For the impermeable slope, the seepage rate $q_s = 0$ in Equation 80 and Equation 82 yields a_* = 1 and b_* = 1 for $L_h = 0$. As a result, the wave overtopping rate q_o is given by $q_o = P_o q_{SWL}$. For the case of combined wave overtopping and overflow, Kobayashi et al. (2007c) expressed the combined rate q_o as:

$$q_o = P_o q_{SWL} + H_{SWL}\sqrt{gH_{SWL}} \quad \text{for} \quad H_{SWL} > 0 \tag{85}$$

with

$$H_{SWL} = \overline{\eta} - R_c \quad \text{at} \quad x = x_{SWL} \tag{86}$$

where H_{SWL} = head for the overflow; $\overline{\eta}$ = MWL above SWL; and R_c = levee crest height above SWL. If $R_c < 0$, the levee crest is below SWL and x_{SWL} is chosen at the seaward edge of the levee crest. For $H_{SWL} > 0$, H_{SWL} is the MWL above the levee crest and $\sqrt{gH_{SWL}}$ may be regarded as the water velocity on the crest.

In summary, Equations 73-86 are essentially empirical and are used in the cross-shore model CSHORE to predict irregular wave runup, overtopping, seepage, and overflow on permeable and impermeable structures. These equations have not been verified for irregular wave overtopping and overflow of dunes. These equations do not predict the spatial variations of the hydrodynamic variables required for the sediment model and the computation of dune profile evolution. Consequently, a hydrodynamic model for the intermittently wet zone landward of the maximum wave setup has been developed in Chapter 8. The formula for P_o given by Equation 78 and the formulas for q_o given by Equations 80 and 85 are removed and replaced by new formulas for P_o and q_o based on the hydrodynamic model for the wet and dry zone. The values of $\overline{\eta}$, σ_r, $R_{1/3}$ and $R_{2\%}$ are computed in CSHORE because this hydrodynamic model does not predict individual wave runup events.

8 Model for Impermeable Wet and Dry Zone

Time-dependent numerical models such as the nonlinear shallow-water wave model by Kobayashi et al. (1989) can predict the water depth and horizontal velocity in the intermittently wet and dry (swash) zone on beaches and inclined structures. However, the time-dependent hydrodynamic computation requires considerable computation time and may not lead to an accurate prediction of dune profile evolution in view of the earlier attempt by Tega and Kobayashi (1996). A time-averaged probabilistic model is developed here to predict the cross-shore variations of the wet probability and the mean and standard deviation of the water depth and cross-shore velocity in the swash. The developed model is very efficient computationally and calibrated using a large number of data sets. The present model is limited to normally incident waves and alongshore uniformity. A sediment transport model in the swash zone is formulated by modifying the sediment transport model in the wet zone.

Water depth and velocity

Van Gent (2002a) and Schüttrumpf and Oumeraci (2005) analyzed the water depth and velocity of waves overtopping of dikes. Kobayashi et al. (2010a) expanded their analyses for the prediction of wave overtopping and overwash as presented in the following.

For normally incident waves on impermeable beaches and inclined structures of alongshore uniformity, the time-averaged cross-shore continuity and momentum equations derived from the nonlinear shallow-water wave equations are expressed as:

$$\overline{hU} = q_o \tag{87}$$

$$\frac{d}{dx}\left(\overline{hU^2} + \frac{g}{2}\overline{h^2}\right) = -gS_{bx}\bar{h} - \frac{1}{2}f_b\overline{|U|U};S_{bx} = \frac{dz_b}{dx} \tag{88}$$

where h and U = instantaneous water depth and cross-shore velocity, respectively; q_o = combined wave overtopping and overflow rate; g = gravitational acceleration; S_{bx} = cross-shore bottom slope; and f_b = bottom friction factor, which is allowed to vary spatially. The wave energy equation corresponding to Equations 87 and 88 was given by Kobayashi and Wurjanto (1992), who used it to estimate the rate of wave energy dissipation due to wave breaking. The wave energy equation is not used in CSHORE because no formula is available to estimate the time-averaged energy dissipation rate in the wet and dry zone.

The instantaneous water depth *h* depends on the cross-shore coordinate *x*. The water depth *h* at given *x* is described probabilistically rather than in the time domain. Kobayashi et al. (1998) analyzed the probability distributions of the free surface elevations measured in the shoaling, surf and swash zones. The measured probability distributions were shown to be in agreement with the exponential gamma distribution which reduces to the Gaussian distribution and the exponential distribution when the skewness approaches zero offshore and two in the swash zone, respectively. The assumption for the Gaussian distribution assumed in Equation 29 has simplified the cross-shore model CSHORE in the wet zone significantly. The assumption of the exponential distribution is made here to simplify the cross-shore model in the wet and dry zone. The probability density function *f*(*h*) is expressed as:

$$f(h)\frac{P_w^2}{\bar{h}}\exp\left(-P_w\frac{h}{\bar{h}}\right) \quad \text{for} \quad h>0 \tag{89}$$

with

$$P_w=\int_0^{\infty} f(h)dh\,;\bar{h}=\int_0^{\infty} hf(h)dh \tag{90}$$

where P_w = wet probability for the water depth $h > 0$; and $\bar{h}$ = mean water depth for the wet duration. The dry probability of $h = 0$ is equal to $(1-P_w)$. The mean water depth for the entire duration is equal to $P_w\bar{h}$. The overbar in Equations 87 and 88 indicates averaging for the wet duration only. The free surface elevation $\left(\eta-\bar{\eta}\right)$ above MWL is equal to $\left(h-\bar{h}\right)$. The standard deviations of η and h are the same and given by

$$\frac{\sigma_\eta}{\bar{h}}=\left(\frac{2}{P_w}-2+P_w\right)^{0.5}; \tag{91}$$

which yields $\sigma_\eta = \bar{h}$ for P_w = 1. This equality was supported by the depth measurements in the lower swash zone by Kobayashi et al. (1998) who assumed P_w =1 in Equation 89.

The cross-shore velocity U depends on x and t and is related to the depth h in the swash zone. The following relationship between U and h may be assumed to express U as a function of h:

$$U = \alpha\sqrt{gh} + U_s \tag{92}$$

where α is a positive constant; and U_s = steady velocity which is allowed to vary with x. The steady velocity U_s is intended to account for offshore return flow on the seaward slope and the downward velocity increase on the landward slope. Holland et al. (1991) measured the bore speed and flow depth on a barrier island using video techniques and obtained $\alpha \simeq 2$ where the celerity and fluid velocity of the bore are assumed to be approximately the same. Tega and Kobayashi (1996) computed wave overtopping of dunes using the nonlinear shallow-water wave equations and showed $\alpha \simeq 2$ for the computed U and h. As a result, use may be made of $\alpha = 2$ as a first approximation. Equation 92 implies that the cross-shore velocity U increases monotonically with the increase of h at given x. Equation 92 yields $U = U_s$ when h = 0, which may be acceptable in view of the very small depth in the wet and dry zone. Using Equations 89 and 92, the mean ($\bar{U}$) and standard deviation (σ_U) of the cross-shore velocity U can be expressed as:

$$\bar{U} = \frac{\sqrt{\pi}}{2}\alpha\left(P_w g\bar{h}\right)^{0.5} + P_w U_s; \tag{93}$$

$$\sigma_U^2 = \alpha^2 g\bar{h} - 2\left(\bar{U} - U_s\right)\left(\bar{U} - P_w U_s\right) + P_w\left(\bar{U} - U_s\right)^2 \tag{94}$$

Equation 92 is substituted into Equations 87 and 88 which are averaged for the wet duration using Equation 89. The continuity Equation 87 yields:

$$\frac{3\sqrt{\pi}\alpha}{4}\bar{h}\left(\frac{g\bar{h}}{P_w}\right)^{0.5} + U_s\bar{h} = q_o \tag{95}$$

After lengthy algebra, the cross-shore momentum Equation 88 is expressed as:

$$\frac{d}{dx}\left(B\frac{g\bar{h}^2}{P_w}+\frac{q_o^2}{\bar{h}}\right)=-gS_{bx}\bar{h}-\frac{f_b}{2}\alpha^2 g\bar{h}G_b(r_s) \qquad (96)$$

with

$$B=\left(2-\frac{9\pi}{16}\right)\alpha^2+1\,;r_s=\frac{3\sqrt{\pi}}{4}\frac{U_s\bar{h}}{q_o-U_s\bar{h}} \qquad (97)$$

The function $G_b(r_s)$ in Equation 96 with $r=r_s$ for simplicity is given by:

$$G_b(r)=1+\sqrt{\pi}r+r^2 \quad \text{for} \quad r\geq 0 \qquad (98)$$

$$G_b(r)=2\exp(-r^2)-r^2-1+\sqrt{\pi}r[2erf(r)+1] \quad \text{for} \quad r<0 \qquad (99)$$

where *erf* is the error function. The function G_b increases monotonically with the increase of *r* and G_b = 0 and 1 for *r* = -0.94 and 0.0, respectively, as shown in Figure 4. For r < -1.5, $G_b \simeq -\left(1+\sqrt{\pi}r+r^2\right)$. *Gb* is a modifier to the time-averaged shear stress, accounting for the probability distribution of the near-bed velocity in random waves.

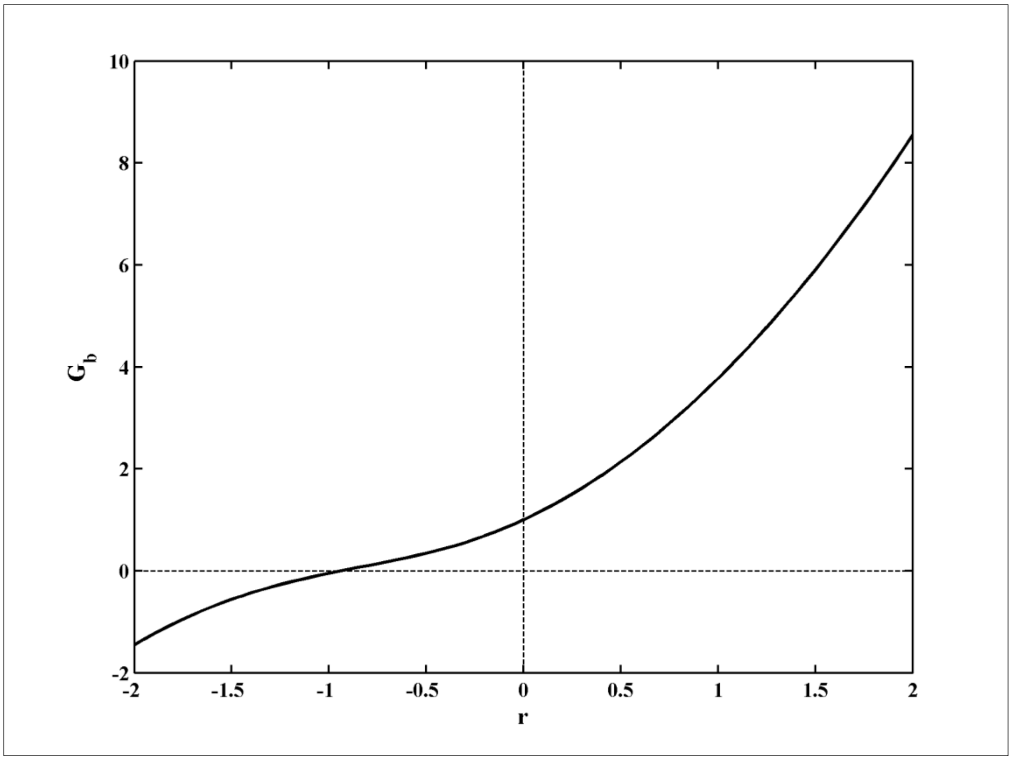

Figure 4. Function *Gb*(*r*) for wet and dry zone.

Equation 95 and 96 are used to predict the cross-shore variation of $\overline{h}$ and U_s for assumed q_o where $\sigma_\eta, \overline{U}$ and σ_U are computed using Equations 91, 93 and 94, respectively. It is necessary to estimate the wet probability P_w empirically. To simplify the integration of the momentum in Equation 96, the following formula is adopted:

$$P_w = \left[(1+A)\left(\frac{\overline{h}_1}{\overline{h}} \right)^n - A\left(\frac{\overline{h}_1}{\overline{h}} \right)^3 \right]^{-1} \; ; A = \frac{q_o^2}{Bg\overline{h}_1^3} \quad for \quad x \le x_c \qquad (100)$$

where $\overline{h}_1$ = mean water depth at the location of P_w = 1; n = empirical parameter for P_w; A = parameter related to the wave overtopping and overflow rate q_o normalized by the depth $\overline{h}_1$ where water is present always. The transition from the wet (P_w = 1) always zone to the wet and dry (P_w < 1) zone may be taken at $x = x_{SWL}$ where x_{SWL} is the cross-shore location of the still water shoreline of an emerged slope (Figure 5) or the seaward edge of a submerged crest as discussed in relation to Equations 85 and 86. Equation 100 is assumed to be valid on the seaward slope and crest in the region of $x \le x_c$ where x_c = landward end of the horizontal crest in Figure 5.

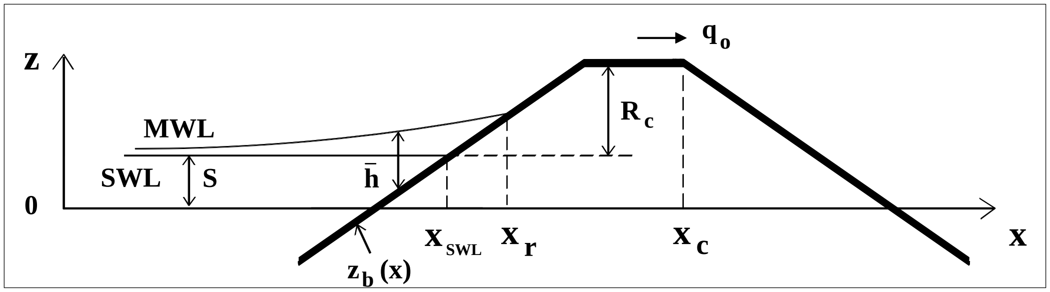

Figure 5. Transition from wet model ($x < x_r$) to wet and dry model ($x > x_{SWL}$) for emerged structure ($R_c > 0$).

Integration of Equation 96 using P_w given by Equation 100 with $\overline{h} = \overline{h}_1$ at $x = x_1$ yields $\overline{h}(x)$ for $x_1 \le x \le x_c$:

$$B_n (1+A)\overline{h}_1 \left[\left(\frac{\overline{h}_1}{\overline{h}} \right)^{n-1} - 1 \right] = z_b(x) - z_b(x_1) + \frac{\alpha^2}{2} \int_{x_1}^{x} f_b G_b dx \qquad (101)$$

where $B_n = B(2-n)/(n-1)$; and $z_b(x)$ = bottom elevation at the cross-shore location *x*. The mean water depth $\bar{h}$ at given *x* is computed by solving Equation 101 iteratively where the bottom friction factor f_b is allowed to vary with *x* and the function G_b given by Equations 98 and 99 depends on r_s defined in Equation 97. The empirical parameter *n* is taken to be in the range of 1 < *n* < 2 so that B_n > 0. The formula for *n* calibrated using the 107 tests of wave overtopping and overflow on a dike by Farhadzadeh et al. (2007) is expressed as $n = 1.01 + 0.98\left[\tanh(A)\right]^{0.3}$ which yields bounds of 1.01 ≤ *n*≤ 1.99.

The wave overtopping and overflow rate q_o is predicted by imposing $U_s = 0$ in Equation 95 at the location of x_c, namely

$$q_o = \frac{3\sqrt{\pi}\alpha}{4}\bar{h}_c\left(\frac{g\bar{h}_c}{P_c}\right)^{0.5} \quad \text{at} \quad x = x_c \tag{102}$$

where $\bar{h}_c$ and P_c are the computed mean depth $\bar{h}$ and wet probability P_w at x_c. The wave overtopping probability P_o may be related to the wet probability P_c at $x = x_c$ where both P_o and P_c are in the range of 0.0-1.0. An empirical relation of $P_o = \left[\tanh(5P_c)\right]^{0.8}$ is fitted for the 107 tests by Farhadzadeh et al. (2007).

On the slope landward of the crest, the wet probability P_w is assumed to be constant and equal to P_c:

$$P_w = P_c \quad \text{for} \quad x \geq x_c \tag{103}$$

Substituting Equation 103 into Equation 96 and integrating the resulting equation from x_c to *x*, the mean depth $\bar{h}(x)$ on the landward slope in the region of $x > x_c$ is expressed as:

$$\frac{\bar{h}}{\bar{h}_c} - 1 + \frac{9\pi a^2}{64B}\left[\left(\frac{\bar{h}_c}{\bar{h}}\right)^2 - 1\right] = \frac{P_c}{2B\bar{h}_c}\left[z_b(x_c) - z_b(x) - \frac{\alpha^2}{2}\int_{xc}^{x} f_b G_b dx\right] \tag{104}$$

where the bottom elevation $z_b(x)$ decreases with the landward increase of x in the region of $x > x_c$. Equation 104 is solved iteratively to compute $\overline{h}$ at a given x.

For assumed q_o, the landward marching computation of $\overline{h}$, σ_η, $\overline{U}$ and σ_U is initiated using the wet model in Chapter 4 from the seaward boundary $x = 0$ to the landward limit located at $x = x_r$ which corresponds to the location where the computed $\overline{h}$ or σ_η becomes negative in the region of $\overline{h}$ less than 1 cm for an emerged crest as shown in Figure 5. For a submerged crest, the landward limit of x_r is taken as x_c. The landward marching computation is continued using the wet and dry model in this section from the location of $x = x_{SWL}$ where $\overline{h} = \overline{h}_1$ in Equation 101 to the landward end of the computation domain or until the mean depth $\overline{h}$ becomes less than 0.001 cm. Then, the rate q_o is computed using Equation 102. This landward computation starting from $q_o = 0$ is repeated until the difference between the computed and assumed values of q_o is less than 1 percent. This convergency is normally obtained after several iterations. The computed values of $\overline{h}, \sigma_\eta, \overline{U}$ and σ_U by the two different models in the overlapping zone of $x_{SWL} < x < x_r$ (see Figure 5) are averaged to smooth the transition from the wet zone to the wet and dry zone.

Kobayashi et al. (2010) compared this hydrodynamic model for the impermeable wet and dry zone with the 107 tests by Farhadzadeh et al. (2007) and the 100 tests conducted by van Gent (2002b) who measured the water depth and velocities on the crest and landward (inner) slopes of six different dikes. The agreement was mostly within a factor of two for the wave overtopping rates and probabilities as well as the water depth, velocity, and discharge on the crest and landward slope exceeded by 2 percent of the incident waves. Kobayashi et al. (2010a) modified Equations 101 and 104 to allow the integration of Equation 96 starting from an arbitrary location landward of the still water shoreline. This modification is necessary for a berm that is slanted downward toward the toe of a dune. The wet probability P_w on the downward berm slope is assumed to be the same as that at the seaward end of this downward slope in the same way as in Equation 103 for the downward dune slope.

Sediment transport

The sediment transport model for the wet zone in Chapter 5 is adjusted for the wet and dry zone. Normally incident waves and alongshore uniformity are assumed here. The Gaussian velocity distribution has been assumed in Chapter 5, whereas *U* in the wet and dry zone is expressed as Equation 92 along with the exponential distribution of *h* given by Equation 89.

The movement of sediment particles is assumed to occur when the instantaneous bottom shear stress given by $0.5\rho f_b U^2$ exceeds the critical shear stress $\rho g(s-1)d_{50}\psi_c$ as has been assumed for Equation 49. The probability P_b of sediment movement is then the same as the probability of $|U| > U_{cb}$ where $U_{cb} = \left[2g(s-1)d_{50}\psi_c f_b^{-1}\right]^{0.5}$. Using Equations 89 and 92, P_b can be shown to be given by:

$$P_b = P_w \quad \text{for} \quad U_s > U_{cb} \tag{105}$$

$$P_b = P_w \exp\left[-\frac{P_w\left(U_{cb}-U_s\right)^2}{\alpha^2 g\bar{h}}\right] \quad \text{for} \quad \left|U_s\right| \le U_{cb} \tag{106}$$

$$P_b = P_w\left\{1-\exp\left[-\frac{P_w\left(U_{cb}+U_s\right)^2}{a^2 g\bar{h}}\right]+\exp\left[-\frac{P_w\left(U_{cb}-U_s\right)^2}{\alpha^2 g\bar{h}}\right]\right\} \quad \text{for} \quad -U_s > U_{cb} \tag{107}$$

where the upper limit of P_b is the wet probability P_w because no sediment movement occurs during the dry duration.

Sediment suspension is assumed to occur when the instantaneous turbulent velocity estimated as $\left(f_b/2\right)^{1/3}|U|$ exceeds the sediment fall velocity w_f as has been assumed for Equation 50. The probability P_s of sediment suspension is then the same as the probability of $|U| > U_{cs}$ where $U_{cs} = w_f\left(2/f_b\right)^{1/3}$. The probability P_s is then given by:

$$P_s = P_w \quad \text{for} \quad U_s > U_{cs} \tag{108}$$

$$P_s = P_w \exp\left[-\frac{P_w\left(U_{cs}-U_s\right)^2}{\alpha^2 g\bar{h}}\right] \quad \text{for} \quad \left|U_s\right| \le U_{cs} \tag{109}$$

$$P_s = P_w \left\{ 1 - \exp\left[-\frac{P_w \left(U_{cs} + U_s \right)^2}{\alpha^2 g \overline{h}} \right] + \exp\left[-\frac{P_w \left(U_{cs} + U_s \right)^2}{\alpha^2 g \overline{h}} \right] \right\} \quad \text{for} \quad -U_s > U_{cs} \qquad (110)$$

which reduces to Equations 105-107 if U_{cs} is replaced by U_{cb}. If $P_s > P_b$, use is made of $P_s = P_b$ because sediment suspension occurs only when sediment movement occurs.

The suspended sediment volume V_s per unit horizontal bottom area is estimated using Equation 51 with $S_{by} = 0$ for alongshore uniformity. In the wet and dry zone, V_s is assumed to be given by:

$$V_s = P_s V_{Bf} \left(1 + S_{bx}^2 \right)^{0.5} \qquad (111)$$

where V_{Bf}= potential suspended sediment volume on a horizontal bottom when P_s=1 . The value of V_{Bf} is assumed to be constant and chosen so that the suspended sediment volume V_s is continuous at $x = x_{SWL}$ at the seaward end of the wet and dry zone. The constant V_{Bf} is based on the assumption that suspended sediment in the swash zone tends to remain suspended. It is noted that P_s given by Equations 108 – 110 decreases landward with the decrease of P_w.

Kobayashi et al. (2010) estimated the cross-shore suspended sediment transport rate q_{sx} is estimated using Equation 52:

$$q_{sx} = a_x \overline{U} V_s \; ; a_x = \left[a + \left(S_{bx} / \tan \varphi \right)^{0.5} \right] \geq a \qquad (112)$$

where $\overline{U}$ is given by Equation 93. The parameter a_x had to be taken as unity in the zone of $\overline{U} > 0$ over the dune crest to predict minor wave overwash. However, Equation 112 was found to underpredict major wave overwash in the three small-scale tests conducted by Figlus et al. (2009) to investigate the transition from minor to major wave overwash of dunes constructed of fine sand. For these tests, suspended load was computed to be dominant. To account for the wave overtopping rate q_o explicitly, Equation 112 is modified as:

$$q_{sx} = \left(a_x \overline{U} + a_o U_o \right) V_s \; ; U_o = q_o / \overline{h} \qquad (113)$$

where a_o = empirical parameter with a_o=0 in Equation 112; and U_o = onshore current due to q_o , which is significant only in the zone of the very small depth $\overline{h}$. The parameter a_x is the same as in Equation 112 without any adjustment in the zone of $\overline{U} > 0$. The calibrated value for the three tests by Figlus et al. (2009) was in the range of a_o = 1.3 – 1.8. However, the range of a_o = 0.1 – 0.5 was necessary for the minor wave overwash data used by Kobayashi et al. (2010a) to calibrate Equations 111 and 112. The accurate prediction of wave overtopping and overwash is very difficult because of the small water depth and large velocity in the zone which is wet intermittently.

The cross-shore bedload transport rate q_{bx} is estimated using Equation 56 for the case of normally incident waves (sin θ = 0) and no longshore current $\left(\overline{V} = 0\right)$ where $\sigma_T = \sigma_U$ for sin θ = 0 in Equation 32. For this case, q_{bx} is given by:

$$q_{bx} = \frac{bP_b\sigma_U^3}{g(s-1)} G_s\left(S_{bx}\right) \tag{114}$$

where the bottom slope function $G_s\left(S_{bx}\right)$ is given by Equations 58 and 59, and the standard deviation σ_U is given by Equation 94 for the wet and dry zone. The parameter b in the wet and dry zone is chosen so that the value of q_b is continuous at $x = x_{SWL}$.

The cross-shore sediment transport rates q_{sx} and q_{bx} computed for the wet zone and the wet and dry zone are averaged in the overlapping zone of $x_{SWL} < x < x_r$ for the smooth transition between the two zones in the same way as the smooth transition of $\overline{h}, \sigma_\eta, \overline{U}$ and σ_U as explained at the end of the "Water depth and velocity" section in this chapter. The linear extrapolation for the case of no overwash given by Equation 60 for scarping is not applied now that the sediment transport in the wet and dry zone is predicted. The continuity equation of bottom sediment given by Equation 61 with q_y = 0 is solved numerically to obtain the bottom elevation at the next time level.

9 Model for Permeable Wet and Dry Zone

The model in Chapter 8 is extended to a permeable wet and dry zone. The extended model is calibrated and verified using available data for stone structures.

A number of time-dependent hydrodynamic models for rubble mound structures have already been developed as reviewed by Losada et al. (2008). These numerical models try to predict the temporal and spatial variations of wave dynamics as accurately as possible. The computation time normally increases with the increase of the resolution and accuracy. The computationally advanced models are used to predict hydrodynamic variables for relatively short durations. To reduce computation time considerably, Kobayashi et al. (2007b) proposed the probabilistic model CSHORE. The time-varying wave variables are expressed using a probability distribution. The spatial variations of the mean and standard deviation are computed using the time-averaged governing equations. The probabilistic time-averaged model requires additional assumptions but its computational efficiency allows the calibration of the model parameters using a large number of tests. This probabilistic model for the wet zone on the permeable armor layer is extended in this section to the wet and dry zone to predict the wave motion above the still water level (SWL). The extended model provides the hydrodynamic input to a damage progression model that predicts the slow evolution of the armor layer profile.

The movement of individual stone units on the armor layer may be computed using the equation of motion for each armor unit (Kobayashi and Otta 1987). The profile evolution of the armor layer may then be predicted by computing the displacements of all the armor units (Norton and Holmes 1992). However, this approach has never been adopted for practical applications probably because of its computation time. The sediment transport model in Chapter 8 is modified in this section to predict the profile evolution of the armor layer in the same manner as the prediction of the beach profile evolution. This simple approach neglects the discrete nature of armor stone units but is very convenient for the prediction of the armor layer profile evolution averaged alongshore where the alongshore averaging reduces the discrete nature.

Water depth and velocity

Figure 6 depicts the permeable stone layer analyzed in this section. Alongshore uniformity and normally incident waves are assumed. The cross-shore coordinate x is positive onshore with x=0 at the offshore location of the wave measurement. The vertical coordinate z is positive upward with z=0 at the datum. The still water level (SWL) above the datum is allowed to vary in time during a storm or an experiment. The upper and lower boundaries of the permeable stone layer are located at $z = z_b(x)$ and $z_p(x)$, respectively, where the lower boundary is assumed to be impermeable to simplify the analysis. The crest height R_c is taken conventionally as the structure height above SWL. The crest location x_c is defined here as the highest and most landward location. The wave overtopping rate is denoted as q_o. The SWL shoreline on the seaward slope is located at x_{SWL}. The mean water level (MWL) is located at $z=\left(S+\overline{\eta}\right)$ where $\overline{\eta}$ is the wave setup above SWL. The mean water depth $\overline{h}$ above $z = z_b$ is given by $\overline{h}=\left(S+\overline{\eta}-z_b\right)$. The cross-shore location x_r is the landward limit of the time-averaged model in the wet zone presented in Chapter 6.

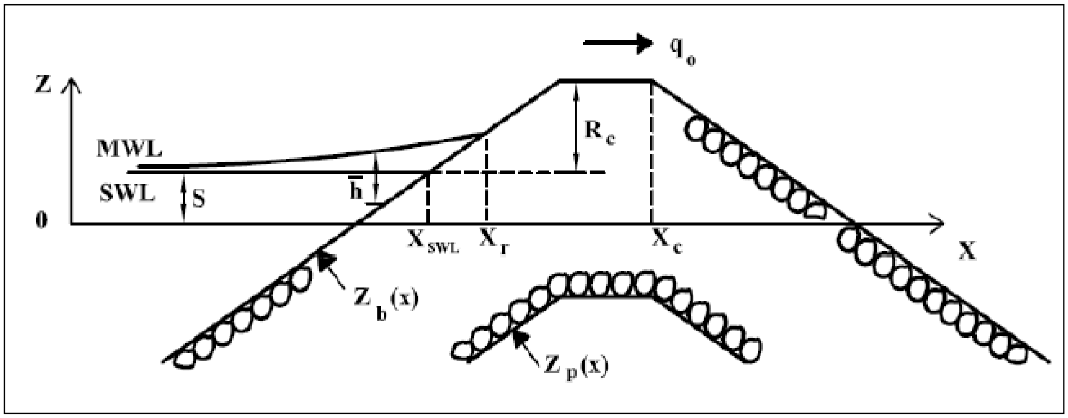

Figure 6. Transition from wet model ($x<x_r$) to wet and dry model ($x>x_{SWL}$) on permeable stone layer.

The time-averaged model for the permeable slope developed by Kobayashi et al. (2007b) has been modified using linear wave and current theory where wave overtopping induces onshore current. The time-averaged continuity, momentum, and wave action equations are used to predict the cross-shore variations of the mean $\overline{U}$ of the depth-averaged cross-shore velocity U, the mean $\overline{\eta}$ of the free surface elevation η above SWL, and the free surface standard deviation σ_η . The overbar denotes time averaging. The root-mean-square (rms) wave height is defined as $H_{rms}=\sqrt{8}\sigma_\eta$.

Linear progressive wave theory is used locally to express the velocity standard deviation σ_U in terms of σ_η. The probability distributions of η and *U* are assumed to be Gaussian. The equivalency of the time averaging and probabilistic averaging is assumed to express the time-averaged terms in the governing equations in terms of $\bar{\eta}, \sigma_\eta, \bar{U}, \sigma_U$. The permeability effects are included in Chapter 6.

The landward-marching computation using this model for the wet zone is continued as long as the computed $\bar{h}$ and σ_η are larger than 0.1 cm. The end location of the computation is denoted as x_r in Figure 6. The time-average model for the wet zone cannot predict wave overtopping. Consequently, a separate model for the wet and dry zone is developed and connected with the model for the wet zone. This procedure is the same as that used in Chapter 8. The time-averaged cross-shore continuity and momentum equations derived from the nonlinear shallow-water wave equations on the permeable slope (Wurjanto and Kobayashi 1993) are expressed as:

$$\frac{d}{dx}\left(\overline{hU}\right) = -\overline{w_p} \tag{115}$$

$$\frac{d}{dx}\left(\overline{hU^2} + \frac{g}{2}\overline{h^2}\right) = -g\bar{h}\frac{dz_b}{dx} - \frac{1}{2}f_b\overline{|U|U} - \overline{u_b w_p} \tag{116}$$

where h and U = instantaneous water depth and cross-shore velocity, respectively; w_p = vertical seepage velocity which is taken to be positive downward; g = gravitational acceleration; z_b =bottom elevation above the datum z=0; f_b = bottom friction factor which is allowed to vary spatially; and u_b = horizontal fluid velocity at $z = z_b$. The last term on the right hand side of Equation 116 represents the time-averaged flux of the horizontal momentum into the permeable layer. The overbar in Equations 115 and 116 for the wet and dry zone indicates time averaging for the wet duration only because no water exists during the dry duration.

The continuity and approximate momentum equations for the flow inside the permeable layer are expressed as

$$\frac{dq_p}{dx} = \overline{w_p} \tag{117}$$

$$\left(\alpha_p + \beta_1 \left|\overline{U_p}\right|\right)\overline{U_p} = -g\frac{d\overline{\eta}}{dx} \tag{118}$$

$$\alpha_p = 1000\left(\frac{1-n_p}{n_p}\right)^2 \frac{\upsilon}{D_{n50}^2}; \beta_1 = \frac{5\left(1-n_p\right)}{D_{n50}n_p^3} \tag{119}$$

where q_p = time-averaged horizontal volume flux in the permeable layer; $\overline{U_p}$ = time-averaged horizontal discharge velocity; α_p and β_1 = coefficients associated with the laminar and turbulent flow resistance in Equation 65, respectively; n_p = porosity of the permeable layer; D_{n50} = nominal stone diameter; and ν = kinetic viscosity of the fluid. Equation 119 is based on the formula developed by van Gent (1995) and calibrated by Kobayashi et al. (2007b). The resistance component associated with the oscillatory flow is simply neglected in Equation 118 which is solved analytically to obtain the discharge velocity $\overline{U_p}$ driven by the horizontal pressure gradient due to $\overline{\eta} = \left(\overline{h} + z_b - S\right)$ where $\overline{h}$ and z_b vary with x. It is noted that Equation 118 retains only the leading terms in the horizontal momentum equation given by Wurjanto and Kobayashi (1993). Adding Equations 115 and 117 and integrating the resulting equation with respect to x, the vertically integrated continuity equation is obtained:

$$\overline{hU} + q_p = q_o \tag{120}$$

where the wave overtopping rate q_o is defined as the sum of the volume fluxes above and inside the permeable layer in the same way as in Equation 62. The volume flux q_p is estimated as:

$$q_p = P_w \overline{U_p}\left(\overline{\eta_p} - z_p\right) \tag{121}$$

where P_w = wet probability defined as the ratio between the wet and entire durations; $\overline{\eta_p}$ = average water level inside the permeable layer; and z_p = elevation of the impermeable lower boundary. The elevation $\overline{\eta_p}$ and z_p are relative to the datum z = 0 in Figure 6 and $\left(\overline{\eta_p} - z_p\right)$ is the thickness of water inside the permeable layer. The elevation $\overline{\eta_p}$ is estimated as:

$$\overline{\eta_p} = P_w z_b + \left(1 - P_w\right) z_p \quad \text{for} \quad z_p \geq S \tag{122}$$

$$\overline{\eta_p} = P_w z_b + (1 - P_w) S \quad \text{for} \quad z_p < S \tag{123}$$

The upper bound of $\overline{\eta_p}$ for $P_w = 1$ is the upper boundary of the permeable layer located at $z = z_b$. The lower bound of $\overline{\eta_p}$ for $P_w = 0$ is the higher elevation of the lower boundary z_p of the permeable layer and the still water level S. The wet probability P_w in Equation 121 ensures that $q_p = 0$ if $P_w = 0$. Equations 121– 123 based on physical reasoning may be crude but are used along with Equations 118 and 119 to estimate q_p for the known $\bar{h}$ and P_w.

The momentum flux in Equation 116 is expressed as:

$$\overline{u_b w_p} = \alpha_m P_w \left(g\bar{h}\right)^{0.5} w_m \tag{124}$$

with

$$\left(\alpha_p + \beta_1 w_m\right) w_m = g \tag{125}$$

where α_m =empirical parameter; and w_m = maximum downward seepage velocity due to the gravity force, obtained by solving Equation 125 analytically. The seepage velocity w_p is assumed to be of the order of w_m or less. The horizontal velocity u_b at $z = z_b$ is assumed to be of the order of $\left(g\bar{h}\right)^{0.5}$. Equation 124 assumes that the downward flux of the horizontal momentum during the wet duration is much larger than the upward momentum flux from the permeable layer.

The cross-shore variation of the mean water depth $\bar{h}$ is obtained by solving the momentum Equation 116 together with the continuity Equation 120. The probability density function *f(h)* in the wet and dry zone is assumed to be exponential and given by:

$$f(h) = \frac{P_w^2}{\bar{h}} \exp\left(-P_w \frac{h}{\bar{h}}\right) \quad \text{for} \quad h > 0 \tag{126}$$

with

$$P_w = \int_0^\infty f(h)\,dh \,; \bar{h} = \int_0^\infty h f(h)\,dh \tag{127}$$

Equations 126 and 127 are the same as Equations 89 and 90 but presented again for clarity. The wet probability P_w equals the probability of the instantaneous water depth $h > 0$. The dry probability of $h = 0$ is equal to $(1 - P_w)$. The mean water depth for the wet duration is $\bar{h}$ but the mean depth for the entire duration is equal to $P_w\bar{h}$. The free surface elevation η above SWL is given by $\eta = (h + z_b - S)$ where z_b and S are assumed to be invariant during the averaging. The standard deviations of η and h are the same and given by:

$$\frac{\sigma_\eta}{\bar{h}} = \left(\frac{2}{P_w} - 2 + P_w\right)^{0.5} \tag{128}$$

which is the same as Equation 91.

The cross-shore velocity U may be related to the depth h in the wet and dry zone in the same way as in Equation 92:

$$U = \alpha\sqrt{gh} + U_s \tag{129}$$

where α = positive constant taken as $\alpha = 2$; and U_s = steady velocity which is allowed to vary with x. The steady velocity U_s is included to account for offshore return flow on the seaward slope and crest and the downward velocity increase on the landward slope. Using Equations 126 and 129, the mean $\bar{U}$ and standard deviation σ_U of the cross-shore velocity U can be expressed as:

$$\bar{U} = \frac{\sqrt{\pi}}{2}\alpha\left(P_w g\bar{h}\right)^{0.5} + P_w U_s \tag{130}$$

$$\sigma_U^2 = \alpha^2 g\bar{h} - 2\left(\bar{U} - U_s\right)\left(\bar{U} - P_w U_s\right) + P_w\left(\bar{U} - U_s\right)^2 \tag{131}$$

Equations 128, 130 and 131 express $\sigma_\eta, \bar{U}, \sigma_U$ in terms of $\bar{h}$, P_w, and U_s which vary with x.

Equation 129 is substituted into Equations 116 and 120 which are averaged for the wet duration using Equation 126. The continuity Equation 120 yields:

$$\frac{3\sqrt{\pi}\alpha}{4}\bar{h}\left(\frac{g\bar{h}}{P_w}\right)^{0.5}+U_s\bar{h}=q\,;q=q_o-q_p \tag{132}$$

where q = volume flux above the permeable layer. After lengthy algebra, the momentum Equation 116 is expressed as:

$$\frac{d}{dx}\left(B\frac{g\bar{h}^2}{P_w}+\frac{q^2}{\bar{h}}\right)=-gh\frac{-dz_b}{dx}-\frac{f_b}{2}\alpha^2 g_b\left(r_s\right)-\alpha_m P_w\left(g\bar{h}\right)^{0.5}w_m \tag{133}$$

with

$$B=\left(2-\frac{9\pi}{16}\right)\alpha^2+1\,;r_s=\frac{3\sqrt{\pi}}{4}\frac{U_s\bar{h}}{q-U_s\bar{h}} \tag{134}$$

where the parameter B is related to the momentum flux term on the left hand side of Equation 116. The function $G_b(r_s)$ in Equation 133 is given by Equations 98 and 99.

Equations 132 and 133 are used to predict the cross-shore variation of $\bar{h}$ and U_s for assumed q_o. It is necessary to estimate the wet probability P_w empirically. To simplify the integration of Equation 133, the following formula is adopted:

$$P_w=\left[\left(1+A_1\right)\left(\frac{\bar{h}_1}{\bar{h}}\right)-A\left(\frac{\bar{h}_1}{\bar{h}}\right)^3\right]^{-1}\,;A=\frac{q^2}{Bg\bar{h}_1^{3}}\,;A_1=\frac{q_1^2}{Bg\bar{h}_1^{3}} \tag{135}$$

where $\bar{h}_1$ and q_1 = mean water depth and volume flux, respectively, at the location of $x = x_1$ where $P_w = 1$; n = empirical parameter for P_w ; and A and A_1 = dimensionless variables related to q and q_1, respectively. The transition from the wet (P_w = 1 always) zone to the wet and dry (P_w <1) zone may be taken at $x_1 = x_{SWL}$ where x_{SWL} is the cross-shore location of the still water shoreline of an emerged crest as shown in Figure 6. Equation 135 is assumed to be valid on the upward slope and horizontal crest in the region of $x_1 \le x \le x_c$ where x_c is the highest and most landward location of the structure.

Integration of Equation 133 for P_w given by Equation 135 starting from $\overline{h} = \overline{h_1}$ at $x = x_1$ yields $\overline{h}(x)$:

$$B_n(1+A_1)\overline{h}_1\left[\left(\frac{\overline{h}_1}{\overline{h}}\right)^{n-1}-1\right] = z_b(x) - z_b(x_1) + \int_{x1}^{x}\left[\frac{f_b}{2}\alpha^2 G_b + \alpha_m \frac{P_w w_m}{(g\overline{h})^{0.5}}\right]dx \quad (136)$$

where $B_n = B(2 - n)/(n-1)$; and $z_b(x)$ = bottom elevation at the cross-shore location x. The mean water depth $\overline{h}$ at given x is computed by solving Equation 136 iteratively. The empirical parameter n is taken to be in the range of $1 < n < 2$ so that $B_n > 0$. The formula for n for the impermeable wet and dry zone in Chapter 8 is adopted and expressed as: $n = 1.01 + 0.98\left[\tanh(A_o)\right]^{0.3}$ where $1.01 \le n \le 1.99$ and $A_o = q_o^2/\left(Bg\overline{h_1}^3\right)$.

On the downward slope in the region of $x > x_c$, the wet probability P_w is assumed to be given by:

$$P_w^{-1} = P_c^{-1} + \frac{q_c^2 - q^2}{Bg\overline{h}^3} \quad (137)$$

where P_c and q_c are the computed wet probability P_w and volume flux q at $x = x_c$. Substituting Equation 137 into Equation 133 and integrating the resulting equation from x_c to x, the mean depth $\overline{h}(x)$ is expressed as:

$$\frac{\overline{h}}{\overline{h}_c} - 1 + \frac{P_c q_c^2}{4gB\overline{h}_c^3}\left[\left(\frac{\overline{h}_c}{\overline{h}}\right)^2 - 1\right] = \frac{P_c}{2Bh_c}\left\{z_b(x_c) - z_b(x) + \int_{xc}^{x}\left[\frac{f_b}{2}\alpha^2 G_b + \alpha_m \frac{P_w w_m}{(g\overline{h})^{0.5}}\right]dx\right\} \quad (138)$$

where h_c is the computed mean depth at $x = x_c$.

The wave overtopping rate q_o is predicted by imposing $U_s = 0$ in Equation 132 at the crest location x_c such that:

$$q_o = \frac{3\sqrt{\pi}\alpha}{4}\overline{h}_c\left(\frac{\overline{h}_c}{P_c}\right)^{0.5} + q_p \quad \text{at} \quad x = xc \quad (139)$$

The wave overtopping probability P_o may be related to the wet probability P_c at $x = x_c$ where both P_o and P_c are in the range of 0.0 – 1.0. The empirical relation of $P_o = \left[\tanh\left(5P_c\right)\right]^{0.8}$ for the impermeable wet and dry zone in Chapter 8 is adopted to estimate P_o.

For assumed q_o, the landward marching computation of $\overline{h}, \sigma_\eta, \overline{U}$ and σ_U is initiated using the wet model in Chapter 6 from the seaward boundary $x = 0$ to the landward limit located at $x = x_r$. The landward marching computation is continued using the wet and dry model in this section from the location of $x = x_{SWL}$ where $\overline{h} = \overline{h_1}$ to the landward end of the computation domain or until the mean depth $\overline{h}$ becomes less than 0.001 cm. The rate q_o is computed using Equation 139 together with the overtopping probability P_o. This landward computation starting from $q_o = 0$ is repeated until the difference between the computed and assumed values of q_o is less than 1%. This convergence is normally obtained after several iterations. The computed values of $\overline{h}, \sigma_\eta, \overline{U}$ and σ_U by the two different models in the overlapping zone of $x_{SWL} < x < x_r$ (see Figure 6) are averaged to smooth the transition from the wet zone to the wet and dry zone.

Farhadzadeh et al. (2009) compared the numerical model with test explained by Kobayashi and de los Santos (2007) and van Gent (2002a). The empirical formula developed using the tests was expressed as:

$$\alpha_m = \alpha\left(\frac{z_b - z_p}{D_{n50}}\right)^{0.3} \tag{140}$$

where the constant α is the same as α = 2 in Equation 129 and $\left(z_b - z_p\right)/D_{n50}$ is the local thickness of the permeable layer normalized by the nominal stone diameter.

For the probability density function $f(h)$ given by Equation 126, the water depth h_e corresponding to the exceedance probability e is given by:

$$h_e = \frac{\overline{h}}{P_w}\ln\left(\frac{P_w}{e}\right) \quad \text{for} \quad P_w > e \tag{141}$$

Using Equation 129, the water velocity U_e and discharge q_e corresponding to the exceedance probability e are expressed as:

$$U_e = \alpha\sqrt{gh_e} + U_s \;;\; q_e = h_e U_e \tag{142}$$

The probability e of $h > h_e$ at given x is not directly related to the probability based on individual overtopping events. The probability 2 percent used by van Gent (2002b) is assumed to correspond to the range of e = 0.01 – 0.02 where Equation 141 is not very sensitive to e = 0.01 – 0.02 as long as the wet probability P_w is larger than about 0.1. The computed values of h_e, U_e and q_e in CSHORE are based on e = 0.01 where use is made of $e = P_w / 1.1$ if P_w <0.011 so that $(P_w / e) \geq 1.1$ in Equation 141. Farhadzadeh et al. (2009) compared the measured and computed values of $h_{2\%}$, $U_{2\%}$, and $q_{2\%}$. The agreement was mostly within the factor of two but the hydrodynamic variables in the wet and dry zone are difficult to predict accurately due to the small water depth and larger velocity during intermittent wave overtopping.

Stone movement

The sediment transport model for the impermeable sand beach in Chapters 5 and 8 is modified to predict the movement of stone armor units on a coastal structure. The probability P_b of stone movement under the Gaussian velocity U in the wet zone is estimated assuming that the stone movement occurs when the absolute value of the instantaneous velocity U exceeds the critical velocity U_{cb} estimated as:

$$U_{cb} = \left[N_c g(s-1) D_{n50}\right]^{0.5} \tag{143}$$

where s and D_{n50} = specific gravity and nominal diameter of the stone, respectively; and N_c = empirical parameter. If the wave height H_c corresponding to U_{cb} is given by $H_c = U_{cb}^2 / g$, then Equation 143 becomes $N_c = H_c / \left[(s-1) D_{n50}\right]$ and N_c may be regarded as the critical stability number for the stone which is of the order of unity (Kobayashi et al. 2003). Equation 49 is based on the critical Shields parameter Ψ_c = 0.05 for the initiation of sand movement. The two parameters are related by $N_c = 2\Psi_c / f_b$ and Equation 49 for the probability P_b is applicable using $\Psi_c = 0.5 f_b N_c$.

Equation 143 is adopted here and N_c is calibrated as N_c = 0.7 using the damage progression tests of a stone structure with s = 2.66 and D_{n50} = 3.64 cm conducted by Melby and Kobayashi (1998). The probability of stone suspension is estimated using Equation 50 where the stone fall velocity w_f is estimated using $w_f = 1.8\left[g(s-1)D_{n50}\right]^{0.5}$ for a sphere (e.g., Jiménez and Madsen 2003). For the stone with s = 2.66 and D_{n50} = 3.64 cm, w_f = 1.4 m/s and the computed probability of suspension of this stone is essentially zero. The stone armor units are assumed to move like bedload particles, although CSHORE also computes the suspended stone transport rate using the formulas developed for sand.

The probability P_b of stone movement in the wet and dry zone is obtained for the probability distribution of U based on Equations 126 and 129. The probability P_b of stone movement is assumed to be the same as the probability of $|U| > U_{cb}$ with U_{cb} given by Equation 143. Then, P_b is given by Equations 105 – 107.

The time-averaged volumetric rate q_b of stone transport is estimated using the formula for bedload given by Equation 114 which is modified as:

$$q_{bx} = bP_b G_s B_r \sigma_U^3 / \left[g(s-1)\right]; B_r = \left(\frac{z_b - z_p}{D_{n50}}\right)^m \leq 1 \qquad (144)$$

where b = bedload parameter specified as b = 0.002 as discussed below Equation 57; G_s = function of the bottom slope given by Equations 58 and 59; B_r = reduction factor due to limited stone availability; m = empirical parameter; and σ_U = velocity standard deviation representing the wave action on the stone. The rate q_{bx} becomes negative (offshore) on the steep slope with $G_s < 0$. The reduction factor B_r is added in CSHORE to account for the thickness $(z_b - z_p)$ of the stone layer where $B_r = 1$ if $(z_b - z_p) > D_{n50}$ and $B_r = 0$ in the zone of $z_b = z_p$ and no stone. The computed profile changes are found to be insensitive to the parameter m in the range of 0.5 to 2.0. The value of m = 1.0 is specified in CSHORE. The rate q_{bx} of stone transport in the wet and dry zone is also estimated using Equation 144 where the parameter b is chosen so that the values of q_{bx} computed for the two different zones are the same at the still water shoreline located at $x = x_{SWL}$. The computed cross-shore variations of q_{bx} in the two zones are averaged in the overlapping zone of $x_{SWL} \leq x \leq x_r$ for the smooth transition between the two zones. The temporal change of the bottom elevation z_b is computed using the conservation equation of stone volume in the same way as in Chapter 8.

Farhadzadeh et al. (2009) compared the numerical model with the three damage progression tests by Melby and Kobayashi (1998). The armor stone was placed in a traditional two-layer thickness with the seaward slope of 1/2. The armor stone was characterized by D_{n50} = 3.64 cm, s = 2.66 and n_p = 0.4 where the maximum seepage velocity was w_m = 8.7 cm/s using Equation 125. The thickness of the armor layer was 7.3 cm. The test duration was in the range of 8.5 to 28.5 hrs. The numerical model overpredicted the deposited area below SWL at the end of the test mostly because it does not account for discrete stone units dislodged and deposited at a distance seaward of the toe of the damaged armor layer. The eroded area above SWL was predicted better. The temporal variation of the eroded area A_e was compared using damage S_e defined as $S_e = A_e / D_{n50}^2$. The numerical model predicted the damage progression well partly because the critical stability number N_c introduced in Equation 143 was calibrated to be N_c = 0.7 for the three damage progression tests. The temporal variations of S_e computed for N_c = 0.7 and 0.6 were fairly sensitive to N_c. The simple criterion of stone movement based on Equation 143 may be improved so as to predict the damage progression more accurately.

10 Sensitivity Tests, Calibration and Model Validation to Field Data

Introduction

The CSHORE model input specification includes eight sediment related parameters influencing the calculated sediment transport and profile evolution. Four of these parameters pertain to the physical characteristics of the sediment comprising the beach profile and therefore should not be adjusted for model calibration purposes. These parameters are the median sediment diameter D_{50} (mm), the sediment fall velocity w_f (m/s), the sediment specific gravity s, and the sediment maximum slope tan Φ. The free parameters include the empirical bedload parameter b, the empirical suspended load parameter a, and two sediment suspension efficiency parameters e_B and e_f for sediment suspension due to energy dissipation from wave breaking and bottom friction respectively. Kobayashi et al. (2008a) calibrated the bedload parameter $b = 0.002$ using 20 water tunnel tests of Ribberink and Al-Salem (1994), the four large-scale flume tests of Dohmen-Janssen and Hanes (2002) and the 24 sheet flow test by Dohmen-Janssen et al. 2002). Based on three small-scale equilibrium profile tests conducted by Kobayashi et al. (2005), the suspended load parameter a was estimated on the order of 0.2. Typical values for the suspension efficiency parameters $e_B = 0.005$ and $e_f = 0.01$ have be assigned although these values are uncertain (Kobayashi 2007a).

In this chapter, the CSHORE model is applied to a suite of 52 cases of storm-induced beach profile change measured in the field. These data sets encompass seven sites along the Atlantic coast and two sites along the Pacific coast and involve several storm events. An initial suite of sensitivity simulations was performed to quantify the relative influence and role of each of the model parameters on the predicted profile change. CSHORE was calibrated for three east and two west coast cases with γ set at the default value of 0.5. Based on these calibrations, new default sediment parameter values were estimated. The full suite of field cases was simulated using the default parameter values.

Sensitivity tests

To determine the sediment parameter sensitivity, CSHORE was run with the initial default values for all but one of the empirical inputs. The variable was systematically varied over a reasonable range of values. The other parameter values were held constant at their respective default values.

Bedload parameter *b*

Figures 7 through 11 illustrate the sensitivity of CSHORE results to the specified value of the bedload parameter b. The six cases illustrated are a high quality and representative data subset used in the sensitivity analysis. The bedload parameter controls the magnitude of the computed bedload sediment transport which is prescribed in CSHORE as onshore-directed. Therefore, as seen in the figures, increasing the value of b results in a reduction of erosion in the swash zone and for larger values, a buildup of sediment in the foreshore is observed. As the value of b decreases the bar feature is positioned further offshore and is less pronounced, again, the result of reduced onshore sand transport counter acting offshore directed suspended sand transport. For these test cases, values of b greater than about 0.005 result in unrealistic accretion of the beach berm feature.

Suspended load parameter *a*

Figures 12 through 16 illustrate the sensitivity of CSHORE results to the specified value of the suspended load parameter a. The suspended load parameter accounts for the onshore-directed wave-related sediment transport through a reduction in the offshore-directed sediment flux due to undertow. The undertow driven erosion of the foreshore/swash zone and volume of sand deposited in the bar feature is unmitigated by the effect of wave transport as the value of a approaches one. Model results are relatively sensitive to the specified value of the suspended load parameter a.

Suspension efficiency parameter e_B

Figures 17 through 21 illustrate the sensitivity of CSHORE results to the specified value of the suspension efficiency parameter e_B. The suspension model is predicated on the importance of energy dissipation in sediment entrainment, and the suspension efficiency parameter e_B is the primary free parameter controlling magnitude of transport. Increasing the value of e_B increases the suspended sediment concentration in the breaking region and increases the estimated erosion on the foreshore and deposition in the

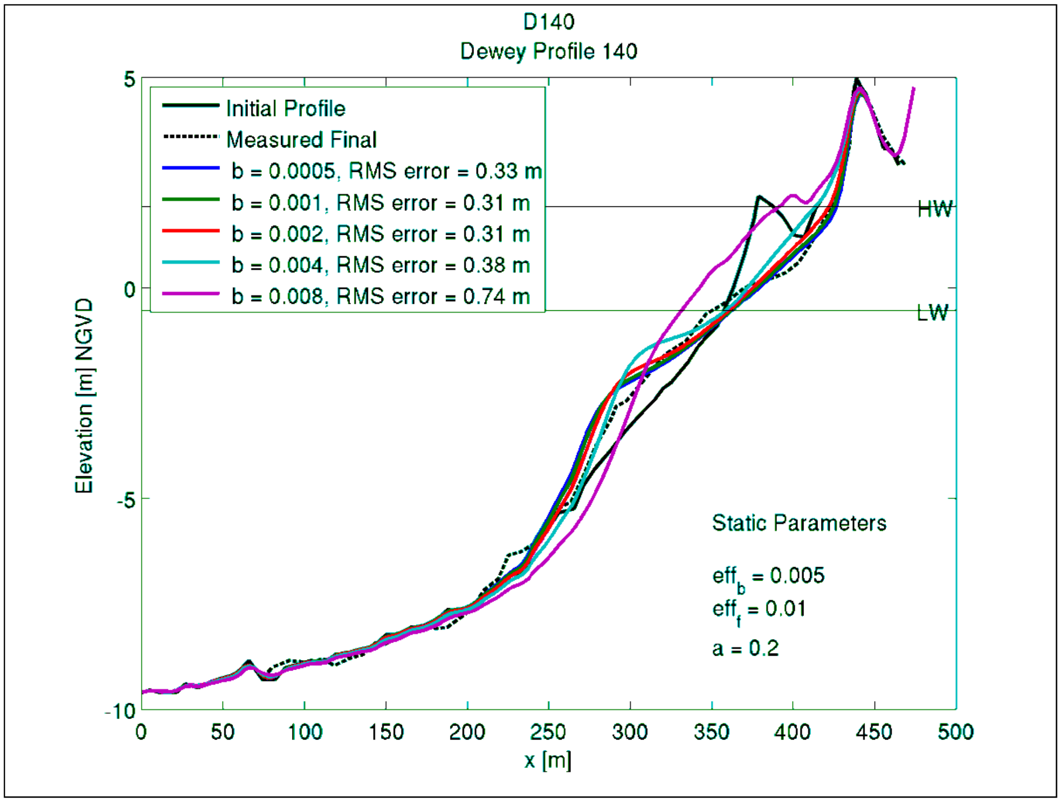

Figure 7. Case D140 – Sensitivity to bedload parameter *b*.

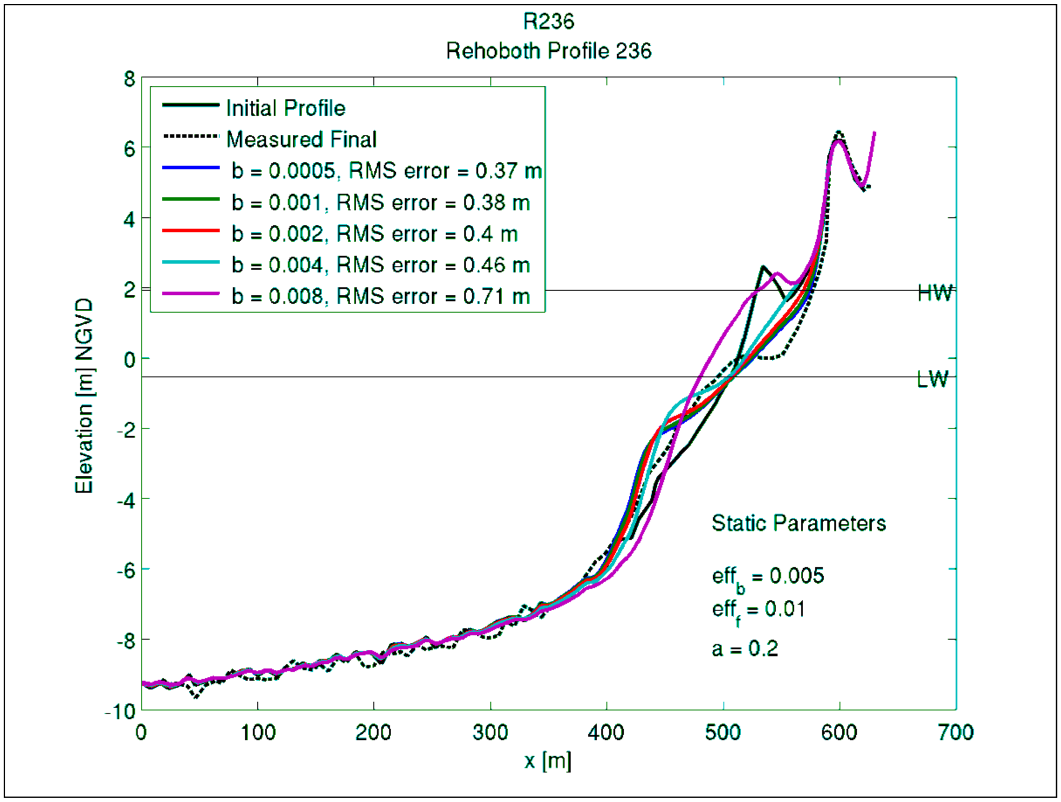

Figure 8. Case R236 – Sensitivity to bedload parameter *b*.

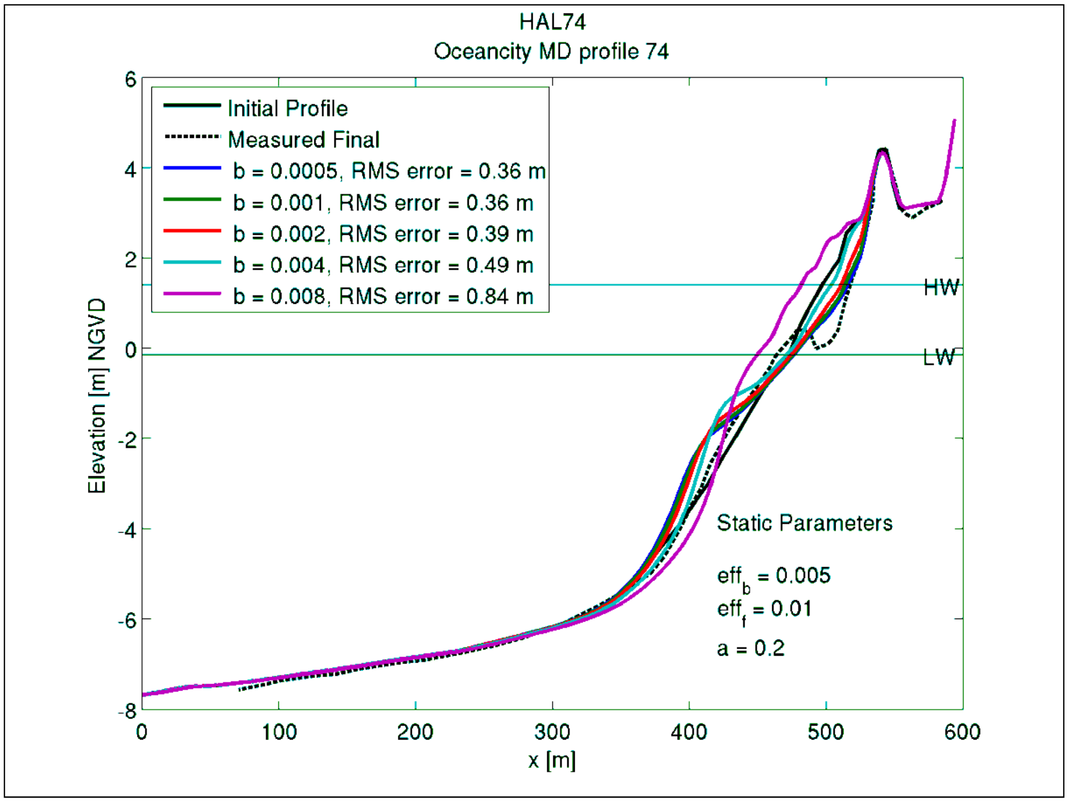

Figure 9. Case HAL74 – Sensitivity to bedload parameter *b*.

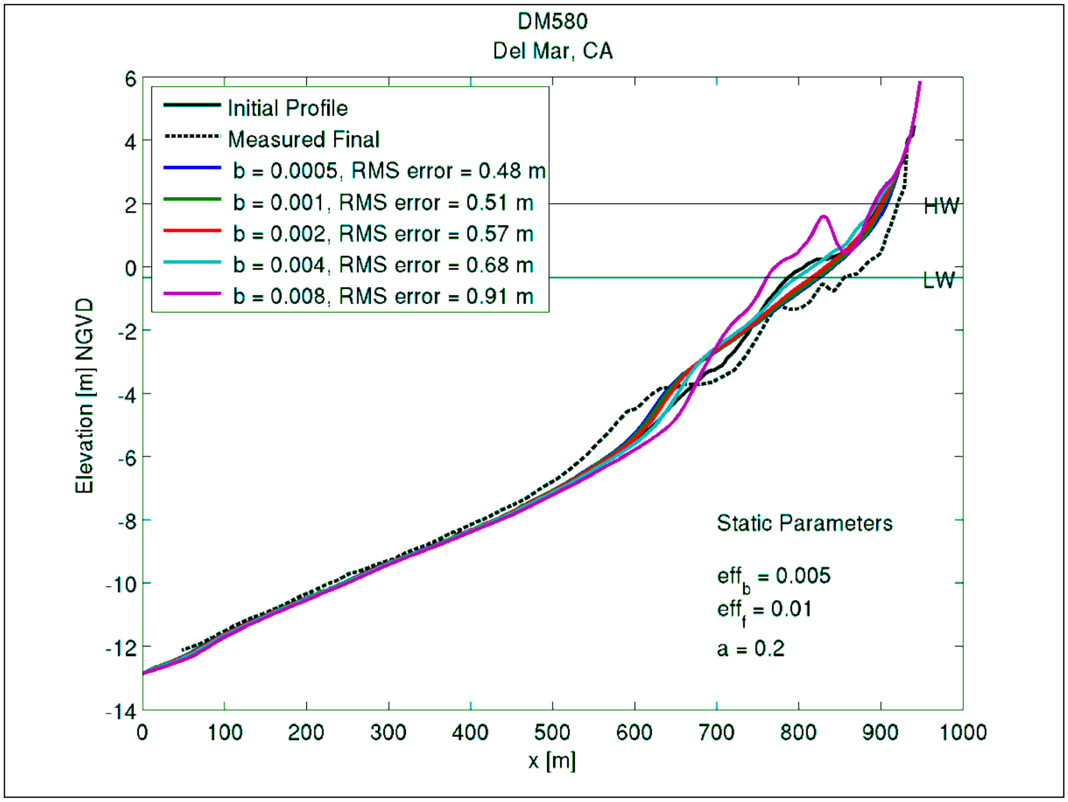

Figure 10. Case DM580 – Sensitivity to bedload parameter *b*.

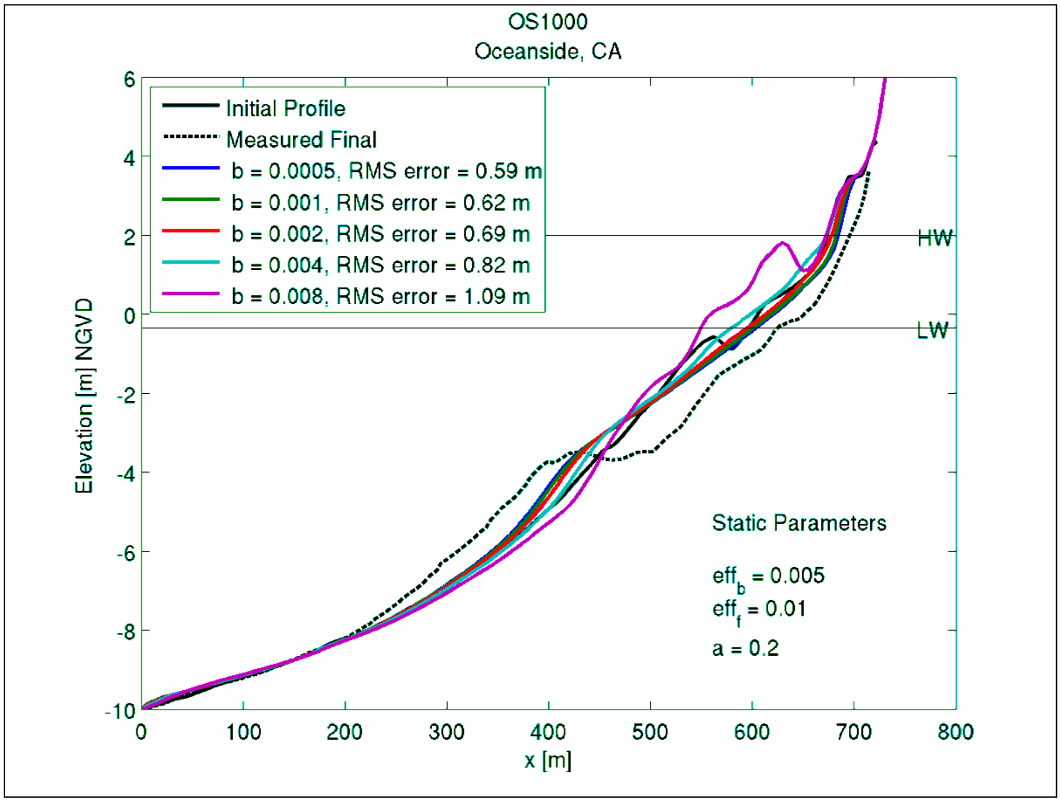

Figure 11. Case OS1000 – Sensitivity to bedload parameter *b*.

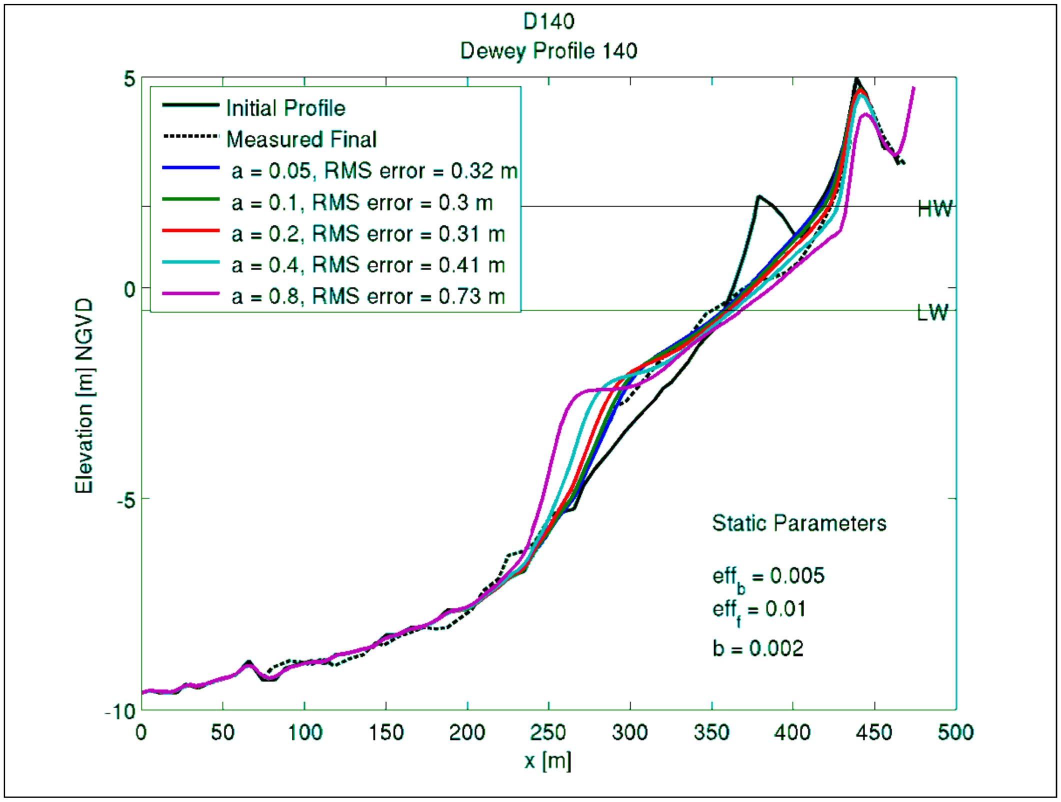

Figure 12. Case D140 – Sensitivity to suspended load parameter *a*.

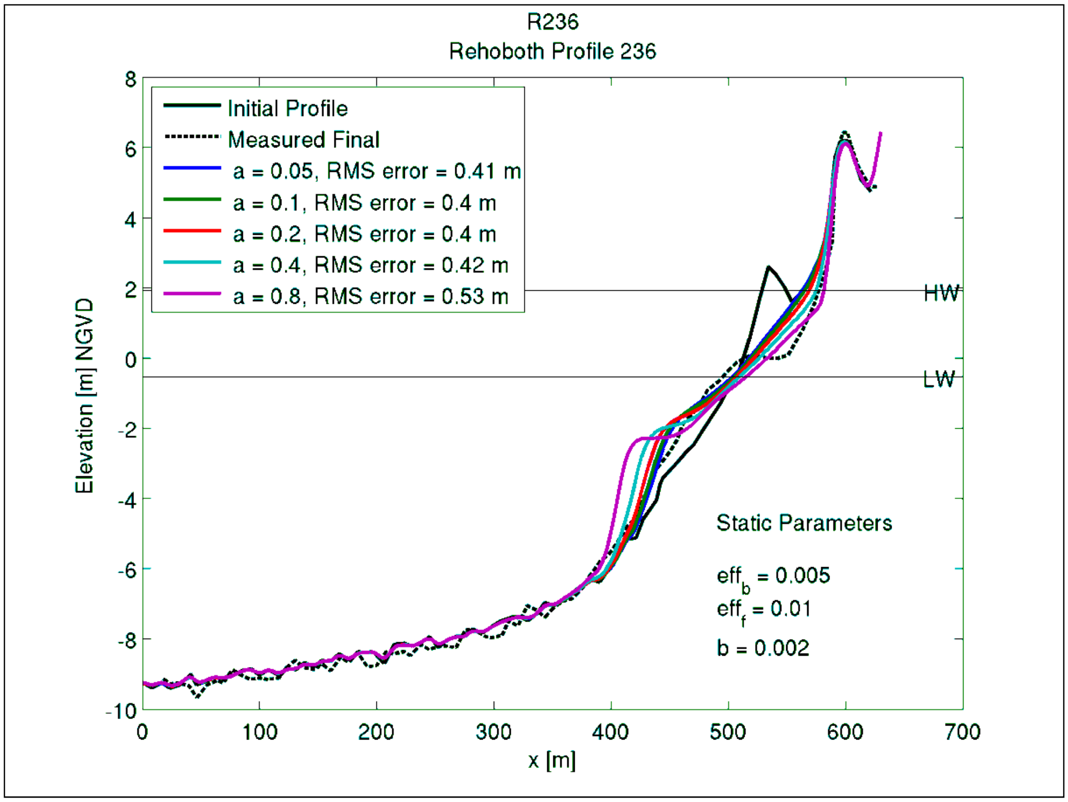

Figure 13. Case R236 – Sensitivity to suspended load parameter *a*.

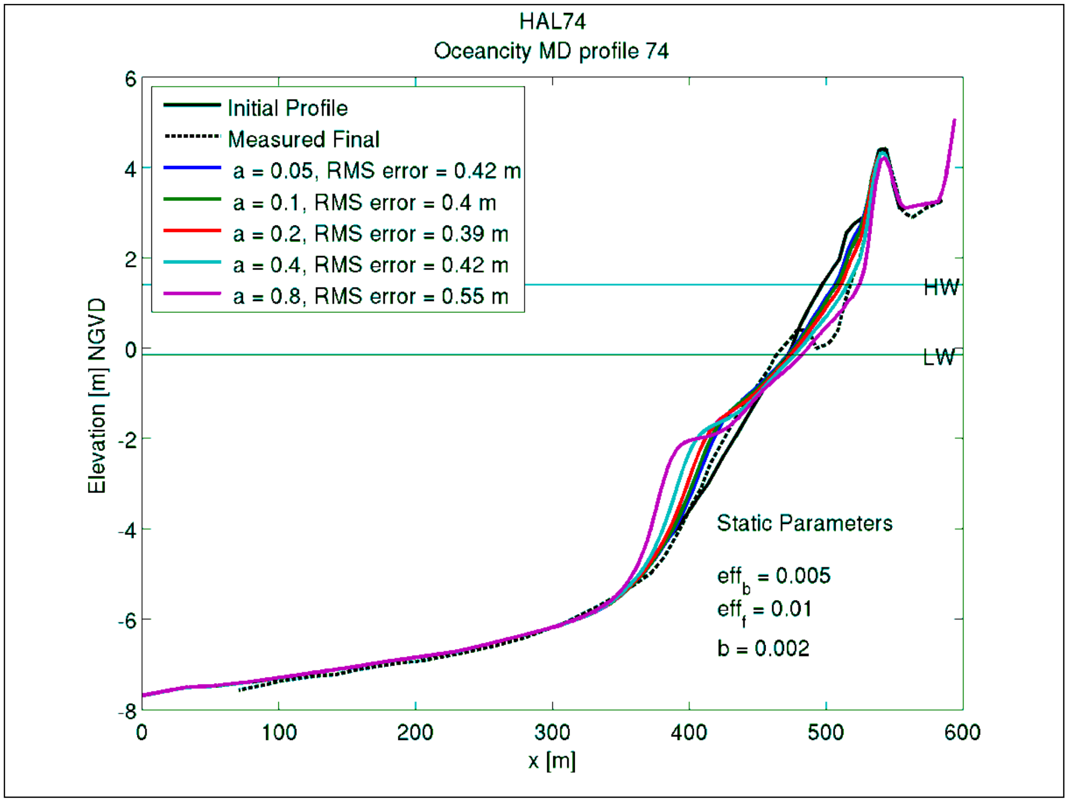

Figure 14. Case HAL74 – Sensitivity to suspended load parameter *a*.

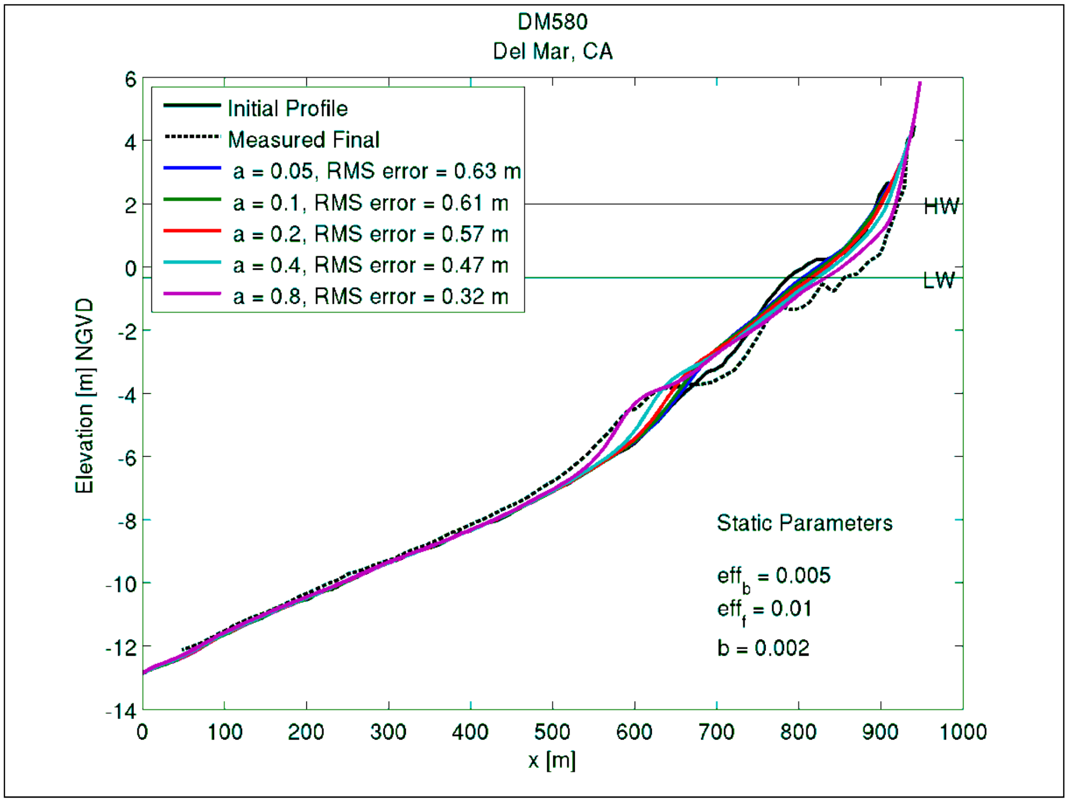

Figure 15. Case DM580 – Sensitivity to suspended load parameter *a*.

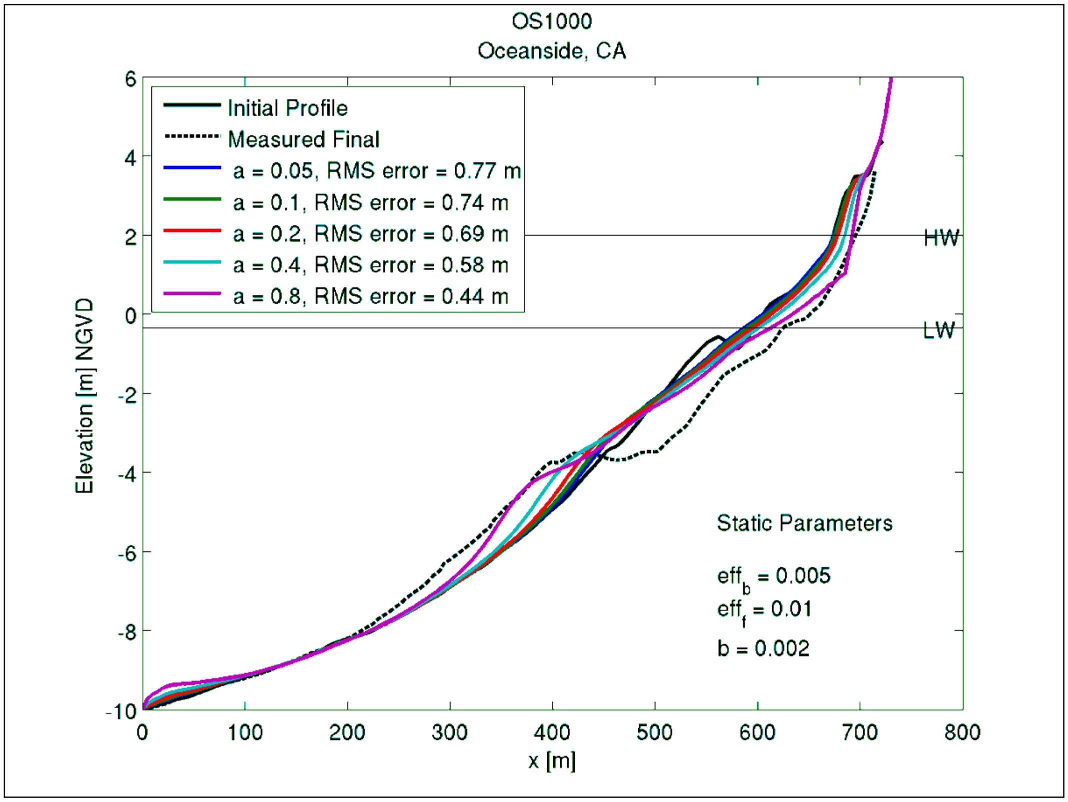

Figure 16. Case OS1000 – Sensitivity to suspended load parameter *a*.

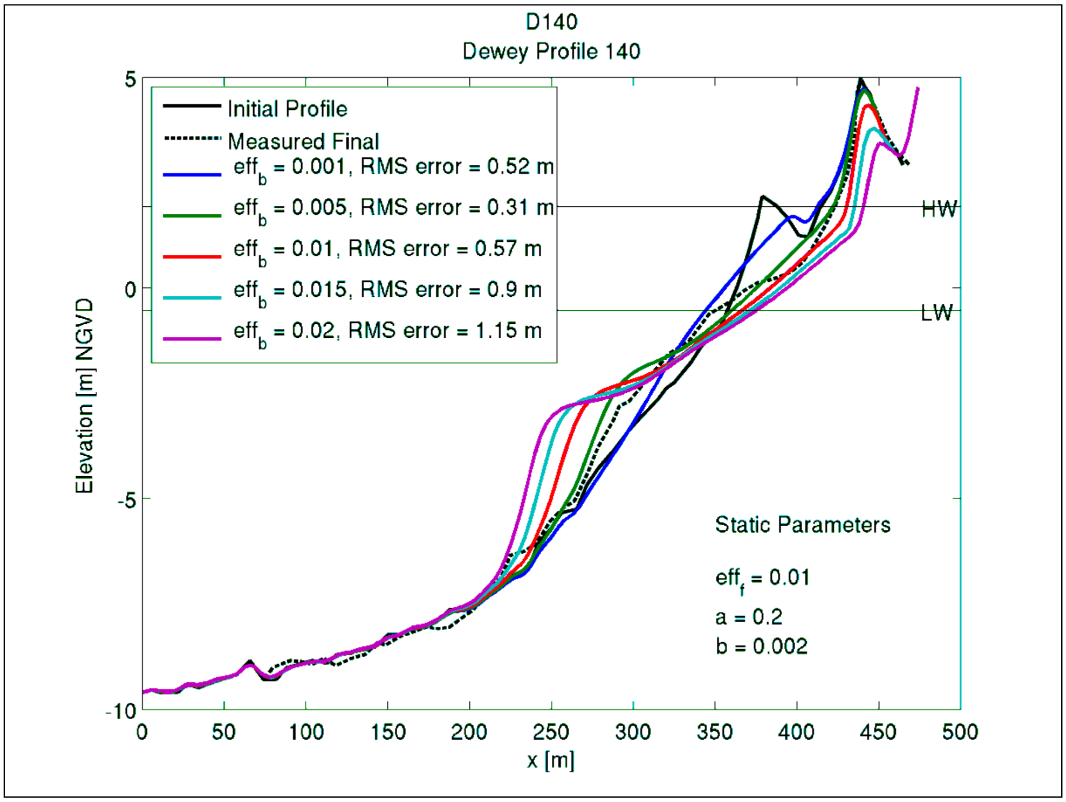

Figure 17. Case D140 – Sensitivity to efficiency parameter e_B.

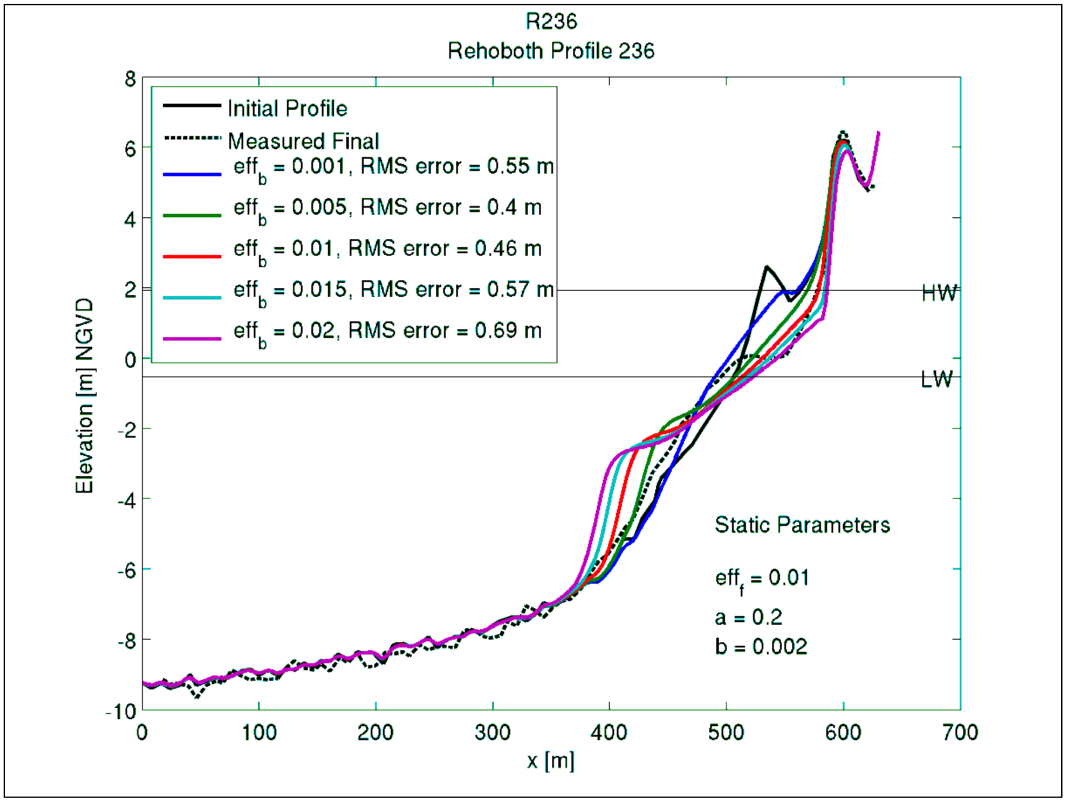

Figure 18. Case R236 – Sensitivity to efficiency parameter e_B.

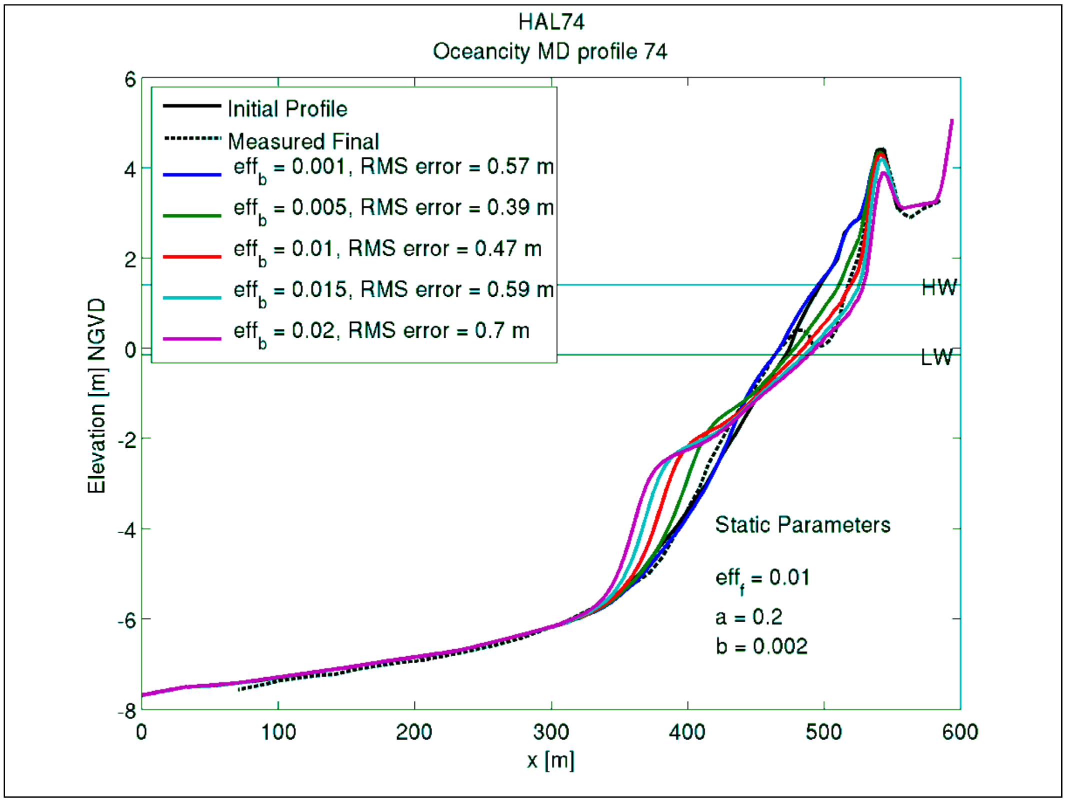

Figure 19. Case HAL74 – Sensitivity to efficiency parameter e_B.

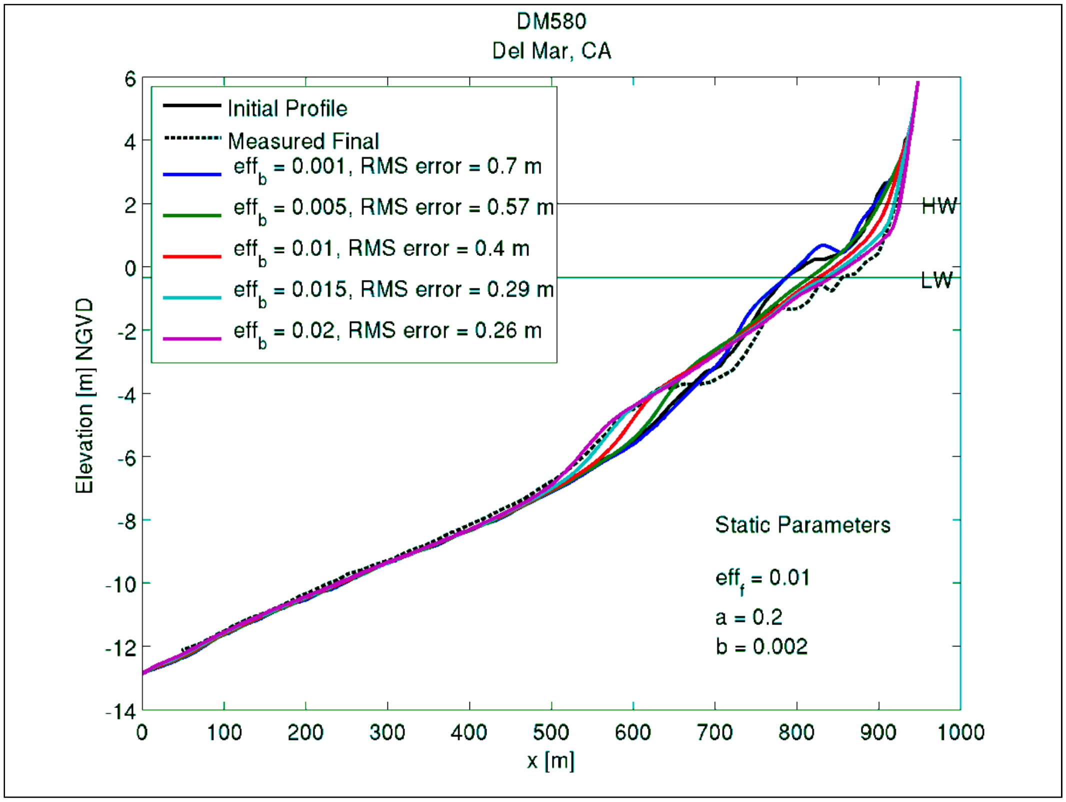

Figure 20. Case DM580 – Sensitivity to efficiency parameter e_B.

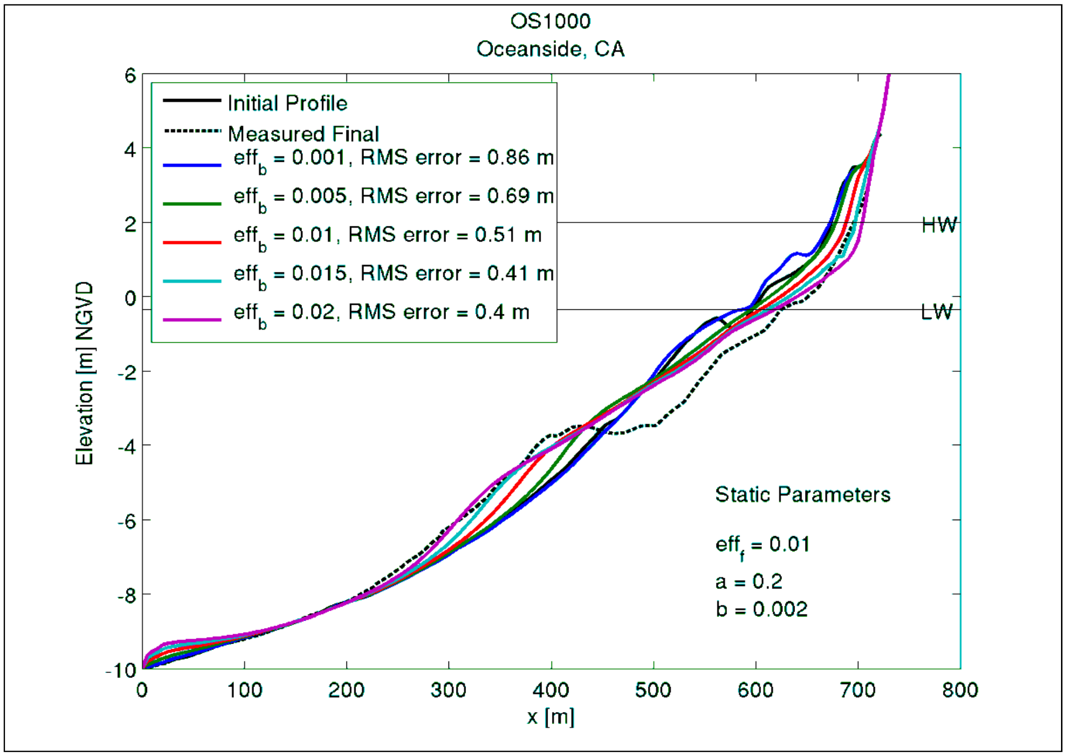

Figure 21. Case OS1000 – Sensitivity to efficiency parameter e_B.

nearshore bar feature. Conversely, a decrease in the value of e_B results in less foreshore erosion and a more subtle bar feature. It appears that the CSHORE results may be more sensitive to changes in the value of e_B than they are to changes in the value of *a*. Although the parameters are associated with different physical mechanisms, both parameters tend to influence the model results in a similar way.

Suspension efficiency parameter e_f

As shown in Kobayashi (2008a) the suspended sediment concentration and transport is driven by both wave breaking dissipation and dissipation in the bottom boundary layer. The magnitude of suspended sediment concentration due to bottom friction is controlled through the efficiency parameter e_f. Figures 22 through 26 illustrate the sensitivity of CSHORE results to the specified value of the suspension efficiency parameter due to bottom friction. In a manner similar to the breaking efficiency, increasing the value of e_f tends to increase the estimated foreshore erosion. Although it may not be evident in this effort the breaking dissipation and bottom friction dissipation can be important suspension mechanisms in different regions of the profile, and therefore increases in these two values can result in divergent profile evolution.

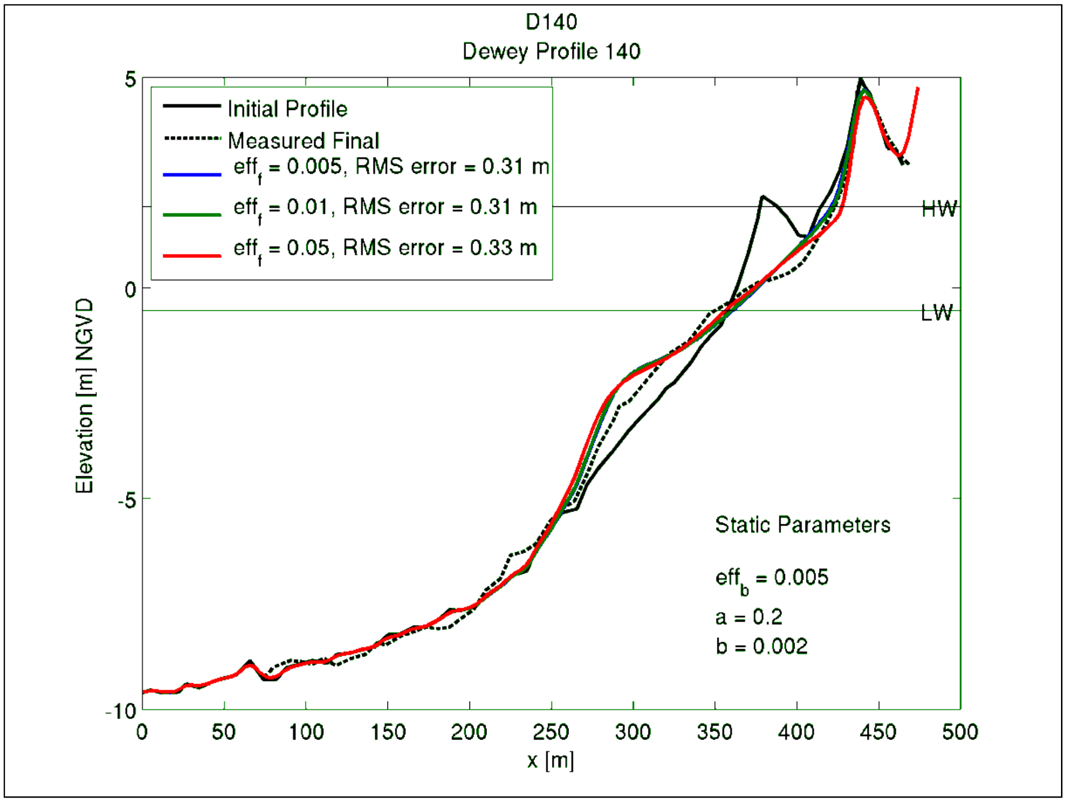

Figure 22. Case D140 – Sensitivity to efficiency parameter e_f.

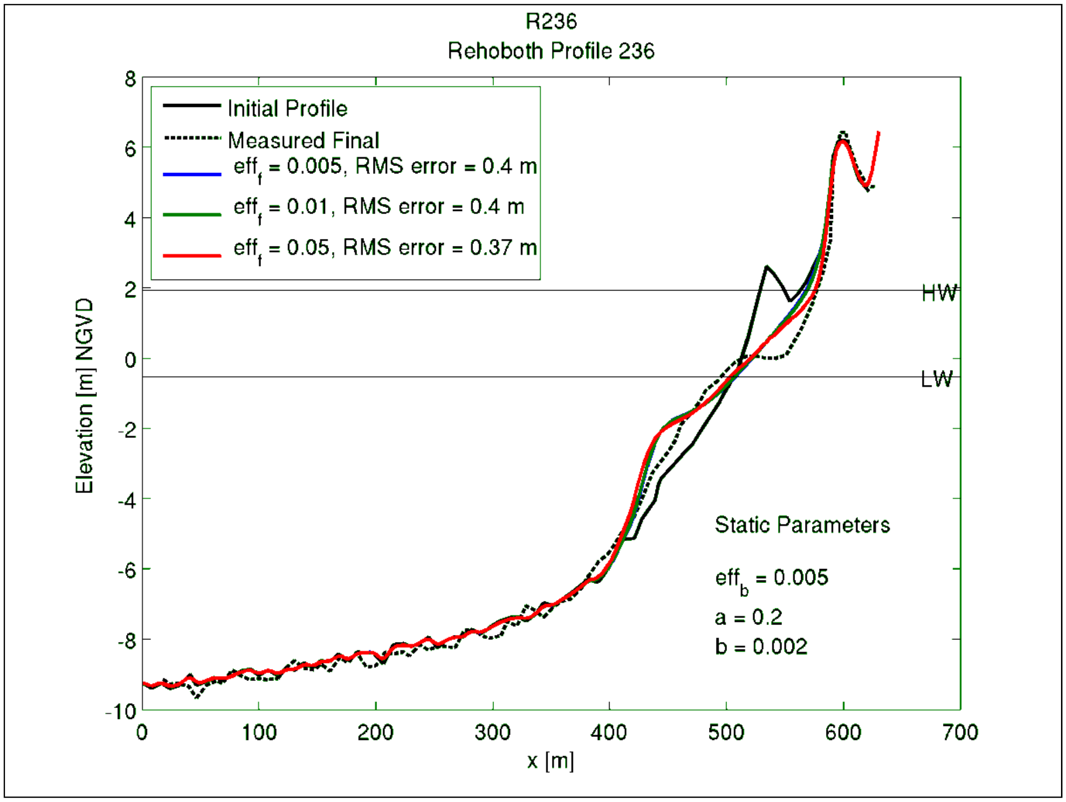

Figure 23. Case R236 – Sensitivity to efficiency parameter e_f.

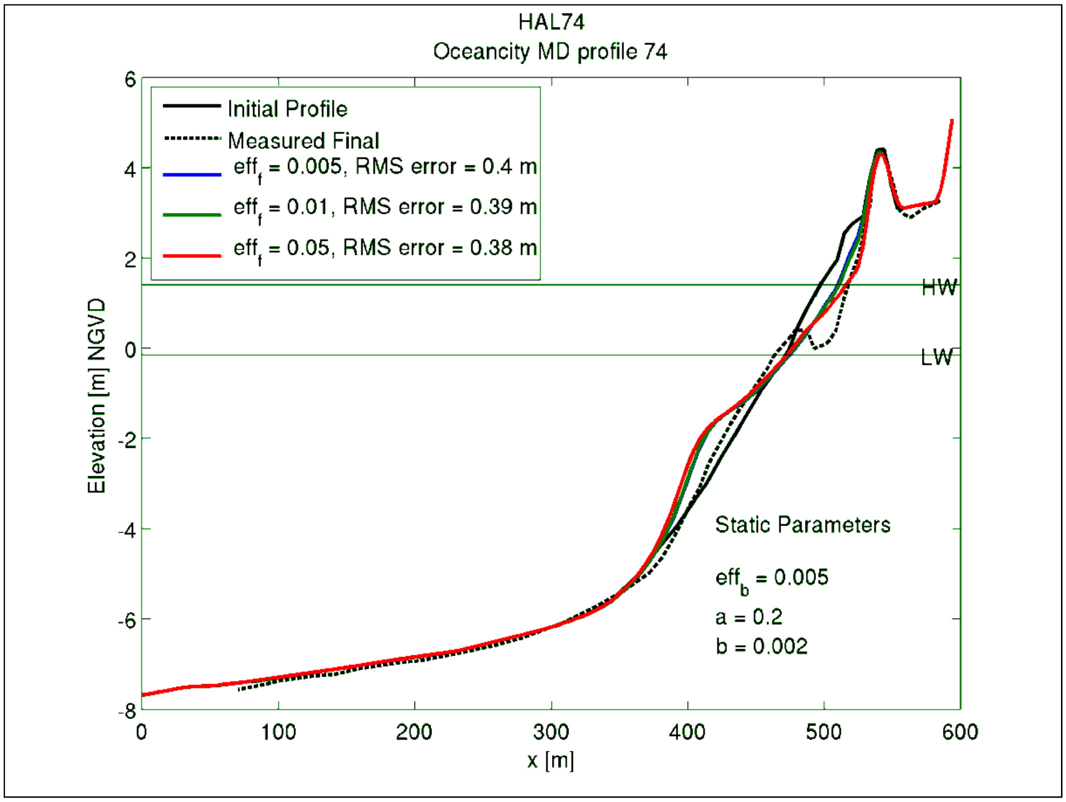

Figure 24. Case HAL74 – Sensitivity to efficiency parameter e_f.

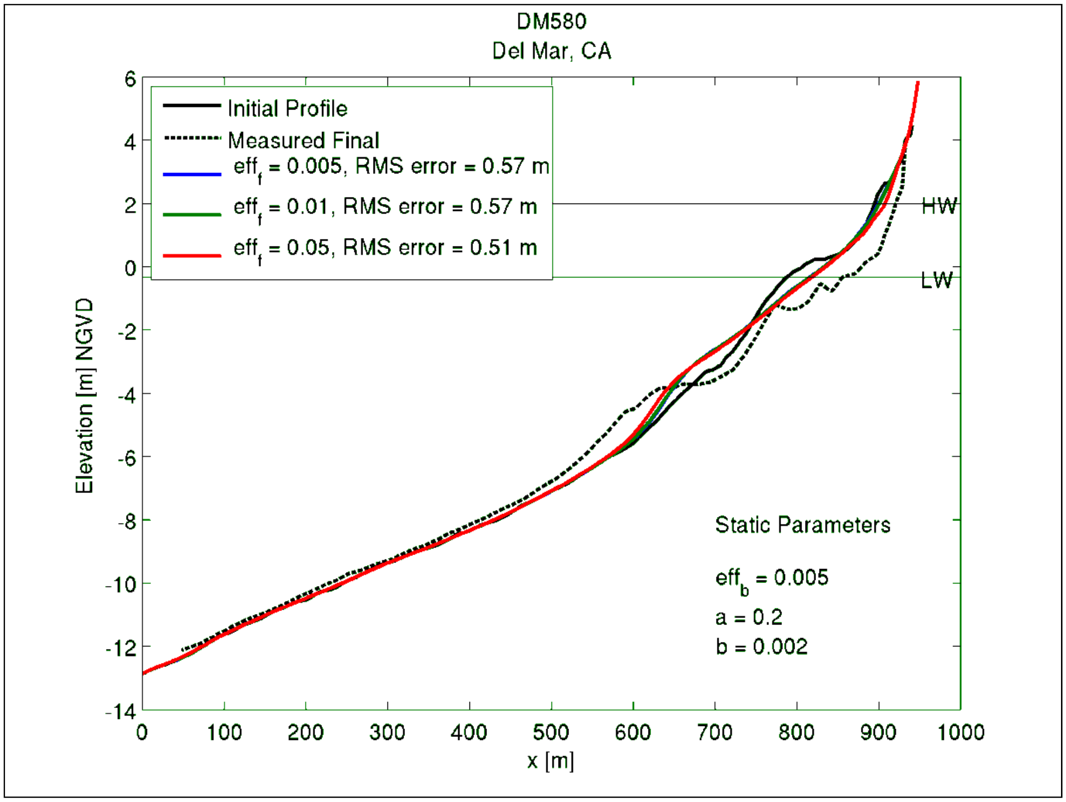

Figure 25. Case DM580 – Sensitivity to efficiency parameter e_f.

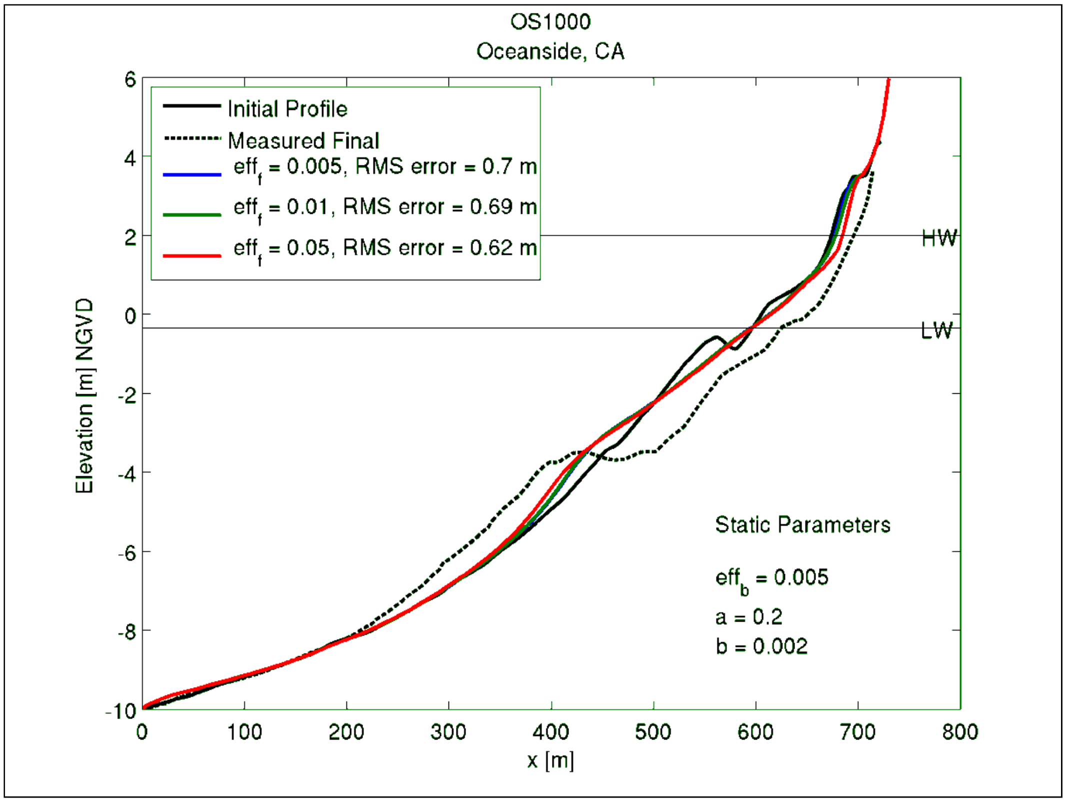

Figure 26. Case OS1000 – Sensitivity to efficiency parameter e_f.

Summary

CSHORE results are more sensitive to changes in the values of the suspended load parameter a and the suspension efficiency parameter e_B than they are to reasonable changes in the value of the bedload parameter b or the suspension efficiency parameter e_f. It is noted that the suspended load parameter a and the suspension efficiency parameter e_B are associated with different physical processes but tend to influence the model results in the same way. That is, increasing the value of either a or e_B will act to increase the amount of erosion at the foreshore and the volume of sand in the nearshore bar feature. The suspension efficiency parameters e_B and e_f influence the magnitude of the calculated suspended sediment transport, and the suspended load parameter a controls the balance between suspended sediment transport directed offshore due to under tow and onshore due to the positive correlation between the time varying cross-shore velocity and suspended sediment concentration. The bedload parameter b influences the magnitude of the onshore directed bedload sediment transport . Increasing the value of b will increase the onshore bedload transport which will tend to decrease the volume in the nearshore bar and reduce foreshore erosion or, at large values of *b*, produce foreshore deposition.

CSHORE calibration

Having identified the role and relative sensitivity of the CSHORE input parameters, appropriate default parameter values to serve as a reasonable starting point for project specific CSHORE calibration are developed herein. In the case that calibration data for CSHORE does not exist, predictions may be made using default parameter settings. Consequently, the approach used in the present study was to perform a detailed calibration for a limited number of field cases (three Atlantic coast cases and two Pacific coast cases) and default parameter values were estimated. The predictive skill of CSHORE was tested by running the model against the larger suite of 52 field cases using the new default parameter value settings. Evaluation of the model performance focuses on simulation of erosion processes at the foreshore and dune with less emphasis on the submerged portion of the beach profile.

Overlap in effect between the CSHORE input parameters tends to complicate the model calibration process; in that the best fit value for one parameter depends to some extent on the values assigned to the other parameters. As a result, a family of different parameter value settings is possible, each leading to a satisfactory calibration result. In the present calibration effort iterative simulations were performed between optimized values of the breaking efficiency parameter and the suspended load parameter. In these simulations optimization was based on minimizing the root mean square error between the measured and computed post-storm beach profile across the entire profile (computational domain). After optimum values for the breaking efficiency and suspended load parameters were determined the value of the bedload parameter was optimized. Next the value of the bottom friction efficiency parameter e_f was optimized.

Suspension efficiency parameter e_B

The value of suspension efficiency parameter e_B, was the first model parameter to be optimized in the calibration process. The suspension efficiency parameter e_B optimized at values ranging from 0.004 to 0.006 for the Atlantic coast calibration cases. For the Pacific coast calibration cases the suspension efficiency parameter e_B optimized at values ranging from 0.01 to 0.02. Default values for the suspension efficiency parameter were set at 0.005 for Atlantic coast applications and twice that, 0.01, for Pacific coast applications. Again, the differences in the Atlantic and Pacific coasts tests are poorly understood, and the larger parameter value for Pacific coast applications relates to the requirement for larger suspended load sediment transport and enhanced erosion.

Suspended load parameter *a*

The suspended load parameter a optimized at values ranging from 0.1 to 0.2 for Atlantic coast applications. The value of the suspended load parameter for the Pacific coast calibration cases ranged between 0.4 and 0.6. The new default value for the suspended load parameter, a, was set at 0.2 for Atlantic coast applications and 0.5 for the Pacific coast. Although the difference in parameter values is not well understood, a distinguishing difference between the Atlantic coast and Pacific coast calibration cases is the relative extent of upper beach erosion. This difference stems from the comparatively mild pre-storm foreshore slopes in the Pacific coast cases (approximately 1 on 35) as compared to the pre-storm foreshore slopes in the Atlantic coast cases (approximately 1 on 18). Whereas, the post-storm foreshore slopes are nearly the same for the Pacific and Atlantic coast cases at 1 on 21 and 1 on 16, respectively. To accommodate prediction of the larger upper beach erosion observed in the Pacific coast calibration cases, the proportion of offshore directed suspended sediment transport had to increase relative to the onshore directed bedload sediment transport, which was achieved in part with larger parameter values for the suspended load parameter a.

Bedload parameter *b*

The calibration process revealed that satisfactory predictions were consistently obtained with a bedload parameter value between 0.001 and 0.002. The new default for both the Atlantic and Pacific coast applications is set at the preliminarily assigned default value of 0.002. It is noted that the bedload parameter is expected to be instrumental in the accretionary phase of profile development. The short-term erosional field cases presented herein are ill-suited to the calibration of longer-term evolution, and additional data may alter this conclusion.

Suspension efficiency parameter e_f

The value of the suspension bottom friction efficiency e_f was selected following the other parameter optimizations. The procedure indicates that changes in the value assigned to this model parameter had very little influence on the predicted beach profile response. The default value for this model parameter remained unchanged at 0.01 for the Atlantic coast cases and, consistent with the breaking efficiency parameter, was doubled for the Pacific coast cases to 0.02.

Summary

CSHORE model results for each of the six calibration cases are illustrated in Figures 27 through 31. Each figure plots the measured initial and final beach profile together with the CSHORE predicted post-storm profile based on the new default parameter values developed as part of the present effort. The Atlantic coast cases are shown in Figures 27 through 29 whereas the Pacific coast cases are shown in Figures 30 and 31.

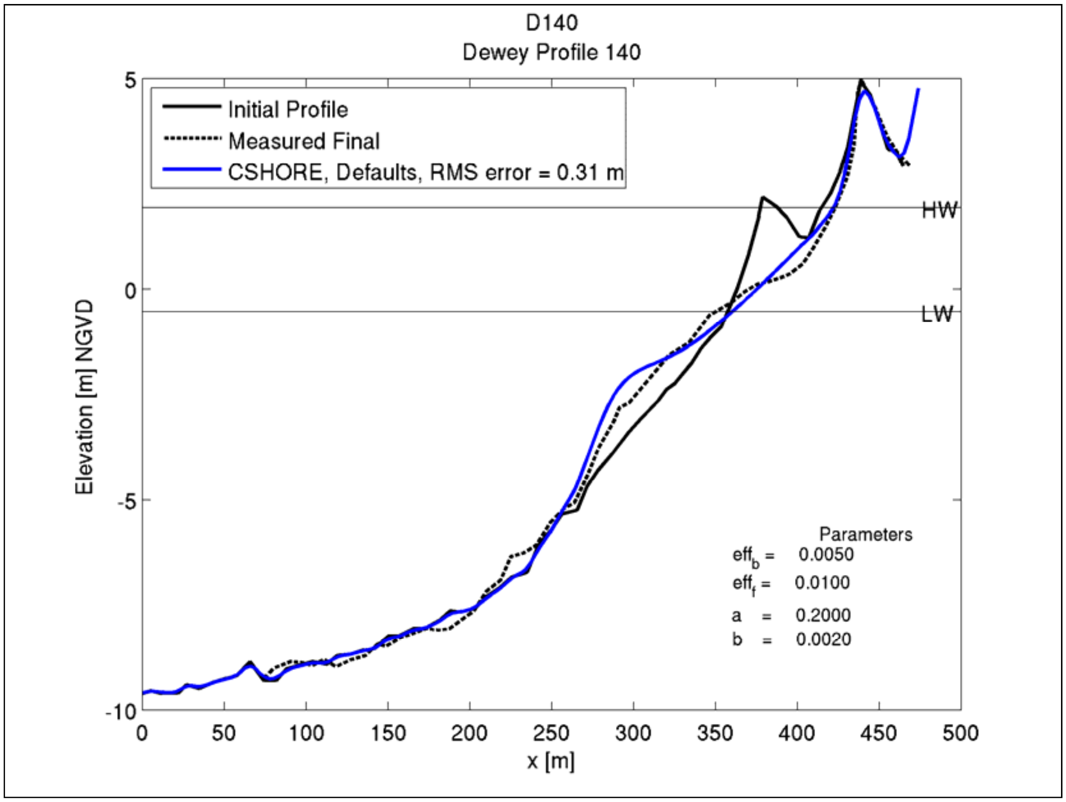

Figure 27. Case D140.

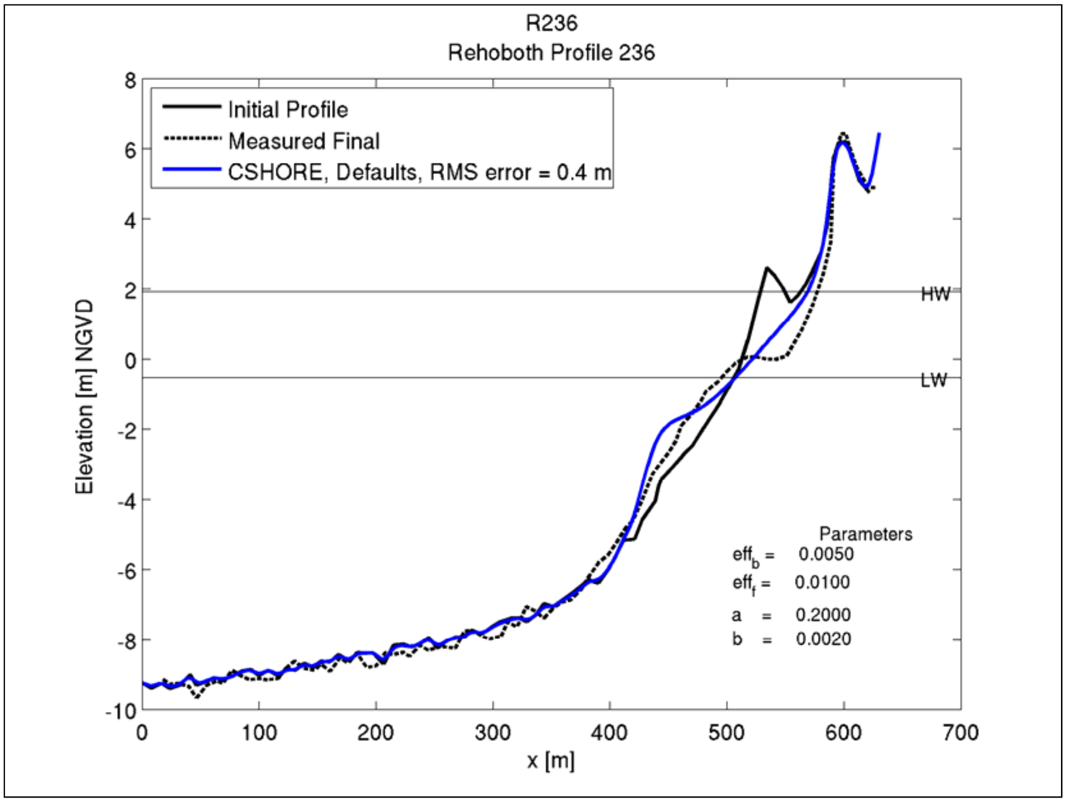

Figure 28. Case R236.

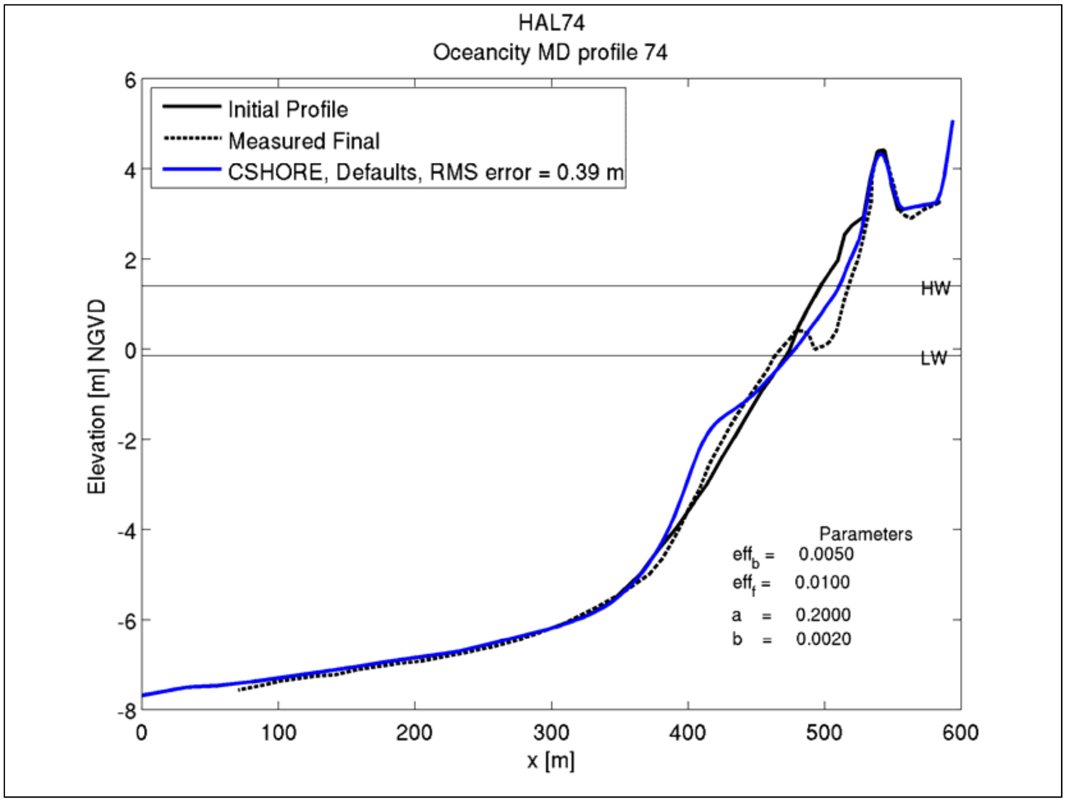

Figure 29. Case HAL74.

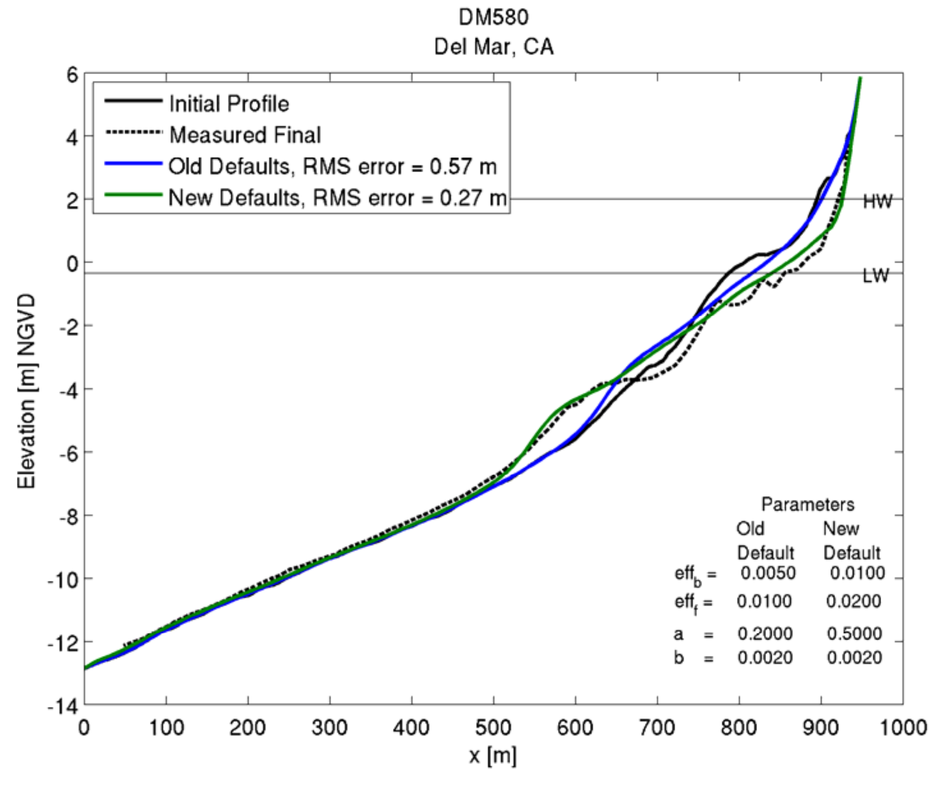

Figure 30. Case DM580.

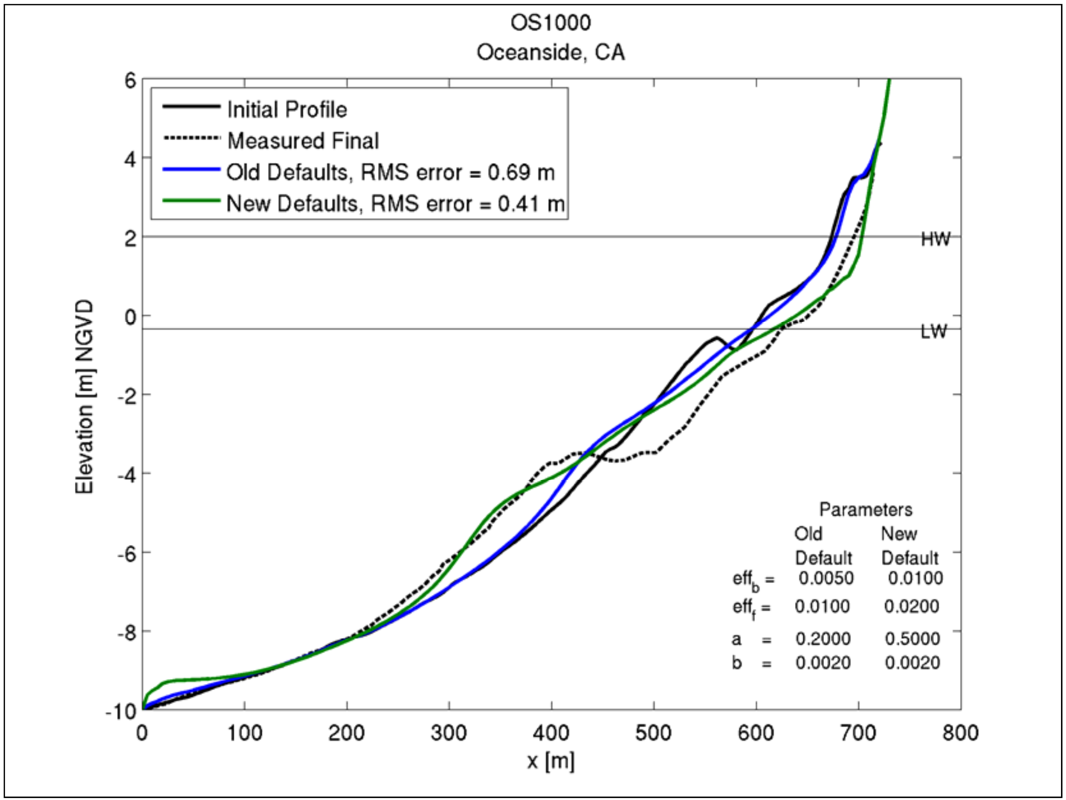

Figure 31. Case OS1000.

Field case studies

Based on the Atlantic coast calibration effort new default parameter values were estimated as follows:

- $b = 0.002$
- $a = 0.2$
- $e_B = 0.005$
- $e_f = 0.01$

Using these default values, CSHORE simulations were performed for a suite of fifty (50) Atlantic coast field cases involving seven different sites and six different storm sequences. The field cases selected for this study are the same data that were used to document the validation of SBEACH (Wise et al. 1996) and represent the best and most readily available records of storm-induced profile response for application and evaluation of CSHORE. The field case studies include Ocean City, MD (a series of storms from October 1991- January 1992); Manasquan/Point Pleasant Beach, NJ (March 1984 storm) Dewey Beach/Rehoboth Beach, DE (December 1992 storm); and Debidue Beach/Myrtle Beach, SC (Hurricane Hugo, September 1989).

Based on the Pacific coast calibration effort new (Pacific coast) default parameter were estimated as:

- $b = 0.002$
- $a = 0.5$
- $e_B = 0.01$
- $e_f = 0.02$

Using these default values, CSHORE simulations were performed for the three available field cases in southern California (Del Mar and Oceanside).

Measuring model performance

The intent of this portion of the study is to illustrate the capability of CSHORE to reproduce storm-induced beach profile change measured in the field and to evaluate model performance through comparison of measured and predicted beach profile response with emphasis on the dune and foreshore. The measures of performance were selected based on the types of information that field engineers require in the assessment of storm damage. These measures include volume change at the foreshore, recession of a specified contour, and landward storm intrusion, see Figure 32 for a schematic.

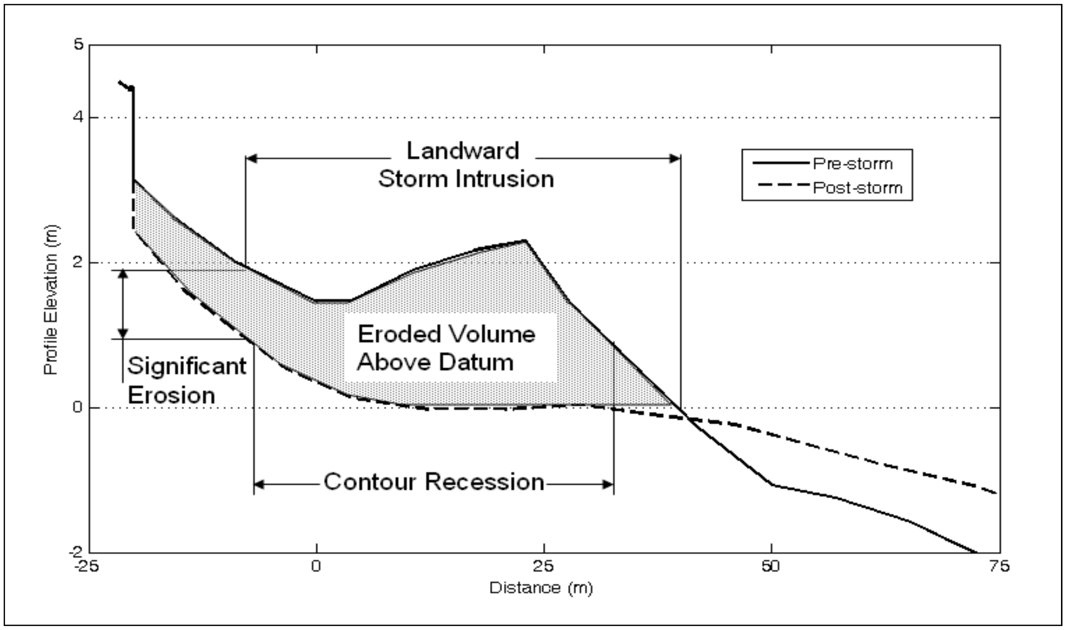

Figure 32. Definition of model performance measures at the foreshore.

Volume change. Volume change at the foreshore is computed as the net gain or loss in volume per unit beach width above some specified elevation. In this study, the reference elevation for volume calculations was set to the National Geodetic Vertical Datum (NGVD) which approximately corresponds to mean sea level at the selected field sites. The measure of volume change is useful in identifying how well CSHORE predicts erosion of the subaerial beach, which is important in defining volume requirements for beach nourishment operations and estimating damages to upland structures. However, in the available data set, volume change is not always a reliable indicator of model accuracy in the prediction of storm erosion. Some of the post-storm surveys occurred well after the end of the erosive wave conditions and include berm features that indicate significant post storm beach profile recovery. In these cases calculation of volume change based on the pre- and post-storm profiles underestimates the erosion generated by the storm and predicted by CSHORE. Consequently, the presence of a post-storm recovery berm must be considered when evaluating model performance using this measure.

Contour recession. Measuring the horizontal recession of a specified contour provides an assessment of how well CSHORE predicts the change of a given morphological feature such as the dune or berm. Contour recession also provides information on the loss of beach width resulting from a storm. For this study, a representative beach contour located between the reference elevation (NGVD) and the dune crest was identified for each field case. Recession of the selected contour from its initial position on the pre-storm profile was determined from the data and compared with simulation results.

Landward storm intrusion. Another measure of beach profile change at the foreshore is the extent of landward storm intrusion. Landward storm intrusion is defined as the landward limit of a specified depth of profile erosion. In this study an erosion depth of 0.3 m was employed for all cases. The measure of storm intrusion distance is often used to quantify the landward extent of potential structural damage caused by erosion and undermining. All measures of landward storm intrusion presented in this report are referenced to the horizontal position of the vertical datum (NGVD) on the initial beach profile

Ocean City, MD

Between late October 1991 and early January 1992 the beach at Ocean City, MD was affected by a series of severe storms. The storms, which included the 30 October 1991 "Halloween storm," 11 November 1991 storm, and 4 January 1992 storm, resulted in large-scale erosion of the constructed foreshore and dune at Ocean City. A major beach nourishment project had recently been completed at Ocean City, the result of a joint effort of the U.S. Army Corps of Engineers, the state of Maryland, Worcester County and the Town of Ocean City (Grosskoph and Stauble 1993). The data used in this case study was collected as part of the project monitoring effort, which included collection of beach profile data by sled surveys and the measurement of local wave conditions and water levels at an offshore gauge. These monitoring data provided a comprehensive set of high-quality data for application of CSHORE. Figures 33-35 present the wave and water elevation time histories recorded by the offshore gauge and used as input to CSHORE for each storm. The wave gauge was located outside the surf zone at a depth of approximately 10 m. Analysis of sediment samples collected as part of the monitoring program indicated a representative median sediment grain size of 0.35 mm. Additional details on the beach nourishment project and monitoring program at Ocean City are provided by Stauble et al. (1993). Impacts of the storms at Ocean City are discussed in a special issue of *Shore and Beach* (Vol. 61 No. 1, 1993).

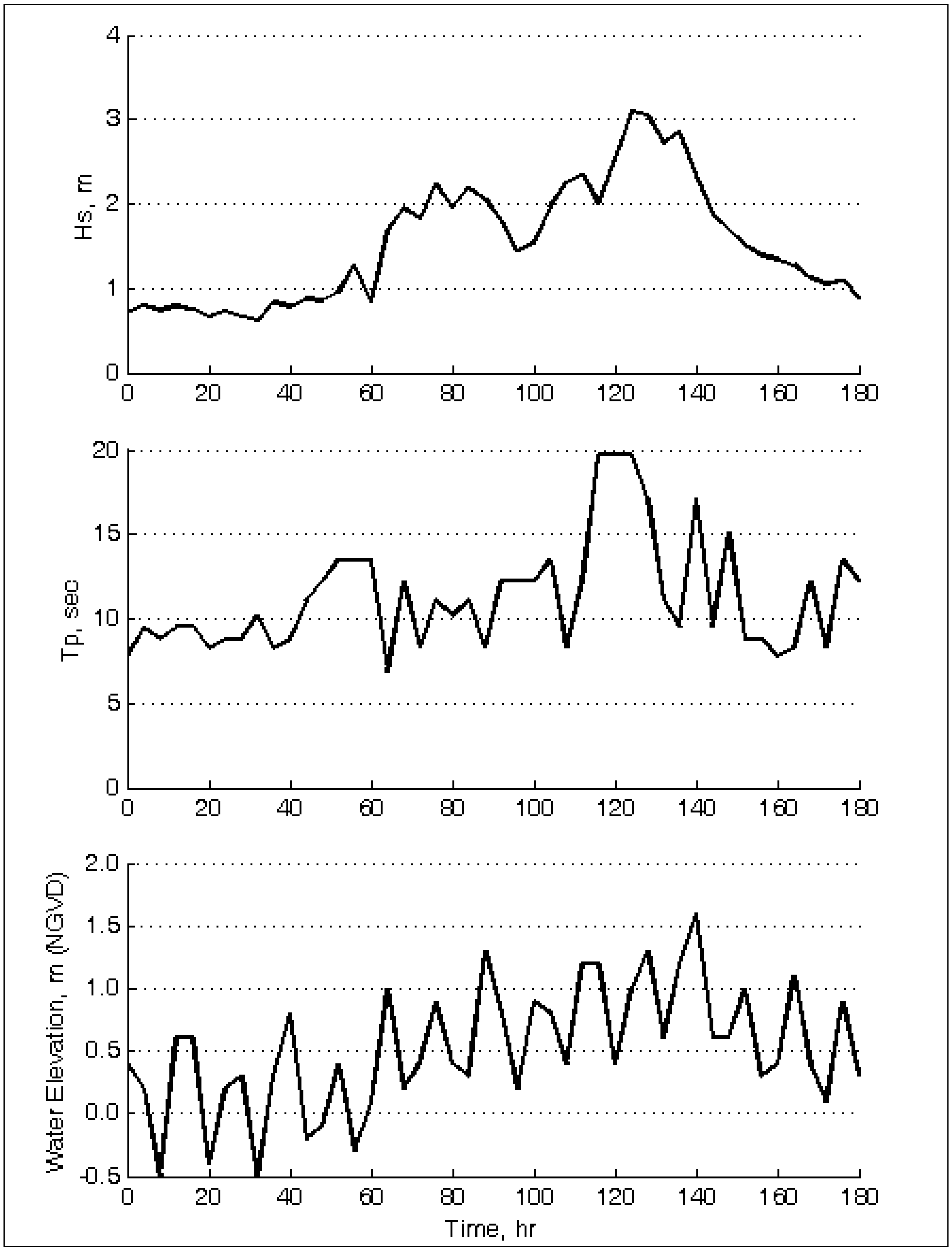

Figure 33. Wave height, wave period, and water elevation time-histories for the Halloween 1991 storm, Ocean City, MD.

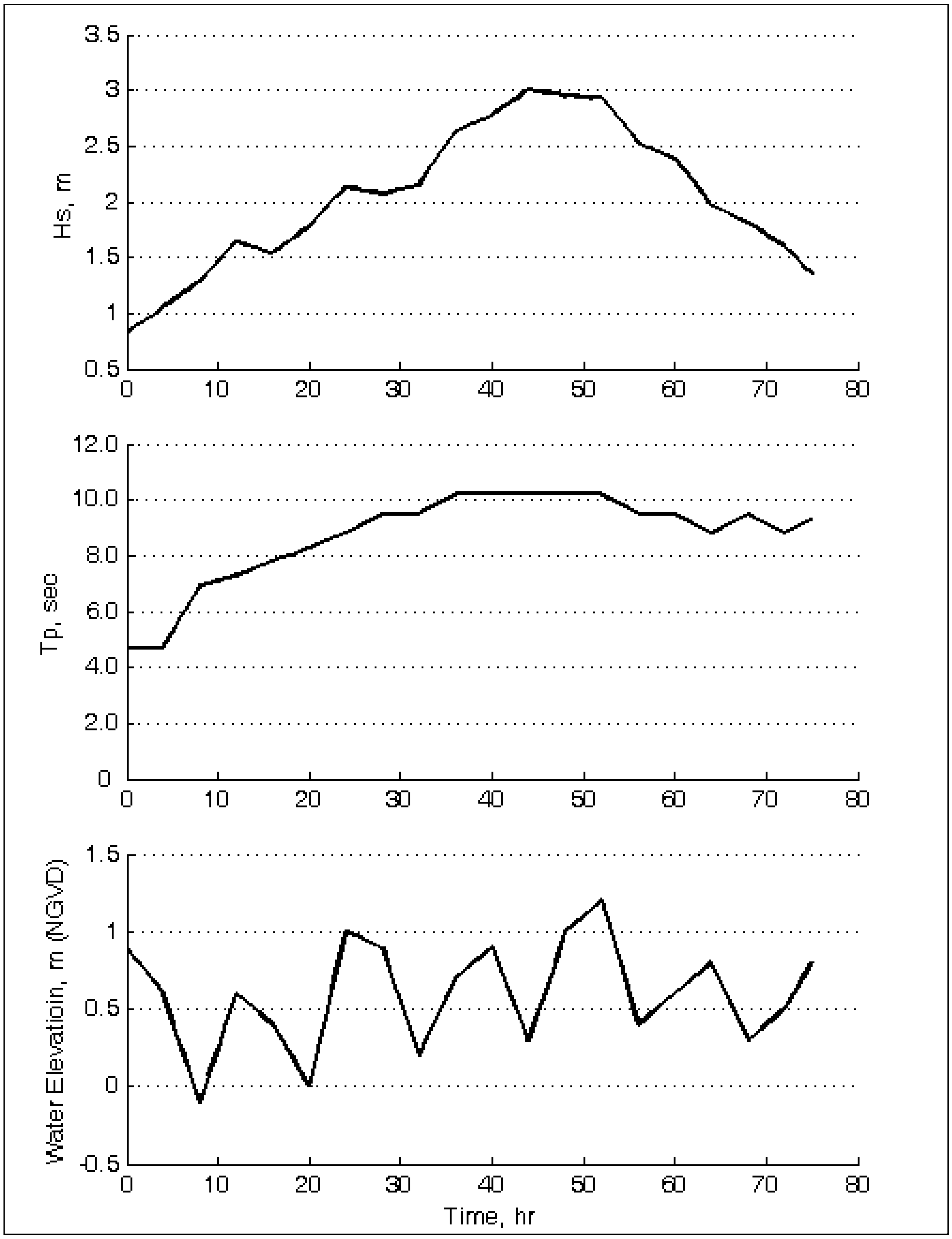

Figure 34. Wave height, wave period, and water elevation time-histories for the 11 November 1991 storm, Ocean City, MD.

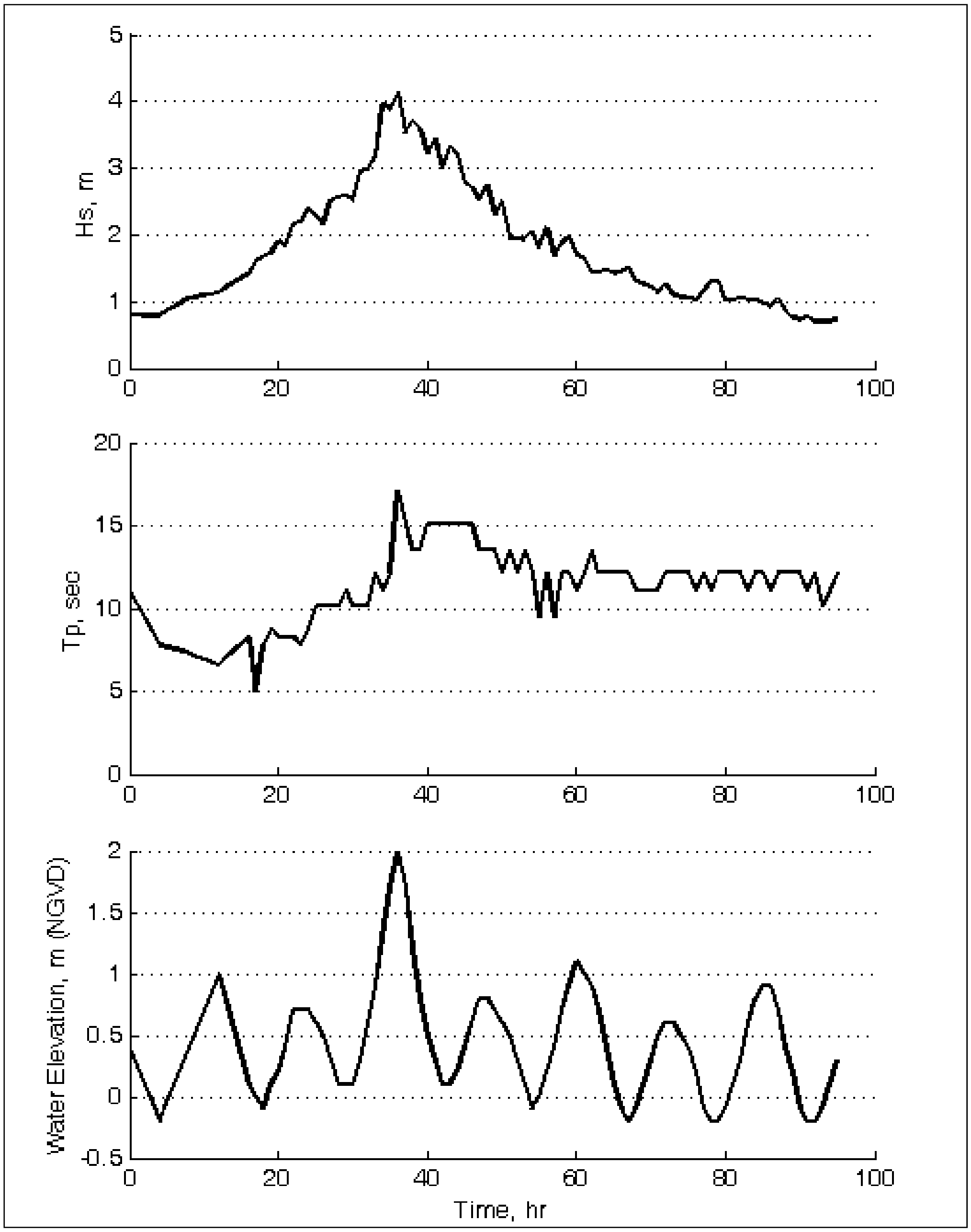

Figure 35. Wave height, wave period, and water elevation time-histories for the 4 January 1992 storm, Ocean City, MD.

Halloween storm. As shown in Figure 33, the Halloween storm produced large waves and high water levels at Ocean City for approximately four days. The maximum measured significant wave height was about 3 m and the peak water level was measured at just over 1.5 m NGVD. Data at six beach profile survey lines were available to model the beach response to the storm. Pre-storm profile surveys were collected in June 1991 and post-storm surveys were collected shortly after the storm. The June surveys were assumed to reasonably characterize the condition of the upper beach profile prior to the storm, as no other significant erosion events occurred between June and October. The storm-induced volume change at each of the six profiles is shown in Figure 36, where it is seen that five of the profiles experienced a net loss of volume and one profile experienced a net gain in volume. The lack of mass conservation at the various profiles indicates that material was redistributed by longshore processes between the surveys. It is believed that most of the sediment redistribution was confined to the subaqueous portion of the profile and that changes on the upper beach profile and dune were dominated by cross-shore sediment transport processes during the storm. Consequently, model results are expected to produce better agreement on the upper beach profile than on the offshore portion of the profile.

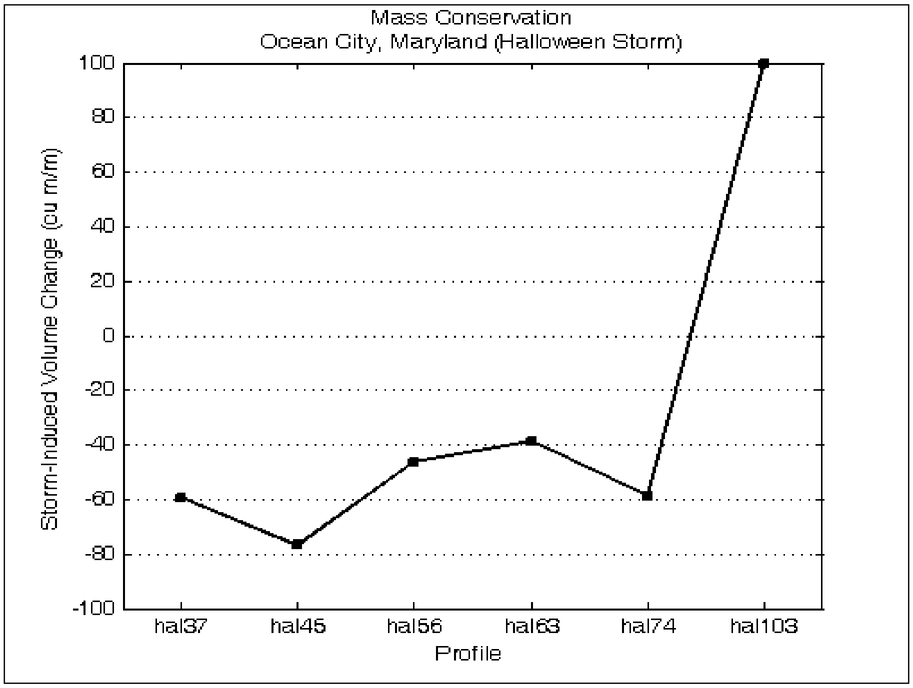

Figure 36. Conservation of mass between beach profile surveys for the Halloween storm, Ocean City, MD.

CSHORE results for the Halloween storm are provided in Figures 37 through 42. The beach profile response to this storm is reasonably well predicted by CSHORE simulations for five of the six profiles. For profiles 37, 63, and 74 predicted erosion above datum compares favorably with the measurements. For profiles 45 and 56, predicted erosion above the datum is slightly less than indicated in the measurements. For profile 103 the predicted erosion largely exceeds the erosion indicated in the measurements. The measured nearshore recovery bar or beach step present in the post-storm profiles is not indicated in the CSHORE results.

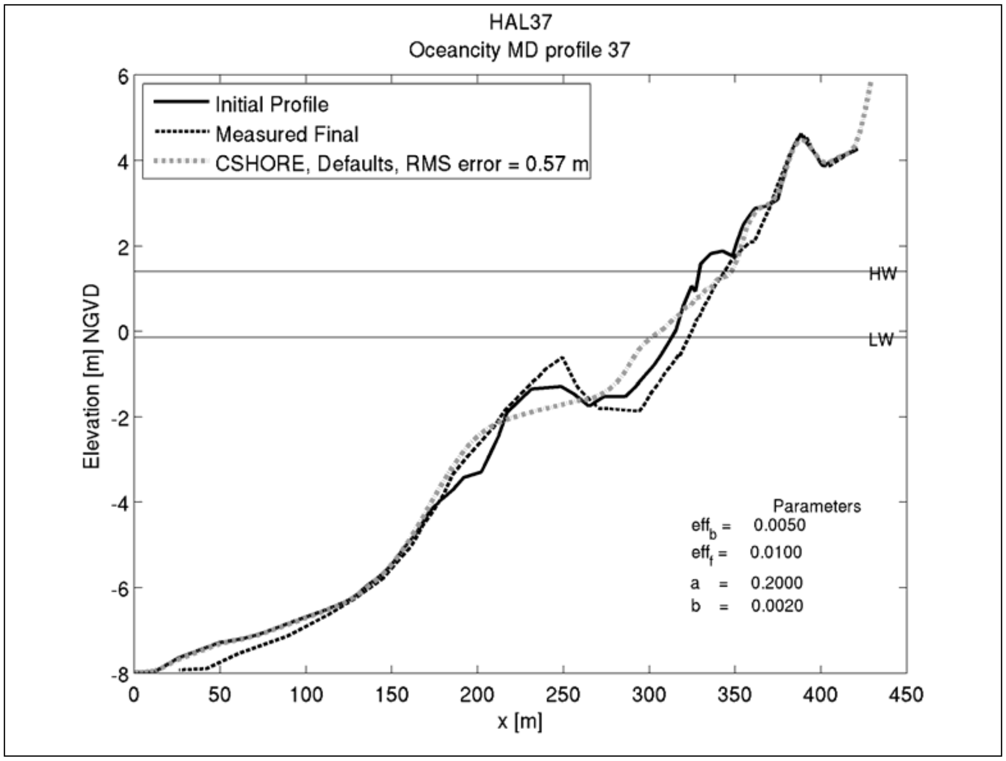

Figure 37. CSHORE simulation of the Halloween storm for Profile 37, Ocean City, MD.

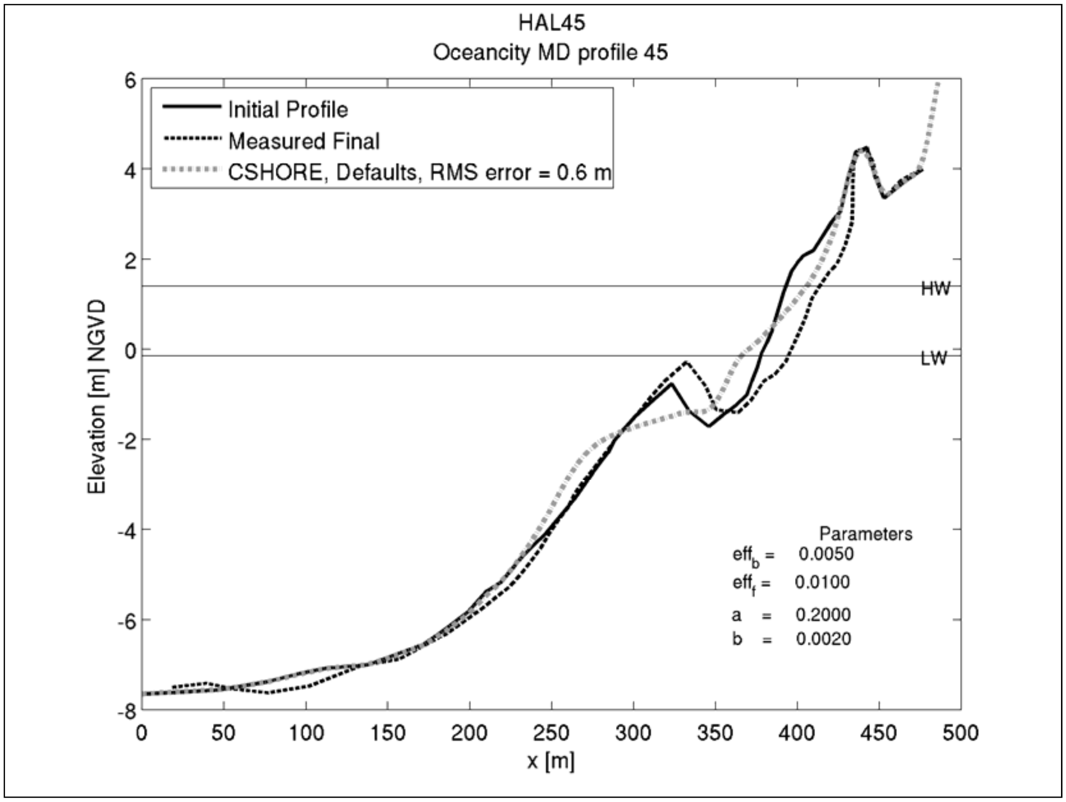

Figure 38. CSHORE simulation of the Halloween storm for Profile 45, Ocean City, MD.

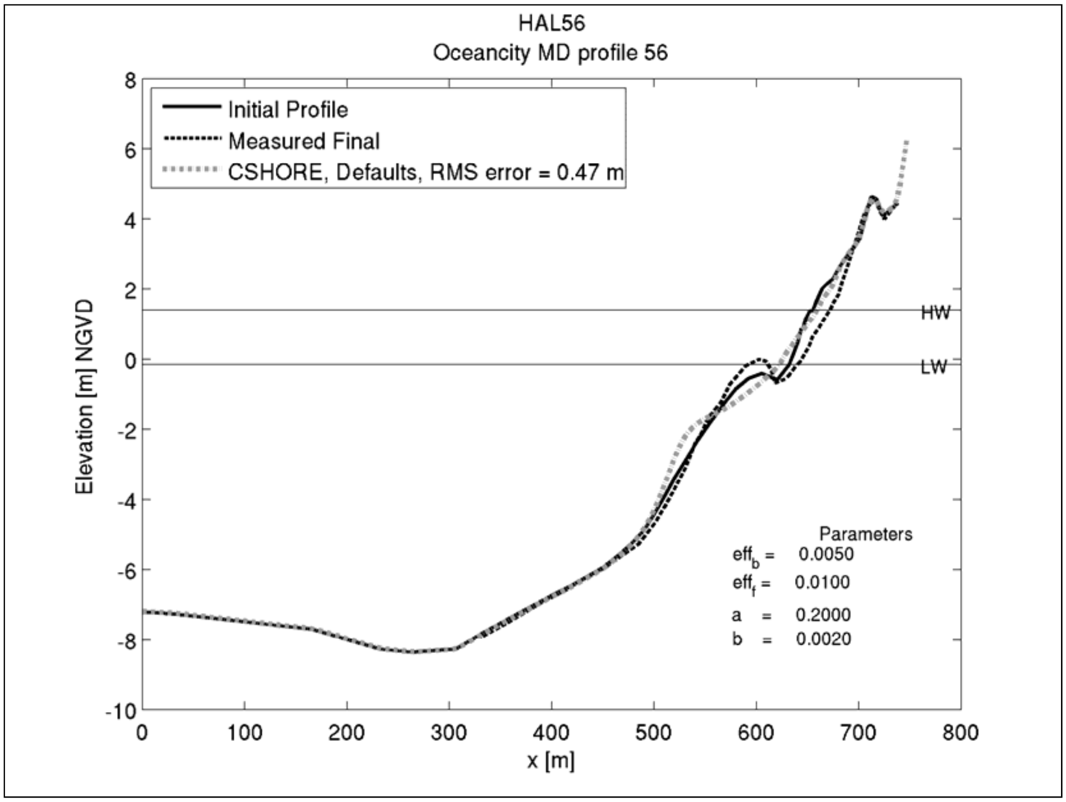

Figure 39. CSHORE simulation of the Halloween storm for Profile 56, Ocean City, MD.

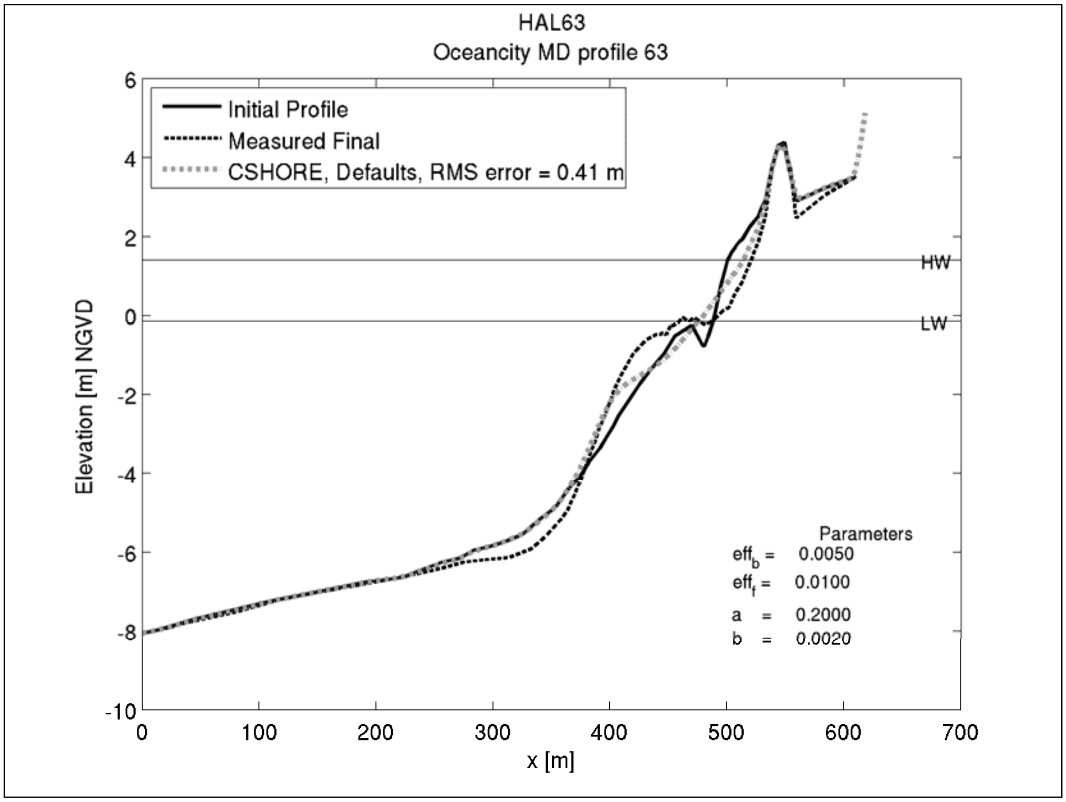

Figure 40. CSHORE simulation of the Halloween storm for Profile 63, Ocean City, MD.

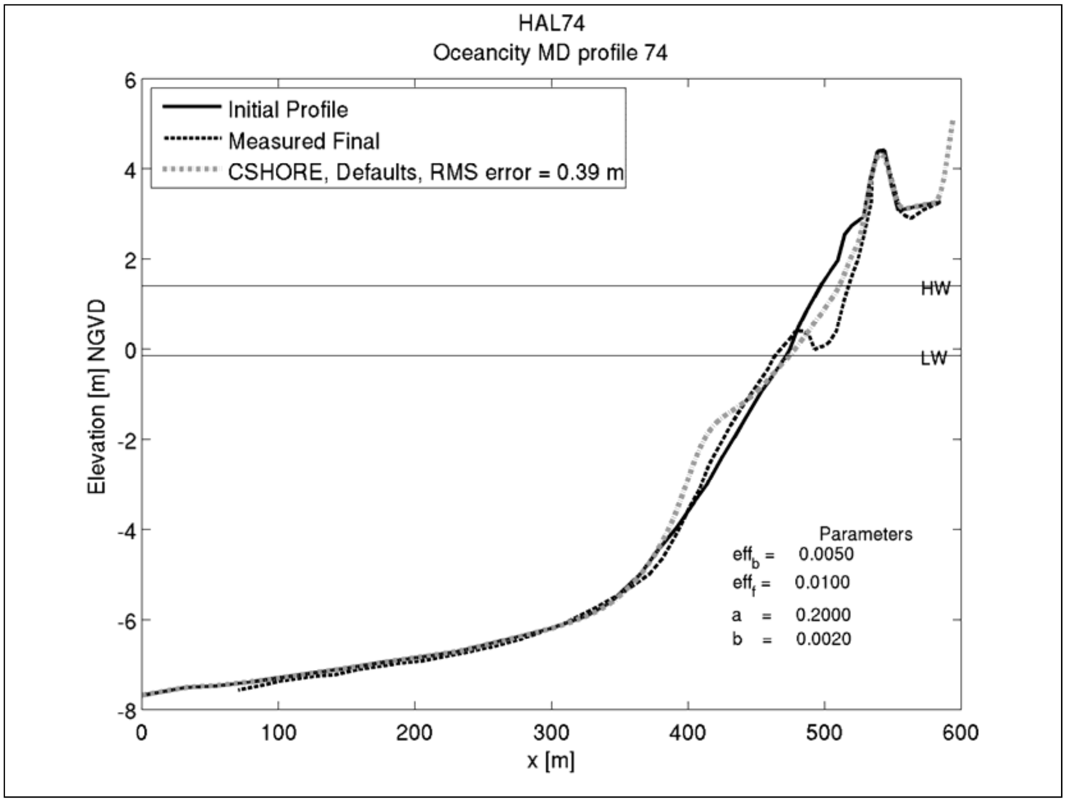

Figure 41. CSHORE simulation of the Halloween storm for Profile 74, Ocean City, MD.

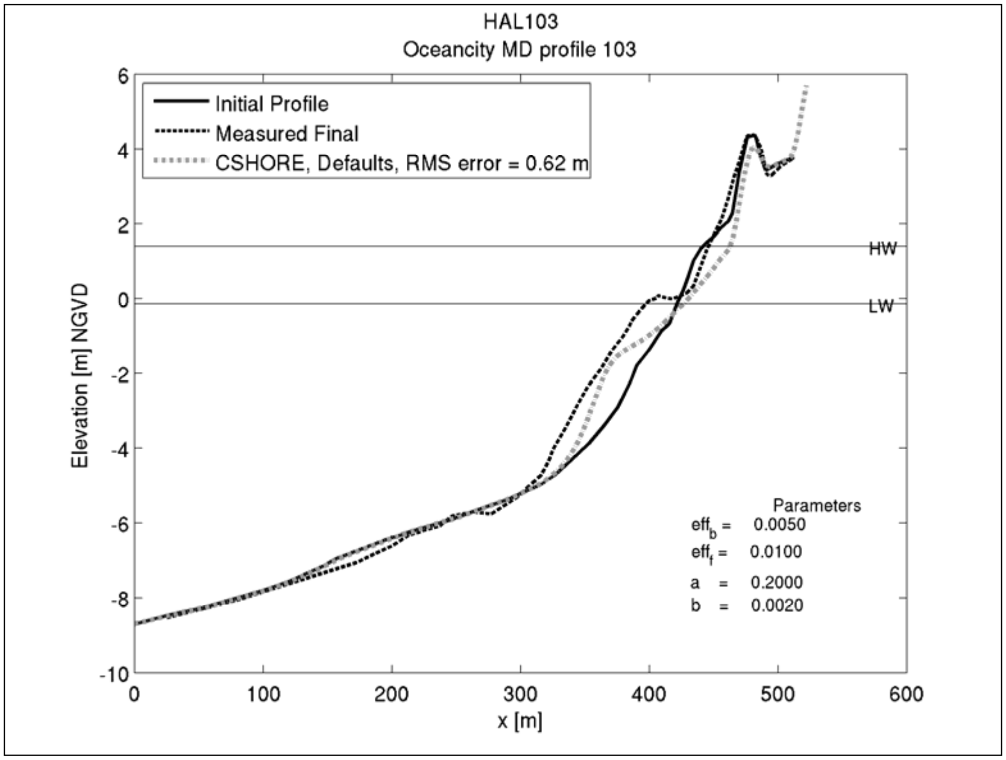

Figure 42. CSHORE simulation of the Halloween storm for Profile 103, Ocean City, MD.

Figures 43 - 45 provide plots of the quantitative model performance measures described above. Figure 71 shows that although the calculated volumetric erosion above NGVD is generally under estimated, the measured profile to profile trends were followed except for profile 103.

Figure 44 shows the measured and calculated recession of the 1.5 m contour. Here it is seen that for four of the six profiles the predicted recession of the 1.5 m contour is within about five or six meters of the measured with a bias for under prediction. The comparisons for profiles 56 and 103 are not as good with an under prediction of about 12 m at profile 56 and an over prediction of about 17 m at profile 103. It is noted that profile 103 gained approximately 100 cu m/m between the pre- and post-storm surveys, which indicates that this profile was heavily influenced by non-uniform longshore sediment transport processes and may explain why the CSHORE predictions are poorest at this profile. Figure 45 shows the comparison between the measured and calculated storm intrusion of the 0.3-m depth of erosion. The difference between the calculated and measured storm intrusion distance is less than about 10 m except for at profile 103, which is considered reasonably good agreement.

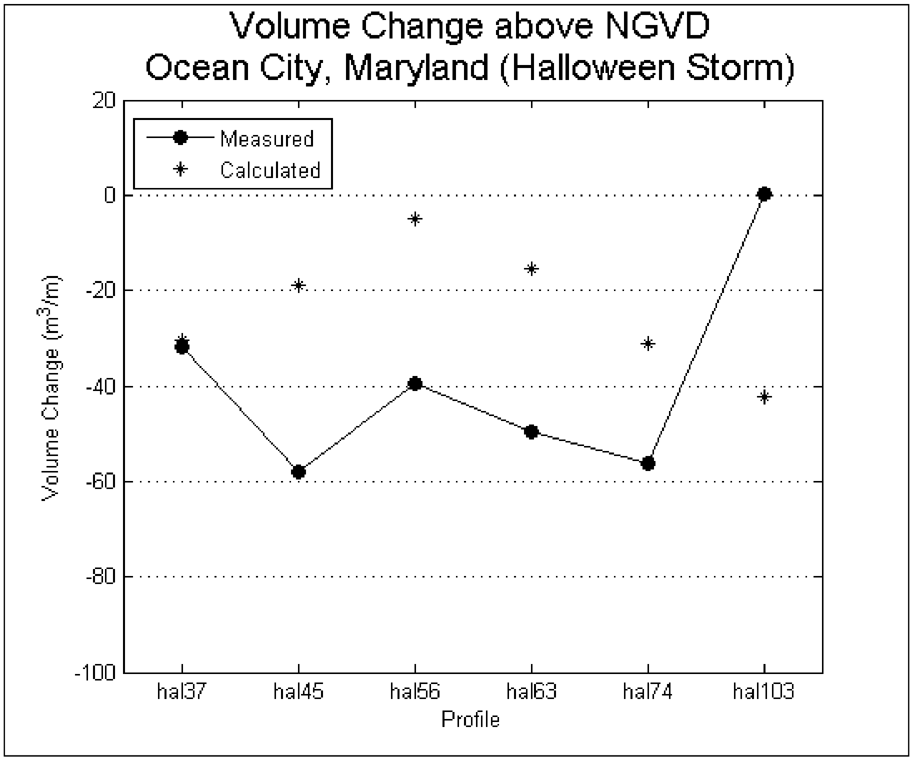

Figure 43. Comparison of measured and calculated volume change above NGVD for the Halloween storm, Ocean City, MD.

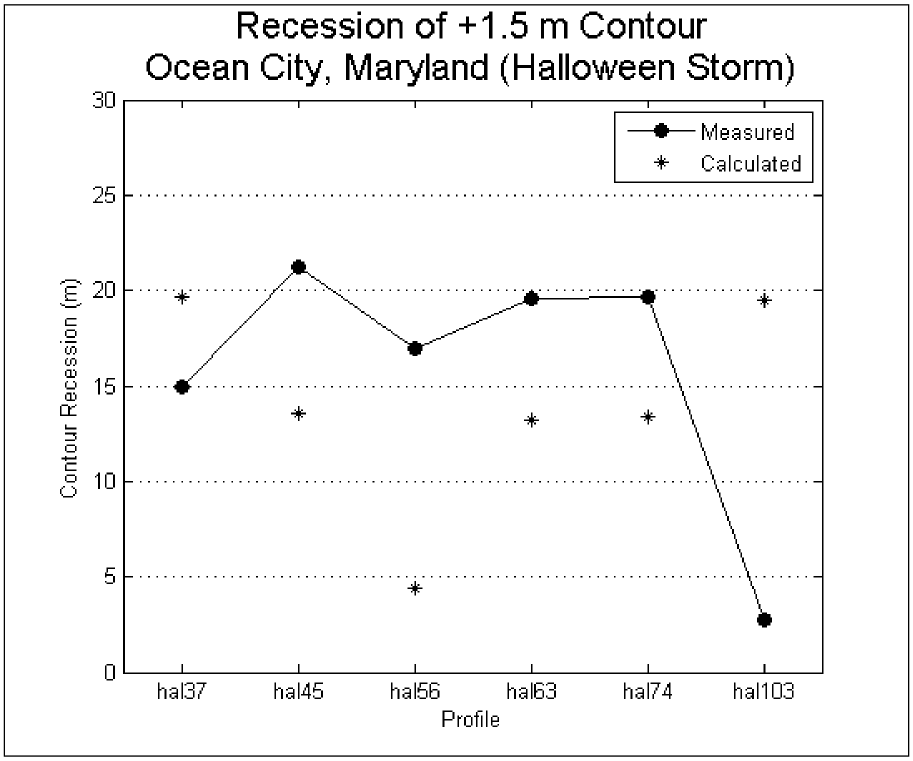

Figure 44. Comparison of measured and calculated recession of the 1.5 m contour for the Halloween storm, Ocean City, MD.

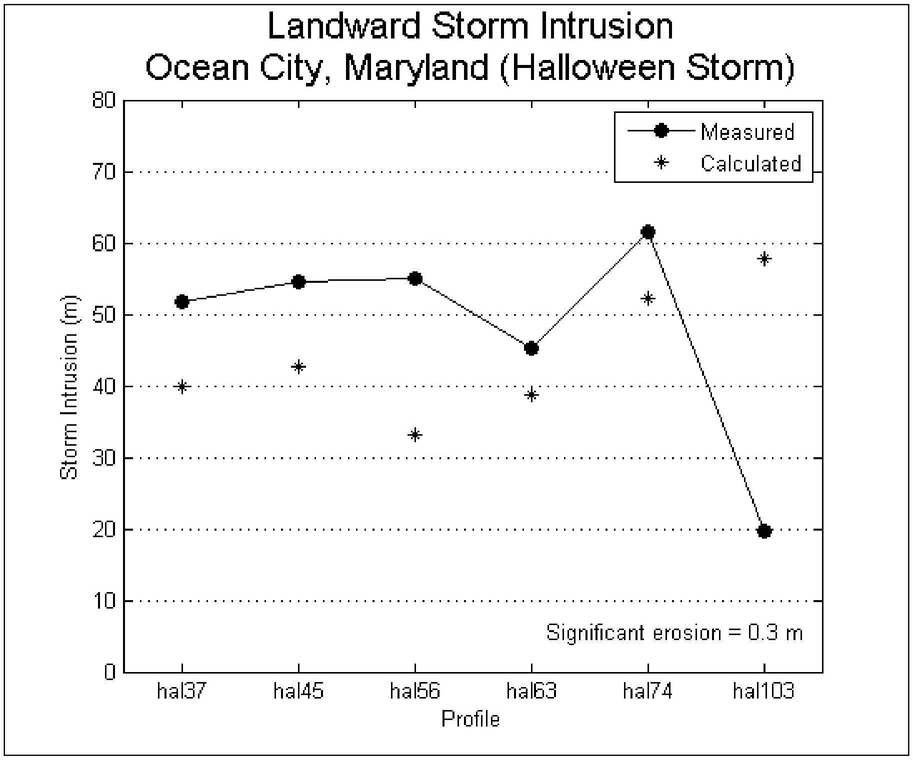

Figure 45. Comparison of measured and calculated storm intrusion for the Halloween storm, Ocean City, MD.

November-January storms. The November-January (NJ) cases involved a combined simulation of the 11 November 1991 storm and the 4 January 1992 storm. It was necessary to combine the two storms because beach profile data were not available between the two events. The wave height and water level time histories are shown in Figures 34 and 35. As indicated in the figures the duration of both storms was approximately three days. The November storm involved a sustained maximum significant wave height of approximately 3 m for about 10 hours and a peak total water elevation of 1.2 m NGVD. The January storm was somewhat more energetic than the November storm with significant wave heights exceeding 3 m for a 15 hour duration peaking at approximately 4 m. The peak total water elevation was measured at 2 m. The January storm is the most energetic of the three Ocean City storms included in this study in terms of maximum significant wave height and peak total water elevation and this storm also produced the most damage in terms of erosion on the upper beach profiles.

For the NJ simulations the beach profiles measured after the Halloween storm served as the pre-storm profiles and beach profile surveys collected soon after the January storm provided the post-storm profiles used for comparison with the model results. Figure 46 illustrates the degree of mass conservation between the pre- and post-storm surveys. Here it is seen that profiles 37 and 103 gained considerable mass between the survey interval whereas mass is nearly conserved at the other profile lines.

The measured and CSHORE predicted beach profile response for the NJ storm series is shown in Figures 47 through 52. These figures indicated that the NJ storm series produced significant dune overwash, a reduction in dune crest elevation and a landward translation of the dune crest at profiles 45, 63, 74 and 103. Although the CSHORE simulations for these profiles included hydrodynamic overtopping of the dune crest the predicted dune crest lowering is far less than indicated in the measurements and no landward translation of the dune crest was predicted. Sensitivity testing showed that the predicted dune lowering could be increased by increasing the value of the breaker ratio γ. However, use of a larger breaker ratio specification in other simulations resulted in predicted dune crest lowering in cases where the measurements indicate no dune crest lowering. These findings indicate that improvements are needed in CSHORE in the area of dune overtopping and overwash processes.

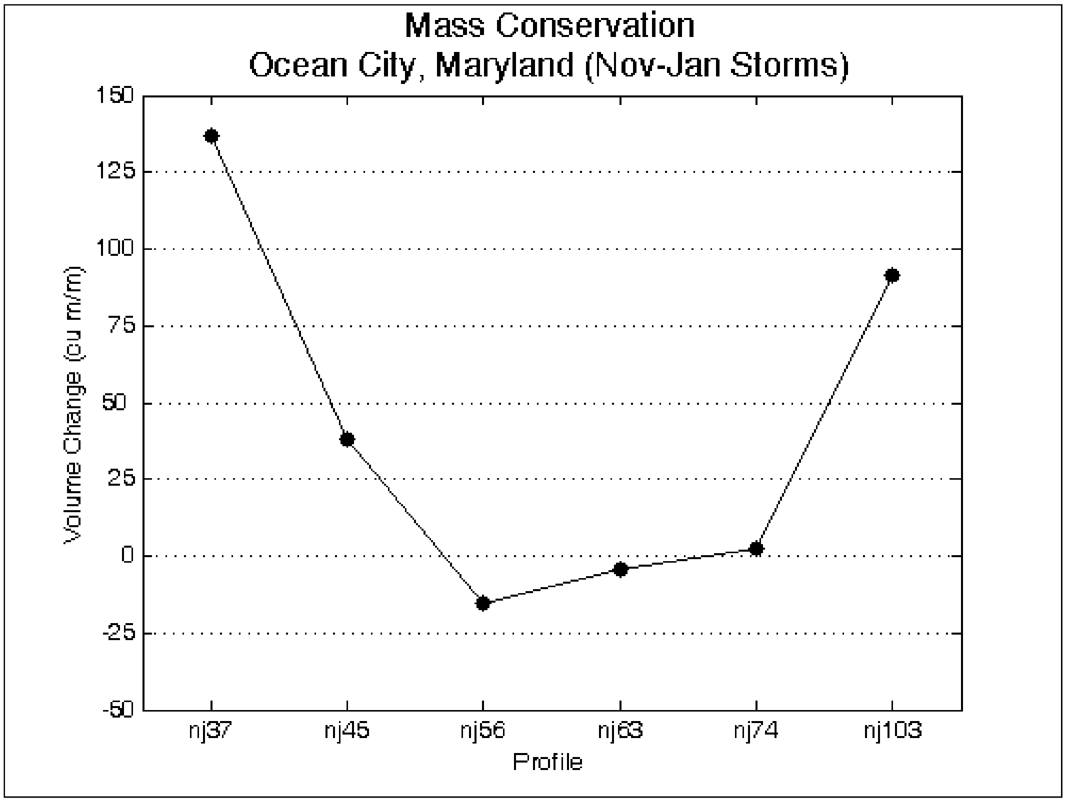

Figure 46. Conservation of mass between beach profile surveys for the NJ storm series, Ocean City, MD.

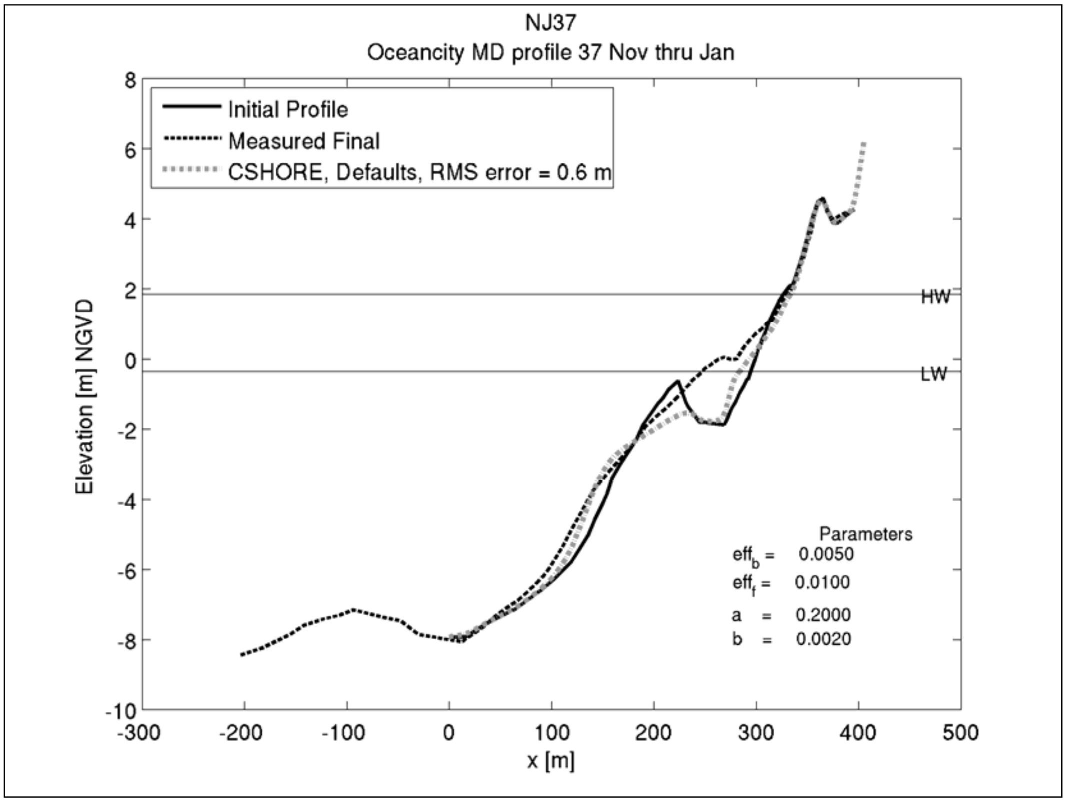

Figure 47. CSHORE simulation of the NJ storm series for Profile 37, Ocean City, MD.

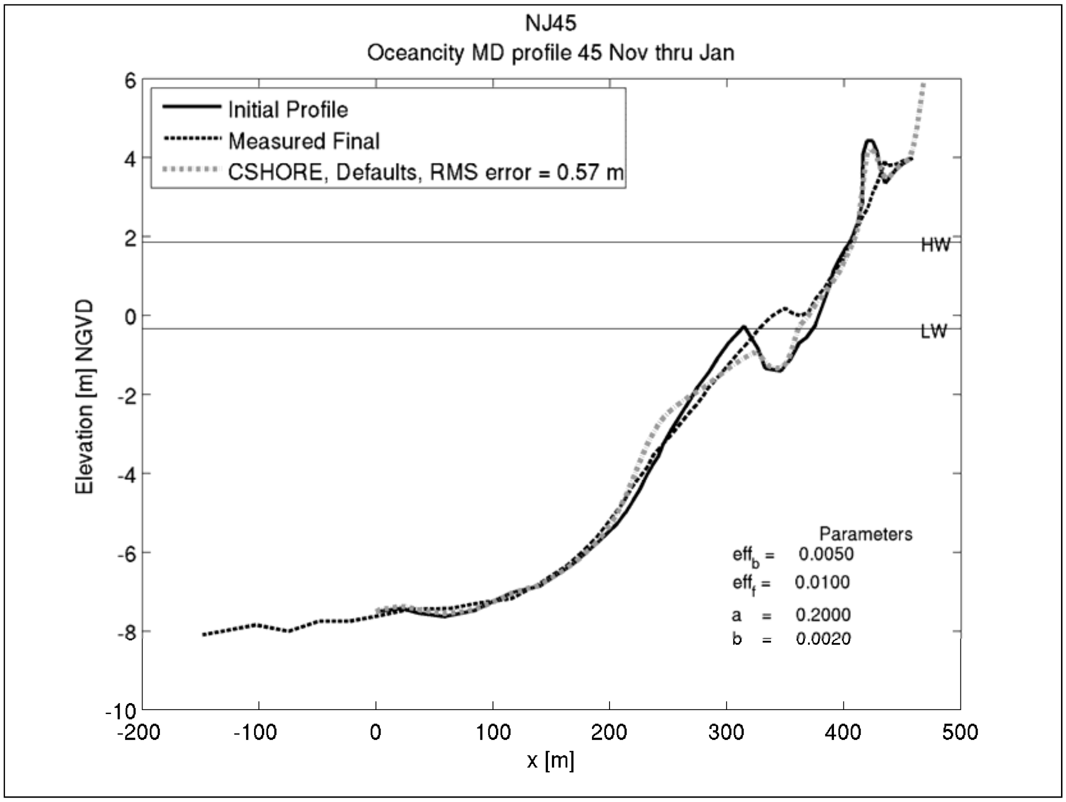

Figure 48. CSHORE simulation of the NJ storm series for Profile 45, Ocean City, MD.

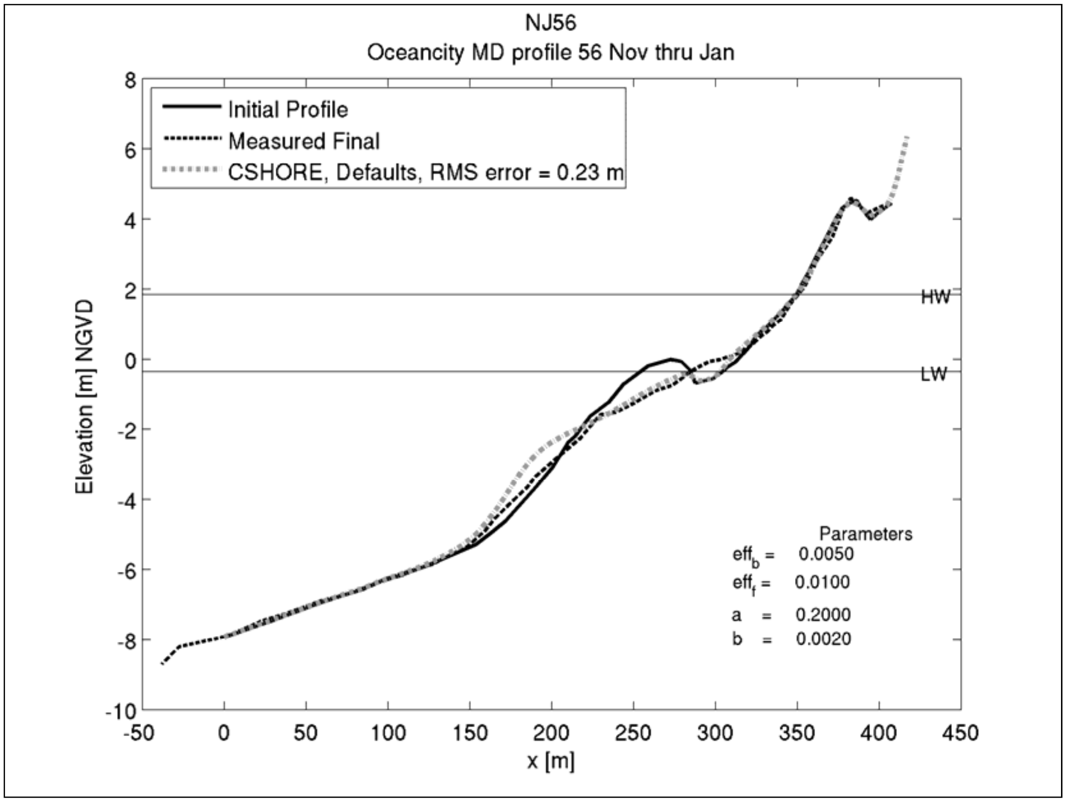

Figure 49. CSHORE simulation of the NJ storm series for Profile 56, Ocean City, MD.

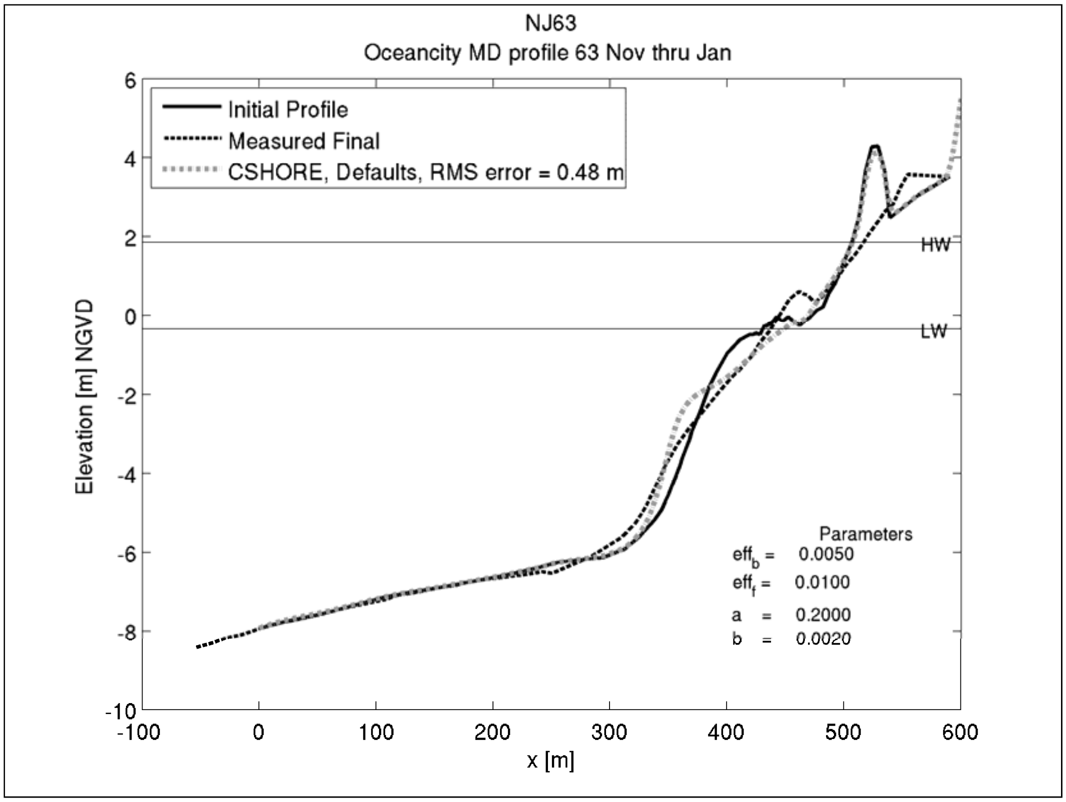

Figure 50. CSHORE simulation of the NJ storm series for Profile 63, Ocean City, MD.

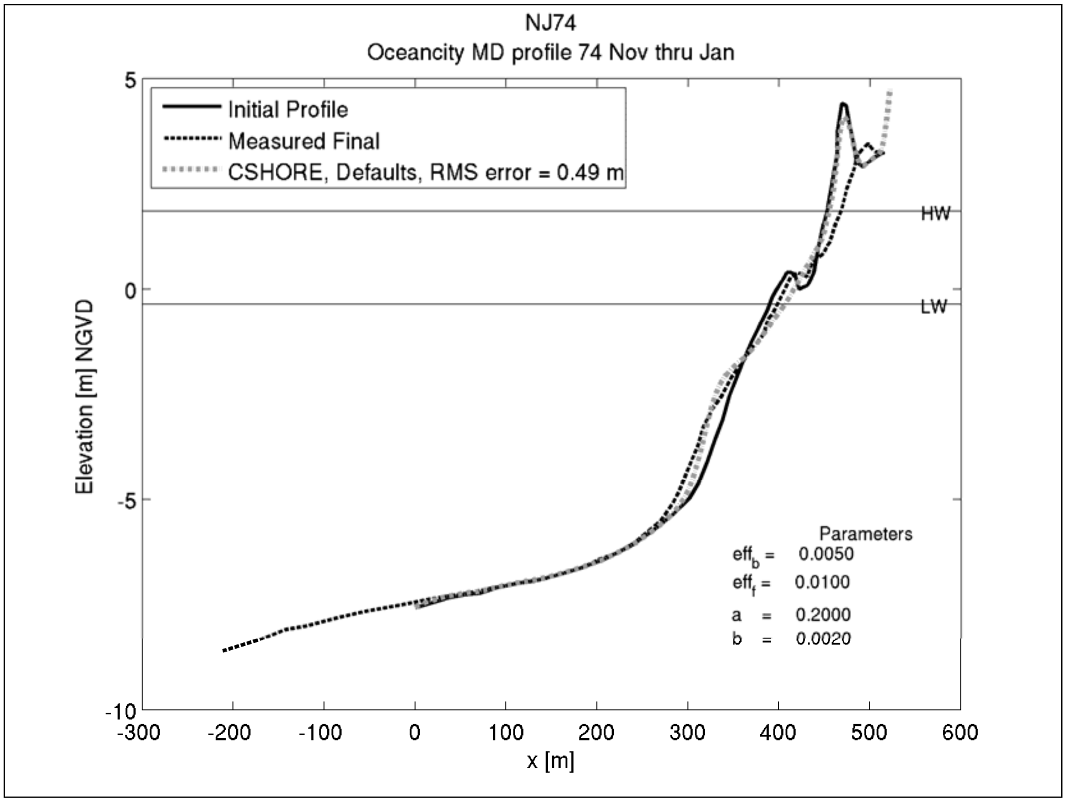

Figure 51. CSHORE simulation of the NJ storm series for Profile 74, Ocean City, MD.

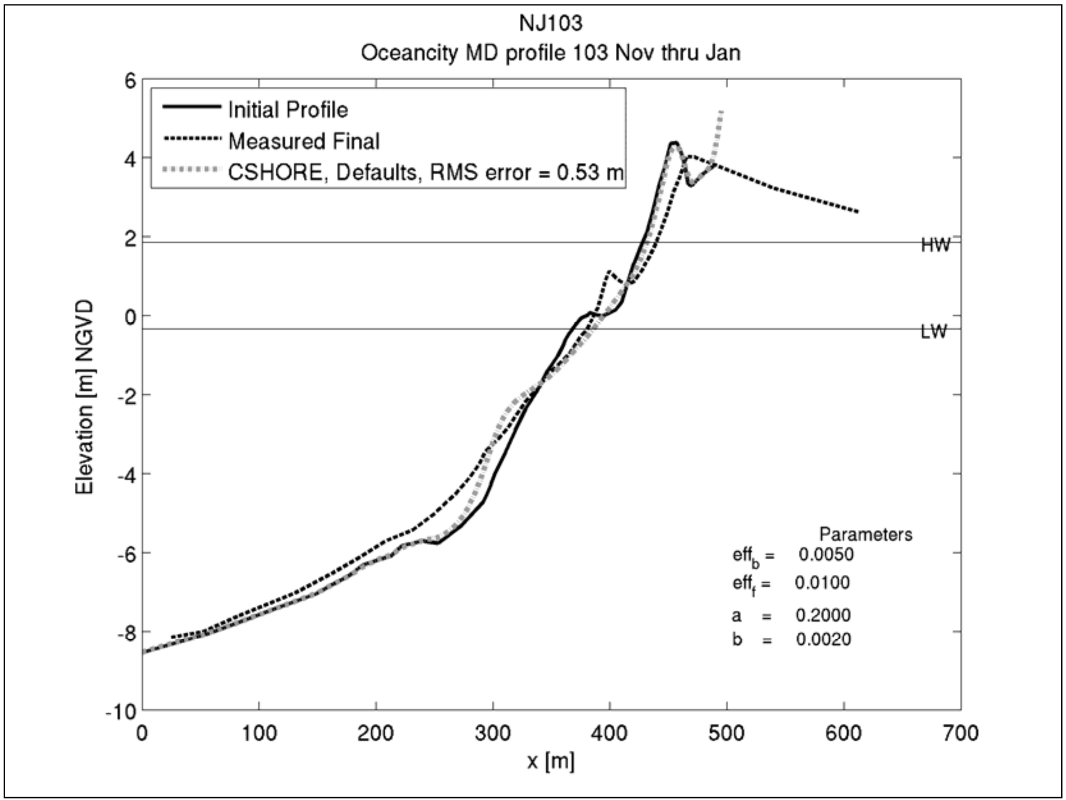

Figure 52. CSHORE simulation of the NJ storm series for Profile 103, Ocean City, MD.

The quantitative model performance measures are illustrated in Figures 53 through 55. In Figure 53 it is seen that the measured and predicted volume change above NGVD compare favorably at profiles 45, 63, and 103 even though the predicted and measured profiles do not. At profile 56 the predicted volume change above NGVD as well as the predicted profile compare well with the measurements. At profile 37 the measurements indicate a net gain of approximately 8 cu m/m whereas the CSHORE simulation estimated a net loss of more than 20 cu m/m. At profile 74 CSHORE underestimates volume loss above NGVD by nearly 25 cu m/m presumably a result of the lack of predicted dune lowering due to dune overwash processes. Figure 54 shows the measured and simulated recession of the 2.5 m contour. The CSHORE simulations indicate recession of the 2.5 m contour at less than 5 m at profiles 37, 45, 56 and 103 whereas the measurements indicate erosion of the 2.5 m contour at 10 to 20 m at the profiles 63 and 74. Measured and computed landward storm intrusion are compared in Figure 55 which, shows that CSHORE predicts a landward storm intrusion that compares favorably to measurements at profiles 45, 74, and 103 but does not simulate the landward storm intrusion well at the other profiles.

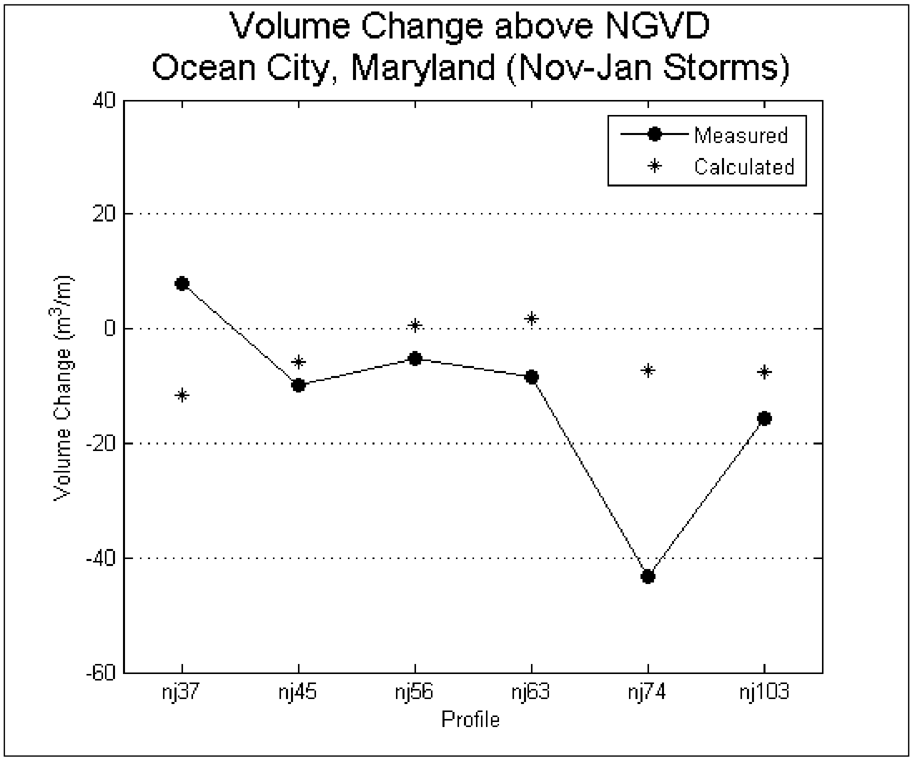

Figure 53. Comparison of measured and simulated volume change above NGVD for the NJ storm series, Ocean City, MD.

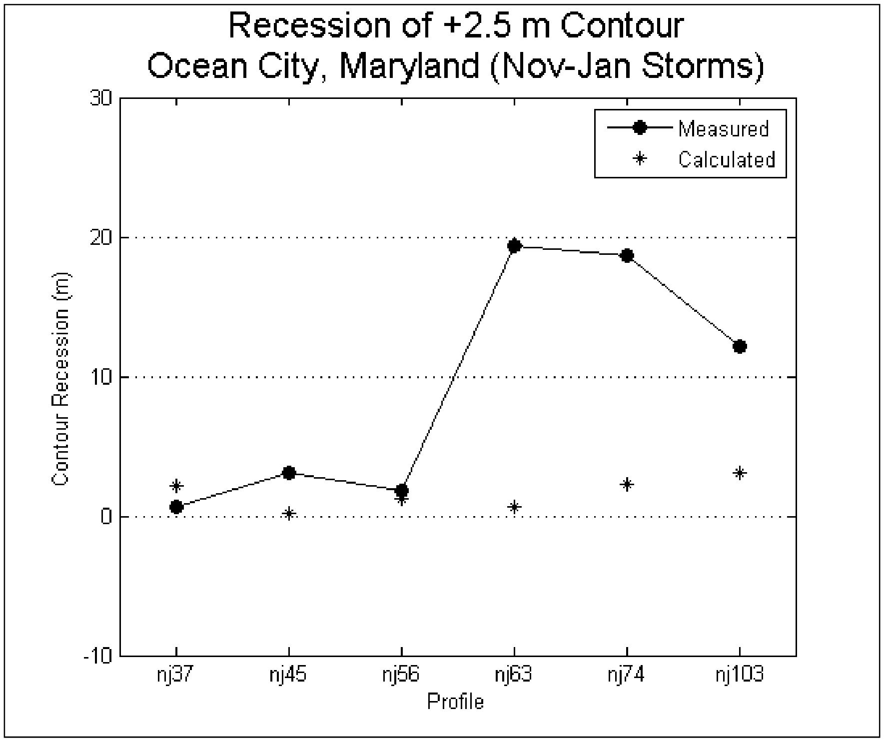

Figure 54. Comparison of measured and simulated recession of the 2.5-m contour for the NJ storm series, Ocean City, MD.

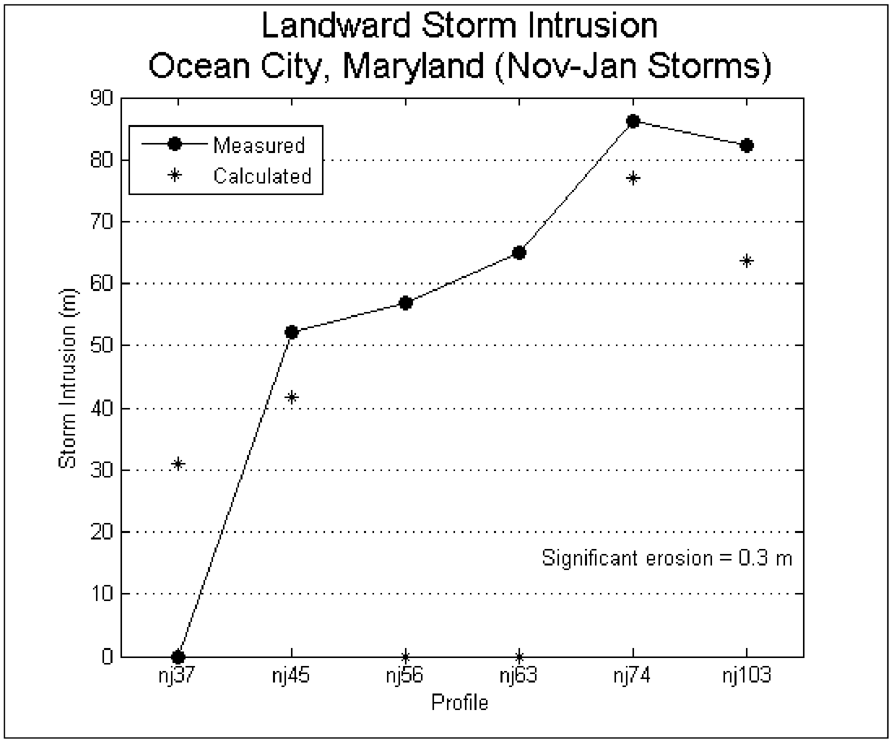

Figure 55. Comparison of measured and simulated storm intrusion for the NJ storm series, Ocean City, MD

October-January storms. The October-January (OJ) cases involved the simulation of the entire three storm sequence for four profile lines that were not surveyed in November 1991 between the Halloween and November storms. For these cases, the pre-storm profiles were from the June 1991 surveys and the post-storm profiles were obtained from the surveys performed after the January storm. Figure 56 shows the extent to which mass was conserved between the pre- and post-storm profiles. Although mass was more or less conserved at profiles 52, 81, and 86, profile 92 gained considerable volume between the surveys.

The CSHORE simulation results for the OJ storm series are shown in Figures 57 through 60. These figures show that the CSHORE simulations provide a good reproduction of the measured storm induced beach profile change in the absence of dune overwash processes. The measured beach profile response for profiles 52 and 92 are reasonably well estimated whereas, the measured dune lowering observed at profiles 81 and 86 is not reproduced by the CSHORE predictions.

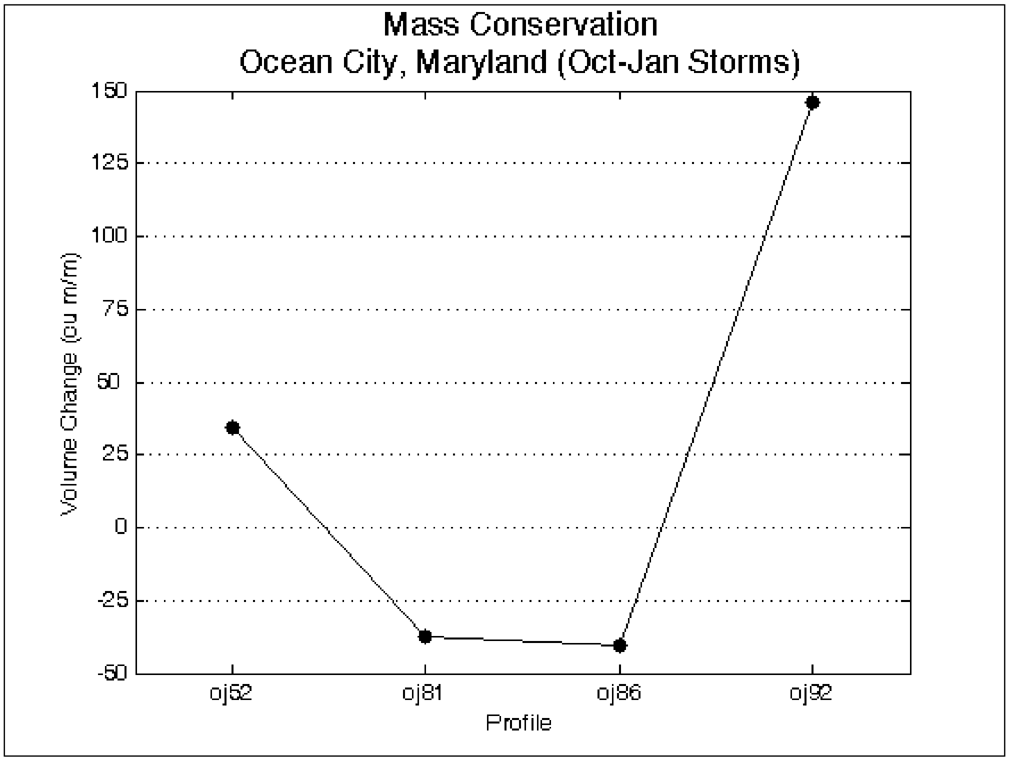

Figure 56. Conservation of mass between beach profile surveys for the OJ storm series, Ocean City, MD.

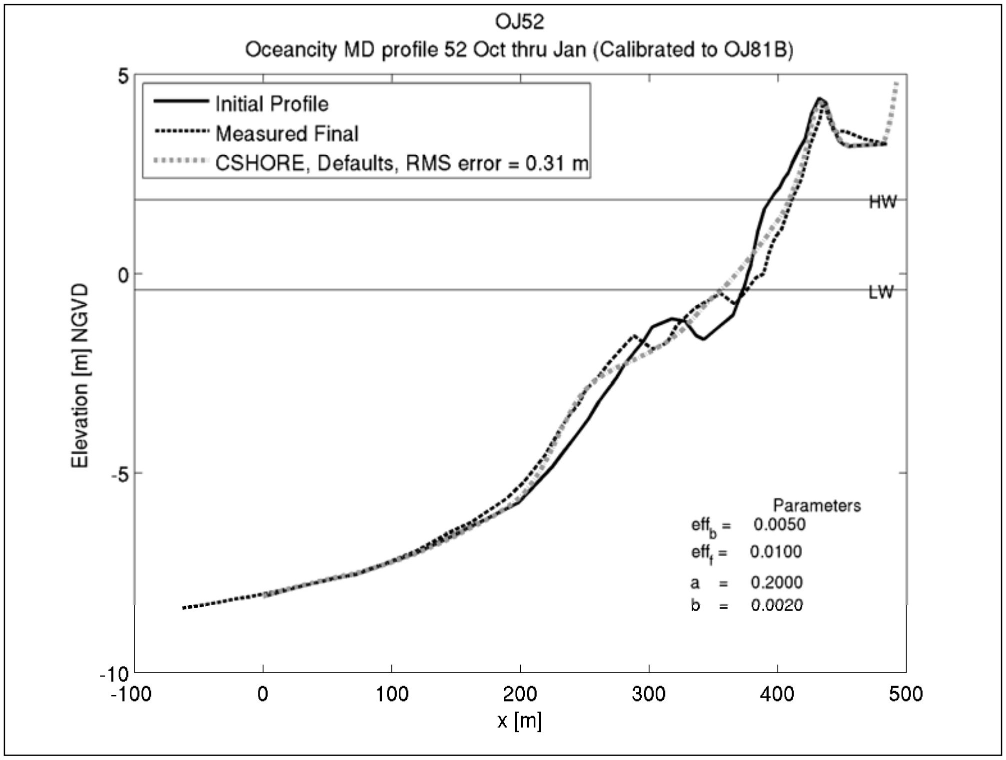

Figure 57. CSHORE simulation of the OJ storm series for profile 52, Ocean City, MD.

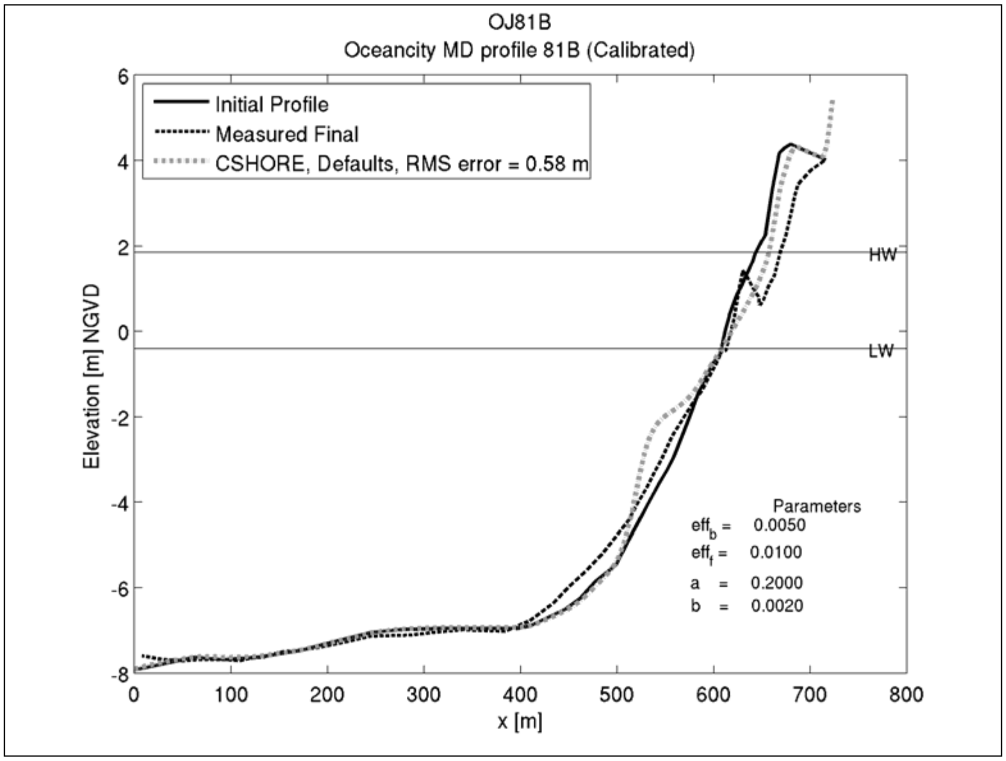

Figure 58. CSHORE simulation of the OJ storm series for profile 81 Ocean City, MD.

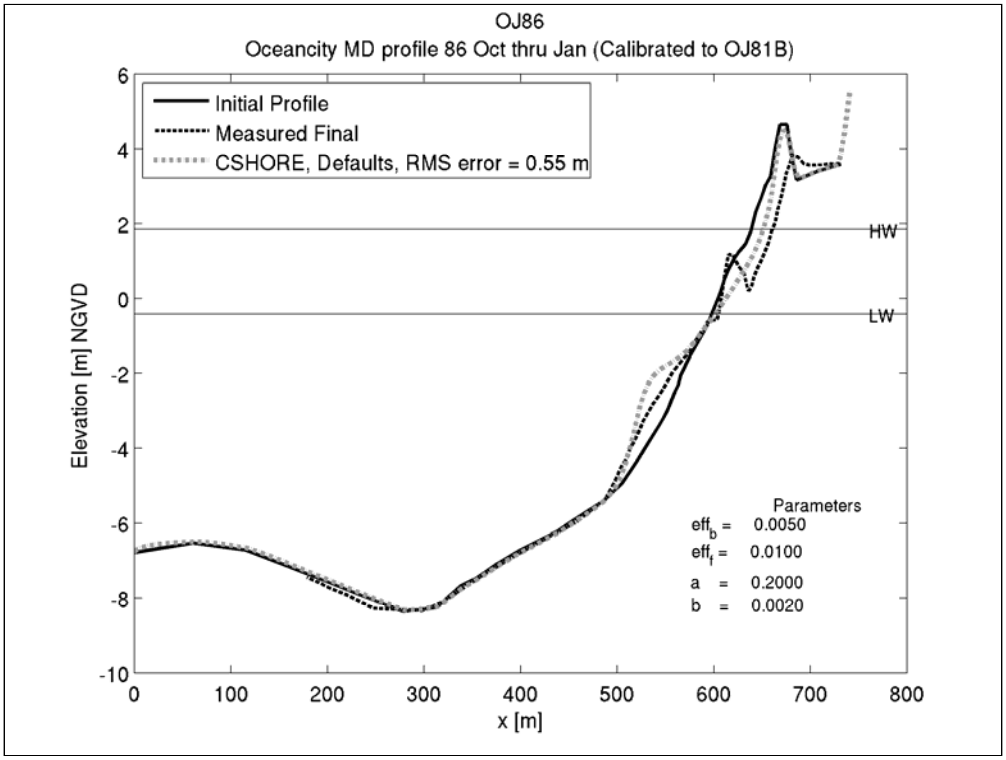

Figure 59. CSHORE simulation of the OJ storm series for profile 86, Ocean City, MD.

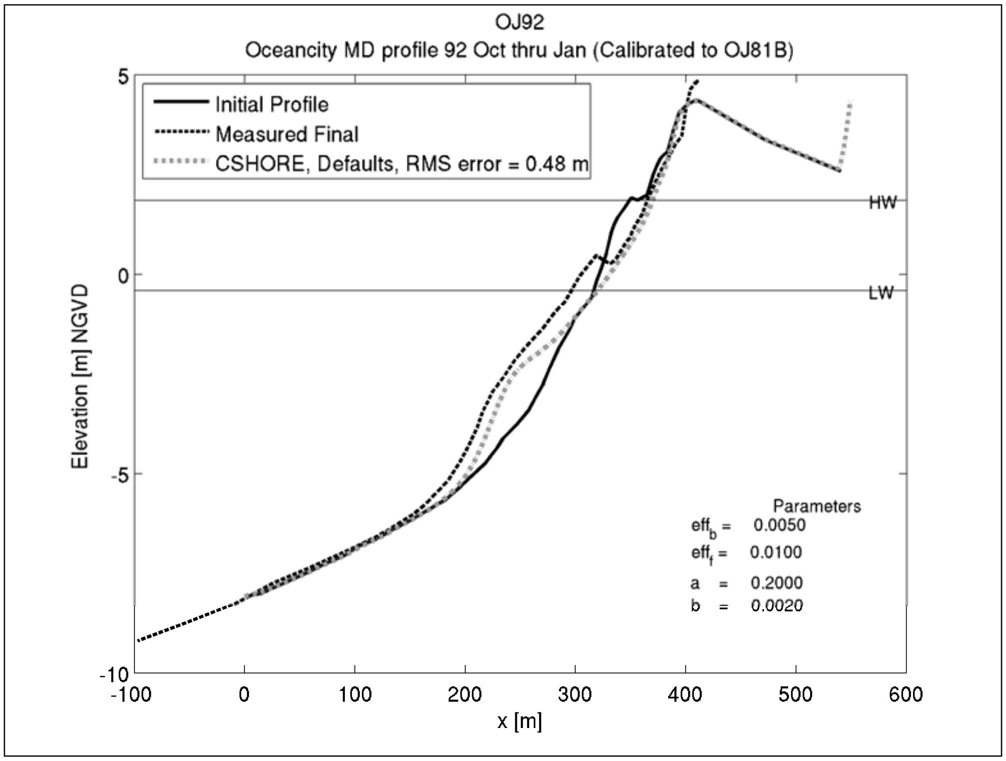

Figure 60. CSHORE simulation of the OJ storm series for profile 92, Ocean City, MD.

The quantitative model performance measures for the OJ storm series cases are illustrated in Figures 61 through 63. In Figure 61 it is seen that the CSHORE predicted volume change above NGVD is within 15 to 20 cu m/m at all profiles except profile 81. Measured and computed recession of the 2.5-m contour is compared in Figure 62 where excellent agreement is observed at profiles 52 and 92, poorest at profile 81 and agreement within about 8 m is observed at profile 86. The predicted and measured storm intrusion distances shown in Figure 63 are within about 10 m at profiles 52 and 86, less than 20 m at profile 92, and just over 20 m at profile 81. It is noted that the measurements show a considerable alongshore variation in the beach profile response between the various profiles whereas the model results are more consistent. These differences can be at least partially explained by noting that the environmental forcing (waves and water levels) in CSHORE is constant between the profiles, whereas the measurements reflect non-uniform beach profile response that arises from non-uniform forcing due to known irregularities in the nearshore bathymetry offshore of Ocean City, MD (see Stauble et al. 1993). Specifically, profiles 81 and 86, are known to lie in an erosional hot spot area that is believed to be associated with offshore shore oblique shoals.

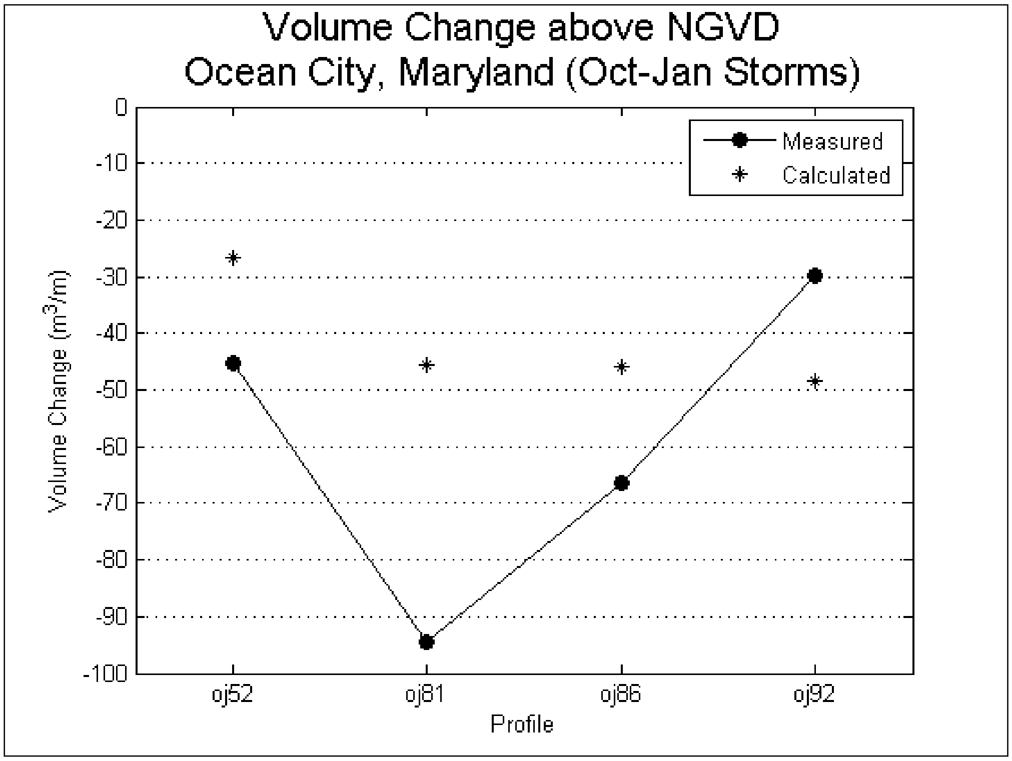

Figure 61. Comparison of measured and simulated volume change above NGVD for the OJ storm series, Ocean City, MD.

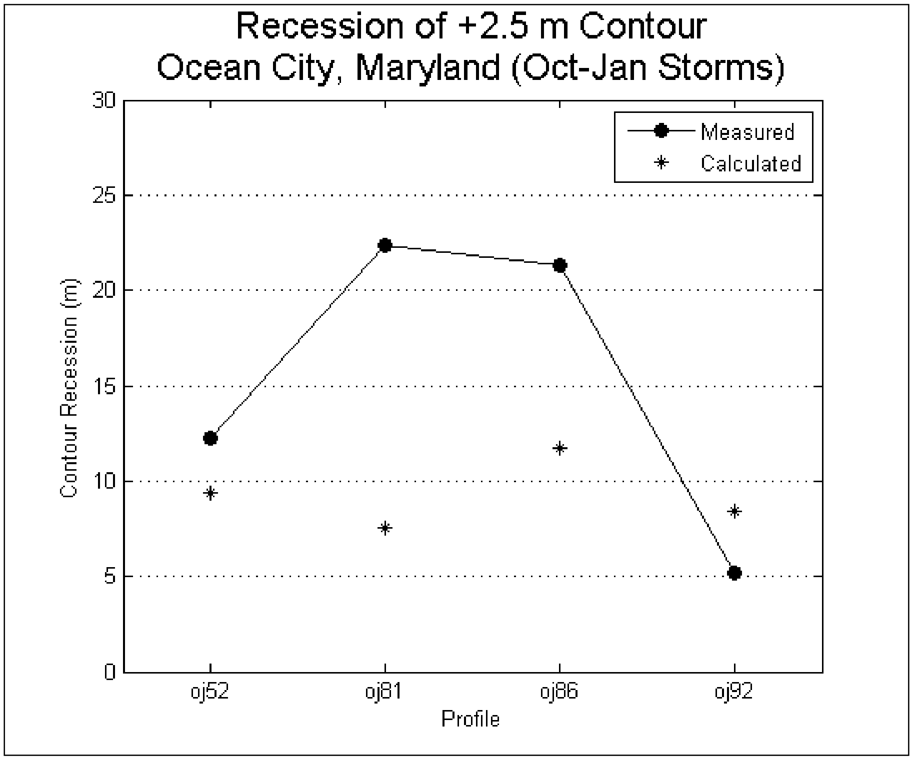

Figure 62. Comparison of measured and simulated recession of the 2.5-m contour for the OJ storm series, Ocean City, MD.

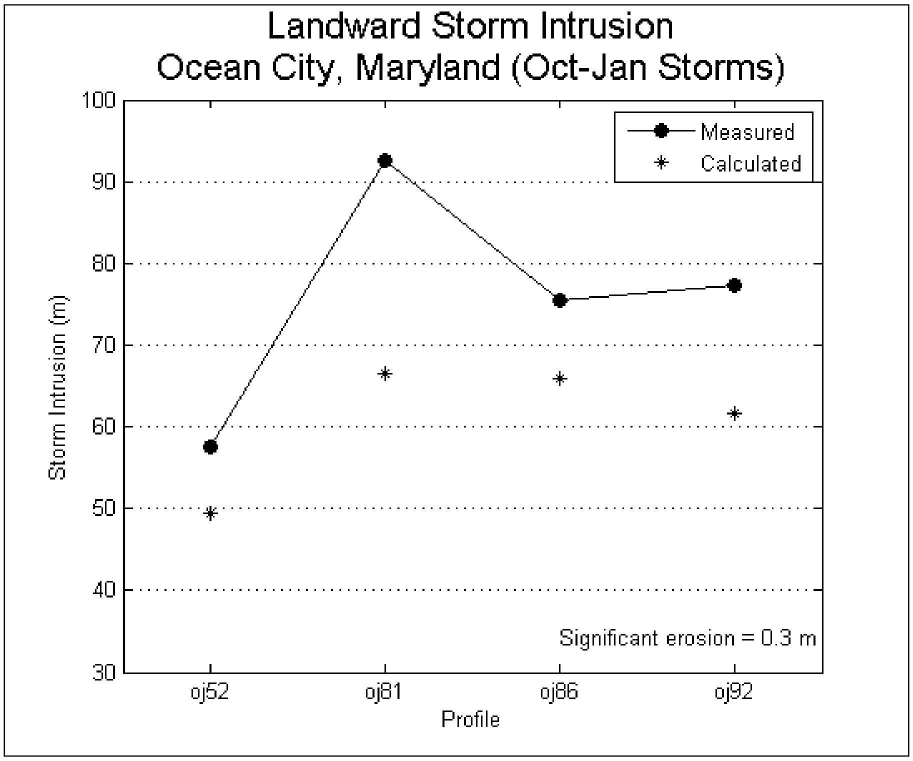

Figure 63. Comparison of measured and simulated storm intrusion for the OJ storm series, Ocean City, MD.

Manasquan and Point Pleasant Beach, NJ

Manasquan and Point Pleasant Beach are the coastal communities immediately to the north and south of Manasquan Inlet on the Atlantic coast of New Jersey. The beach at Manasquan is relatively narrow with short groins spaced at 200 to 300-m intervals. Point Pleasant Beach on the other hand has a comparatively wide beach with no littoral structures other than the south jetty at Manasquan Inlet. These contrasting beach conditions are explained by the net northerly longshore sand transport regime and the inlet stabilization structures at Manasquan Inlet. Blockage of the net longshore transport rate by the jetties at Manasquan Inlet produces both the wide beaches in Point Pleasant Beach and the comparatively narrow beaches in Manasquan.

A northeaster impacted these two beaches between 28 and 30 March 1984 causing severe erosion. The effects of this storm were captured by profile surveys conducted by the U.S. Army Engineer District (USAED), Philadelphia, as part of the Corps of Engineers Monitoring of Completed Coastal Projects (MCCP) program. Subaerial profile surveys at the two beaches were taken approximately two days before the storm and again three to four days after the storm. Subaqueous profile surveys were taken approximately three months before and two weeks after the storm. The subaerial and subaqueous profiles were combined to obtain an approximation of the pre- and post-storm profiles. Wave data for the northeaster were provided by a waverider buoy located at a depth of 15.2 m operated as another element of the MCCP program. Water level data were obtained through a National Oceanographic Service (NOS) maintained tide gauge located near the shoreward side of Manasquan Inlet. The time histories of the wave and water level data are shown in Figure 64. The storm duration was approximately 2 days with a peak significant wave height of 7 m and a peak water level of 2 m NGVD.

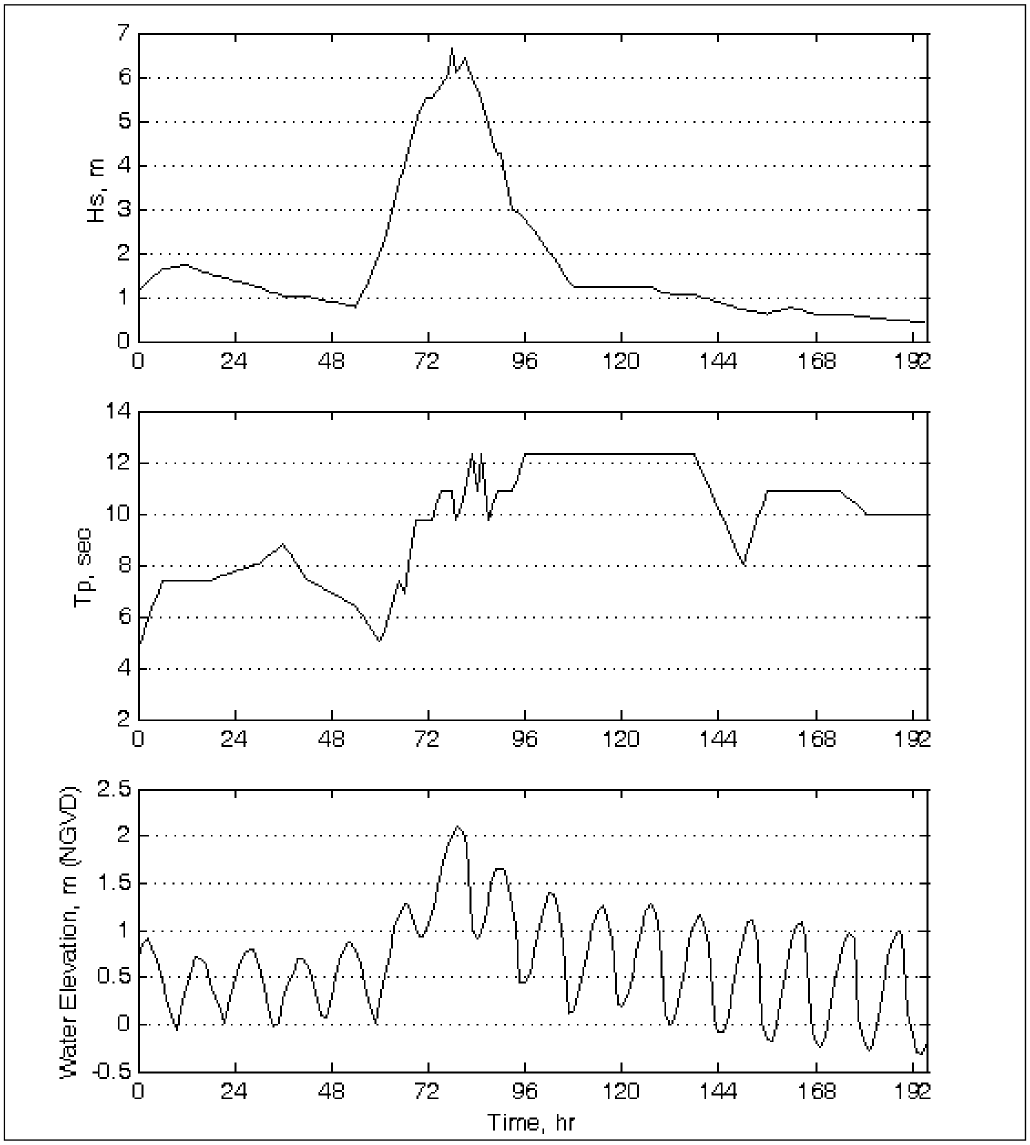

Figure 64. Wave height, wave period, and water elevation time-histories for the March 1984 storm, Manasquan/Point Pleasant Beach, NJ.

Manasquan. The total volume change per unit width of beach based on the pre- and post-storm beach profiles at the Manasquan is illustrated in Figure 65. The beach at Manasquan is located on the north side of Manasquan Inlet. The beach profiles at Manasquan are numbered in order with distance from the inlet jetty with profile M1 being the closest and M9 the most distant. As seen in Figure 65, mass conservation between the pre- and post-storm beach profiles at Manasquan was poor. Five of the nine profiles were found to have either gained or lost more than 100 cu m/m. These large volumetric changes are presumed to be attributed to the long time interval between the subaqueous profile surveys, gradients in the longshore sand transport due to the inlet structures, or possible survey error.

CSHORE simulation results for the March 1984 storm at Manasquan are illustrated in Figures 66 to 74. In general, the CSHORE predictions underestimate the measured beach profile response in terms of total volumetric erosion particularly erosion high on the beach profile.

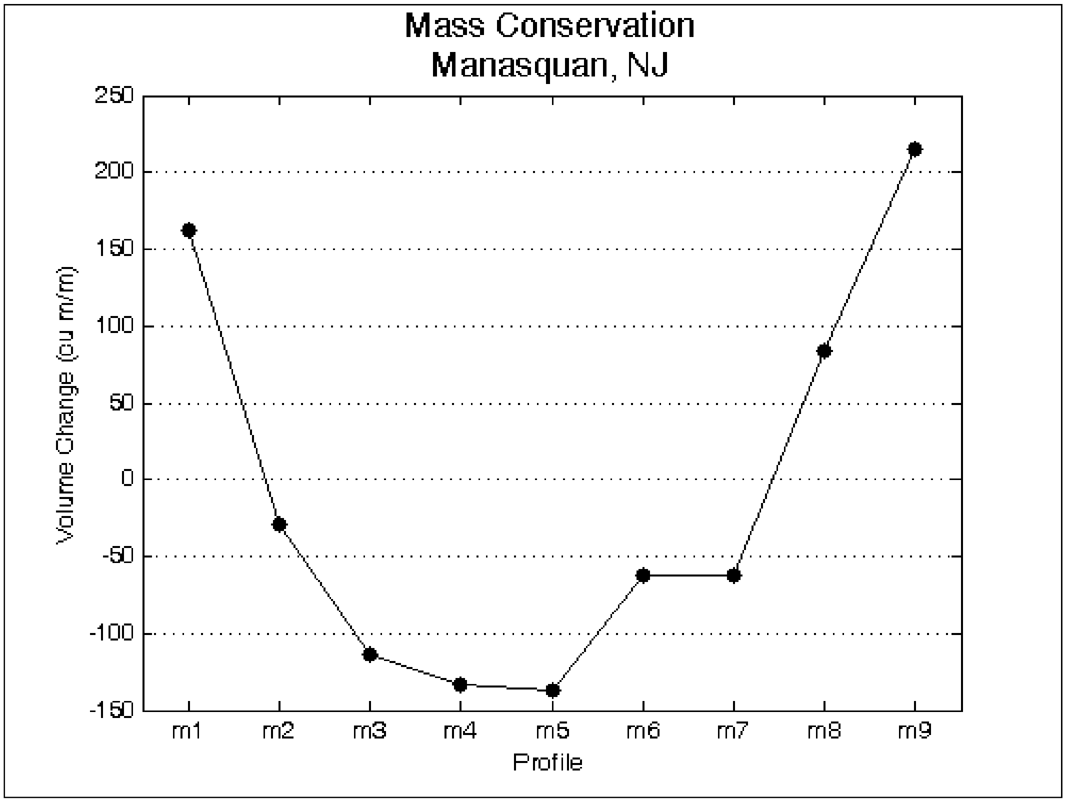

Figure 65. Conservation of mass between beach profile surveys for the March 1984 storm, Manasquan, NJ.

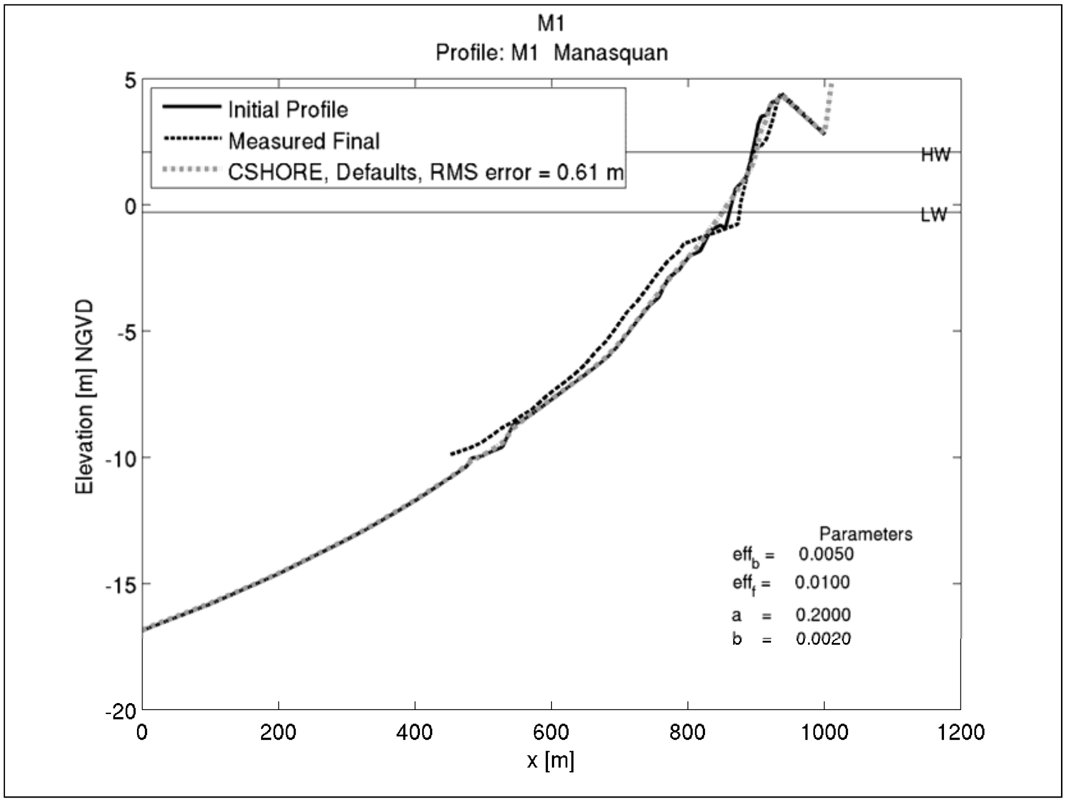

Figure 66. CSHORE simulation of the March 1984 storm for profile M1, Manasquan, NJ.

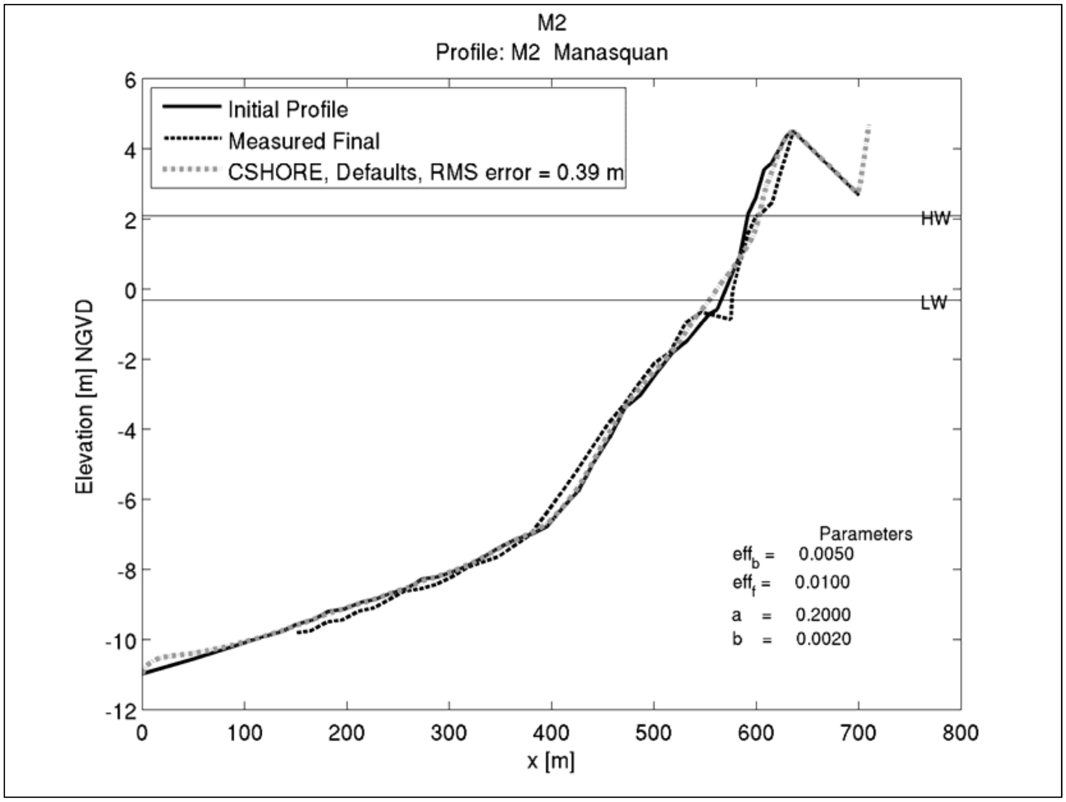

Figure 67. CSHORE simulation of the March 1984 storm for profile M2, Manasquan, NJ.

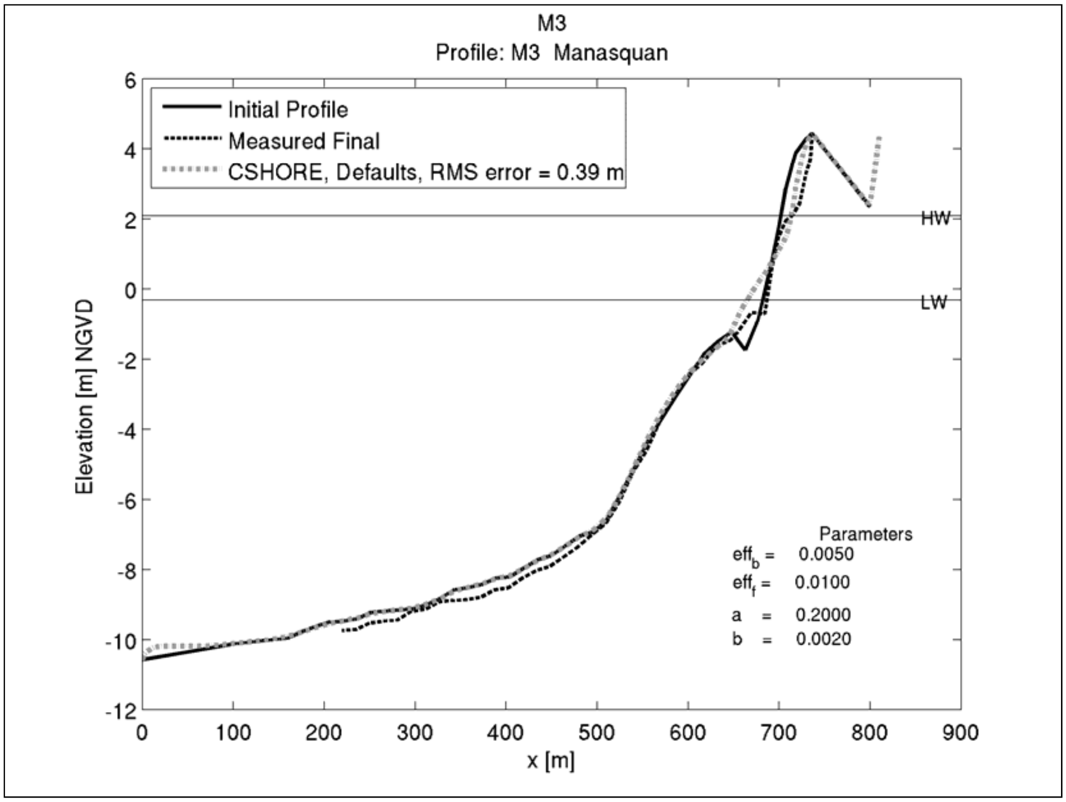

Figure 68. CSHORE simulation of the March 1984 storm for profile M3, Manasquan, NJ.

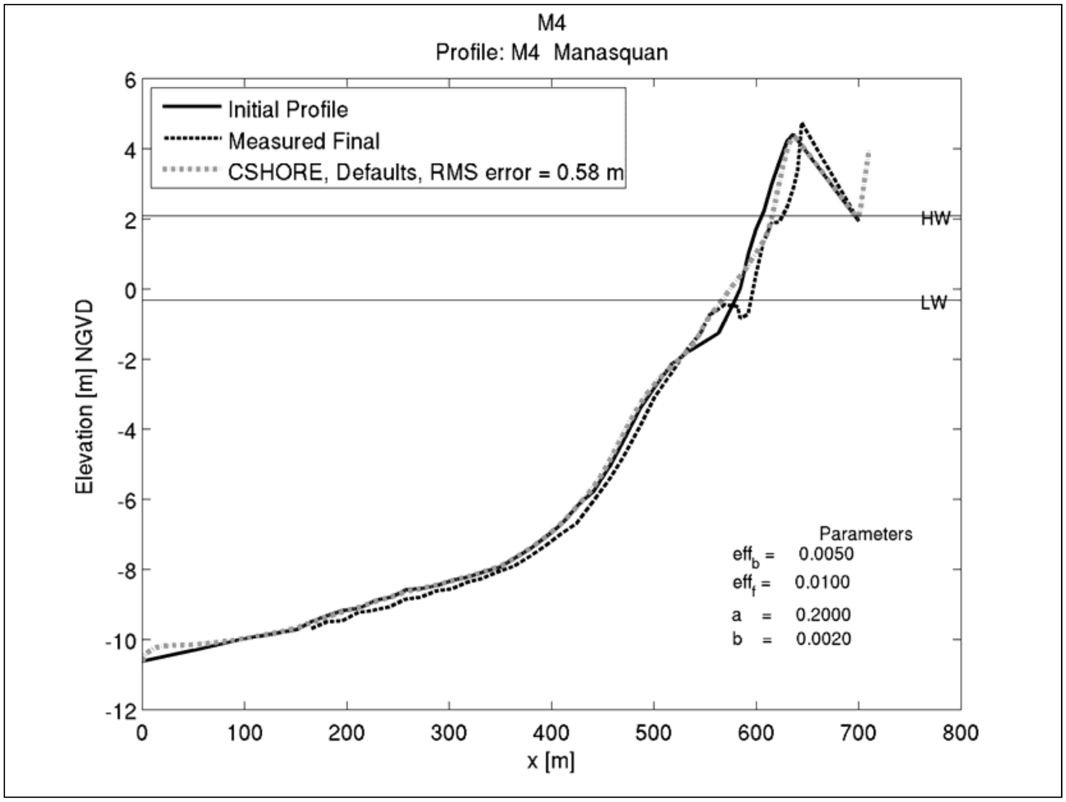

Figure 69. CSHORE simulation of the March 1984 storm for profile M4, Manasquan, NJ.

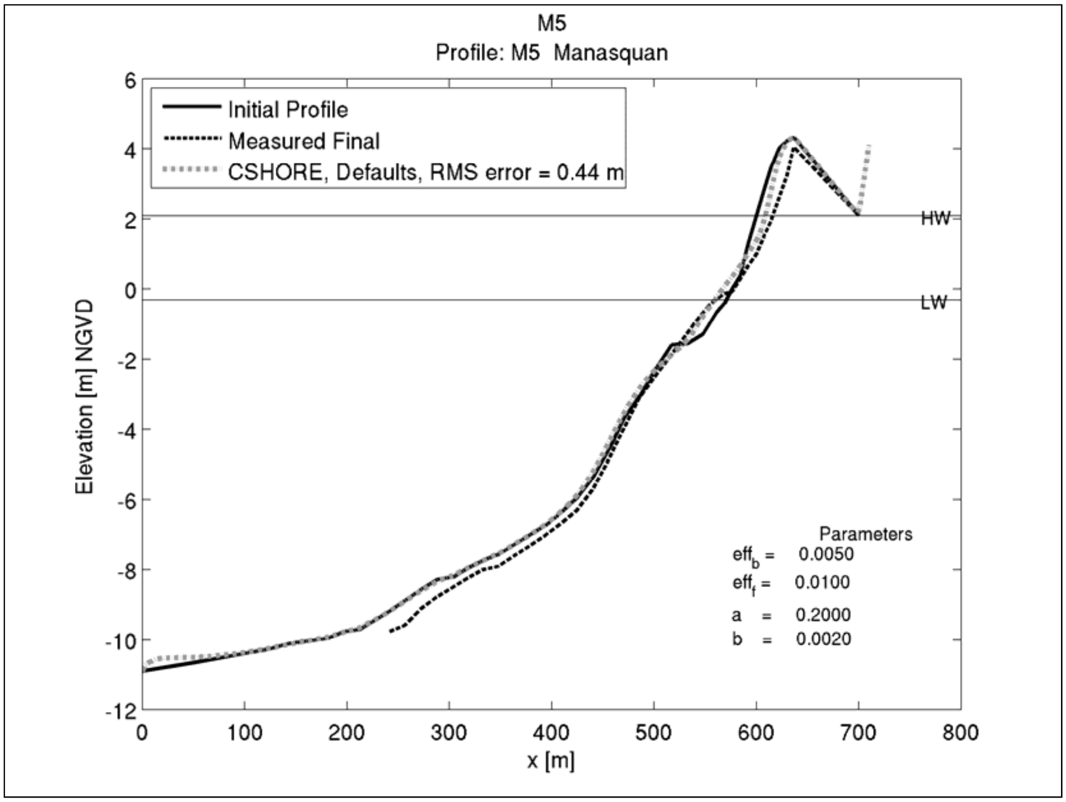

Figure 70. CSHORE simulation of the March 1984 storm for profile M5, Manasquan, NJ.

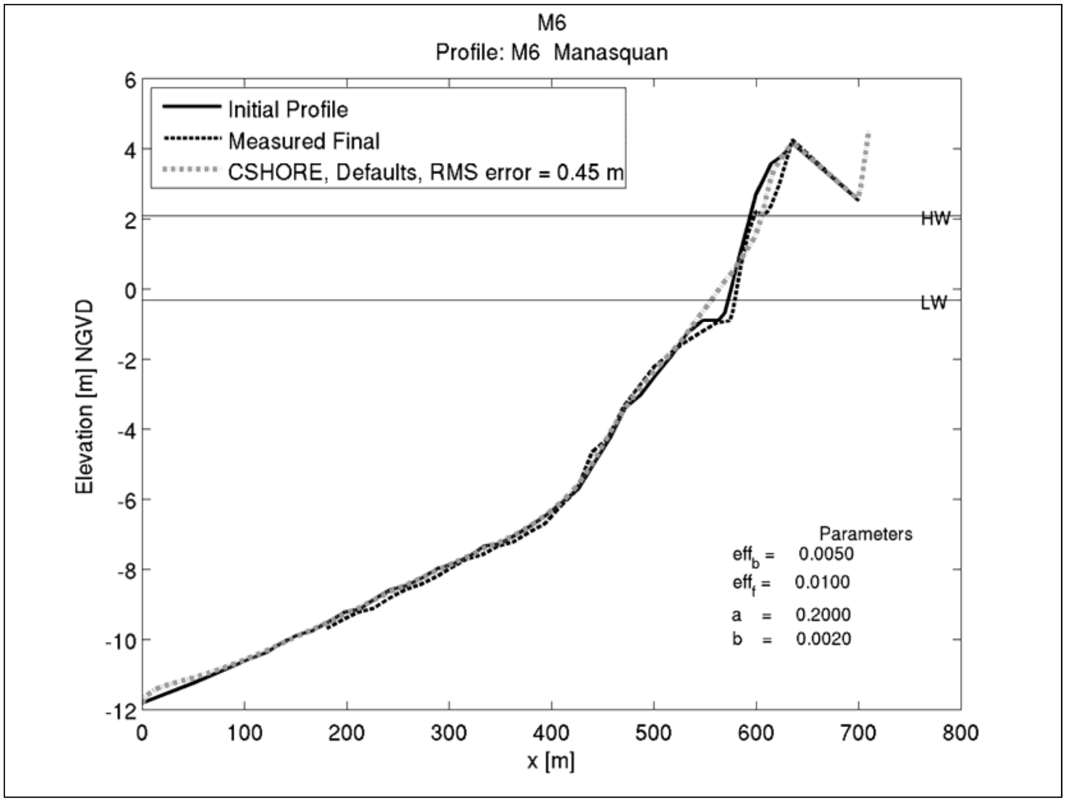

Figure 71. CSHORE simulation of the March 1984 storm for profile M6, Manasquan, NJ.

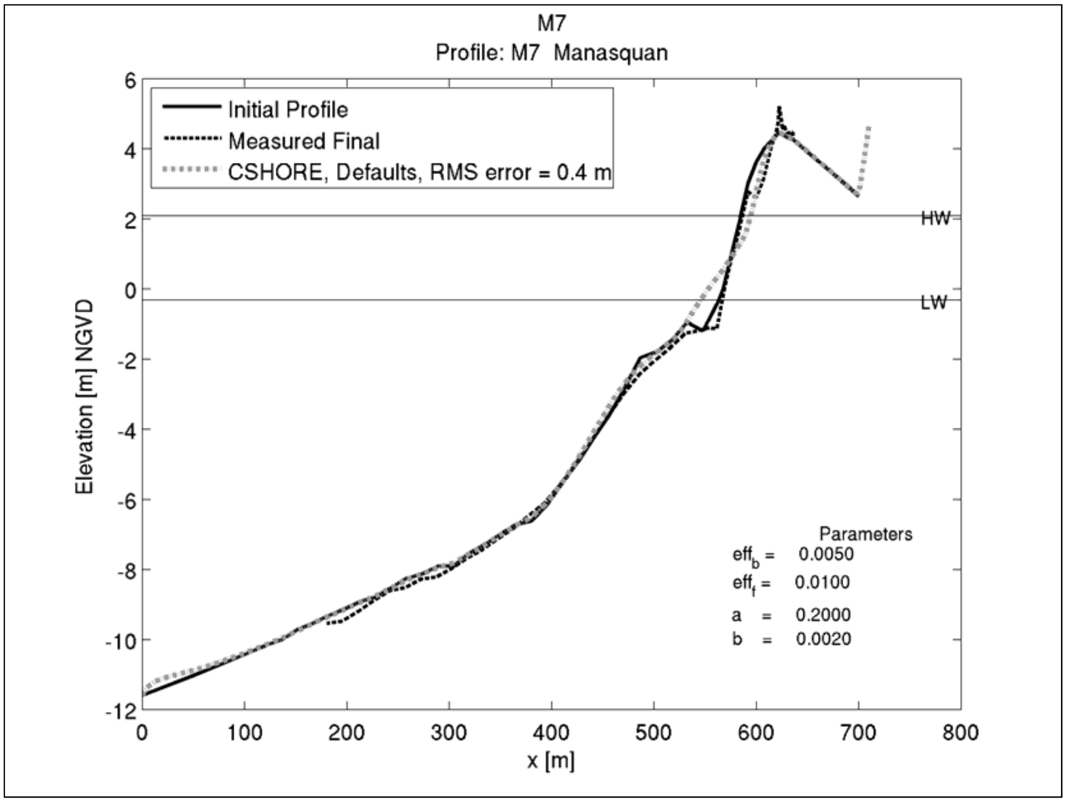

Figure 72. CSHORE simulation of the March 1984 storm for profile M7, Manasquan, NJ.

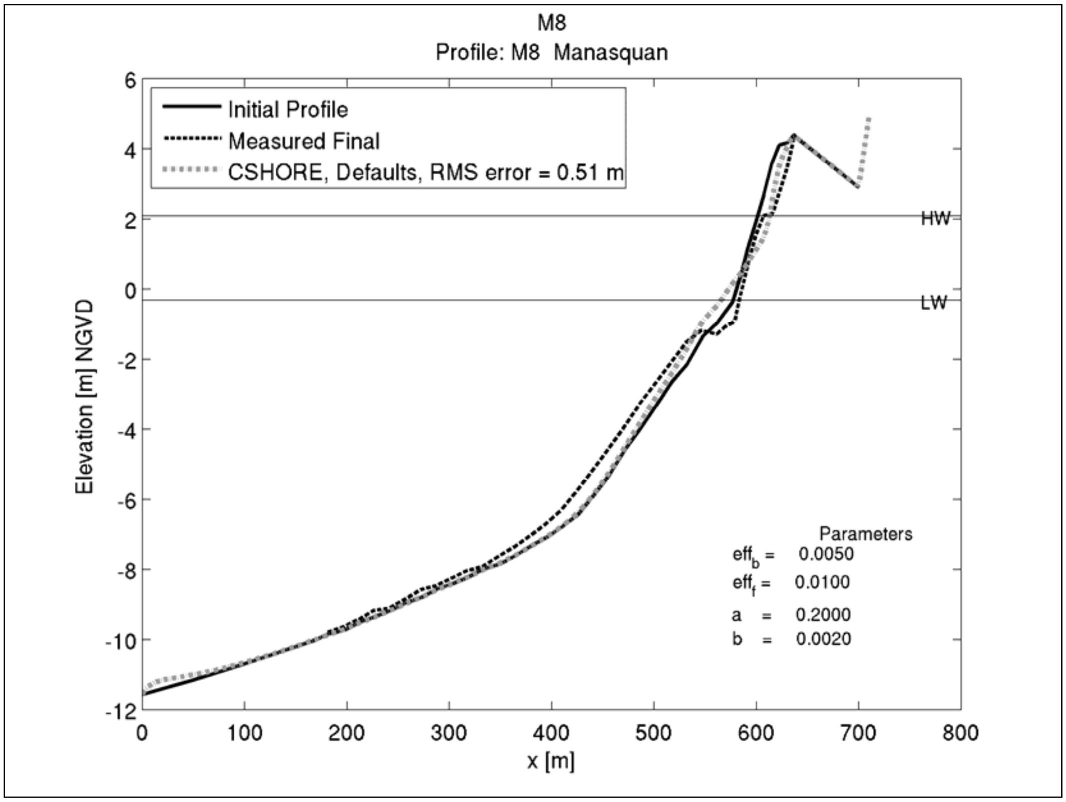

Figure 73. CSHORE simulation of the March 1984 storm for profile M8, Manasquan, NJ.

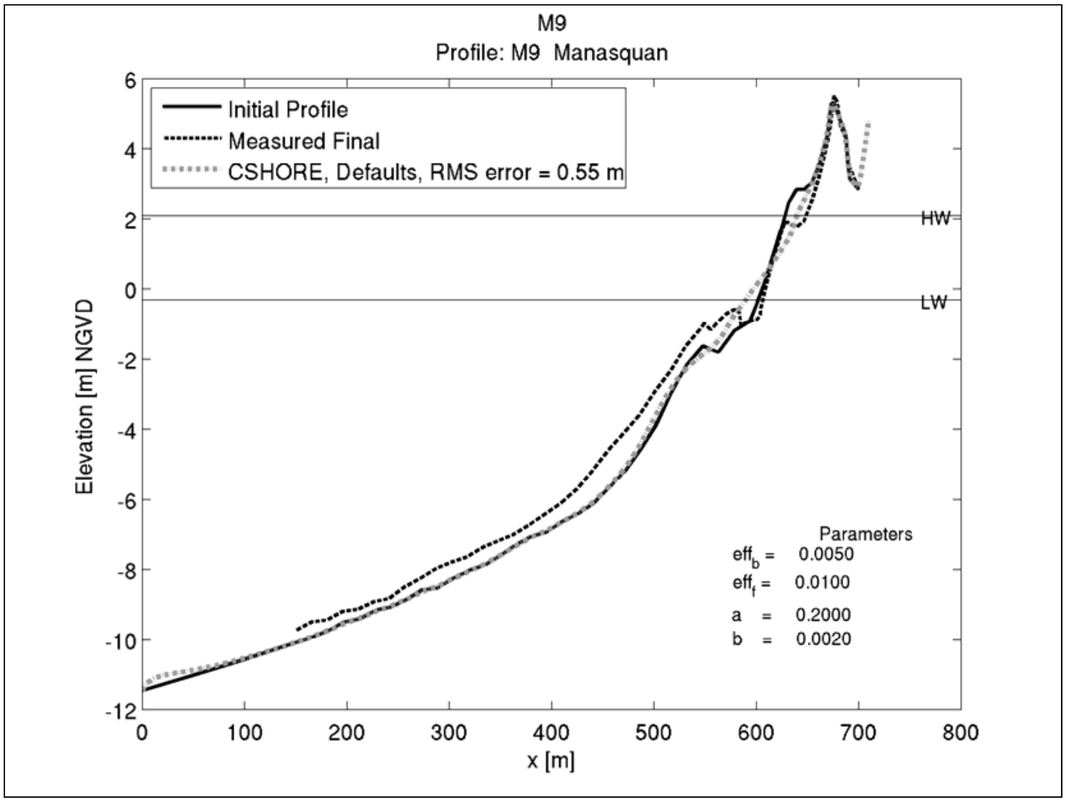

Figure 74. CSHORE simulation of the March 1984 storm for profile M9, Manasquan, NJ.

A curious characteristic of the Manasquan beach profile response to the March 1984 storm is the lack of significant erosion between the elevations of 0 and 2 m NVGD with an associated large amount of erosion above the 2 m elevation. The specific cause of this unusual beach profile response is unknown although it could be that the reduced erosion in the 0 to 2 m elevation range is the result of the rapid development of a post-storm recovery berm in the waning stages of the storm and prior to the post-storm profile surveys.

The quantitative model performance measures for the March 1984 storm at Manasquan are illustrated in Figures 75 through 77. Figure 75 shows that the predicted volume loss above NGVD is consistently under predicted, except at profile M7. Predicted recession of the 3.75 m contour is consistently under estimated by 1 to 12 m in the model simulations, as seen in Figure 76. The measurement of landward storm intrusion illustrated in Figure 77 shows that the CSHORE predictions also under estimated the storm intrusion distance at all profiles by approximately 3 to 12 m.

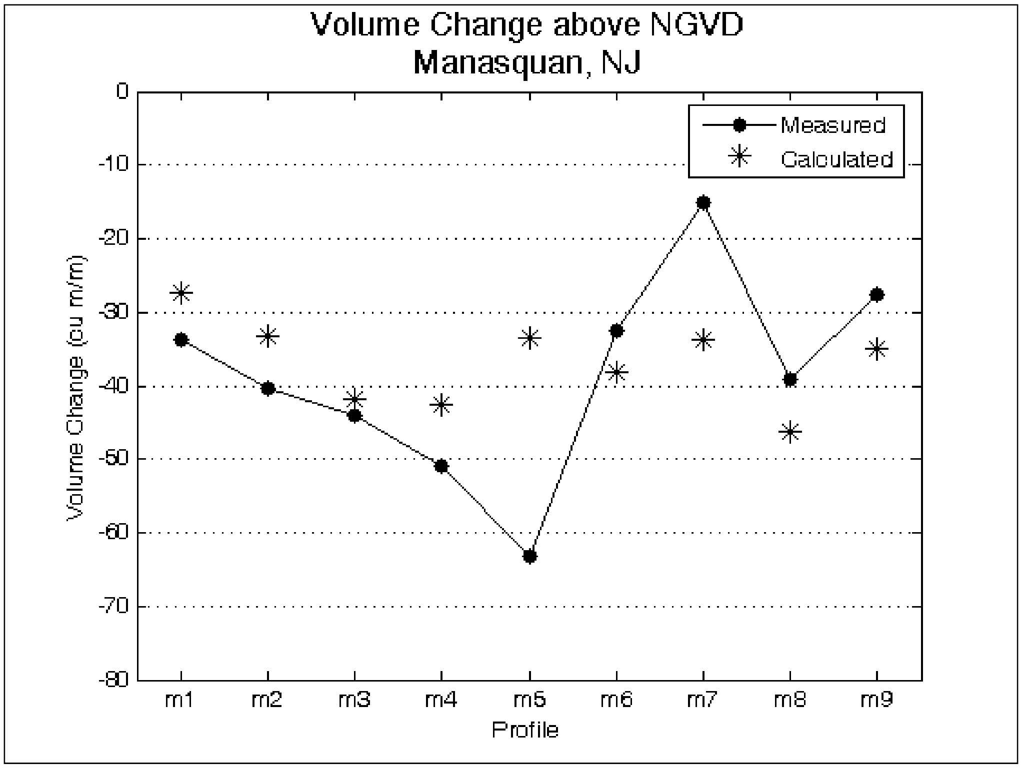

Figure 75. Comparison of measured and simulated volume change above NGVD for the March 1984 storm, Manasquan, NJ.

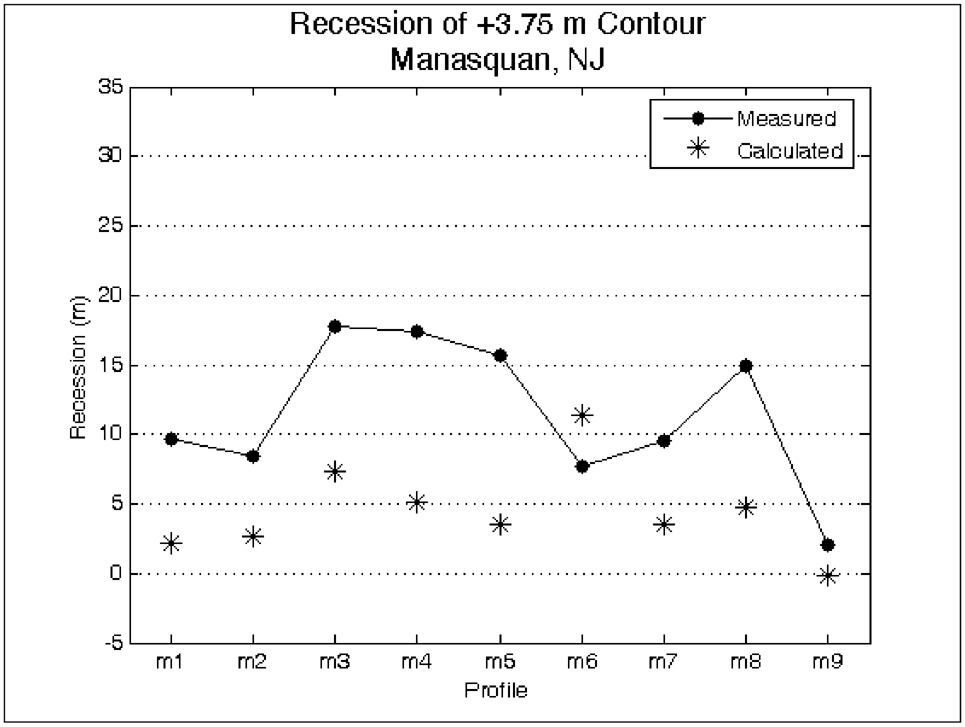

Figure 76. Comparison of measured and simulated recession of the 3.75-m contour for the March 1984 storm, Manasquan, NJ.

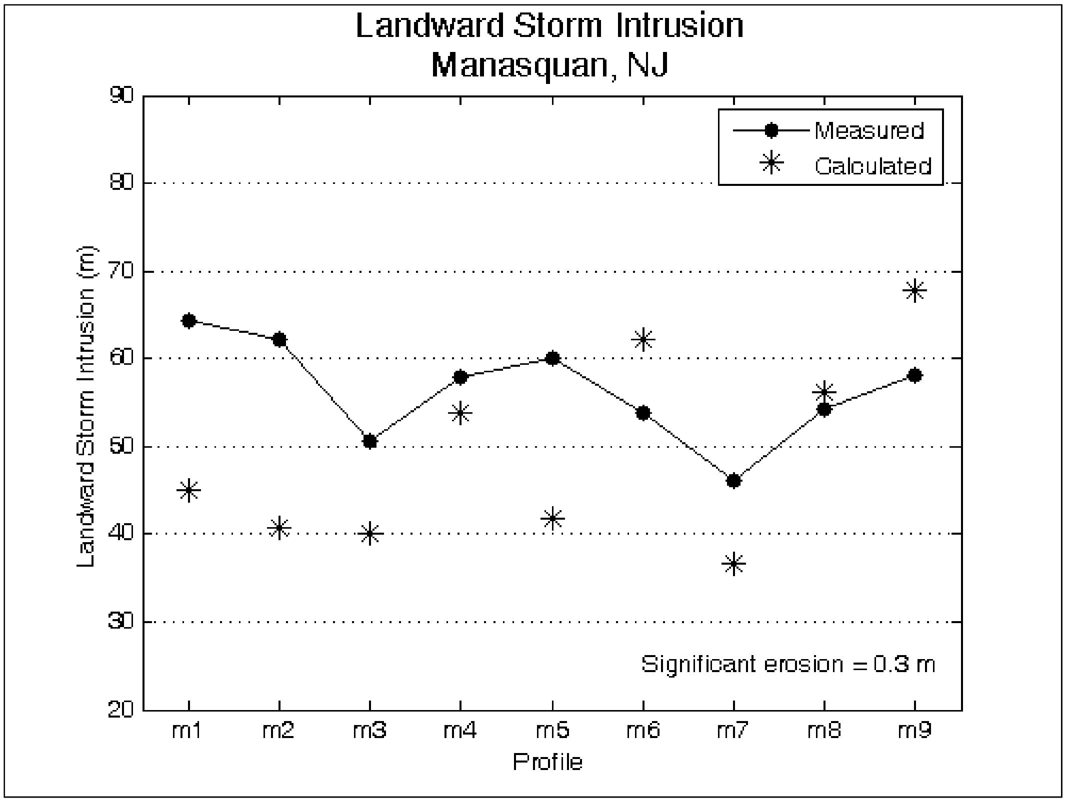

Figure 77. Comparison of measured and simulated storm intrusion for the March 1984 storm, Manasquan, NJ.

Point Pleasant Beach. Eight profiles were surveyed at Point Pleasant Beach located south of Manasquan Inlet. The profiles at Point Pleasant Beach are numbered in order with distance from the inlet. Profile P1 was closest to the inlet jetty and profile P8 was the most distant. Figure 78 shows the total measured volume change between the pre- and post-storm profile surveys. In this figure it is seen that seven of the eight profiles experienced a net loss of volume between the pre- and post-storm surveys. The smaller magnitude of the net volume changes at the Point Pleasant Beach profiles compared to Manasquan profiles indicates better mass conservation. The Point Pleasant Beach profiles experienced more erosion and recession of the upper profile than was observed on the Manasquan profiles. Nearly all of the Point Pleasant Beach post-storm profiles contained a ridge at the shoreline which is likely the development of a post-storm recovery berm formed by long period waves in the waning stages of the storm.

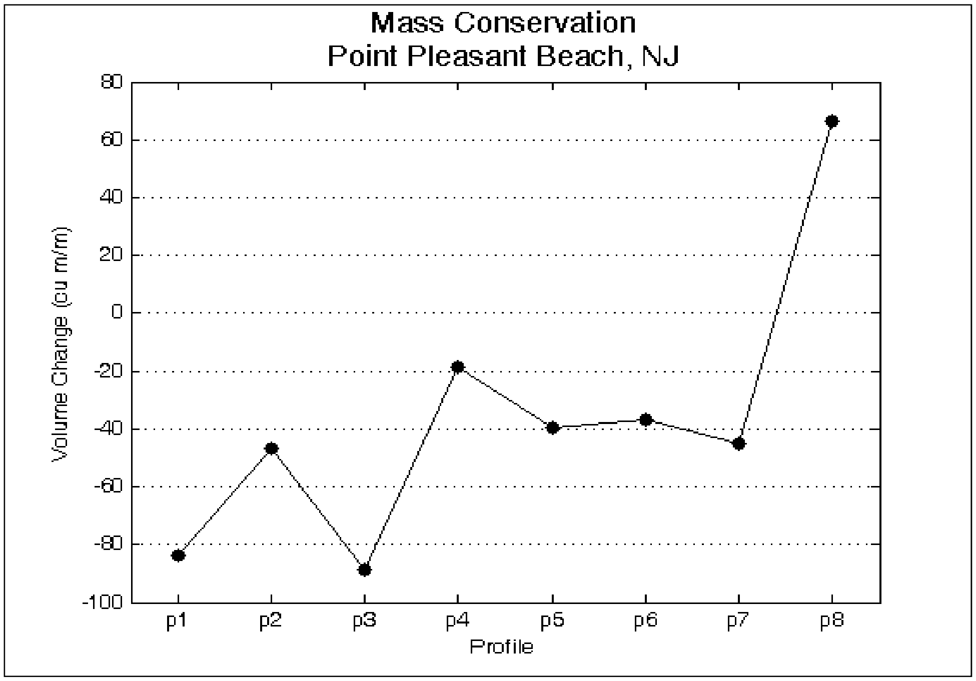

Figure 78. Conservation of mass between beach profile surveys for the March 1984 storm, Point Pleasant Beach, NJ.

CSHORE simulation results for the March 1984 storm at Point Pleasant Beach are illustrated in Figures 79 through 86. Overall, the CSHORE predictions underestimate the measured beach profile erosion on the beach profile above the 2 m NGVD elevation. Erosion on the subaerial profile between the 0 and 2 m NGVD contours is over estimated in the CSHORE results. However, the presence of a post-storm recovery berm in the measured profile data may be masking the storm generated erosion in this elevation range.

The quantitative model performance measures for the March 1984 storm at Point Pleasant Beach are illustrated in Figures 87 through 89. Figure 87 shows that the predicted volume loss above NGVD is in good agreement with the measurements (differences are less than 10 cu m/m) for five of the eight profiles although the measured and predicted post-storm profiles (Figures 79-86) show that the model predictions underestimated erosion high on the profile. The predictive skill implied by the volume loss above NGVD performance measure is tempered by the lack of predictive skill illustrated by the performance measures of contour recession and storm intrusion. Figure 88 shows that recession of the 2.75 m contour is dramatically underestimated in the CSHORE predictions for six of the eight Point Pleasant Beach profiles. Likewise, the extent of landward storm intrusion is also under estimated at all the Point Pleasant Beach profiles except P1.

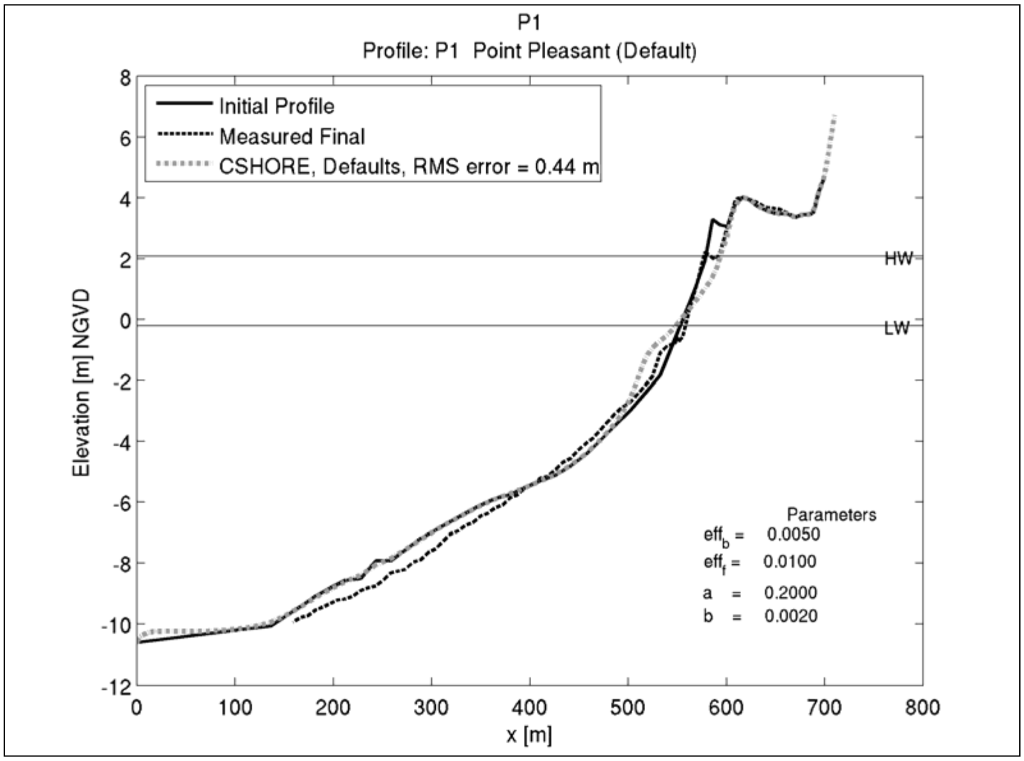

Figure 79. CSHORE simulation of the March 1984 storm for profile P1, Point Pleasant Beach, NJ.

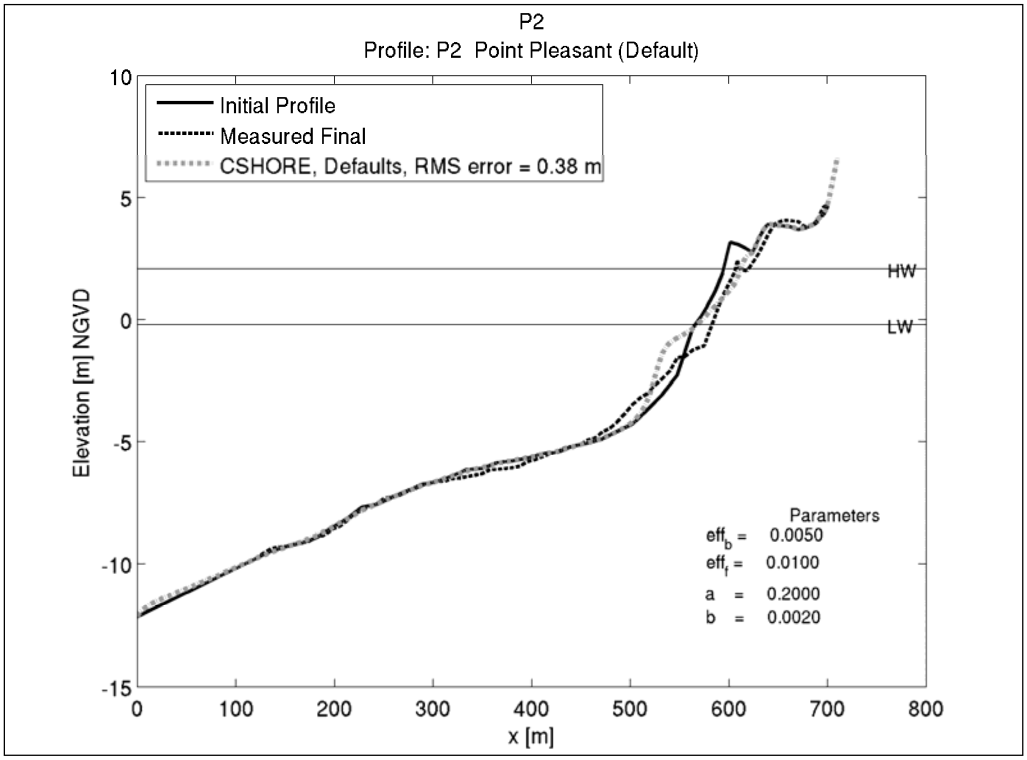

Figure 80. CSHORE simulation of the March 1984 storm for profile P2, Point Pleasant Beach, NJ.

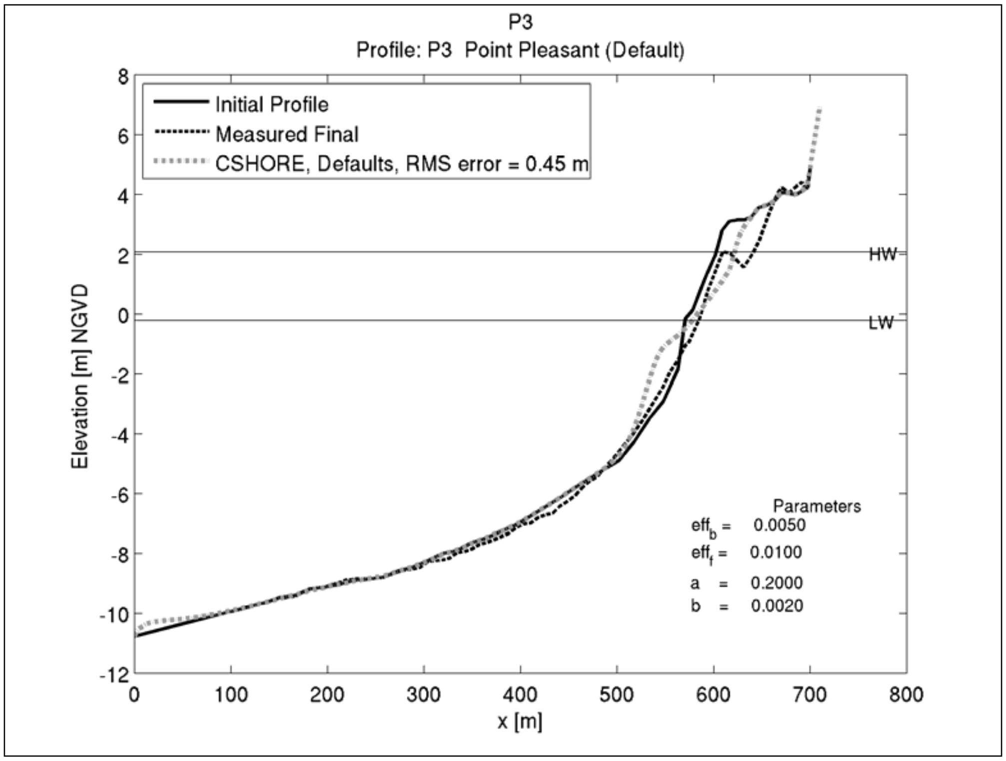

Figure 81. CSHORE simulation of the March 1984 storm for profile P3, Point Pleasant Beach, NJ.

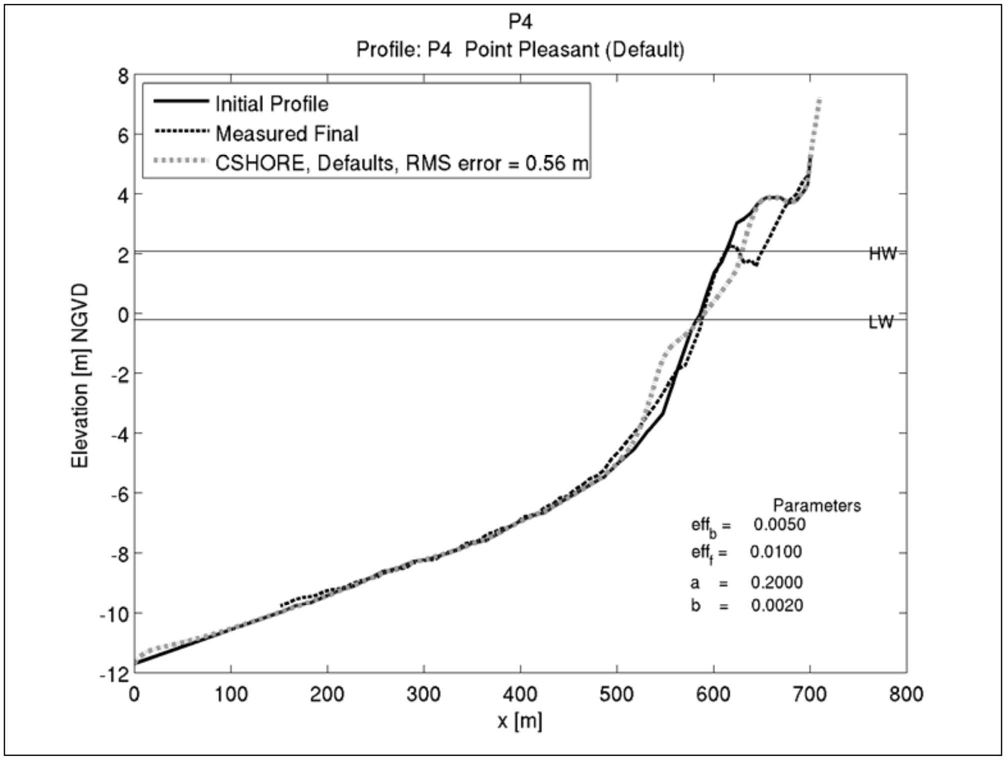

Figure 82. CSHORE simulation of the March 1984 storm for profile P4, Point Pleasant Beach, NJ.

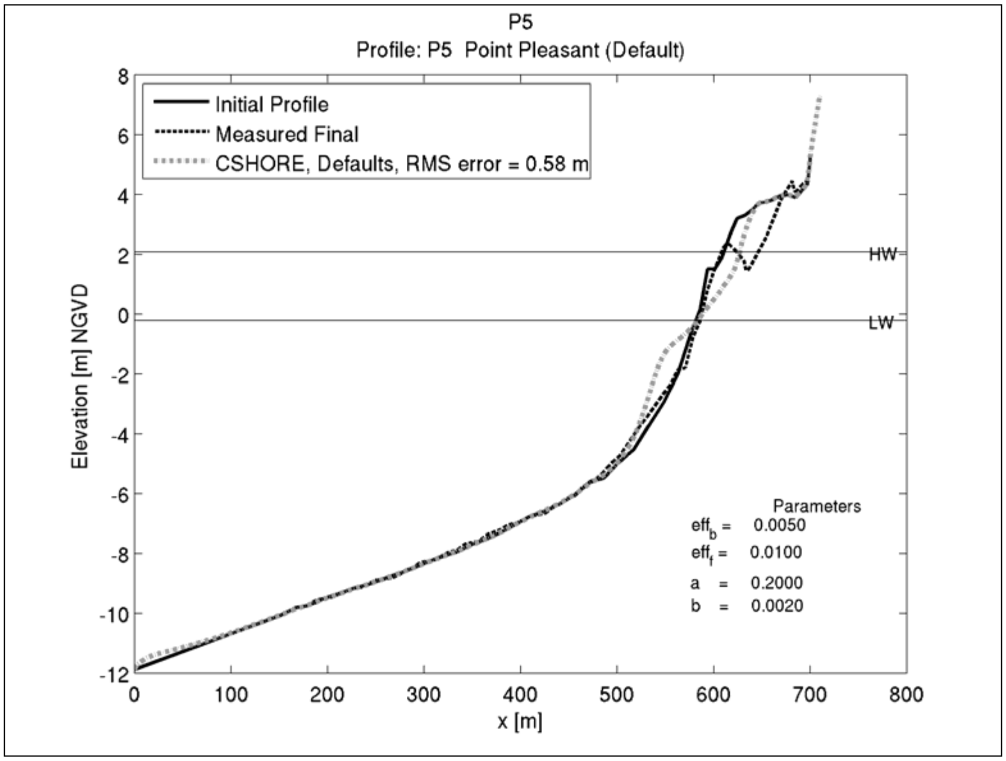

Figure 83. CSHORE simulation of the March 1984 storm for profile P5, Point Pleasant Beach, NJ.

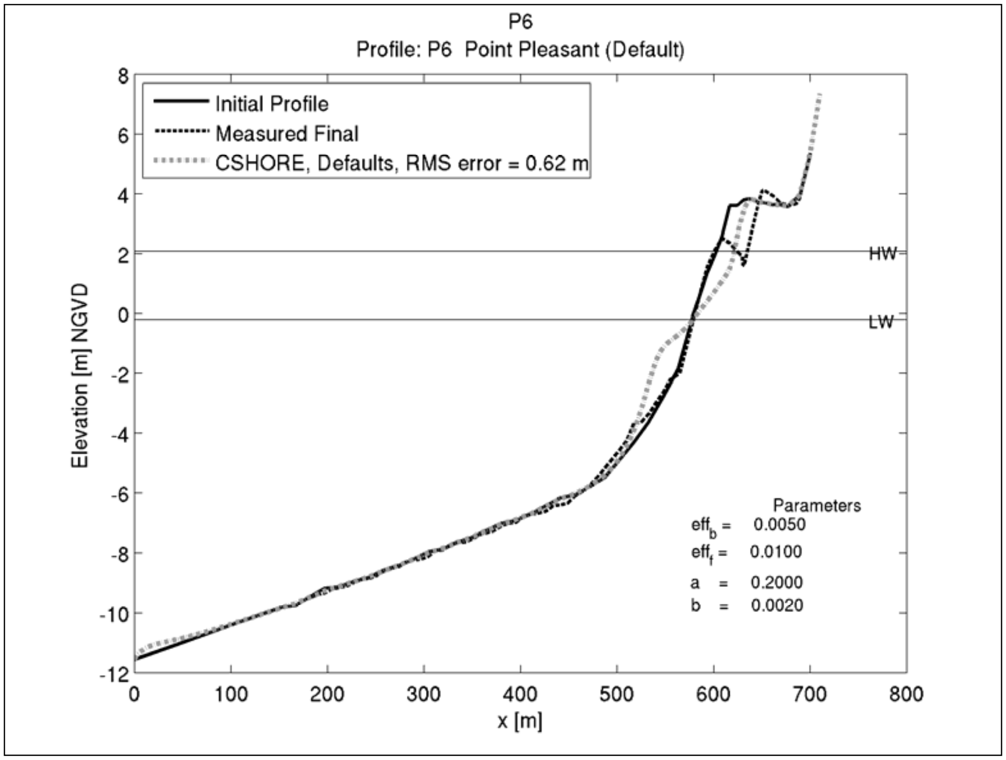

Figure 84. CSHORE simulation of the March 1984 storm for profile P6, Point Pleasant Beach, NJ.

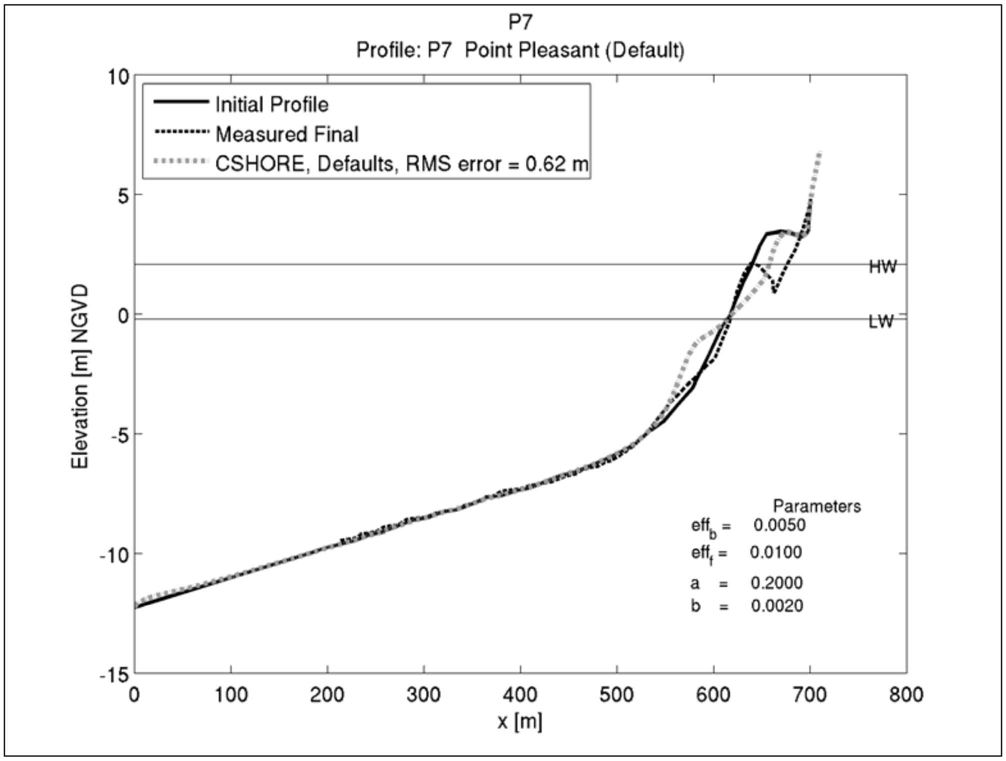

Figure 85. CSHORE simulation of the March 1984 storm for profile P7, Point Pleasant Beach, NJ.

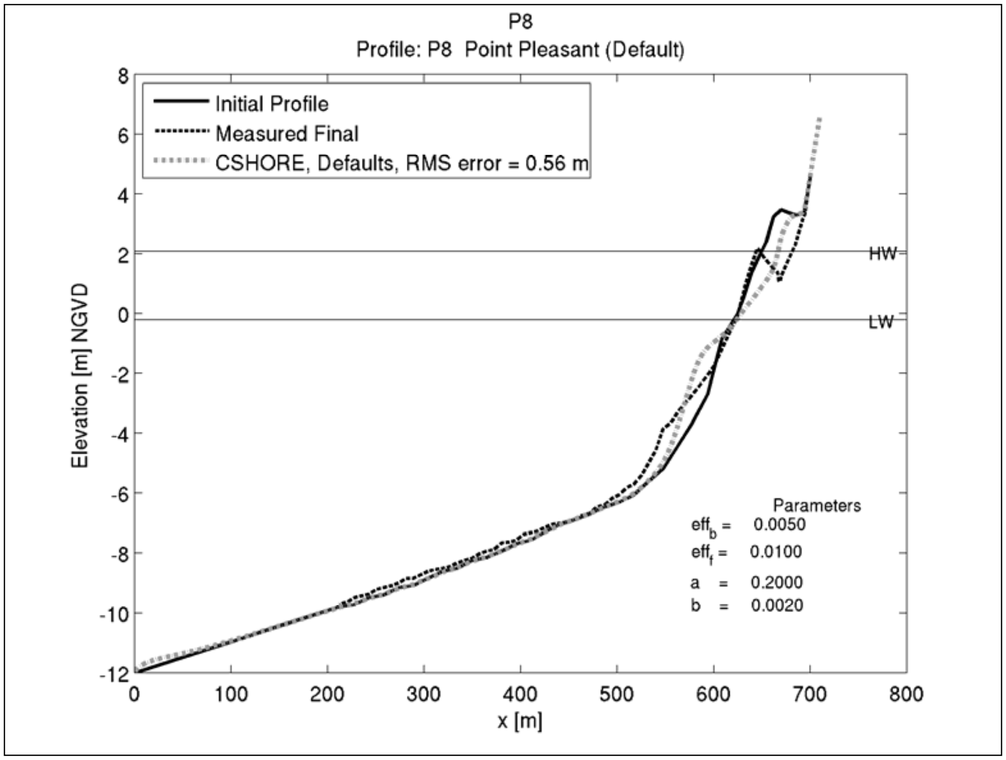

Figure 86. CSHORE simulation of the March 1984 storm for profile P8, Point Pleasant Beach, NJ.

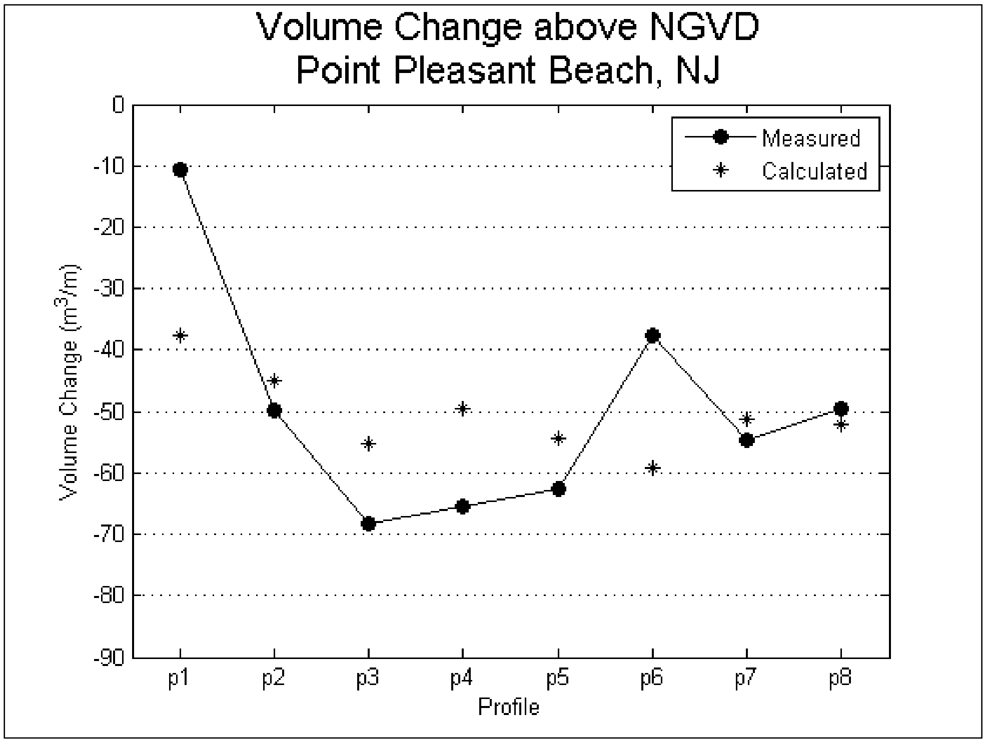

Figure 87. Comparison of measured and simulated volume change above NGVD for the March 1984 storm, Point Pleasant Beach, NJ.

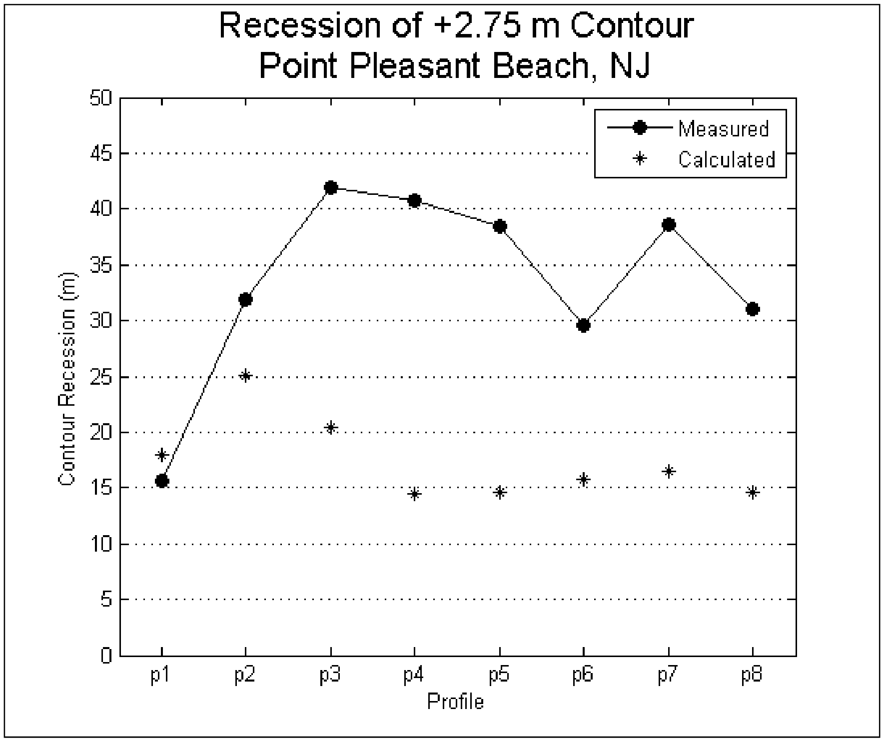

Figure 88. Comparison of measured and simulated recession of the 2.75-m contour for the March 1984 storm, Point Pleasant Beach, NJ.

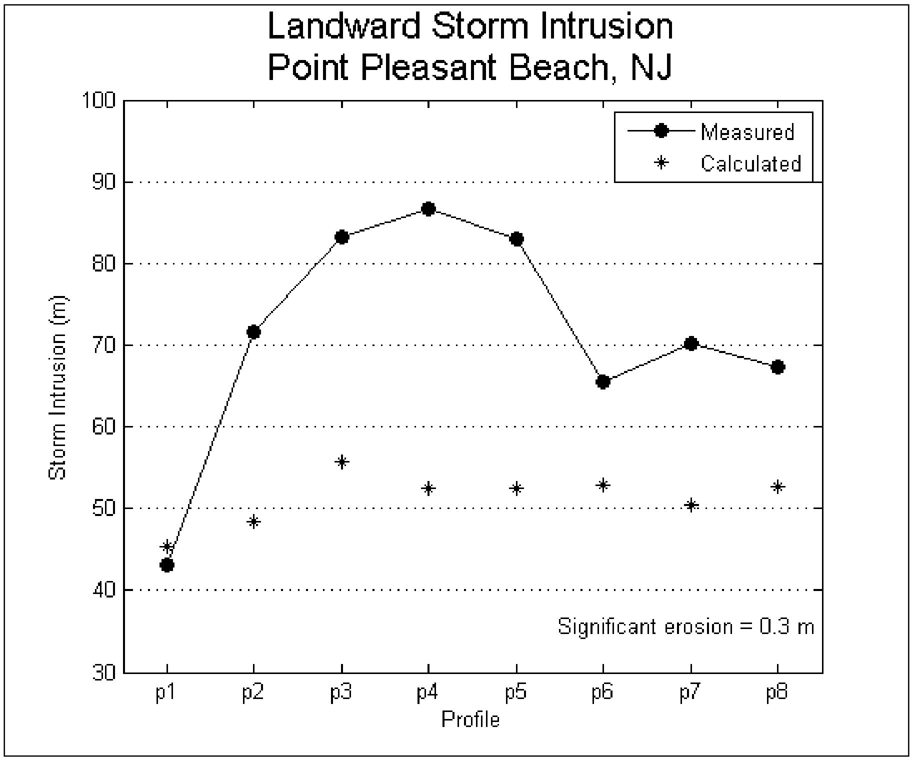

Figure 89. Comparison of measured and simulated storm intrusion for the March 1984 storm, Point Pleasant Beach, NJ.

Dewey Beach and Rehoboth Beach, NJ

The communities of Dewey Beach and Rehoboth Beach on the east coast of Delaware were impacted by a northeaster storm event on 10 December 1992. The beach response to the storm was captured by profile surveys collected by the USACE, Philadelphia, as part of an ongoing feasibility study. Pre-storm profiles were surveyed on 29 October 1992 and post-storm surveys were performed after passage of the storm on 18 December 1992. Wave conditions during the storm were recorded by a wave gauge located at a depth of approximately 9 m offshore of Dewey Beach. Tide information was available from a nearby tide gauge located at Lewes, DE. The time histories of wave and water level information for the 10 December storm event are plotted in Figure 90. The storm had a peak significant wave height of 4 m and a peak total water elevation of just less than 2 m NGVD over a duration of approximately four days. The sediment grain size for the Dewey Beach and Rehoboth Beach CSHORE simulations was specified at 0.33 mm, based on the sediment analyses performed as part of the USAED, Philadelphia project feasibility study.

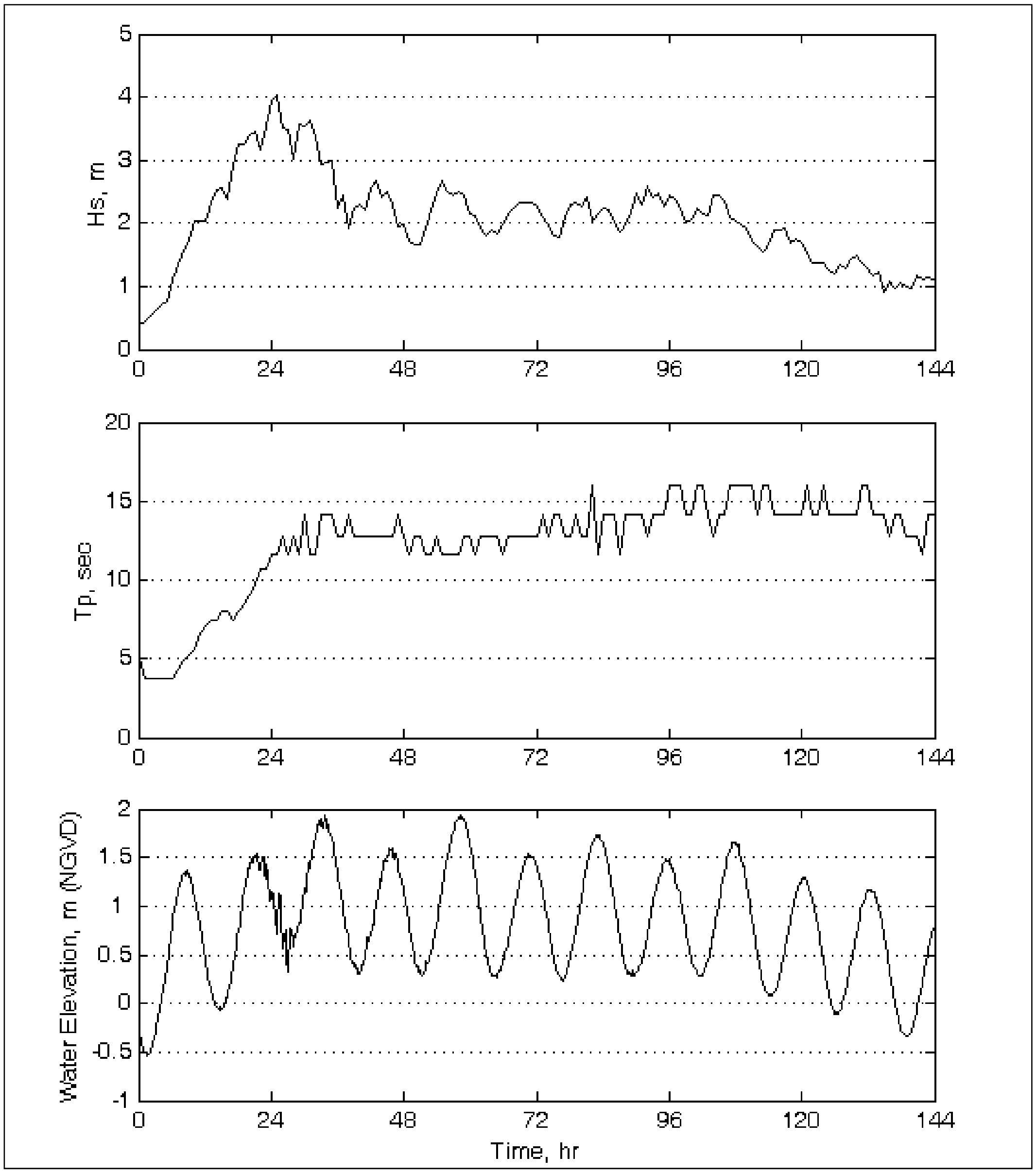

Figure 90. Wave height, wave period, and water elevation time-histories for the December 1992 storm, Dewey Beach/Rehoboth Beach, DE.

Dewey Beach. Pre- and post-storm profile measurements were available for seven profile lines at Dewey Beach. Figure 91 shows the storm induced volume change between the pre- and post-storm surveys at each profile line. The figure shows that a net volume loss was experienced at all of the Dewey Beach profile lines. The greatest volume loss was found at profile 240 with a loss of approximately 120 cu m/m whereas mass was nearly conserved at profile 140 where the volume loss was less than 10 cu m/m.

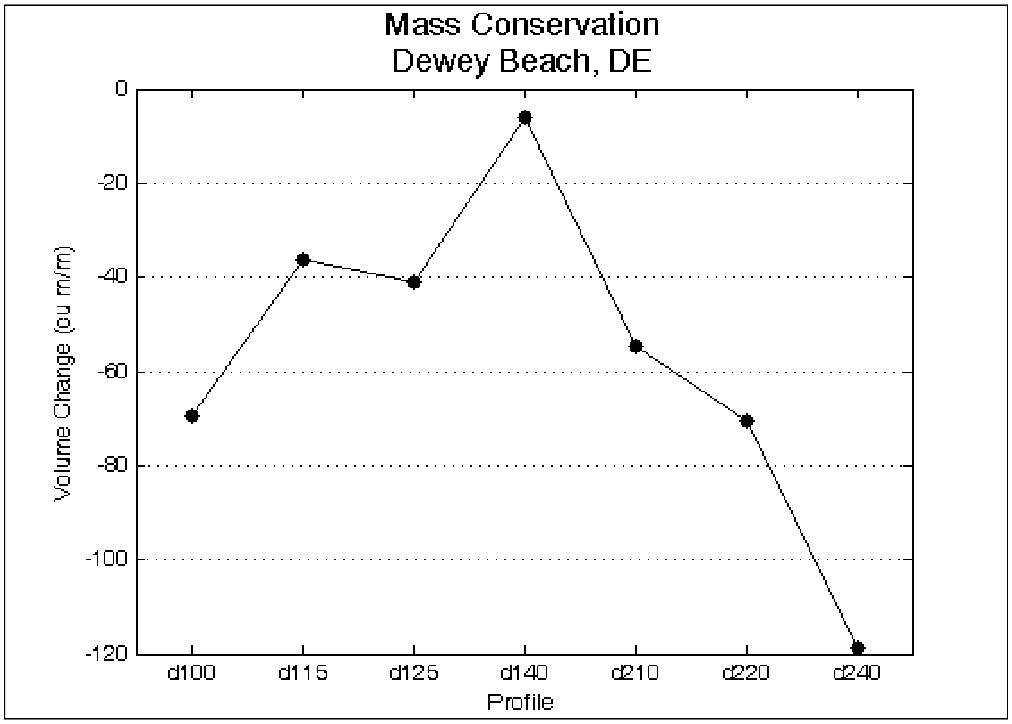

Figure 91. Conservation of mass between beach profile surveys for the December 1992 storm, Dewey Beach, DE.

The CSHORE simulations of storm induced beach profile change at Dewey Beach provided remarkably good agreement with the measured profile changes as illustrated in Figures 92 through 98. Near complete erosion of the beach berm together with moderate erosion of the seaward face of the dune with deposition in an offshore bar feature is typical of measured and predicted beach profile response to the December 1992 storm at Dewey Beach. CSHORE accurately predicted the position and form of the offshore bar particularly on profiles 140, 210, 220, and 240. Erosion of the upper beach is also accurately predicted except for the near horizontal swash platform at about 0 NGVD evident in most of the measured profiles.

The quantitative model performance measures for the December 1992 storm at Dewey Beach are illustrated in Figures 99 through 101. Figure 99 shows that the difference between the measured and computed volume change above 0 NGVD is less than 10 cu m/m for two of the seven Dewey Beach profiles but greater than or equal to about 20 cu m/m for the remainder. The predicted recession of the 1.5-meter contour differs from the measured by less than 10 m in all Dewey Beach cases (Figure 100). The comparison of measured and simulated storm intrusion distance in Figure 101 also shows very good agreement with model estimates within 5 m of the measurements.

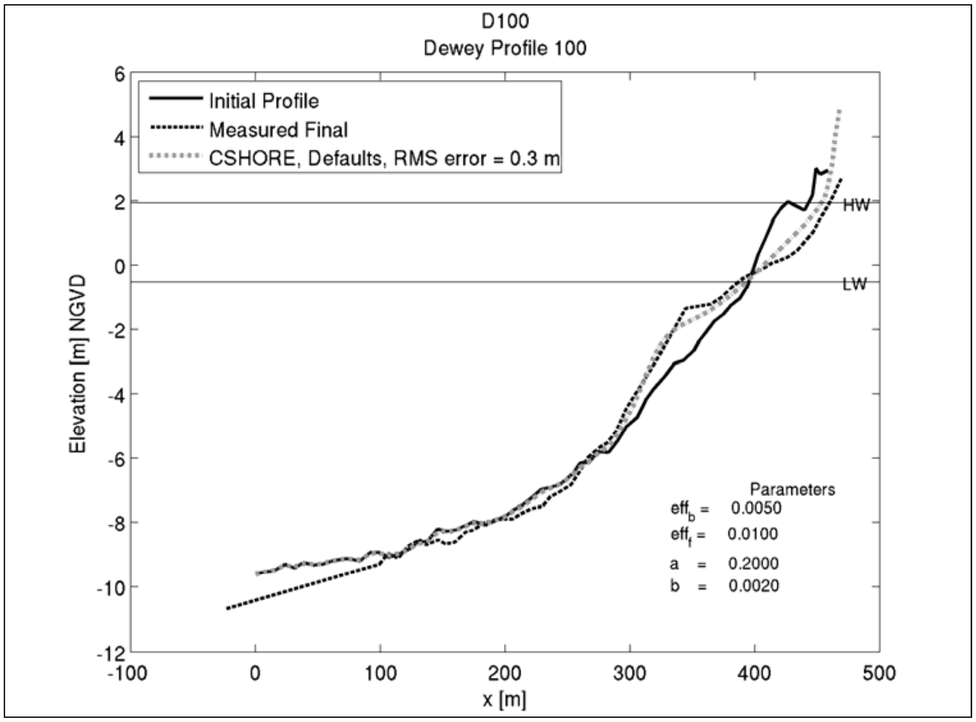

Figure 92. CSHORE simulation of the December 1992 storm for profile D100, Dewey Beach, DE.

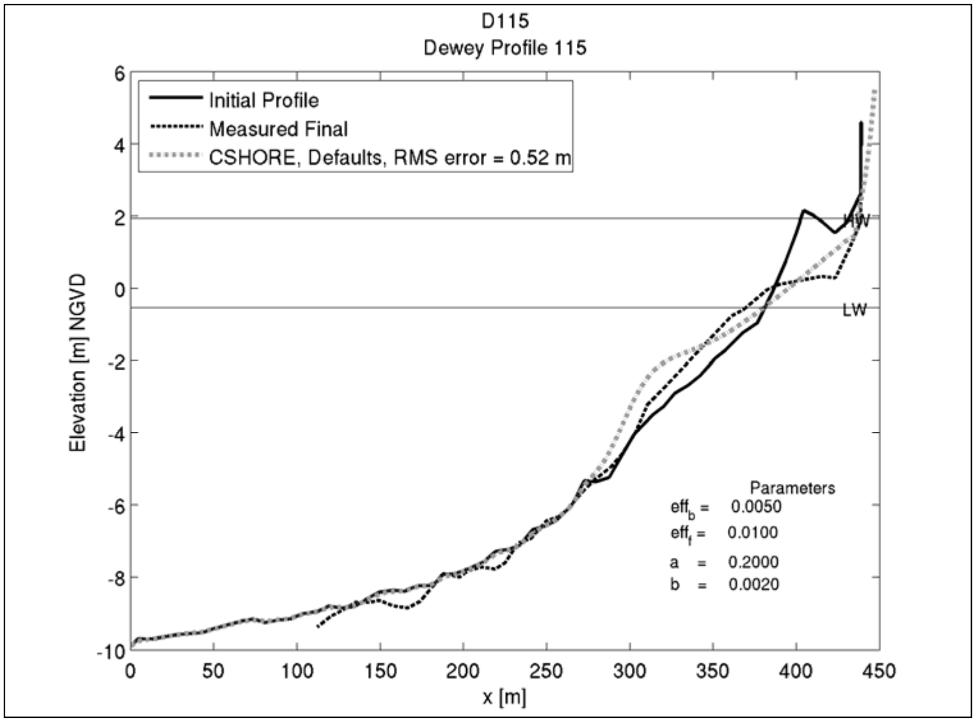

Figure 93. CSHORE simulation of the December 1992 storm for profile D115, Dewey Beach, DE.

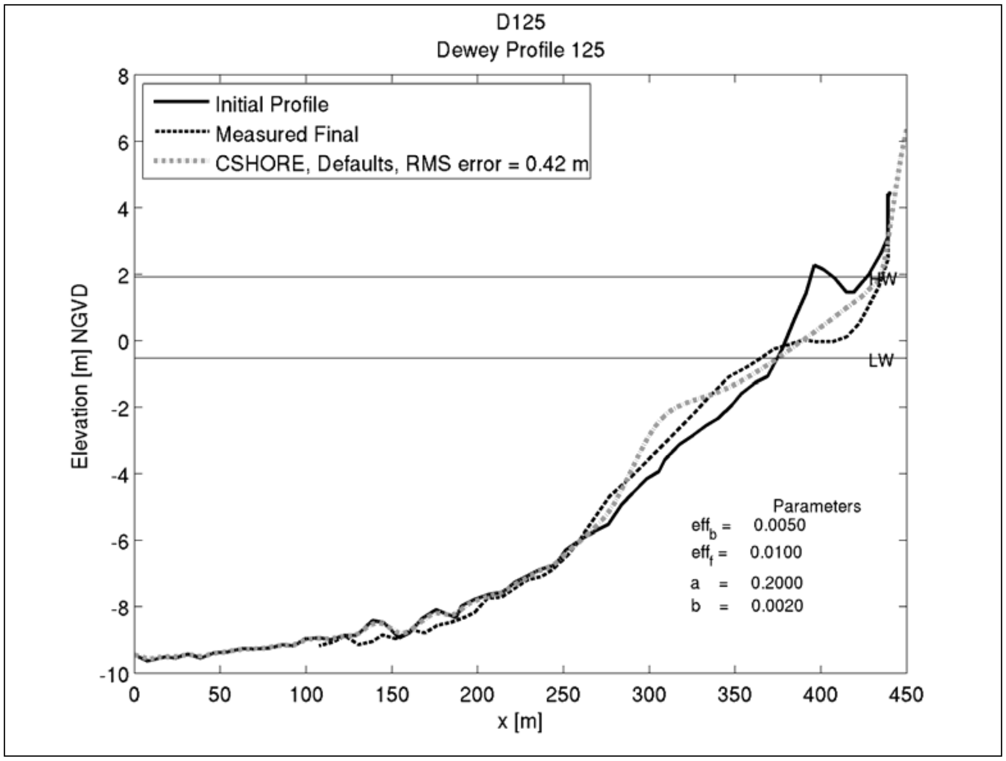

Figure 94. CSHORE simulation of the December 1992 storm for profile D125, Dewey Beach, DE.

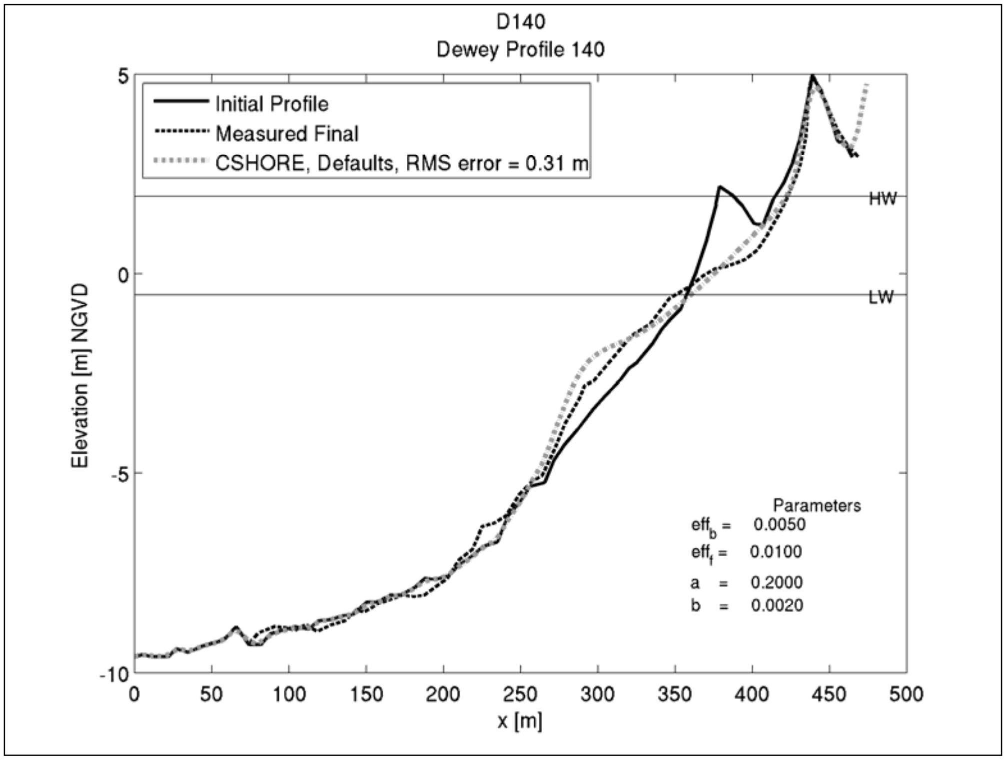

Figure 95. CSHORE simulation of the December 1992 storm for profile D140, Dewey Beach, DE.

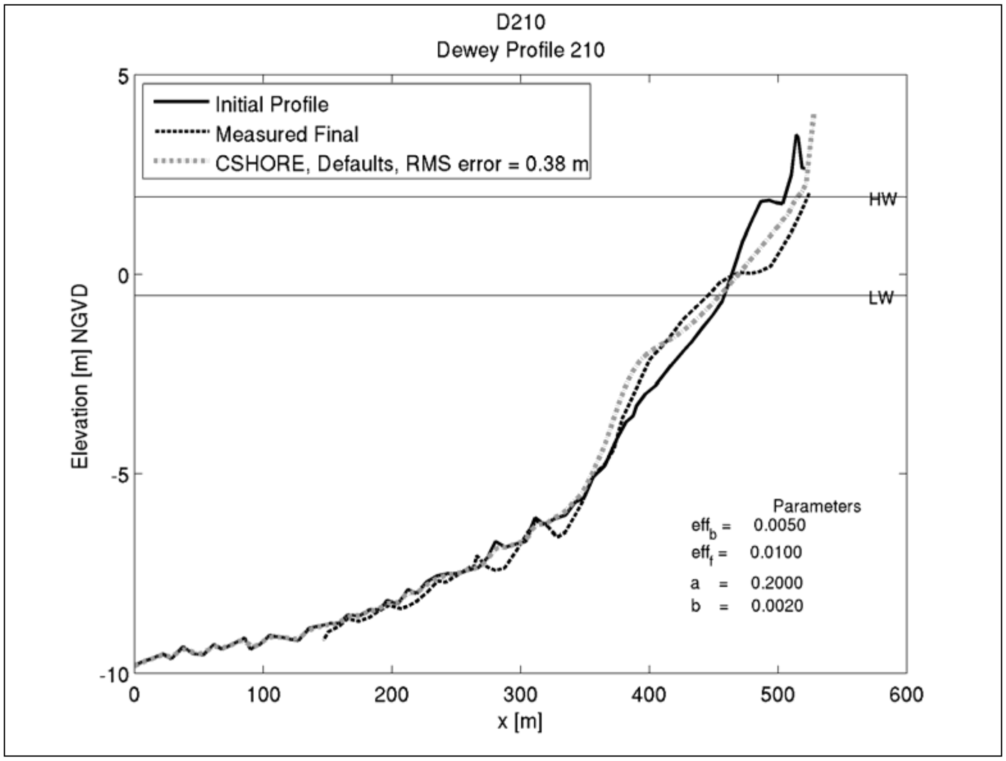

Figure 96. CSHORE simulation of the December 1992 storm for profile D210, Dewey Beach, DE.

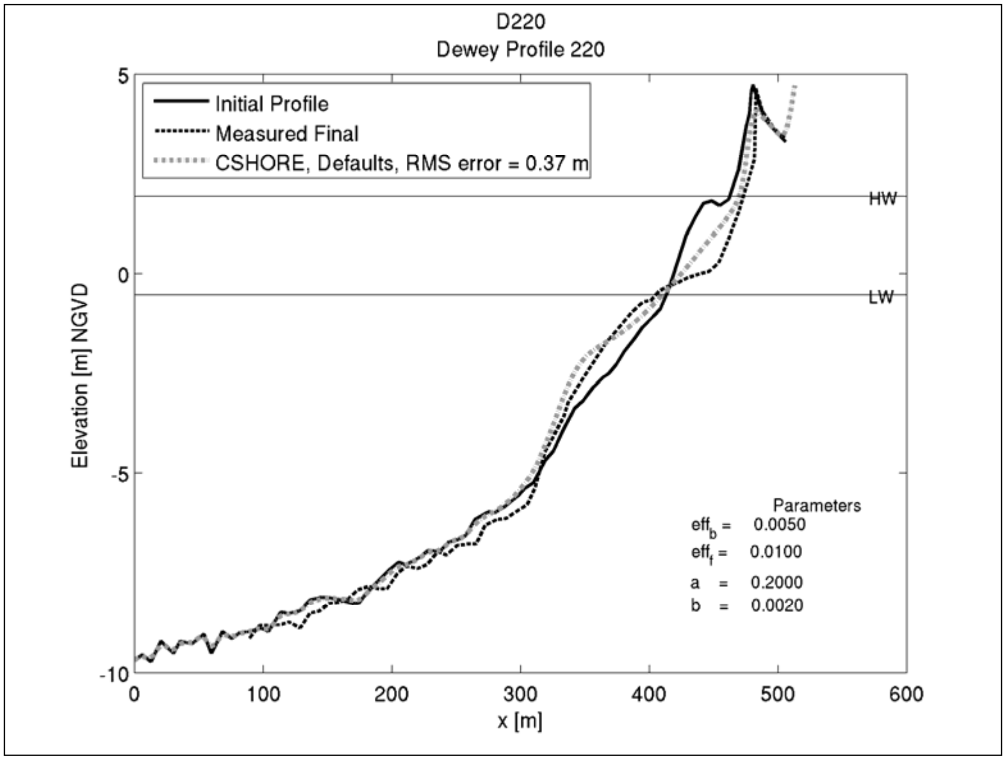

Figure 97. CSHORE simulation of the December 1992 storm for profile D220, Dewey Beach, DE.

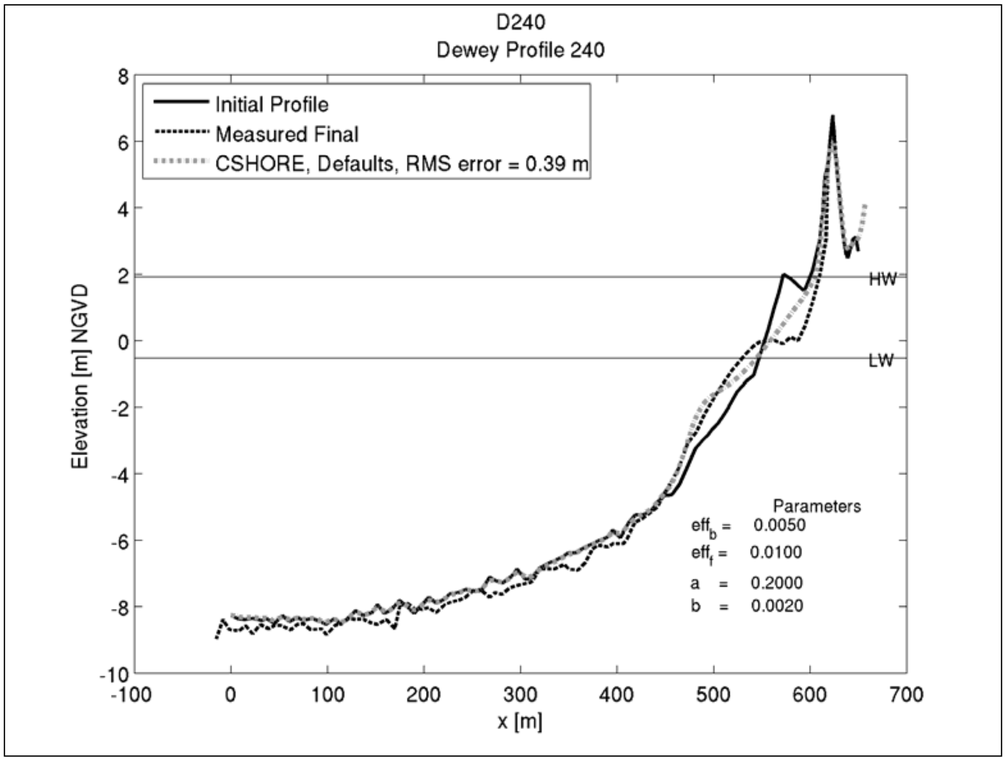

Figure 98. CSHORE simulation of the December 1992 storm for profile D240, Dewey Beach, DE.

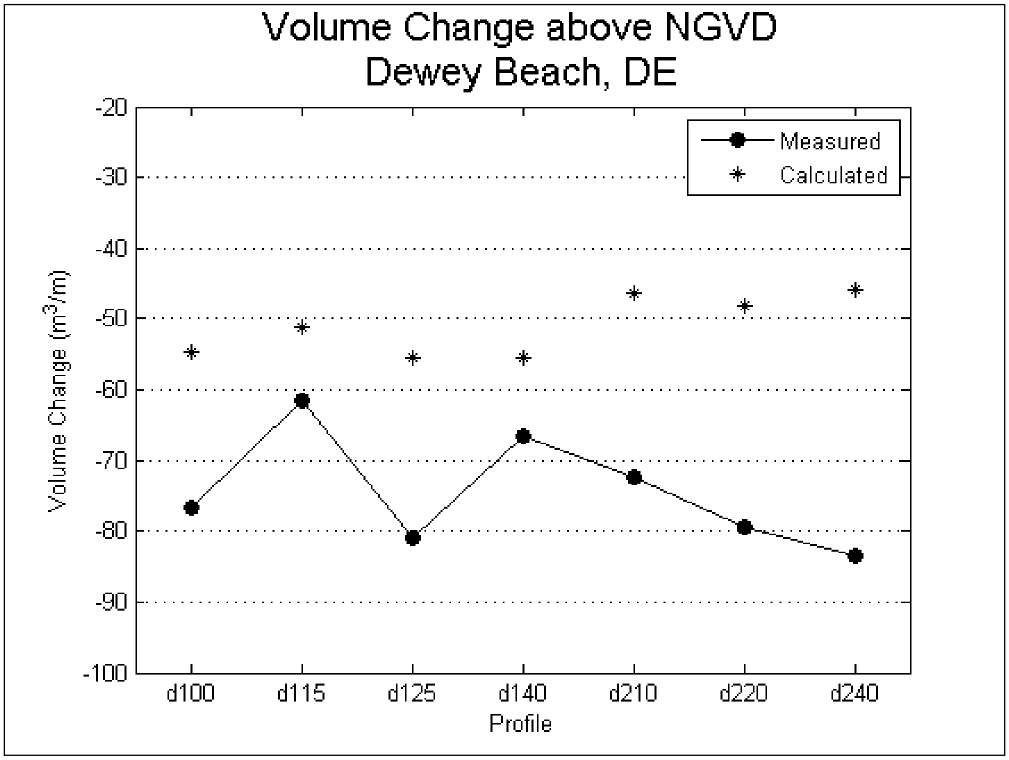

Figure 99. Comparison of measured and simulated volume change above NGVD for the December 1992 storm, Dewey Beach, DE.

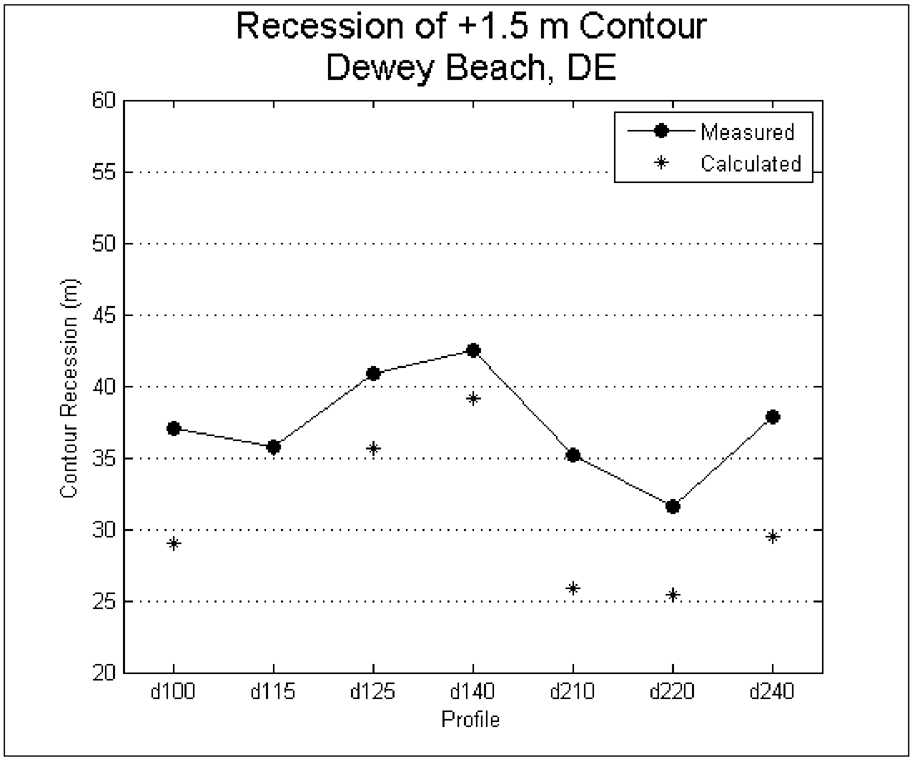

Figure 100. Comparison of measured and simulated recession of the 1.5-m contour for the December 1992 storm, Dewey Beach, NJ.

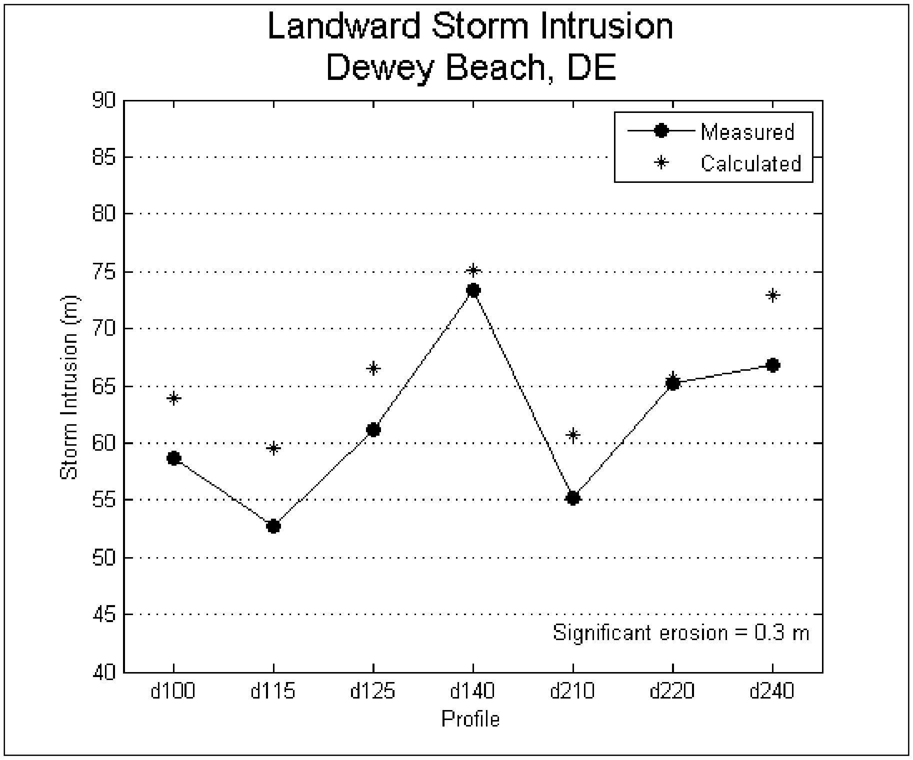

Figure 101. Comparison of measured and simulated storm intrusion for the December 1992 storm, Dewey Beach, NJ.

Rehoboth Beach. Rehoboth Beach lies approximately 1.5 miles north of Dewey Beach along the Delaware coast. Pre- and post-storm profile measurements at Rehoboth Beach were available at eight profile lines to model the beach response to the December 1992 storm. Figure 102 shows the storm induced volume change between the pre- and post-storm surveys for each of the Rehoboth Beach profiles. Mass was reasonably conserved at four of the Rehoboth Beach profiles (117, 200, 215, and 224) whereas net volumetric losses of 40 to 60 cu m/m were experienced at the other four profiles (122, 131, 138, and 236).

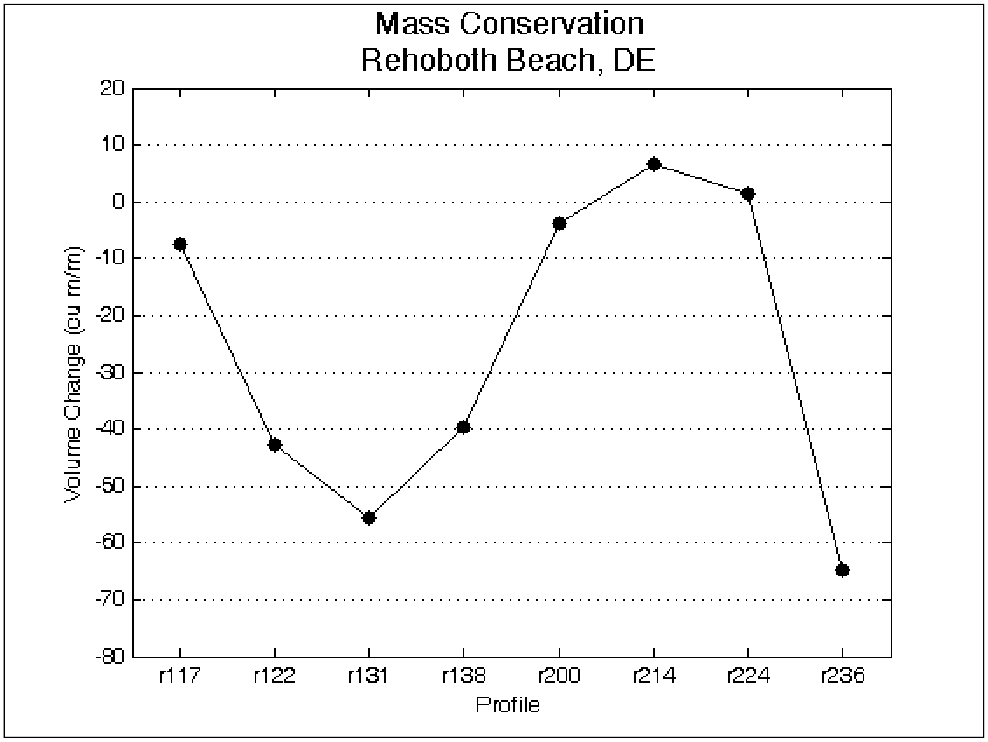

Figure 102. Conservation of mass between beach profile surveys for the December 1992 storm, Rehoboth Beach, DE.

The CSHORE simulation results for the December 1992 storm at Rehoboth Beach, DE are illustrated in Figures 103 through 110. These figures show the presence of an approximately 50 m wide berm backed by a dune or seawall in the pre-storm profiles. The CSHORE simulations predicted complete erosion of the berm feature together with slight erosion low on the seaward face of the dune in good agreement with the measured post-storm profiles. Profiles 117, 122, and 200 of the Rehoboth Beach data set included a seawall landward of the beach berm. Although CSHORE does not presently include a seawall boundary condition the predicted beach profile response is excellent seaward of the seawall position.

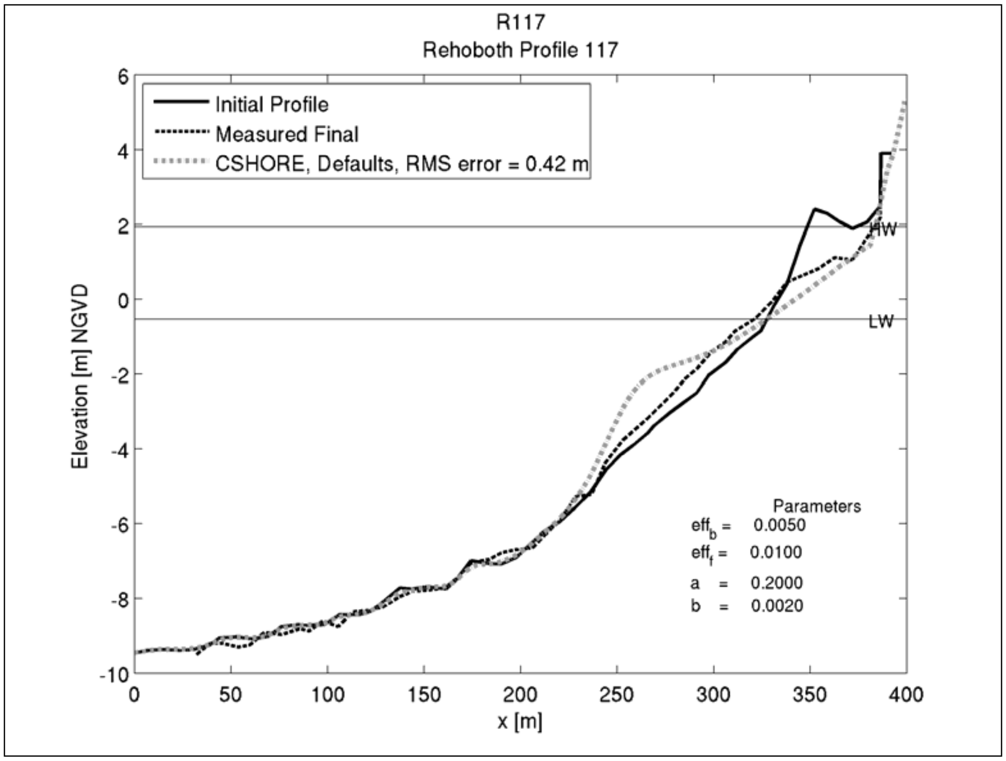

Figure 103. CSHORE simulation of the December 1992 storm for profile R117, Rehoboth Beach, DE.

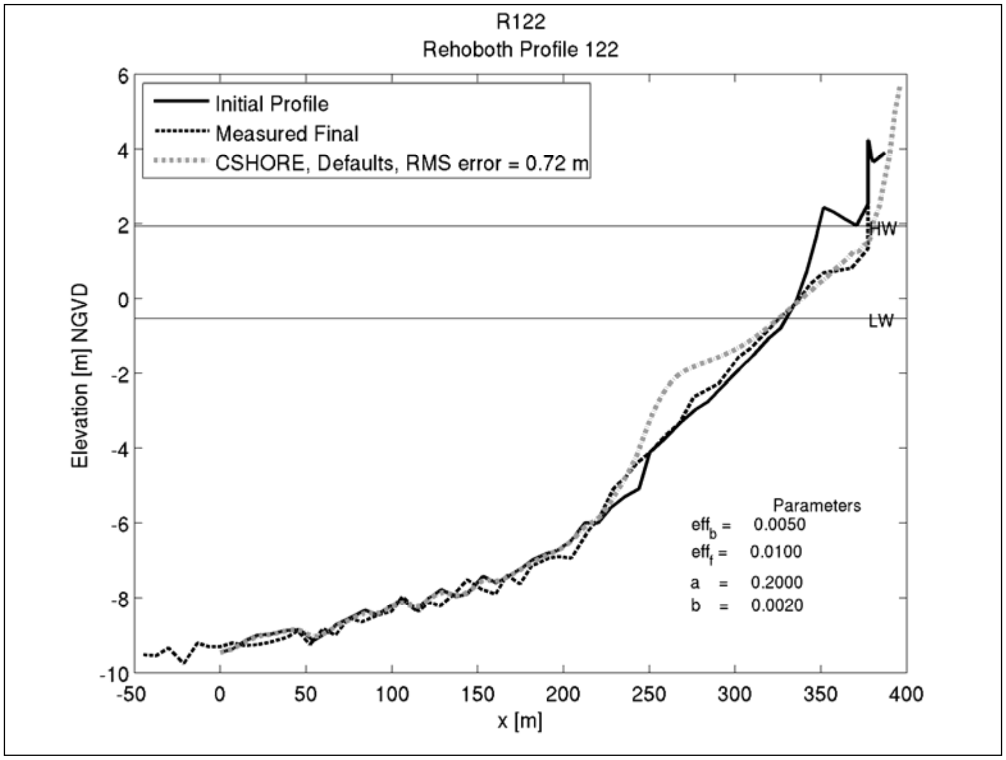

Figure 104. CSHORE simulation of the December 1992 storm for profile R122, Rehoboth Beach, DE.

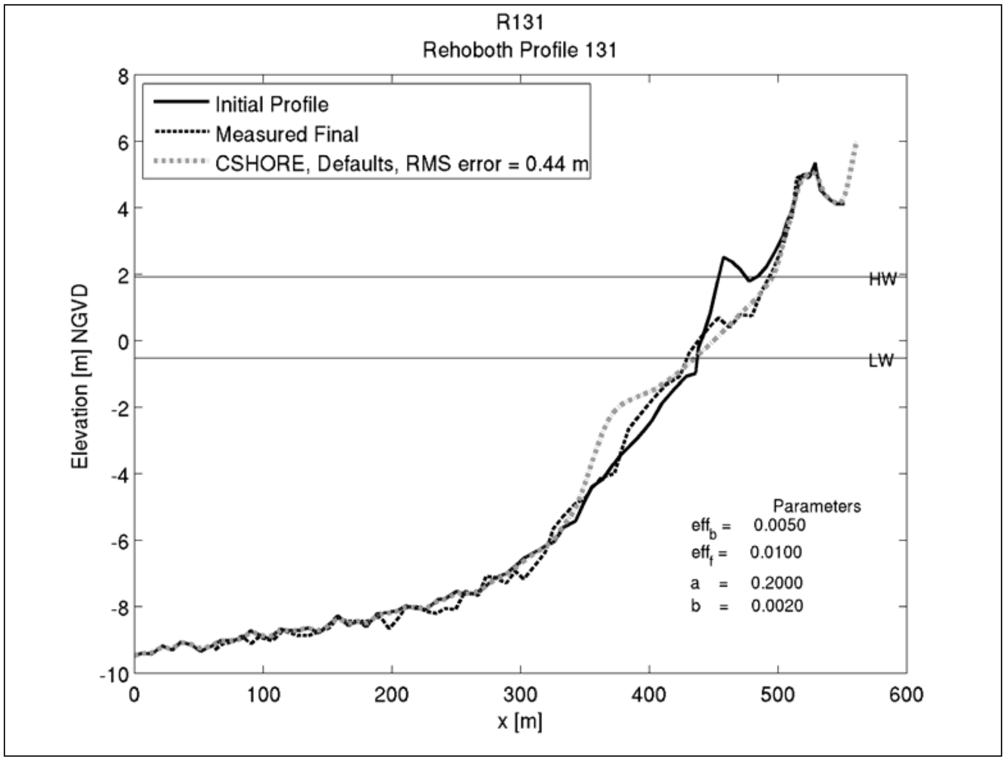

Figure 105. CSHORE simulation of the December 1992 storm for profile R131, Rehoboth Beach, DE.

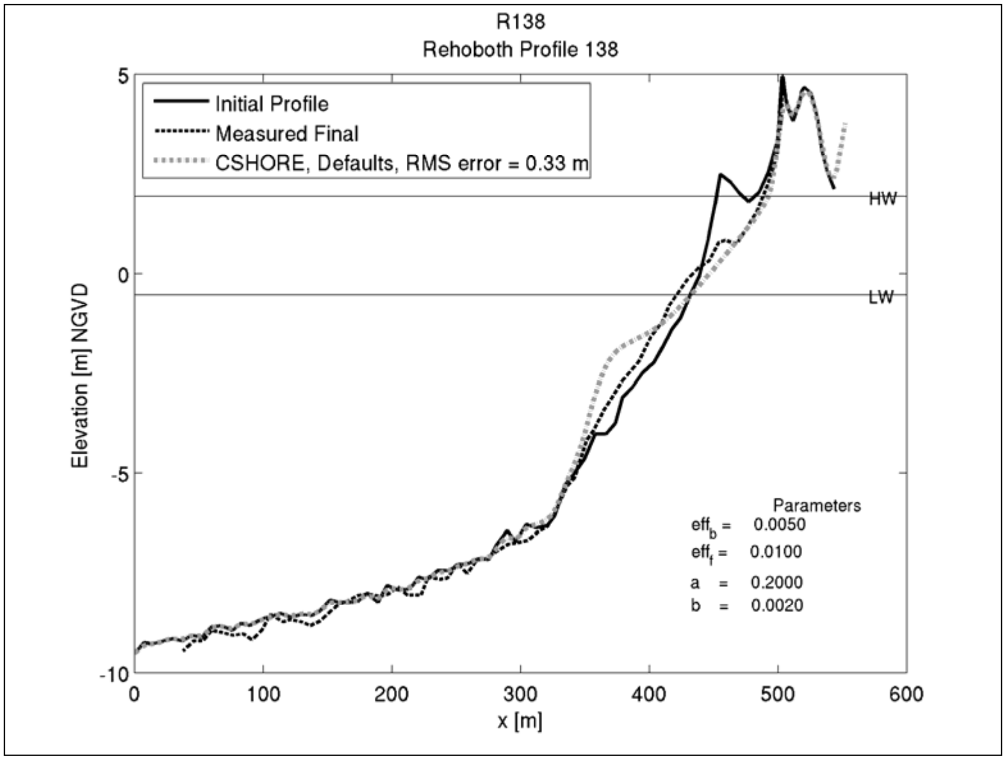

Figure 106. CSHORE simulation of the December 1992 storm for profile R138, Rehoboth Beach, DE.

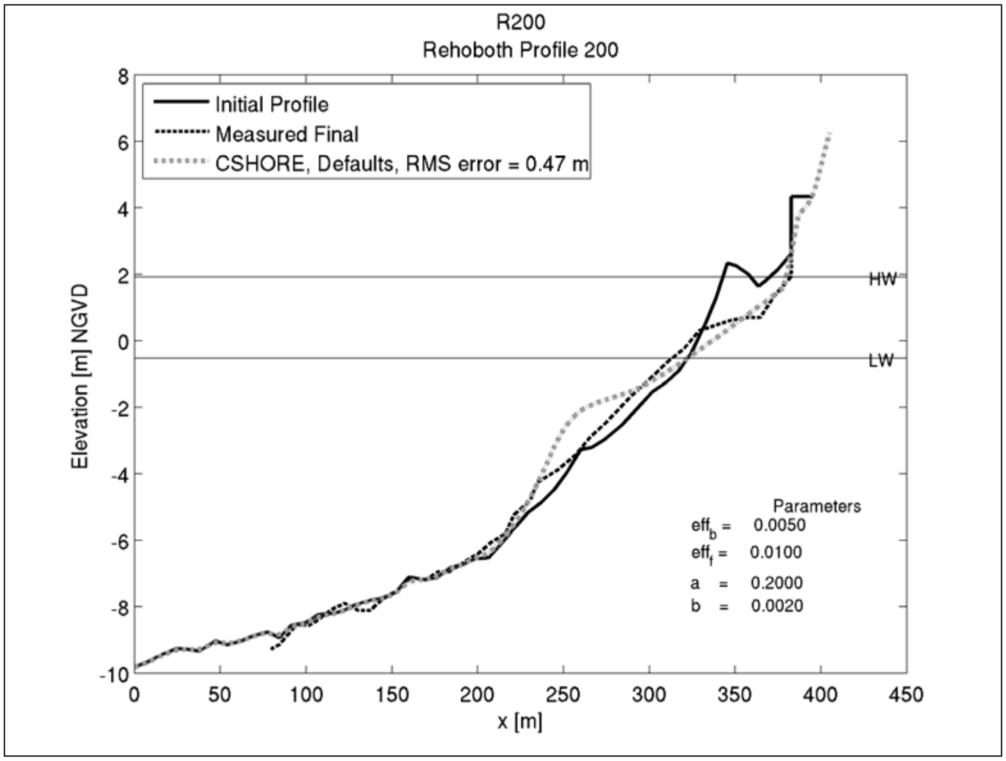

Figure 107. CSHORE simulation of the December 1992 storm for profile R200, Rehoboth Beach, DE.

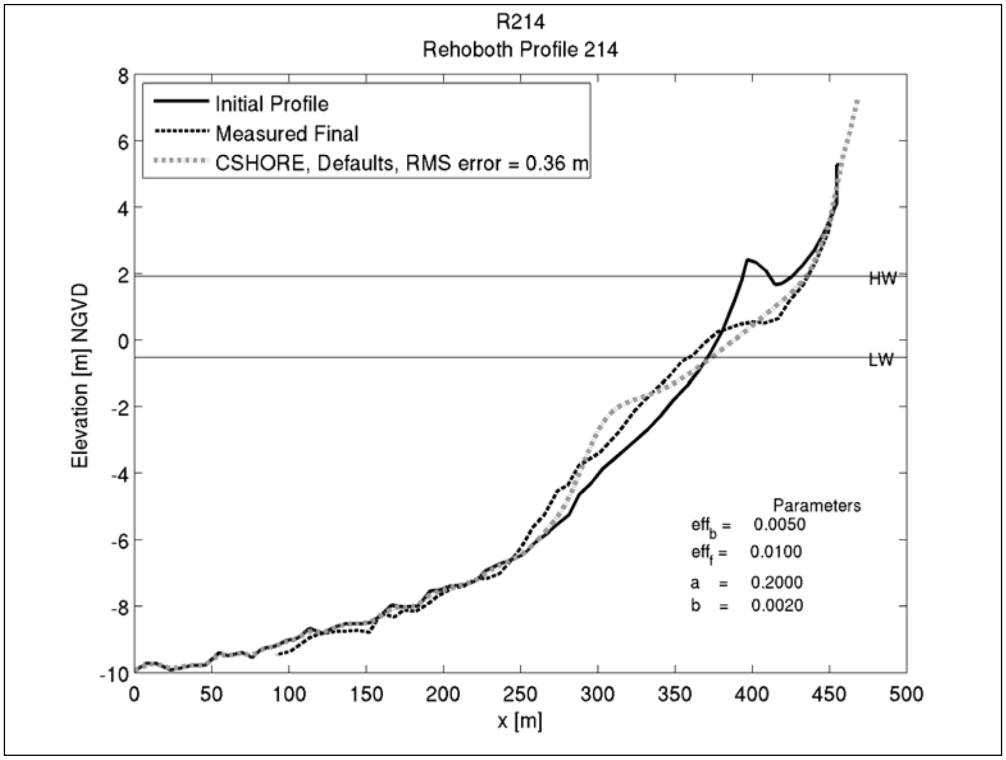

Figure 108. CSHORE simulation of the December 1992 storm for profile R214, Rehoboth Beach, DE.

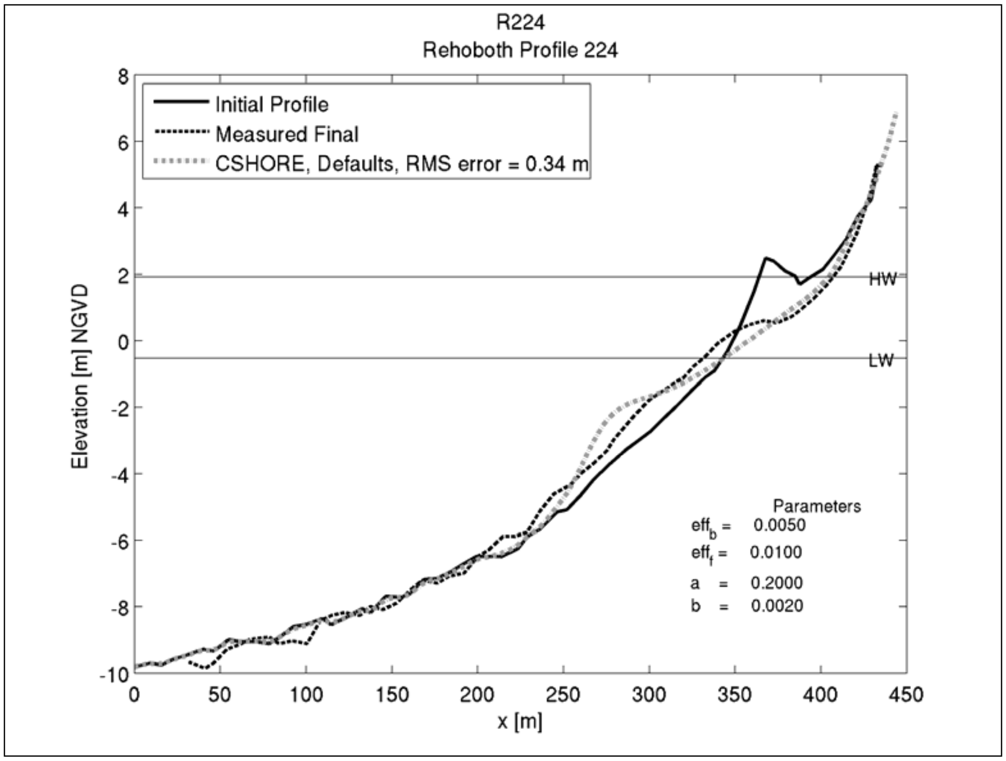

Figure 109. CSHORE simulation of the December 1992 storm for profile R224, Rehoboth Beach, DE.

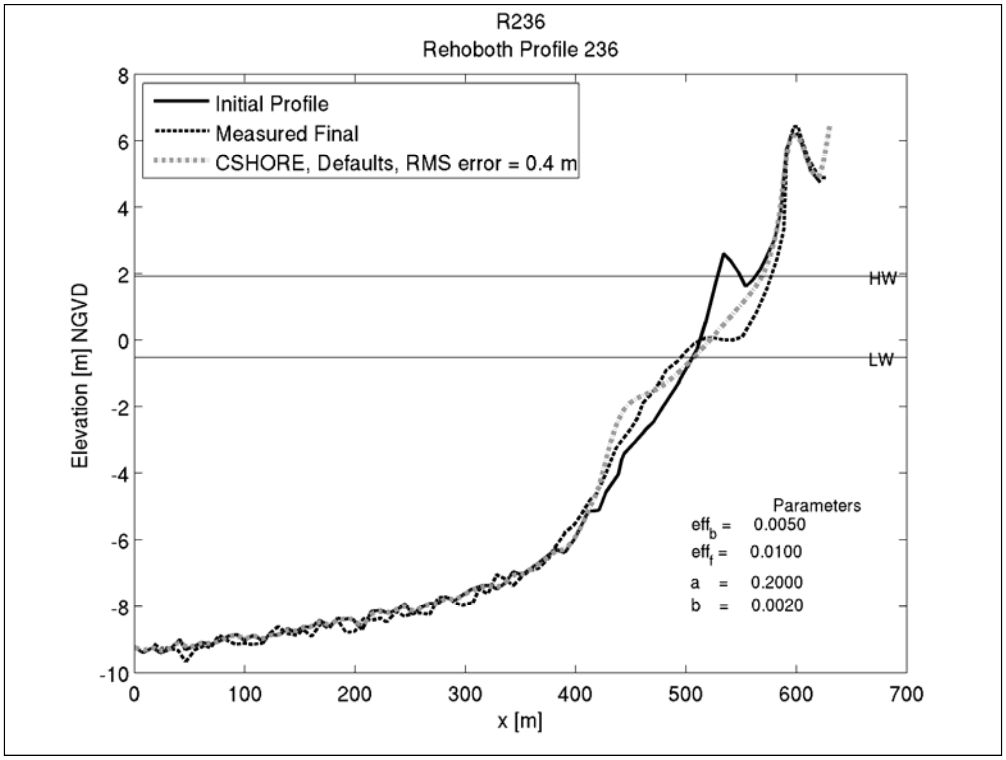

Figure 110. CSHORE simulation of the December 1992 storm for profile R236, Rehoboth Beach, DE.

The quantitative model performance measures for the December 1992 storm at Rehoboth Beach are illustrated in Figures 111 through 113. Figure 111 shows that overall the CSHORE predictions of volumetric change above NGVD compare well with measured values with the exception of profile 236. In five of the profiles the volumetric change estimate was within about 10 cu m/m, profile R117 was within 15 cu m/m, and profile R236 was under estimated by approximately 40 cu m/m. Some of the overestimation of volume change above NGVD could be attributed to the presence of a post-storm recovery berm in the measured post-storm profiles. Figure 112 shows the measured and calculated recession of 2 m contour where it is seen that the difference between the predicted and measured recession is less than 5 m for all but one of the profiles and approximately 9 m at the other profile. Figure 113 shows good agreement between the measured and calculated landward storm intrusion distance. The measured and computed storm intrusion distances for the Rehoboth Beach simulations differ by less than 10 m for five of the eight profiles. The greatest difference is approximately 18 m at profile 236.

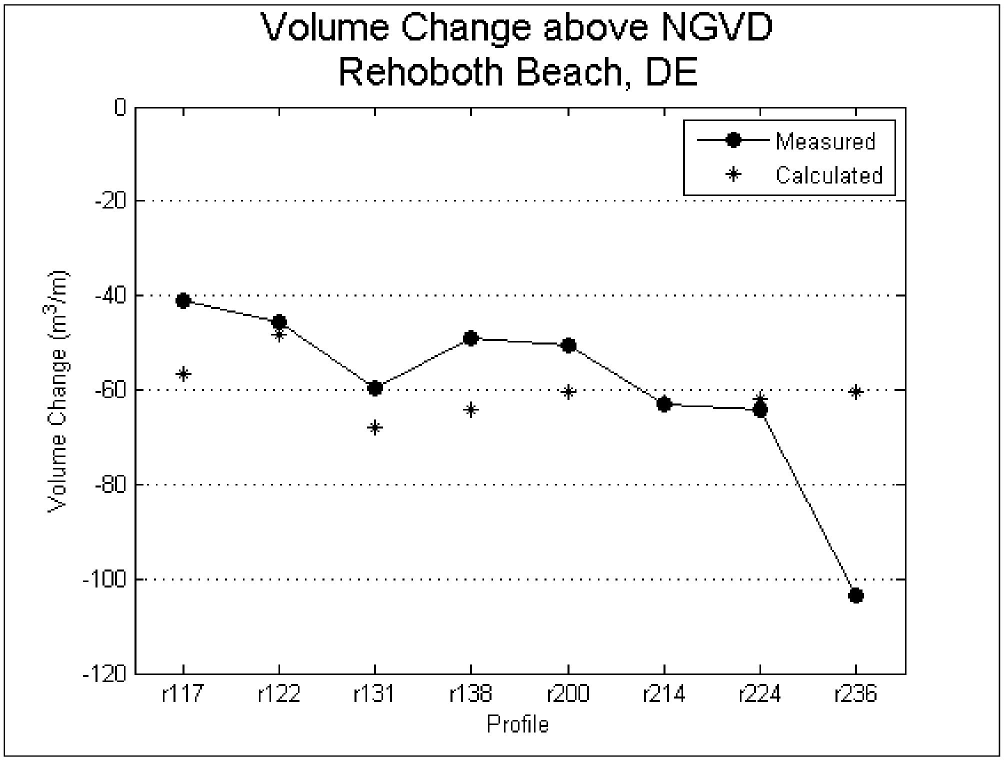

Figure 111. Comparison of measured and simulated volume change above NGVD for the December 1992 storm, Dewey Beach, DE.

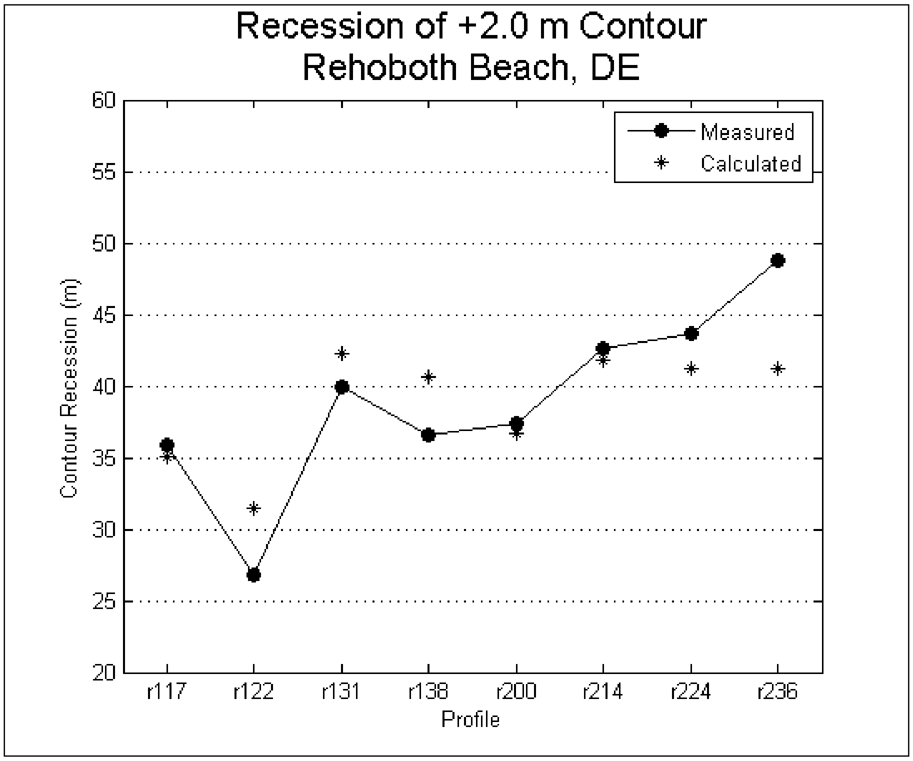

Figure 112. Comparison of measured and simulated recession of the 1.5-m contour for the December 1992 storm, Dewey Beach, NJ.

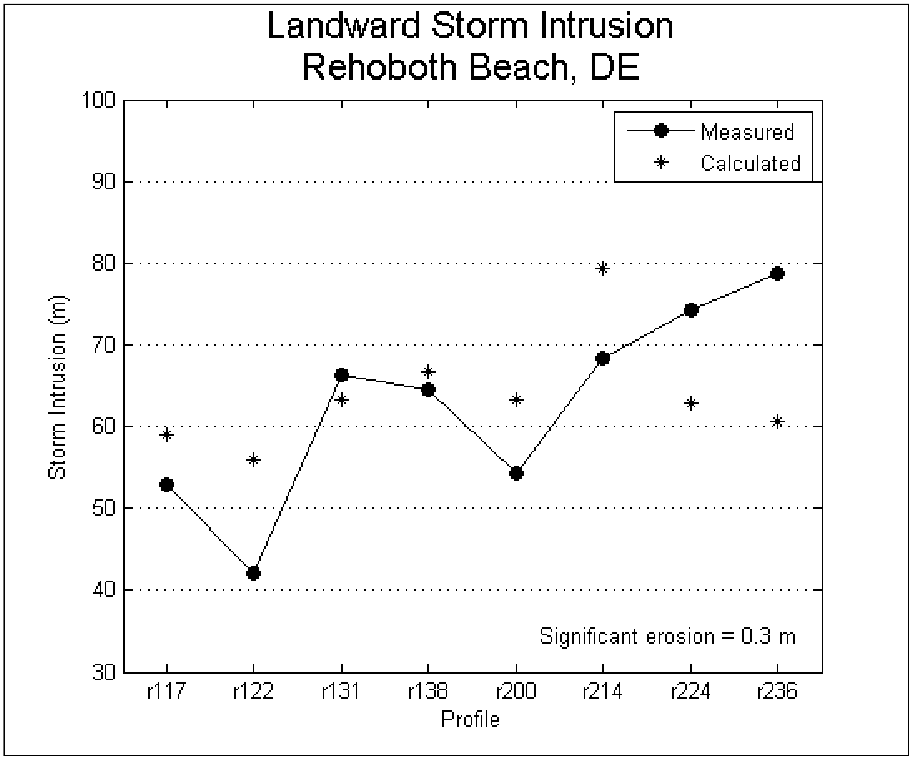

Figure 113. Comparison of measured and simulated storm intrusion for the December 1992 storm, Dewey Beach, NJ.

Debidue Beach and Myrtle Beach, SC

Hurricane Hugo made landfall near Charleston, SC on 22 September 1989. The beaches along the South Carolina coast north of Charleston were exposed to strong onshore winds and high waves and water levels. The extreme erosional effects of Hurricane Hugo were capture by beach surveys performed by Coastal Science and Engineering Inc. and the U.S. Army Corps of Engineers, Waterways Experiment Station, Coastal Engineering Research Center (Stauble et al. 1990). Beach profile data collected at Debidue Beach and Myrtle Beach in June 1989 provided the pre-storm profiles for modeling the beach response to Hurricane Hugo. A single post-storm profile collected within a week of the passing of the hurricane was available for simulating the impact of the hurricane at Debidue Beach and Myrtle Beach. A median sediment grain size of 0.20 mm was specified in the model simulations as a representative value for both beaches.

Water surface elevations during Hurricane Hugo were recorded by a tide gauge located in Winyah Bay, approximately 10 miles south of Debidue Beach and 40 miles south of Myrtle Beach. These tide gauge data represented the best available estimates of the total water level variations produced by the hurricane at both beaches. It is believed that the actual storm surge at the study sites was probably somewhat lower than the measurements since the beaches were located farther north away from the center of the storm. Hindcast wave information was used as input for the CSHORE simulation because no local measurements were available. To account for spatial variation in wave conditions, wave information from different hindcast stations were used for the two beaches. The time histories of the hindcast wave height and period and measured water level used in the modeling are shown in Figures 114 and 115. As indicated in the figures the peak hindcast significant wave height at Debidue Beach was approximately 6 m whereas at Myrtle Beach the peak hindcast significant wave height was approximately 4 m. The differences in the hindcast wave conditions at the two sites are primarily related to the distance from the storm center to the subject beach. The maximum water elevation measured at the Winyah Bay tide gauge was just less than 2.5 m NGVD.

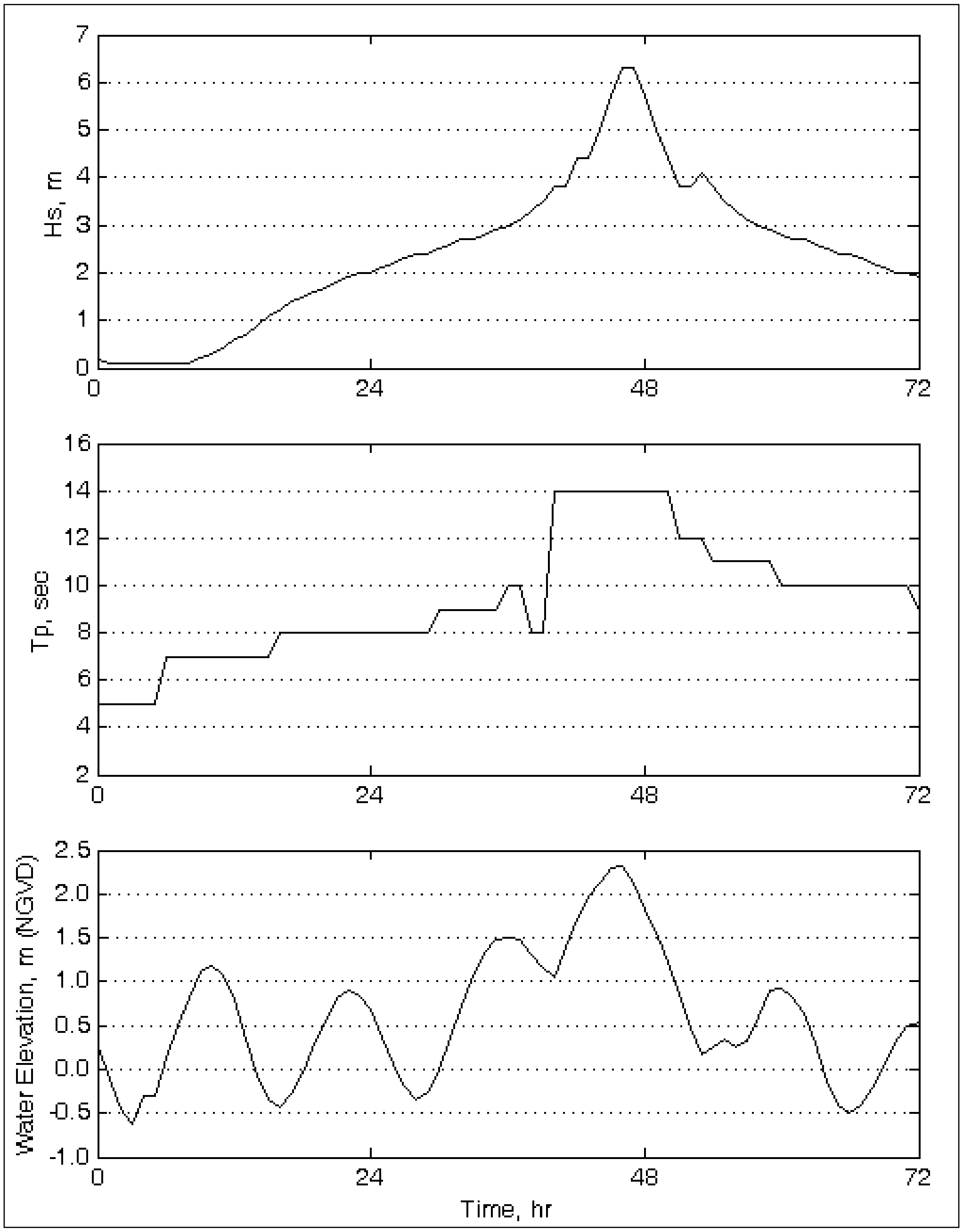

Figure 114. Wave height, wave period and water elevation time-histories for Hurricane Hugo, Debidue Beach, SC.

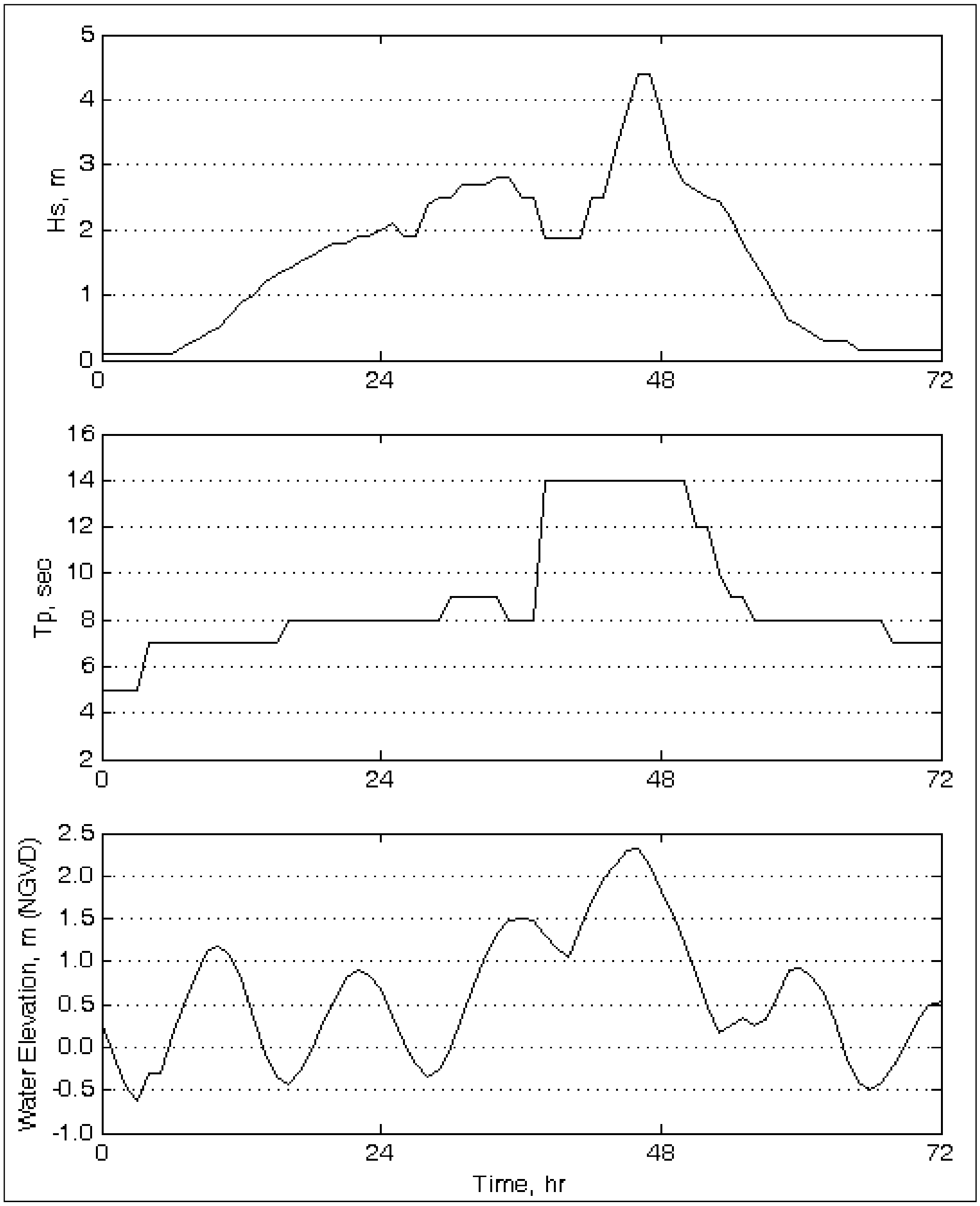

Figure 115. Wave height, wave period and water elevation time-histories for Hurricane Hugo, Myrtle Beach, SC.

CSHORE simulation results for Hurricane Hugo at Debidue Beach and Myrtle Beach are presented in Figures 116 and 117. Figure 116 shows that CSHORE significantly under predicted the near complete erosion of the berm and rather wide foredune indicated in the post-storm measured profile. The measured post-storm profile also indicates considerably more nearshore deposition between -4 m and +1 m NGVD than predicted by CSHORE. Figure 117 shows that the measured upper beach profile erosion due to Hurricane Hugo at Myrtle Beach is significantly under predicted in the CSHORE simulation.

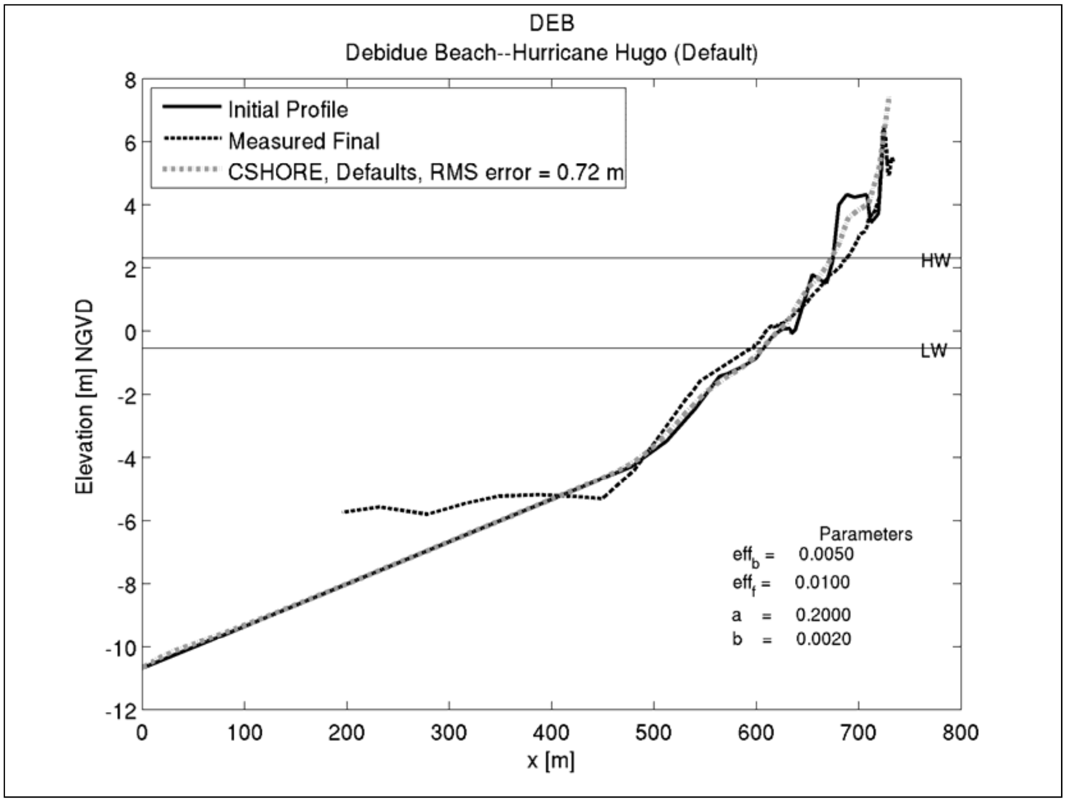

Figure 116. CSHORE simulation of Hurricane Hugo, Debidue Beach, SC.

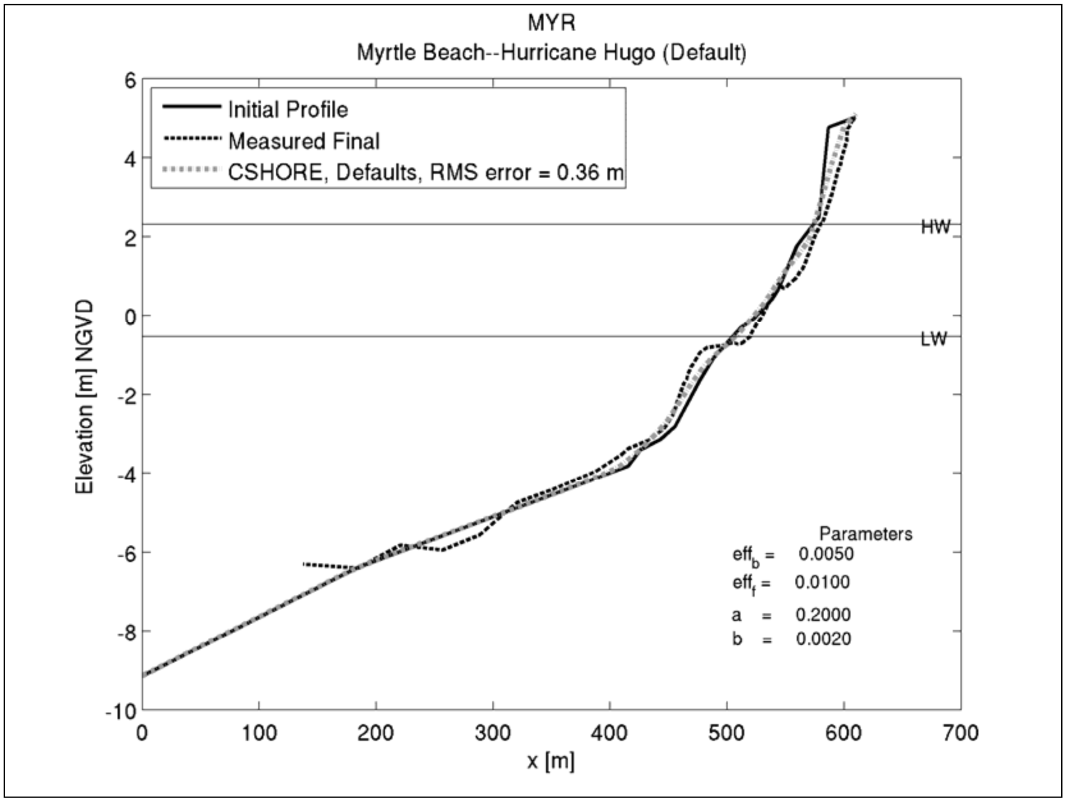

Figure 117. CSHORE simulation of Hurricane Hugo, Myrtle Beach, SC.

The quantitative model performance measures for Hurricane Hugo and Debidue Beach and Myrtle Beach are presented in Figures 118 through 120. Figure 118 shows that the CSHORE calculated erosion volume above NGVD was approximately 50 cu m/m and 33 cu m/m less than indicated by the pre- and post-storm profile measurements. Recession of the 3.5 m NGVD contour presented in Figure 119 was under estimated by approximately 20 m at Debidue Beach and 7 m at Myrtle Beach.

The landward storm intrusion distance was also under estimated by 8 m and 5 m as indicated in Figure 120.

Southern California Field Cases

On January 18, 1988 a significant coastal storm impacted the beaches of southern California. Wave and water level information for this storm was obtained from measurements at Wave Gauge 051 of the Coastal Data Information Program (CDIP, http://cdip.ucsd.edu/) operated and maintained by Scripps Institute of Oceanography, University of California, San Diego. This storm event was the largest recorded wave event at Wave Gauge 051 in the interval September 1, 1983 through June 13, 1988. A peak

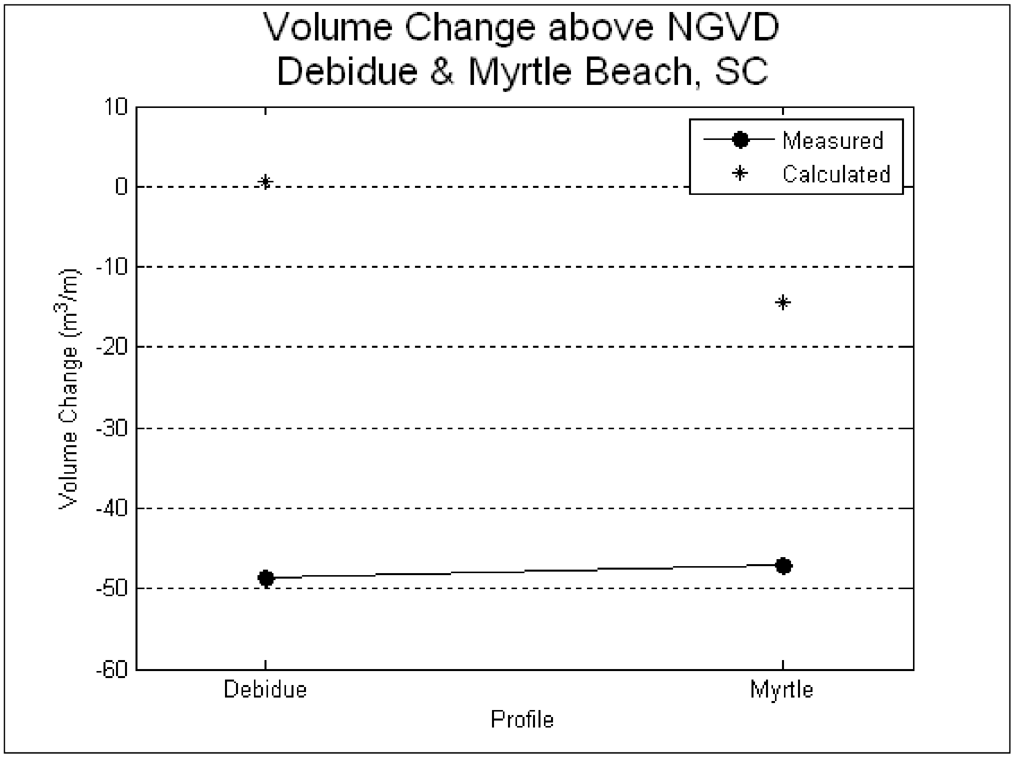

Figure 118. Comparison of measured and simulated volume change above NGVD for Hurricane Hugo, Debidue Beach and Myrtle Beach, SC.

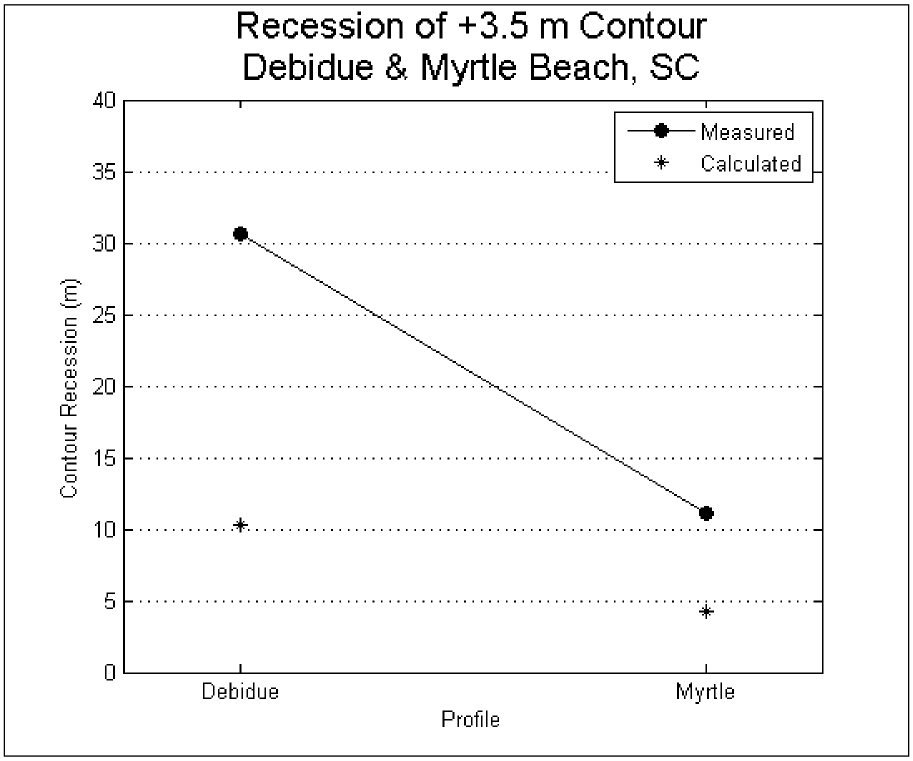

Figure 119. Comparison of measured and simulated recession of the 3.5-m contour for Hurricane Hugo, Debidue Beach and Myrtle Beach, SC.

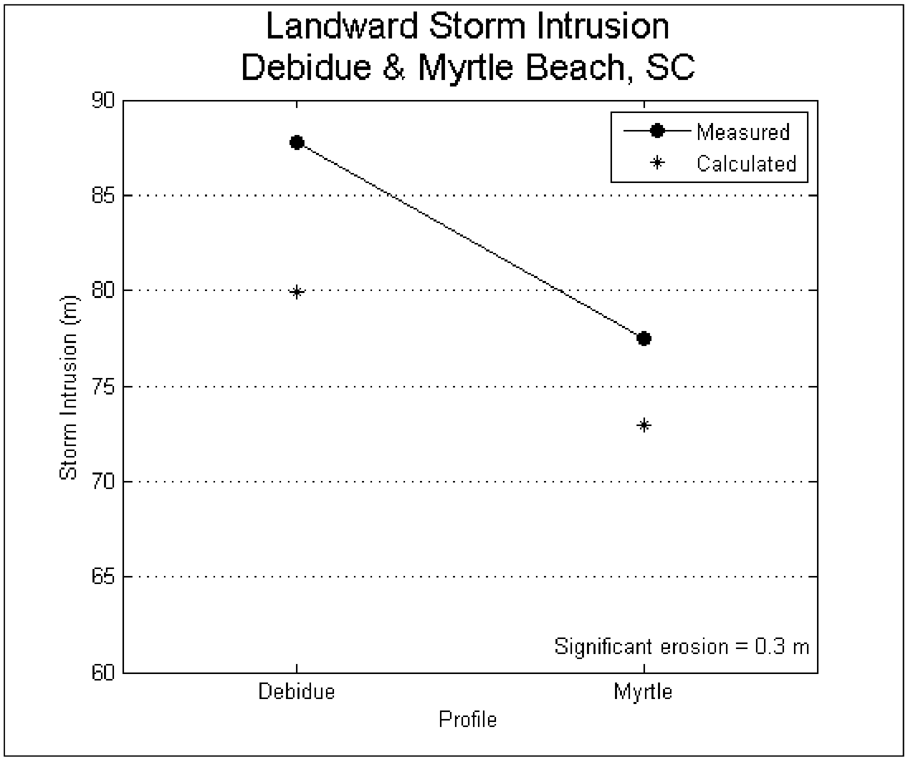

Figure 120. Comparison of measured and simulated storm intrusion for Hurricane Hugo, Debidue Beach and Myrtle Beach, SC.

significant wave height of 4.52 m was recorded on January 18, 1988, which is nearly five times larger than the mean recorded significant wave height of 0.92 m for the previous five years. The time histories of the measured significant wave height, peak wave period, and total water elevation are plotted in Figure 121. Here it is seen that although the storm generated very large wave conditions there is no statistically significant rise in the mean water level relative to the tidal variation of about 2 m. Pre- and post-storm beach profile surveys are available at Oceanside and Del Mar, CA for modeling the beach profile response to the January 1988 storm. The pre-storm profile survey was obtained in September 1987 and the post-storm profile survey was conducted soon after passage of the storm in late January 1988. Mean sediment grain sizes of 0.17 mm and 0.18 mm were specified for the Oceanside and Del Mar profiles, respectively based on sediment sampling.

CSHORE simulation results for the January 1988 storm at Oceanside and Del Mar, CA are illustrated in Figures 122 and 123. As seen in Figure120 both the post-storm measured profile and the CSHORE prediction indicate that the storm produced complete erosion of the berm at Oceanside, CA. The CSHORE simulation predicts development of an offshore bar feature in agreement with the measured profile but under predicts the development of a trough landward of the bar and erosion of the forshore slope between the -4 m contour and MLLW shoreline. At Del Mar (Figure 123) storm induced erosion above the 1 m contour is well predicted as is the development and position of the offshore bar feature. As in the Oceanside case the model does not predict development of a trough feature landward of the bar.

The quantitative model performance measures for the Oceanside and Del Mar, CA field cases are presented in Figures 124 through 126. In Figure 124 it is seen that the measured volumetric erosion above MLLW varies from approximately 95 cu m/m at Oceanside to about 100 cu m/m at Del Mar. The CSHORE predicted volumetric erosion above MLLW is within 1 cu m/m of measurements at Del Mar and approximately 13 cu m/m at Oceanside, and is viewed as good agreement. Measured and computed recession of the +3.0 m contour is compared in Figure 125 where it is seen that the model predictions are within about 1 or 2 m of the measurements. The difference between the measured and computed landward storm intrusion distance is seen in Figure 126 to be approximately 2 m at Oceanside and 5 m at Del Mar. Overall, the Oceanside and Del Mar California beach profile response to the January 1988 storm event is well predicted by CSHORE using the west coast default parameter values.

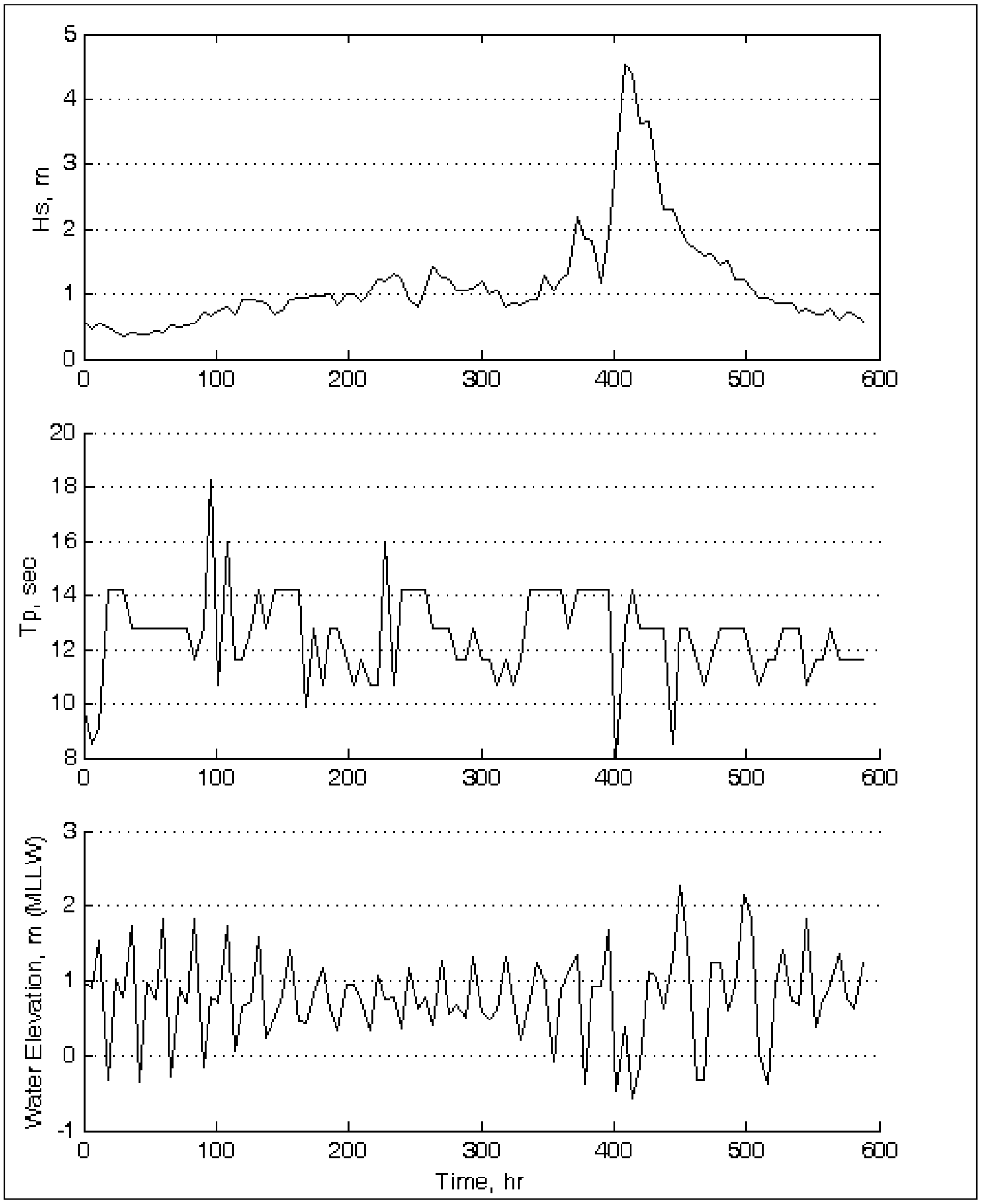

Figure 121. Wave height, wave period and water elevation time-histories for the January 1988 storm, Oceanside and Del Mar, CA.

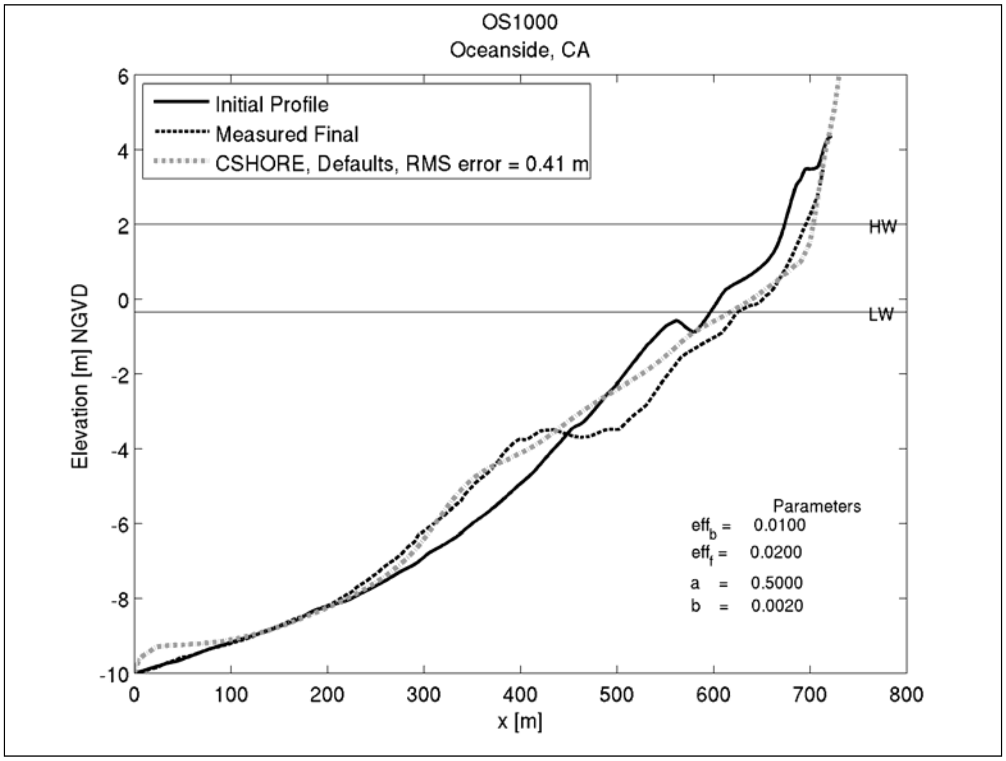

Figure 122. CSHORE simulation of January 1988 storm, Oceanside, CA.

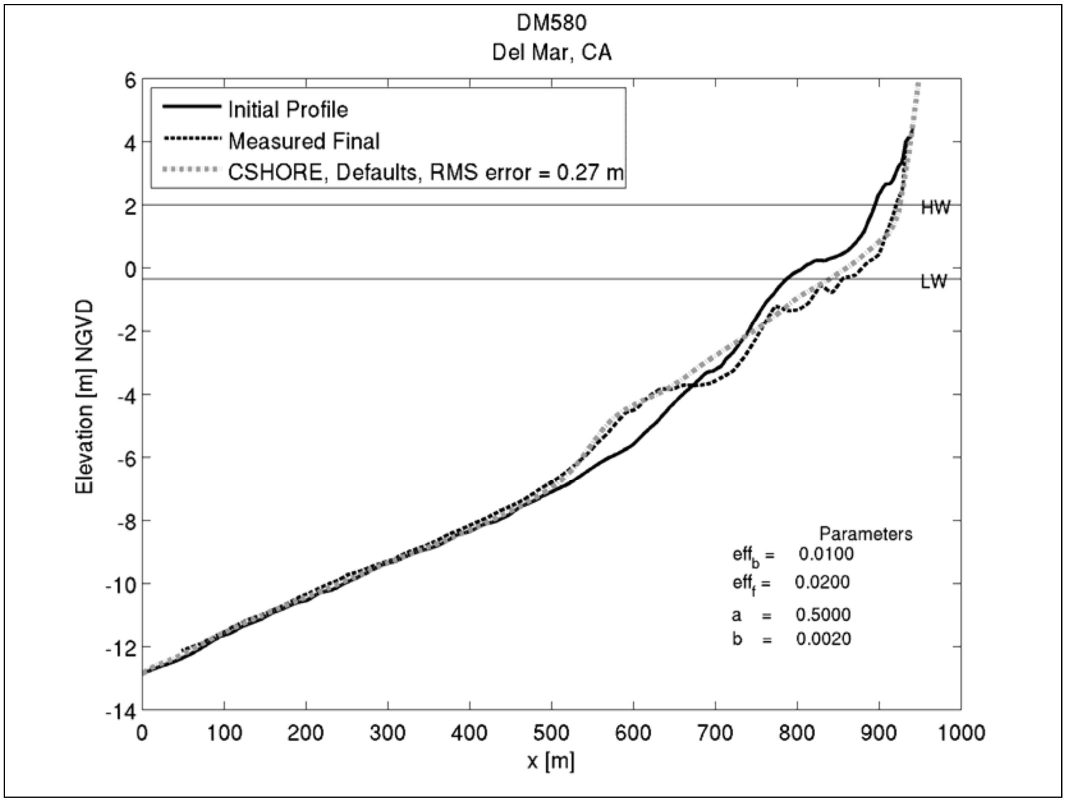

Figure 123. CSHORE simulation of January 1988 storm, Del Mar, CA.

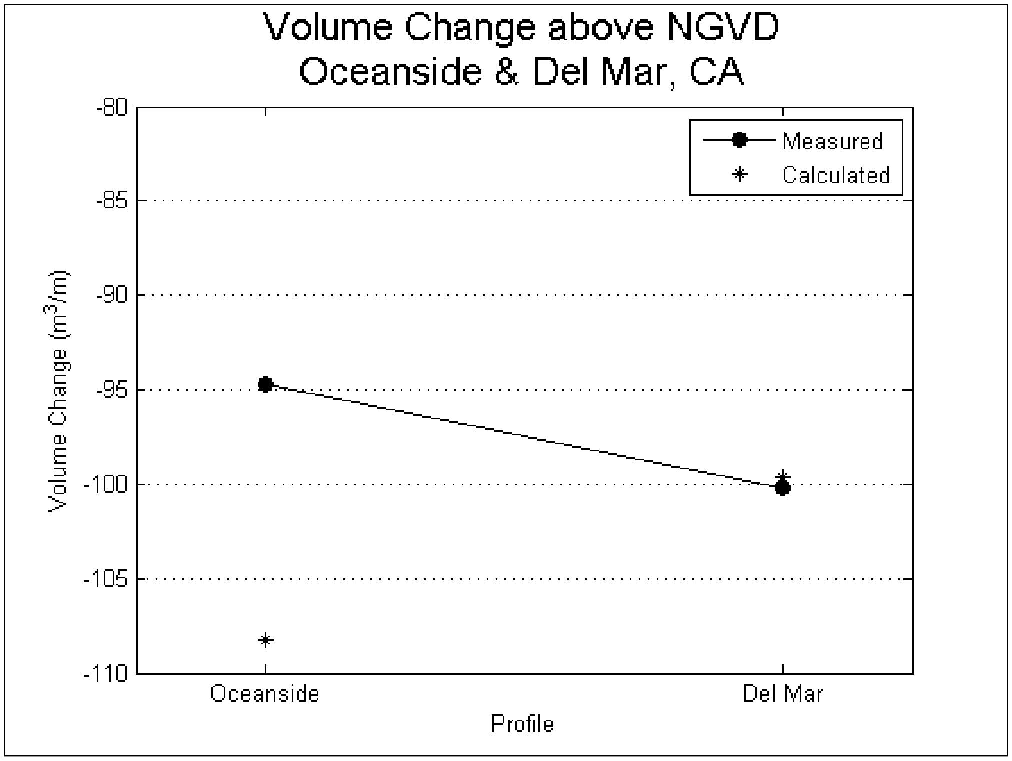

Figure 124. Comparison of measured and simulated volume change above MLLW for the January 1988 storm, Oceanside and Del Mar, CA.

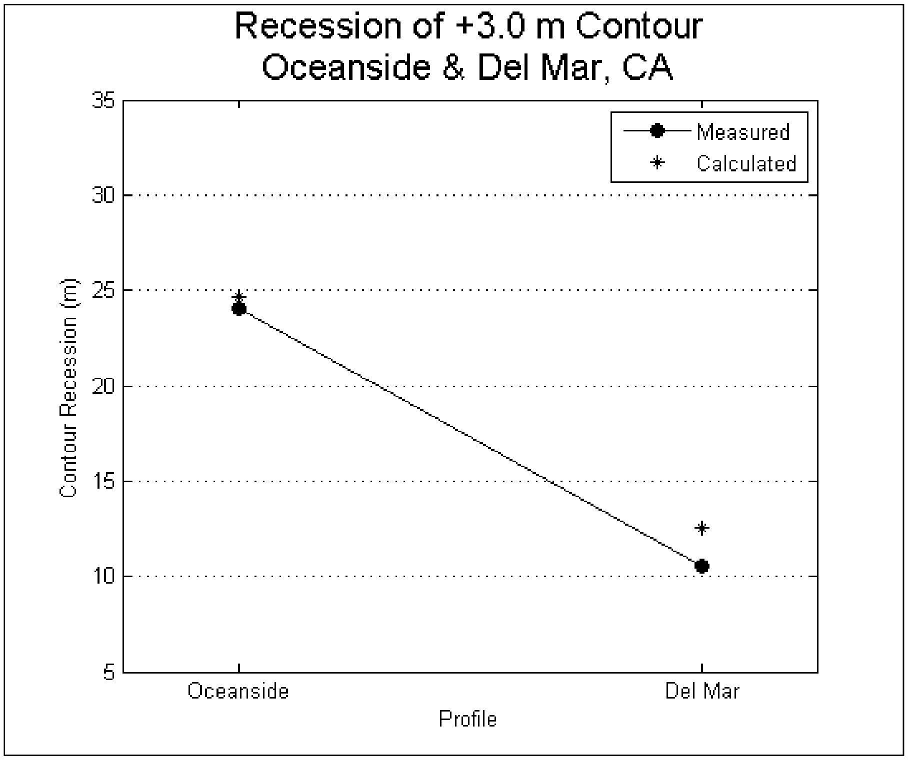

Figure 125. Comparison of measured and simulated recession of the 3.0-m contour for the January 1988 storm, Oceanside and Del Mar, CA.

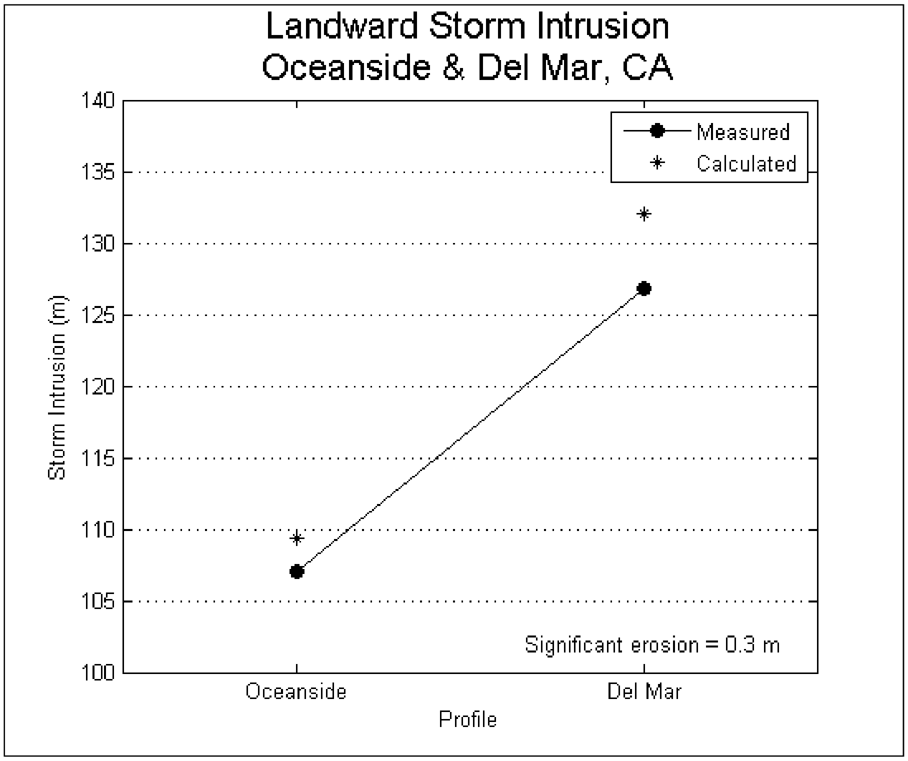

Figure 126. Comparison of measured and simulated storm intrusion for the January 1988 storm, Oceanside and Del Mar, CA.

11 Conclusions

The cross-shore model CSHORE is presented, including formulation documentation and validation test cases. The combined wave current model CSHORE based on the time-averaged continuity, cross-shore momentum, longshore momentum, wave action and roller energy equations predicts the cross-shore variations of the mean and standard deviation of the free surface elevation and depth-averaged cross-shore and longshore velocities under normally or obliquely incident irregular breaking waves. The sediment transport formulas for the cross-shore and longshore transport rates of suspended sediment and bedload on sand beaches are relatively simple and require the hydrodynamic input variables which can be predicted efficiently and fairly accurately using existing wave and current models. The CSHORE model has been compared with a number of small-scale and large-scale laboratory data and is ready for practical applications. CSHORE has been extended to the intermittently wet and dry zone for the prediction of wave overwash, levee erosion and deformation of a low-crested stone structure.

The beach erosion predictive capability of the CSHORE numerical simulation model was evaluated in field case studies using data describing severe beach erosion at nine different sites for eight storms. Seven of the field sites were located on the mid-Atlantic east coast (South Carolina to New Jersey) and two were located on the southern California coast. Model performance focused on the capability of the model to predict erosion of the beach berm and dune. Model performance was quantified by comparison of measured and calculated volume change, recession of select profile contours, and the landward progression of damaging erosion (0.3 m vertical erosion). CSHORE was applied to the field data sets using default parameter values estimated based on site-specific calibration of the model at three of the field sites. Overall the model provided satisfactory estimates of storm induced beach erosion for various pre-storm beach profile shapes and conditions. These field applications of CSHORE demonstrated model effectiveness in simulating beach erosion but also identified areas requiring research and model refinement. Dune lowering and landward translation of the dune crest due to overwash processes during the January 4, 1991 storm at Ocean City, MD was under predicted by CSHORE. The magnitude of upper beach erosion was also under predicted for Hurricane Hugo at

Debidue Beach and Myrtle Beach, SC as well as at six of the eight profiles at Point Pleasant Beach, NJ due to a northeaster storm event in March 1984. Improvements are needed in the area of sediment transport and morphology evolution in the intermittently wet zone.

References

Agarwal, A., N. Kobayashi, and B. D. Johnson. 2006. Longshore suspended sediment transport in surf and swash zones. *Proceedings 30th International Conference on Coastal Engineering*, J. M. Smith (ed.). Singapore: World Scientific Publishing Company, 2,498-2,510.

Agarwal, A., and N. Kobayashi. 2005. Time-averaged model for longshore current and sediment transport in surf and swash zones. Research Report No. CACR-05-07. Newark, DE: Center for Applied Coastal Research, University of Delaware.

Apotsos, A., B. Raubenheimer, S. Elgar, and R.T. Guza. 2008. "Testing and calibrating parametric wave transformation models on natural beaches." *Coastal Engineering*, 55, 224-235.

Bagnold, R. A. 1966. An approach to the sediment transport problem from general physics. Professional Paper 422-I:I1-I37. Reston, VA: U.S. Geological Survey

Bailard, J. A. 1981. An energetics total load sediment transport model for a plane sloping beach. *Journal of Geophysical Research* 86:10,938-10,954.

Battjes, J. A., and M. J. F. Stive. 1985. Calibration and verification of a dissipation model for random breaking waves. *Journal of Geophysical Research* 90(C5):9,159-9,167.

Becker, J. M., Y. L. Firing, J. Aucan, R. Holman, M. Merrifield, and G. Pawlak. 2007. Video-based observations of nearshore sand ripples and ripple migration. *Journal of Geophysical Research* 112, C01007, doi10.1029/2005JC003451.

Buck, M., N. Kobayashi, A. Payo, and B. D. Johnson. 2008. Berm and dune erosion. *Proceedings 31st Coastal Engineering Conference*. World Scientific Publishing Company, 1749-1761.

Buck, M., N. Kobayashi, A. Payo, and B. D. Johnson. 2007. Experiments and numerical model for berm and dune erosion. Research Report No. CACR-07-03. Newark, DE: Center for Applied Coastal Research, University of Delaware.

Chaudhry, M. H. 1993. *Open-channel flow*. Englewood Cliffs, NJ: Prentice Hall.

Dalrymple, R. A. 1988. Model for refraction of water waves. *Journal of Waterway, Port, Coastal, and Ocean Engineering* 114(4):423-435.

Dean, R. G. 1991. Equilibrium beach profile: Characteristics and applications. *Journal of Coastal Research* 7:53-84.

de los Santos, F. J., and N. Kobayashi. 2006. Irregular wave seepage and overtopping of cobble beaches and revetments. Research Report No. CACR-06-01. Newark, DE: Center for Applied Coastal Research, University of Delaware.

de los Santos, F. J., and N. Kobayashi. 2005. Irregular wave setup and runup on cobble beaches and revetments. Research Report No. CACR-05-06. Newark, DE: Center for Applied Coastal Research, University of Delaware.

de los Santos, F. J., N. Kobayashi, and M. Losada. 2006. Irregular wave runup and overtopping on revetments and cobble beaches. *Proceedings 30th International Conference on Coastal Engineering*, J. M. Smith (ed.). Hackensack, NJ: World Scientific Publishing Company, 4,667-4,679.

Dohmen-Janssen, C. M., and D. H. Hanes. 2002. Sheet flow dynamics under monochromatic nonbreaking waves. *Journal of Geophysical Research* 107(C10), 3,149, doi:10.1029/2001JC001045.

Dohmen-Janssen, C. M., D. F. Kroekenstoel, W. N. Hassan, and J. S. Ribberink. 2002. Phase lags in oscillatory sheet flow: Experiments and bed load modeling. *Coastal Engineering* 47:295-327.

EurOtop Manual. 2007. Wave overtopping of sea defences and related structures: Assessment manual. www.overtopping-manual.com.

Farhadzadeh, A., N. Kobayashi, and J. A. Melby. 2008. Wave overtopping and overflow on inclined structures. *Proceedings 31st Coastal Engineering Conference*. Singapore: World Scientific Publishing Company, 2996-3008.

Farhadzadeh, A., N. Kobayashi, J. A. Melby, and C. Ricottilli. 2007. Experiments and numerical modeling of wave overtopping and overflow on dikes. Research Report No. CACR-07-02. Newark, DE: Center for Applied Coastal Research, University of Delaware.

Farhadzadeh, A., N. Kobayashi, and J.A. Melby. 2009. Wave Overtopping and Damage Progression on Rubble Mound Structures. Newark, DE: Research Report No. CACR-09-05. Center for Applied Coastal Research, University of Delaware.

Farhadzadeh, A., N. Kobayashi, and J.A. Melby. 2010. Evolution of Damaged Armor Layer Profile. *Proceedings of 32nd Coastal Engineering Conference*, Structures, 40, 1-13.

Feddersen, F., R. T. Guza, S. Elgar, and T. H. C. Herbers. 2000. Velocity moments in alongshore bottom stress parameterization. *Journal of Geophysical Research* 105(C4):8,673-8,686.

Figlus, J., and N. Kobayashi. 2007. Seasonal and yearly profile changes of Delaware beaches. Research Report No. CACR-07-01. Newark, DE: Center for Applied Coastal Research, University of Delaware.

Figlus, J., N. Kobayashi, C. Gralher, and V. Iranzo. 2009. "Experimental and numerical study on transition from minor to major wave overwash of dunes." Res. Rep. No. CACR-09-04. Newark, DE: Center for Applied Coastal Research, University of Delaware.

Figlus, J., N. Kobayashi, C. Gralher, and V. Iranzo. 2010. "Wave-Induced Overwash and Destruction of Sand Dunes." *Proceedings of 32nd Coastal Engineering Conference*, Sediment, 34, 1-13.

Gallagher, E. L., S. Elgar, and R. T. Guza. 1998. Observations of sand bar evolution on a natural beach. *Journal of Geophysical Research* 103:3,203-3,215.

Gencarelli, R., B. D. Johnson, N. Kobayashi, and G. R. Tomasicchio. 2007. Dune erosion and breaching. *Proceedings Coastal Structures 2007*. Venice, Italy.

Gencarelli, R., G. R. Tomasicchio, N. Kobayashi, and B. D. Johnson. 2008a. Beach profile evolution and dune erosion due to the impact of Hurricane Isabel. *Proceedings 31st Coastal Engineering Conference*. Singapore: World Scientific Publishing Company, 1697-1709.

Gencarelli, R., G. R. Tomasicchio, N. Kobayashi, and B. D. Johnson. 2008b. Effects of Hurricane Isabel along the North Carolina coastline: Beach profile evolution and dune erosion. *Proceedings 3rd International Short Conference on Applied Coastal Research*. Lecce, Italy, 200-210.

Grosskopf, W.G. and D.K. Stauble. 1993. "Atlantic coast of Maryland (Ocean City) shoreline protection project," *Shore and Beach* 61(1), 3-7.

Headquarters, U.S. Army Corps of Engineers. 2002. *Coastal Engineering Manual*. EM 1110-2-1100. Washington, DC.

Henderson, S. M., J. S. Allen, and P. A. Newberger. 2004. Nearshore bar migration predicted by an eddy-diffusive boundary layer model. *Journal of Geophysical Research* 109, C06024, doi:10.1029/2003JC02137.

Hoefel, F., and S. Elgar. 2003. Wave-induced sediment transport and sandbar migration. *Science* 299:1,885-1,887.

Holland, K. T., R. A. Holman, and A. H. Sallenger, Jr. 1991. Estimation of overwash bore velocities using video techniques. *Proceedings Coastal Sediments'91*. Reston, VA: ASCE, 489-497.

Jiménez, J.A., and O.S. Madsen. 2003. "A simple formula to estimate settling velocity of natural sediments." *Journal of Waterway, Port, Coastal, and Ocean Engineering*, 129(2), 70-78.

Johnson, B. D., and N. Kobayashi. 2000. Free surface statistics and probabilities in surf zones on beaches. *Proceedings 27th Coastal Engineering Conference*. ASCE, 1,022-1,035.

Johnson, B. D., and N. Kobayashi. 1998. Nonlinear time-averaged model in surf and swash zones. *Proceedings 26th Coastal Engineering Conference*. ASCE, 2,785-2,798.

Johnson, B., M. Gravens, T. Wamsley, and N. Kobayashi. 2009. A Predictive Model for Beach Profile Evolution. *Proceedings of Coastal Dynamics 2009*, Tokyo, Japan, Paper No. 64.

Johnson, B. and Grzegorzewski, A.S. 2011. Modeling Nearshore Morphologic Evolution of Ship Island During Hurricane Katrina. *Proceedings 7th International Symposium on Coastal Engineering and Science of Coastal Sediment Processes*, pp 1797-1810.

Kamphuis, J. S. 1991. Alongshore sediment transport rate. *Journal of Waterway, Port, Coastal, and Ocean Engineering* 117(6):624-640.

Kearney, P. G., and N. Kobayashi. 2000. Time-averaged probabilistic model for irregular wave runup on coastal structures. *Proceedings 27th Coastal Engineering Conference*. ASCE, 2,004-2,017.

Kobayashi, N. 2008. Efficient wave and current models for coastal structures and sediments. In: *Nonlinear Wave Dynamics*. Singapore: World Scientific Publishing Company, 1-21.

Kobayashi, N. 2006. Time-averaged wave models for coastal structures and sediments. *Proceedings 2nd International Short Course and Workshop on Coastal Processes and Port Engineering*. Cosenza, Italy, 61-75.

Kobayashi, N. 1999. Wave runup and overtopping on beaches and coastal structures. In: *Advances in Coastal and Ocean Engineering* 5, Philip L-F Liu (ed.). Singapore: World Scientific Publishing Company, 95-154.

Kobayashi, N., A. Agarwal, and B. D. Johnson. 2007a. Longshore current and sediment transport on beaches. *Journal of Waterway, Port, Coastal, and Ocean Engineering* 133(4):296-304.

Kobayashi, N., M. Buck, A. Payo, and B. D. Johnson. 2009a. Berm and dune erosion during a storm. *Journal of Waterway, Port, Coastal, and Ocean Engineering,* ASCE, 135(1), 1-10.

Kobayashi, N., D. T. Cox, and A. Wurjanto. 1990. Irregular wave reflection and runup on rough impermeable slopes. *Journal of Waterway, Port, Coastal, and Ocean Engineering* 116(6):708-726.

Kobayashi, N., and F. J. de los Santos. 2007. Irregular wave seepage and overtopping of permeable slopes. *Journal of Waterway, Port, Coastal, and Ocean Engineering* 133(4):245-254.

Kobayashi, N., F. J. de los Santos, and P. G. Kearney. 2008b. Time-averaged probabilistic model for irregular wave runup on permeable slopes. *Journal of Waterway, Port, Coastal, and Ocean Engineering* 134(2):88-96.

Kobayashi, N., G. S. DeSilva, and K. D. Watson. 1989. Wave transformation and swash oscillation on gentle and steep slopes. *Journal of Geophysical Research* 94(C1):951-966.

Kobayashi, N., A. Farhadzadeh, and J. A. Melby. 2007c. Structures of storm surge disaster prevention. *Proceedings 4th International Workshop on Coastal Disaster Prevention*. Yokohama, Japan, 41-49.

Kobayashi, N. and A. Farhadzadeh. 2009. "Dune Erosion and Overwash." *Proceedings of Coastal Dynamics 2009*. Tokyo, Japan, Paper No. 81.

Kobayashi, N., A. Farhadzadeh, J. Melby, B. Johnson, and M. Gravens. 2010. "Wave Overtopping of Levees and Overwash of Dunes." Journal of Coastal Research, 26(5), 888-900.

Kobayashi, N., A. Farhadzadeh, and J.A. Melby. 2010b. “Wave Overtopping andDamage Progression of Stone Armor Layer.” *Journal of Waterway, Port, Coastal and Ocean Engineering*. 136(5), 257-265.

Kobayashi, N., J. Figlus, and M. Buck. 2008e. Beach nourishment and dune erosion. *Proceedings 3rd International Short Conference on Applied Coastal Research*. Lecce, Italy: Department of Innovation Engineering, University of Salento, 71-98.

Kobayashi, N., M. N. Herrman, B. D. Johnson, and M. D. Orzech. 1998. Probability distribution of surface elevation in surf and swash zones. *Journal of Waterway, Port, Coastal, and Ocean Engineering* 124(3):99-107.

Kobayashi, N., and B. D. Johnson. 2001. Sand suspension, storage, advection, and settling in surf and swash zones. *Journal of Geophysical Research* 106:9,363-9,376.

Kobayashi, N., and B. D. Johnson. 1998. Computer program CSHORE for predicting cross-shore transformation of irregular breaking waves. Research Report No. CACR-98-04. Newark, DE: Center for Applied Coastal Research, University of Delaware.

Kobayashi, N., L. E. Meigs, T. Ota, and J. A. Melby. 2007b. Irregular breaking wave transmission over submerged porous breakwaters. *Journal of Waterway, Port, Coastal, and Ocean Engineering* 133(2):104-116.

Kobayashi, N., and A. K. Otta. 1987. Hydraulic stability analysis of armor units. *Journal of Waterway, Port, Coastal, and Ocean Engineering* 113(2):171-186.

Kobayashi, N., A. Payo, and L. Schmied. 2008a. Cross-shore suspended sand and bedload transport on beaches. *Journal of Geophysical Research* 113, C07001, doi:10.1029/2007JC004203.

Kobayashi, N., A. Payo, and B. D. Johnson. 2009b. Suspended sand and bedload transport on beaches. In: *Handbook of Coastal and Ocean Engineering*. Singapore: World Scientific Publishing Company, Chapter 28, 807-823.

Kobayashi, N., B. Pozueta, and J. A. Melby. 2003. Performance of coastal structures against sequences of hurricanes. *Journal of Waterway, Port, Coastal, and Ocean Engineering* 129(5):219-228.

Kobayashi, N., and Y. Tega. 2002. Sand suspension and transport on equilibrium beach. *Journal of Waterway, Port, Coastal, and Ocean Engineering* 128(6):234-248.

Kobayashi, N., and A. Wurjanto. 1992. Irregular wave setup and run-up on beaches. *Journal of Waterway, Port, Coastal, and Ocean Engineering* 118(4):368-386.

Kobayashi, N., and A. Wurjanto. 1990. Numerical model for waves on rough permeable slopes. *Journal of Coastal Research* SI(7):149-166.

Kobayashi, N., H. Zhao, and Y. Tega. 2005. Suspended sand transport in surf zones. *Journal of Geophysical Research* 110, C12009, doi:10.1029/2004JC002853.

Kriebel, D. L., and R. G. Dean. 1985. Numerical simulation of time-dependent beach and dune erosion. *Coastal Engineering* 9:221-245.

Large, W. G., and S. Pond. 1981. Open ocean momentum flux measurements in moderate to strong winds. *Journal of Physical Oceanography* 11:324-336.

Lentz, S., R. T. Guza, S. Elgar, F. Feddersen, and T. H. C. Herbers. 1999. Momentum balances on the North Carolina inner shelf. *Journal of Geophysical Research* 104(C8):18,205-18,226.

Losada, I. J., J. L. Lara, R. Guanche, and J. M. Gonzalez-Ondina. 2008. Numerical analysis of wave overtopping of rubble mound breakwaters. *Coastal Engineering* 55:47-62.

Madsen, O. S., T. A. Chisholm, and L. D. Wright. 1994. Suspended sediment transport in inner shelf waters during extreme storms. *Proceedings 24th Coastal Engineering Conference*. Reston, VA: ASCE, 1,849-1,864.

Madsen, O. S., and W. D. Grant. 1976. Quantitative description of sediment transport by waves. *Proceedings 15th Coastal Engineering Conference*. Reston, VA: ASCE, 1,093-1,112.

Masselink, G., M. J. Austin, T. J. O'Hare, and P. E. Russell. 2007. Geometry and dynamics of wave ripples in the nearshore zone of a coarse sandy beach. Journal of *Geophysical Research* 112, C10022, doi:10.1029/2006JC003839.

Mei, C. C. 1989. *The applied dynamics of ocean surface waves.* Singapore: World Scientific Publishing Company.

Meigs, L. E., and N. Kobayashi. 2004. Time-averaged model for irregular breaking waves on porous structures and beaches. Research Report No. CACR-04-02. Newark, DE: Center for Applied Coastal Research, University of Delaware.

Meigs, L. E., N. Kobayashi, and J. A. Melby. 2004. Cobble beaches and revetments. *Proceedings 29th Coastal Engineering Conference*. Singapore: World Scientific Publishing Company, 3,865-3,877.

Melby, J. A., and N. Kobyashi. 1998. Progression and variability of damage on rubble mound breakwaters. *Journal of Waterway, Port, Coastal, and Ocean Engineering* 124(6):286-294.

Nairn, R. B., and H. N. Southgate. 1993. Deterministic profile modelling of nearshore processes. Part 2. Sediment transport and beach profile development. *Coastal Engineering* 19:57-96.

Neves, M. G., M. T. Reis, I. J. Losada, and K. Hu. 2008. Wave overtopping of Póvoa de Varzin breakwater: Physical and numerical simulations. *Journal of Waterway, Port, Coastal, and Ocean Engineering* 134(4):226-236.

Norton, P.A., and P. Holmes. 1992. Armor displacements on reshaping breakwaters. *Proceedings 23rd Coastal Engineering Conference*. Singapore: World Scientific Publishing Company, 1448-1460.

Ota, T., N. Kobayashi, and A. Kimura. 2006. Irregular wave transformation over deforming submerged structures. *Proceedings 30th International Conference on Coastal Engineering*, J. M. Smith (ed.). Singapore: World Scientific Publishing Company, 4,945-4,956.

Ota, T., Y. Matsumi, N. Kobayashi, and A. Kimura. 2007. Influence of damage progression on performance of rubble mound breakwaters. *Proceedings Coastal Structures 2007*. Venice, Italy.

Payo, A., N. Kobayashi, and K. H. Kim. 2006. Beach nourishment strategies. *Proceedings 30th International Conference on Coastal Engineering*, J. M. Smith (ed.). Singapore: World Scientific Publishing Company, 4,129-4,140.

Payo, A., N. Kobayashi, and F. Yamada. 2009. Suspended sand transport along pier depression. *Journal of Waterway, Port, Coastal, and Ocean Engineering*, ASCE, 135(5), 245-249.

Phillips, O. M. 1977. *The dynamics of the upper ocean*. Cambridge, The United Kingdom: Cambridge University Press.

Powell, M. D., P. J. Vickery, and T. A. Reinhold. 2003. Reduced drag coefficient for high wind speeds in tropical cyclones. *Nature* 422:279-283.

Ribberink, J. S. 1998. Bed-load transport for steady flow and unsteady oscillatory flows. *Coastal Engineering* 34:59-82.

Ribberink, J. S., and A. A. Al-Salem. 1994. Sediment transport in oscillatory boundary layers in cases of rippled beds and sheet flow. *Journal of Geophysical Research* 99:12,707-12,727.

Ruessink, B. G., J. R. Miles, F. Feddersen, R. T. Guza, and S. Elgar. 2001. Modeling the alongshore current on barred beaches. *Journal of Geophysical Research* 106(C10):22,451-22,463.

Schmied, L., N. Kobayashi, A. Payo, and J. A. Puleo. 2006a. Cross-shore sediment transport and beach profile change. Research Report No. CACR-06-03. Newark, DE: Center for Applied Coastal Research, University of Delaware.

Schmied, L. D., N. Kobayashi, J. A. Puleo, and A. Payo. 2006b. Cross-shore suspended sand transport on beaches. *Proceedings 30th International Conference on Coastal Engineering*, J. M. Smith (ed.). Singapore: World Scientific Publishing Company, 2,511-2,523.

Schüttrumpf, H., and H. Oumeraci. 2005. Layer thickness and velocities of wave overtopping flow at sea dikes. *Coastal Engineering* 52:473-495.

Seymour, R., R. T. Guza, W. O'Reilly, and S. Elgar. 2005. Rapid erosion of a small southern California beach fill. *Coastal Engineering* 52:151-158.

Shi, F., J. T. Kirby, and D. M. Hanes. 2007. An efficient model-splitting method for a curvilinear nearshore circulation model. *Coastal Engineering* 54:811-824.

Smith, J. M., A. R. Sherlock, and D. T. Resio. 2001. STWAVE: Steady-state spectral wave model user's manual for STWAVE, version 3.0. Coastal and Hydraulics Laboratory Special Report ERDC/CHL SR-01-1. Vicksburg, MS: U.S. Army Engineer Research and Development Center.

Stauble, D.K., W.C. Eiser, W.A. Birkemeier, L.Z. Hales, and W.C. Seabergh. 1990. "Erosion characteristics of Hurricane Hugo on beaches of South Carolina," *Shore and Beach* 58(4), 23-36.

Stauble, D.K., A.W. Garcia, N.C. Kraus, W.G. Grosskopf, and G.P. Bass. 1993. "Beach nourishment project response and design evaluation, Ocean City, Maryland; Report 1, 1988-1992," Technical Report CERC-93-13, Coastal Engineering Research Center, U.S. Army Engineer Waterways Experiment Station, Vicksburg, MS.

Svendsen, I. A., K. Haas, and Q. Zhao. 2002. Quasi-3D nearshore circulation model SHORECIRC version 2.0. Research Report No. CACR-02-01. Newark, DE: Center for Applied Coastal Research, University of Delaware.

Tega, Y., and N. Kobayashi. 1996. Wave overwash of subaerial dunes. *Proceedings 25th Coastal Engineering Conference*. Reston, VA: ASCE, 4,148-4,160.

Thornton, E. G., R. T. Humiston, and W. Birkemeier. 1996. Bar/trough generation on a natural beach. *Journal of Geophysical Research* 101:12,097-12,110.

Trowbridge, J., and D. Young. 1989. Sand transport by unbroken water waves under sheet flow conditions. *Journal of Geophysical Research* 94:10,971-10,991.

van Gent, M. R. A. 2002a. Wave overtopping events at dikes. *Proceedings 28th Coastal Engineering Conference*. Singapore: World Scientific Publishing Company, 2,203-2,215.

van Gent, M. R. A. 2002b. Low-exceedance wave overtopping events: Measurements of velocities and the thickness of water-layers on the crest and inner slope of dikes. Delft Cluster Report DC030202/H3803. Delft, The Netherlands: Delft Hydraulics Laboratory.

van Gent, M. R. A. 2001. Wave runup on dikes with shallow foreshores. *Journal of Waterway, Port, Coastal, and Ocean Engineering* 127(5):254-262.

van Gent, M. R. A. 1995. Porous flow through rubble-mound material. *Journal of Waterway, Port, Coastal, and Ocean Engineering* 121(3):176-181.

van Gent, M. R. A., E. M. Coeveld, D. J. R. Walstra, J. van de Graaff, H. J. Steetzel, and M. Boers. 2006. Dune erosion tests to study the influence of wave periods. *Proceedings 30th International Conference on Coastal Engineering*, J. M. Smith (ed.). Singapore: World Scientific Publishing Company, 2,779-2,791.

van Rijn, L. C., D. J. R. Walstra, B. Grasmeijer, J. Sutherland, S. Pan, and J. P. Sierra. 2003. The predictability of cross-shore bed evolution of sandy beaches at the time scale of storms and seasons using process-based Profile models. *Coastal Engineering* 47:295-327.

Wise, R.A., J. Smith, and M. Larson. 1996. SBEACH: Numerical model for simulating storm-induced beach change; Report 4, Cross-shore transport under random waves and model validation with SUPERTANK and field data, Technical Report CERC-89-9, Coastal Engineering Research Center, U.S. Army Engineer Waterways Experiment Station, Vicksburg, MS.

Wurjanto, A., and N. Kobayashi. 1993. Irregular wave reflection and runup on permeable slopes. *Journal of Waterway, Port, Coastal, and Ocean Engineering* 119(5):537-557.

Zhao, H., and N. Kobayashi. 2005. Suspended sand transport in surf zones on equilibrium beaches. Research Report No. CACR-05-01. Newark, DE: Center for Applied Coastal Research, University of Delaware.

REPORT DOCUMENTATION PAGE

Form Approved
OMB No. 0704-0188

1. REPORT DATE *(DD-MM-YYYY)*
September 2012

2. REPORT TYPE
Final Report

3. DATES COVERED *(From - To)*

4. TITLE AND SUBTITLE

Cross-Shore Numerical Model CSHORE for Waves, Currents, Sediment Transport and Beach Profile Evolution

5a. CONTRACT NUMBER

5b. GRANT NUMBER

5c. PROGRAM ELEMENT NUMBER

6. AUTHOR(S)

Bradley D. Johnson, Mark B. Gravens, and Nobuhisa Kobayashi

5d. PROJECT NUMBER

5e. TASK NUMBER

5f. WORK UNIT NUMBER

7. PERFORMING ORGANIZATION NAME(S) AND ADDRESS(ES)

Coastal and Hydraulics Laboratory
U.S. Army Engineer Research and Dev. Ctr.
3909 Halls Ferry Road
Vicksburg, MS 39180

Center for Applied Coastal Research
Ocean Engineering Laboratory
University of Delaware

8. PERFORMING ORGANIZATION REPORT NUMBER

ERDC/CHL TR-12-22

9. SPONSORING / MONITORING AGENCY NAME(S) AND ADDRESS(ES)

U.S. Army Corps of Engineers
441 G Street NW
Washington, DC 20314-1000

10. SPONSOR/MONITOR'S ACRONYM(S)

11. SPONSOR/MONITOR'S REPORT NUMBER(S)

12. DISTRIBUTION / AVAILABILITY STATEMENT
Approved for public release; distribution is unlimited.

13. SUPPLEMENTARY NOTES

14. ABSTRACT

The majority of the world shoreline is experiencing some form of erosion, which will become more serious if the mean sea level rise accelerates because of the greenhouse effect. Nourishment and maintenance of wide sand beaches for developed coastal communities will become more expensive unless the present nourishment design method is improved by the development of a reliable morphological model. Concurrently, the recent increase of coastal storm damage necessitates s the development of numerical models for predicting the damage progression and breaching of coastal stone structures and earthen levees during extreme storms. This report summarizes the continuing effort to improve our quantitative understanding of beach morphology and structural damage progression with the goal to develop simple and robust models that are suited for engineering applications. Our effort for the last 10 years has produced the cross-shore numerical model CSHORE, which is presently limited to the case of alongshore uniformity. CSHORE consists of the following components: a combined wave and current model based on time-averaged continuity, cross-shore and longshore momentum, wave action, and roller energy equations; a sediment transport model for suspended sand and bedload; a permeable layer model to account for porous flow and energy dissipation; empirical formulas for irregular wave runup, overtopping and seepage; and a probabilistic model for an intermittently wet and dry zone for the purpose of predicting wave overwash and structural damage progression.
(continued)

15. SUBJECT TERMS

Beach erosion
Dune erosion
Flooding
Modeling
Morphology
Nearshore
Sediment transport
Storm

16. SECURITY CLASSIFICATION OF:			**17. LIMITATION OF ABSTRACT**	**18. NUMBER OF PAGES**	**19a. NAME OF RESPONSIBLE PERSON: Bradley Johnson**
a. REPORT	**b. ABSTRACT**	**c. THIS PAGE**			**19b. TELEPHONE NUMBER *(include area code)***
Unclassified	Unclassified	Unclassified	Unclassified	158	(305) 650-0506

Standard Form 298 (Rev. 8-98)
Prescribed by ANSI Std. 239.18